SEISMIC EVALUATION OF HOLLOW CORE PRESTRESSED CONCRETE BRIDGE COLUMN-PILES IN WASHINGTON STATE

Tasha Tardieu

A thesis

submitted in partial fulfillment of the

requirements for the degree of

Master of Science in Civil Engineering

University of Washington

2019

Committee:

John F. Stanton

Paolo M. Calvi

Dawn E. Lehman

Marc O. Eberhard

Program Authorized to Offer Degree:

Civil and Environmental Engineering

University of Washington

Abstract

Seismic Evaluation of Hollow Core Prestressed Concrete Bridge Column-Piles in Washington State

Tasha Tiffany Tardieu

Co-Chairs of the Supervisory Committee:
John F. Stanton
Civil and Environmental Engineering
Paolo M. Calvi
Civil and Environmental Engineering

The Washington State Department of Transportation (WSDOT) began a bridge seismic retrofit program in 1990 in order to address the earthquake risks associated with state-owned bridges. The majority of these bridges were constructed prior to the development of current seismic design standards, and one class of bridges built during that era represents a particular cause for concern. In that class of bridges, hollow precast, prestressed concrete piles were installed in the ground, and they projected above ground level to form the columns. Cap beams were then cast in place, and connected to the column-piles by means of concrete plugs cast into the tops of the columns.

Previous, but limited, research experiments have shown that these hollow, prestressed concrete columns and piles show minimal ductility under cyclic lateral loading and fail suddenly, because the wall of the column spalls both inwards and outwards. Jacketing is effective only in preventing the outward spalling. Because many of these hollow-column bridges form part of the state's "Seismic Lifeline Routes", they are slated for retrofit in the near future. This research project was conducted to determine the behavior of both as-built and retrofitted hollow, precast, prestressed concrete column-pile bridges under static and seismic loadings. The findings of the research are intended to inform WSDOT's plans for the retrofit scheme to be used in the field.

Under elastic conditions, the peak moment demand occurs at the top of the columns, adjacent to the cap beam; the moments below grade are approximately half as large. Therefore, the proposed

retrofit concept for these column-piles involves cutting back the top of the hollow column-pile wall directly below the cap beam to reduce the column moment demand at the top. The exposed plug, and the column corresponding to the plug region, should be jacketed to create a ductile fuse in that location. A simple analytical study of the column-piles considered their behavior under lateral loading and explored the effects of various parameters such as the length of the column, the length of the below-ground pile, the soil stiffness, the presence of a continuous deck and the consequences of inelastic deformation of the plug. The results showed that the potential retrofit would improve the seismic performance of the column-pile system so that it could in most cases withstand the 1000-year design earthquake. Two experimental programs were conducted in order to validate the feasibility of the retrofit concept.

The first experimental program was a parametric study to investigate the shear friction strength at the interface between the pile wall and the plug, since the gravity load from the superstructure would have to be transferred to the pile by this mechanism if the pile wall was removed below the cap beam, as suggested in the retrofit method. The second experimental program was a scaled cantilever column bending test of the as-built column-to-cap beam connection, in which the column was subjected to reversed cyclic displacement.

The results of the second experimental program showed that the existing column-piles perform better than previous research programs suggest. However, since the existing field conditions differ among the bridges, further study is needed to qualify which conditions lead to the greatest vulnerability, and hence guide the prioritization of bridges in the retrofit program.

Further analytical work is needed, using more sophisticated modeling techniques and the geometry and soil properties of particular bridges, to determine more precisely the piles' vulnerability under different earthquake intensities. Further experiments are also needed to verify the choice and effectiveness of the retrofit details.

TABLE OF CONTENTS

LIST OF FIGURES

LIST OF TABLES

NOTATION LIST

A_{cv} = area of concrete considered to be engaged in interface shear transfer

A_{hollow} = net area of hollow column

A_{ps} = total area of prestressing

A_{sp} = cross-sectional area of spiral reinforcement

A_{str} = cross-sectional area per prestressing strand

A_{vf} = area of interface shear reinforcement crossing the shear place within the area Acv

c = cohesion factor

c_{c_plug} = clear cover from inner surface of column-pile wall to longitudinal reinforcement of plug

d_b = diameter of reinforcing bars

D_{core} = center to center diameter of spiral reinforcement

DCR = demand-to-capacity ratio

D_i = inner diameter of hollow column-pile

D_o = outer diameter of hollow column-pile

D_{plug} = diameter of plug

d_{sp} = diameter of spiral reinforcement

d_{str} = diameter of prestressing strand

E_i = modulus of elasticity of material, i

f'_c = specified 28-day concrete compressive strength

f_{ci} = initial stress in concrete due to prestressing (with respect to net area of hollow column)

F_{EQ} = earthquake amplification factor

F_f = friction force

F_i = initial tensile force per prestressing strand

f_{pu} = minimum ultimate strength of prestressing strands

f_{sp} = stress in spiral steel

f_y = yield stress of steel reinforcement

K = stiffness of structural system

K_{lat} = equivalent linear system lateral stiffness

K_{el} = equivalent elastic stiffness of uncracked wall of plug specimen

L_{cr} = critical length to inflection for shear failure

L_{col} = above ground length of column-pile

L_d = development length of reinforcement

L_{inf} = length to contraflexure

L_{pile} = below grade length of column-pile

L_{plug} = length of plug

L_{wall} = length of wall of column

m = mass of the superstructure elements

M_{col} = moment demand at top of column

M_{pile} = moment demand of column below grade

$M_{n\_combined}$ = nominal moment capacity of column-pile in plug region

M_{n_hollow} = nominal moment capacity of hollow column-pile section

M_{n_plug} = nominal moment capacity of plug only

n_{cr} = number of cracks

p = radial stress in plug specimen

P_c = permanent net compressive force normal to the shear plane (clamping force)

PGA = peak ground acceleration

$P_{residual}$ = load that caused the plug to displace an additional 0.75 inches vertically beyond the initial displacement at the peak load

Q = applied lateral load

r = radius of element

S_a = spectral acceleration

S_d = spectral displacement

s_{wire} = pitch of spiral reinforcement

s_{max} = maximum spacing of spiral reinforcement

s_{min} = minimum spacing of spiral reinforcement

T = period of structural system

t_j = thickness of jacket

t_{sp} = effective thickness of spiral reinforcement = A_{sp}/s

t_{wall} = thickness of wall

V_{ni} = nominal interface shear resistance

α = scale factor for rotational stiffness at top of the column element

β_{soil} = modulus of soil subgrade reaction

$\varepsilon_{h,z}$ = measured hoop strain at height, z

ε_{hoop_ave} = average hoop strain

ε_{sp} = hoop strain in spiral reinforcement

μ = coefficient of friction

ν = Poisson's ratio

ρ_{filled} = volumetric spiral ratio (with respect to total area of filled column)

ρ_{hollow} = volumetric spiral ratio (with respect to net area of hollow column)

ρ_s = volumetric ratio of spiral or seismic hoop reinforcement

σ_j = hoop stress in external jacket

σ_{sp} = hoop stress in spiral reinforcement

ACKNOWLEDGEMENTS

I would like to thank my advisors, Professor John Stanton and Professor Paolo Calvi for their invaluable guidance and support throughout this research project. I would especially like to acknowledge their patience and the many hours they gave to answering all of my questions as they arose. I would also like to thank Professor Dawn Lehman and Professor Marc Eberhard for serving on my committee.

I would like to recognize and thank all those who helped with construction and testing in the Structures Lab. It truly was a team effort and I could not have done it without the following people: Vince Chaijaroen for his practical guidance and wizardry; Sam Turner, Austin Anderson and Tommy Tang for their height, strength and climbing abilities (and good taste in ice-cream); Kristina Tsvetanova, Ingimar Jóhannsson, Otgonchimeg Davaadorj, and Alec Yeutter for their solidarity and help whenever needed; and all others who helped on test days and cast days. I am forever grateful.

Monetary support and project guidance from the Washington State Department of Transportation is greatly appreciated. Also, thank you to Concrete Technology Corporation and Oldcastle Precastle for the manufacture of the test specimens, and to Combined Construction for the donation of carbon fiber wrap material and labor.

This degree would not have been completed without the support of my fellow graduate students at the University of Washington over the past three years. Thank you for the time spent in and out the walls of More Hall, for the knowledge and insights in our field and for the wonderful friendships we share. Special thanks to Sarah Wichman, Samar Kenkre, Audrey Davaadorj, Givens Lam and Chris Pyke.

Finally, and most importantly, thank you to my family, friends and mentors who got me to, and through, graduate school.

DEDICATION

To my parents, Robert and Susan, and my sister, Krystle for your unwavering support and love from 4000 miles away and to my nephew, Krystian for always making me smile. I could not have done it without you.

Chapter 1. INTRODCUTION

1.1 BACKGROUND

The state of Washington is ranked nationally as the state with the second highest risk of economic loss caused by earthquakes, according to a 2008 Federal Emergency Management Agency study. These losses would be amplified if transportation infrastructure were damaged since the movement of key personnel and emergency responders would be limited. Seattle is especially dependent on its bridges that form hundreds of miles of its critical highway networks, such as Interstate 5 and Interstate 405. Multiple studies exploring the impact of megathrust or Seattle fault earthquakes have found that the city's transportation system would be severely impacted by these types of earthquakes (Seattle Office of Emergency Management).

The Washington State Department of Transportation (WSDOT) undertook a large-scale bridge retrofit program beginning in 1991. The program was developed in order to address the seismic risk associated with the nearly 3,000 state-owned bridges that WSDOT maintains. The majority of these bridges were constructed prior to the implementation of current seismic design standards. In particular, hollow prestressed concrete piles were used as the foundation of 22 bridges in Washington State which were built in the 1960's and 1970's. These piles were typically driven into the ground with the upper end projecting above ground to form the columns of the bridge. Cap beams were then cast-in-place over the columns with a longitudinally reinforced solid plug section that extended a short distance into the top of the hollow section. A typical cross-section of these bridges is illustrated in Figure 1-1.

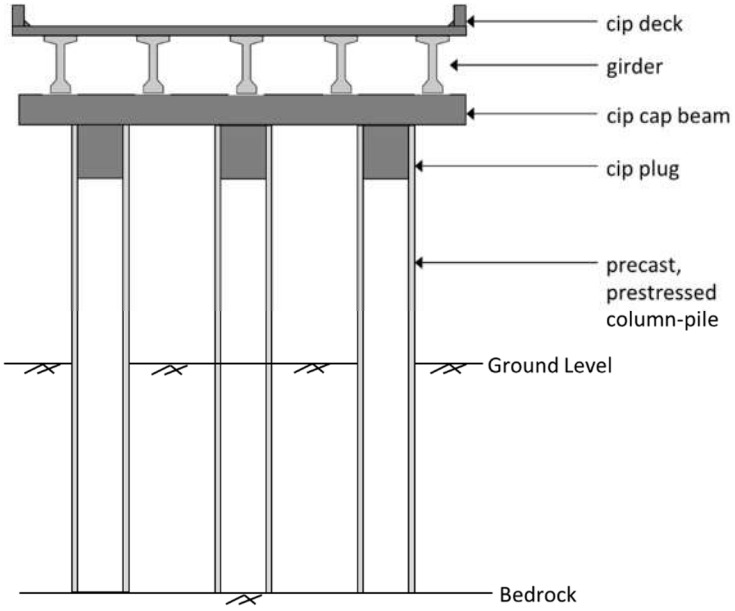

Figure 1-1. Typical Cross-section of bridge founded on Hollow Prestressed Concrete Column-Piles

The hollow core prestressed concrete column-piles are a part of the state's retrofit program after previous research experiments showed that these systems fail suddenly and show no ductile behavior due to minimal energy absorbing hysteretic behavior (Budek, A., Benzoni, G., Priestley, M.J., 1997). With this knowledge, WSDOT intends to retrofit the affected bridges in coming years but to date, there has been no research indicating what the most appropriate fix would be to increase the ductility of the system. This is the overarching objective of this research program.

1.1.1 *Reference Bridges*

The project sponsor Washington State Department of Transportation (WSDOT) asked the research team to focus on a few bridges that form a part of the I-5 highway system that runs north to south through the state, and another that is a part of the I-405 highway that runs parallel to I-5 on the east side of Lake Washington. The I-5 highway is Washington's busiest roadway and sees over 250,000 vehicles daily (Gutman, 2018). In a large seismic event, damage to this highway would hinder travel through the city and cause significant traffic delays and/or high economic losses. The I-405 highway is a part of the state's "lifeline route" to facilitate transportation needs in the event

of a disaster and serves the tech-concentrated regions of Bellevue and Kirkland. The bridges that form the basis of the study are described below and further details are provided in Appendix A.

1.1.1.1 Ravenna Boulevard Overcrossing

The Ravenna Boulevard Overcrossing is located in the Ravenna neighborhood of Seattle near NE 63rd Street and 8th Avenue NE. The bridge is 1,310 feet long and has 19 spans, supporting two lanes of traffic on each of three sections. It was constructed between 1960 and 1962 and is made up of precast, prestressed concrete girders and columns. The columns are hollow with a 48-inch outer diameter and a 5-inch thick wall, and extend into the ground to act as pile shafts. The above ground height of the columns varies from 15 to 27 feet and they are spaced at 18 feet centers for every bent (Greenwood, 2008). At the top of the columns, there is a four-foot long inner plug of reinforced concrete with longitudinal bars that extend into the cap beam. The cap beam is 54 inches by 36 inches in cross-section and is typically supported by four to seven columns.

The columns on Ravenna Bridge were all post-tensioned except for two which were pre-tensioned test piles. According to historical documents obtained from WSDOT, there are a few construction details to note. Firstly, the post-tensioned piles were line-cast with metal ducts in the walls. The spaces between the ends of the piles were blocked and the whole line was post-tensioned. The ducts were grouted, after which the anchors (which were present only on the end piles of the line) were cut, leaving the prestressing forces to be transferred by bond alone. On the other hand, two of the piles were pre-tensioned by a separate company after construction workers reported seeing large longitudinal cracks form while driving the post-tensioned piles. The pre-tensioned piles were manufactured and driven to compare the development of cracks which the contractor noted was minor for the two test piles in the soil conditions present on site. The researchers inspected the columns at the Ravenna Bridge, and saw long cracks along the height of the column, especially to the north end of the bridge where the first piles were driven (See Figure 1-2). These cracks also aligned well with the strands of the column, which were detected using a rebar locator but the precise cause of the cracks is unknown.

Figure 1-2. Longitudinal cracks on columns of Ravenna Bridge

Lastly, while most piles had to be cut off to the correct height, some piles had to be extended. From the contractor's explanation of the pile extensions it is unclear whether they were solid or hollow and, reinforced or not further adding to the uncertainty of the as-built conditions of the columns.

1.1.1.2 East Galer St. to Lakeview Boulevard Viaduct

The East Galer St. to Lakeview Boulevard Viaduct (we will refer to it as the Galer-Lakeview Bridge) is located at the intersection of three major neighborhoods in Seattle – Eastlake, South Lake Union and Capitol Hill. The viaduct consists of three bridges approximately 1691 feet long with 19 spans, supporting multiple lanes of traffic. This bridge began construction shortly after the Ravenna Bridge and was completed one year after it. The Galer-Lakeview Bridge is of a similar design to the Ravenna Bridge but with one major difference. While the Ravenna Bridge was made up of hollow core columns that extended below ground to act as pile shafts, the contractor of the Galer-Lakeview Bridge stated that they chose to follow an alternative method of construction of the piles. From the drawings, this alternative method was to cast a 4'-6" solid, reinforced concrete pile with a bell footing below ground and have the hollow core column sit aboveground only, on top of the solid pile (See Figure 1-3). The effect that this method of construction would have on the response of the column-piles to seismic forces as compared to the Ravenna Bridge was unknown to the researchers.

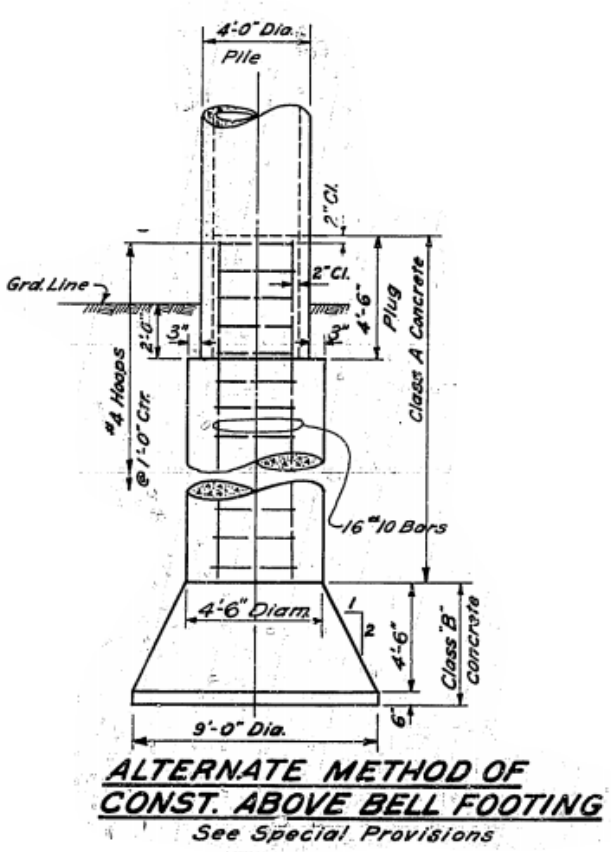

Figure 1-3. Alternative Method of Pile Construction for East Galer St. Bridge

Another potential difference between the two bridges upon initial investigation of existing drawings and reports was that, although the Galer-Lakeview Bridge called for almost identical post-tensioned piles to the Ravenna Bridge, the contractor on the project was the same contractor who supplied the two pre-tensioned test piles to the Ravenna Bridge project. This suggests that the piles on the Galer-Lakeview Bridge were actually pre-tensioned but this had to be confirmed by the researchers.

1.1.1.3 L^E Line Bridge over Slide (South 184th Street to South 144th Street)

The L^E Line Bridge over Slide is located to the south of Seattle in the Tukwila neighborhood. The bridge is 515 feet long and consists of five spans. Construction of the original bridge took place between 1965 and 1966, and the bridge was widened in 1994. The two exterior piers consist of hollow core columns that were filled with cylinder concrete while the interior piers consist of four hollow core prestressed columns each. These columns were 4'-6" in diameter, that is, six inches

wider than the previous two bridges and were pre-tensioned rather than post-tensioned. The bridge is built over a steep gradient in the transverse direction so that the columns on each pier have a height gradient between 15% and 25%. Lastly, the cross beam on the Slide Bridge is quite shallow at three feet deep and five and a half feet wide which is much different than the previous bridges described. These design components suggest a different failure mode from what is expected for the hollow columns but this was not certain.

1.1.1.4 Green River Bridge

The Green River Bridge is located along the I-405 highway system between Tukwila and South Renton. The bridge is the only one of the four investigated that crosses over water and is very short compared to the others, with three spans covering 245 feet all together. The two interior piers consist of ten and eleven hollow core pre-tensioned columns topped by a precast box girder beam. The Green River Bridge was originally constructed in 1964 and widened by 2 piers in 1988 to accommodate HOV lanes. The lengths of the plugs at the tops of these columns are typically longer than seen in the other bridges, usually between five and seven feet. However, the pile design details are similar between this bridge and the Slide Bridge above (See Figure 1-4) with more strands and plug bars than in the earlier bridges. Additionally, these columns consisted of hoop ties evenly spaced through the length of the plug around the longitudinal reinforcement.

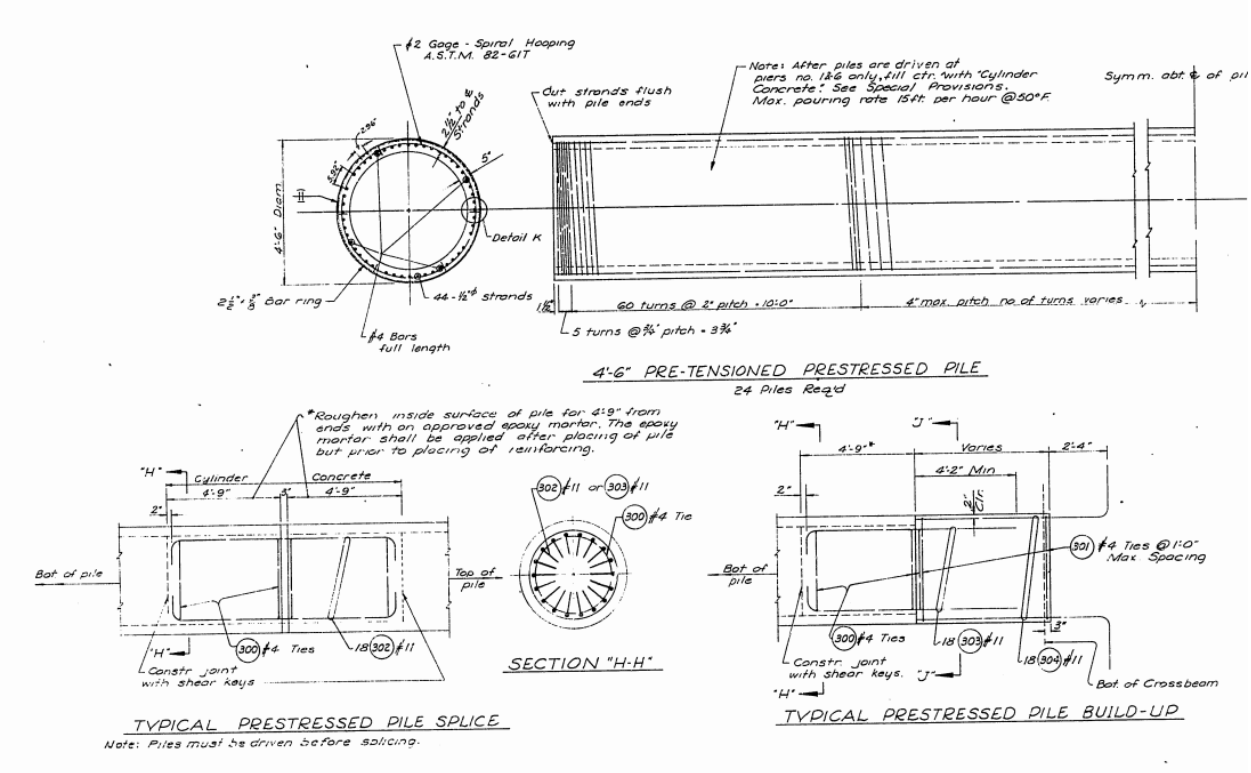

Figure 1-4. Typical Details for Pretensioned Pile

1.2 RESEARCH MOTIVATION

The seismic performance of bridges built with these hollow, precast, prestressed column-piles is uncertain. Hollow sections have been shown to have little flexural ductility because they fail prematurely by internal spalling (implosion) when bent into the inelastic range. Consequently the usual solution of external confinement such as jacketing the column does nothing to prevent this failure mode.

Two locations in the column-pile are particularly susceptible to large moments which can trigger this mode of failure. These are at the cap-beam-column connection and below grade (See Figure 1-5). The presence of the solid concrete plug at the cap beam connection prevents the inward implosion of the hollow section under large moments but depending on the length of the plug and the moment gradient along the length of the column, there exists the risk of a hollow section flexural failure just after the plug ends where one would expect a sudden change in the column's flexural capacity. A potential way to reduce the risk of hollow column failure at this location would

be to cut and remove the outer wall over a short distance directly below the cap beam and to confine the left behind plug with a jacket in order to provide a ductile fuse (See Figure 1-5). However, this requires the plug to carry the axial load from the superstructure and transfer it to the column through the action of interface shear friction, the feasibility of which would need to be investigated. This is especially true given the unknown surface roughness conditions of the field columns.

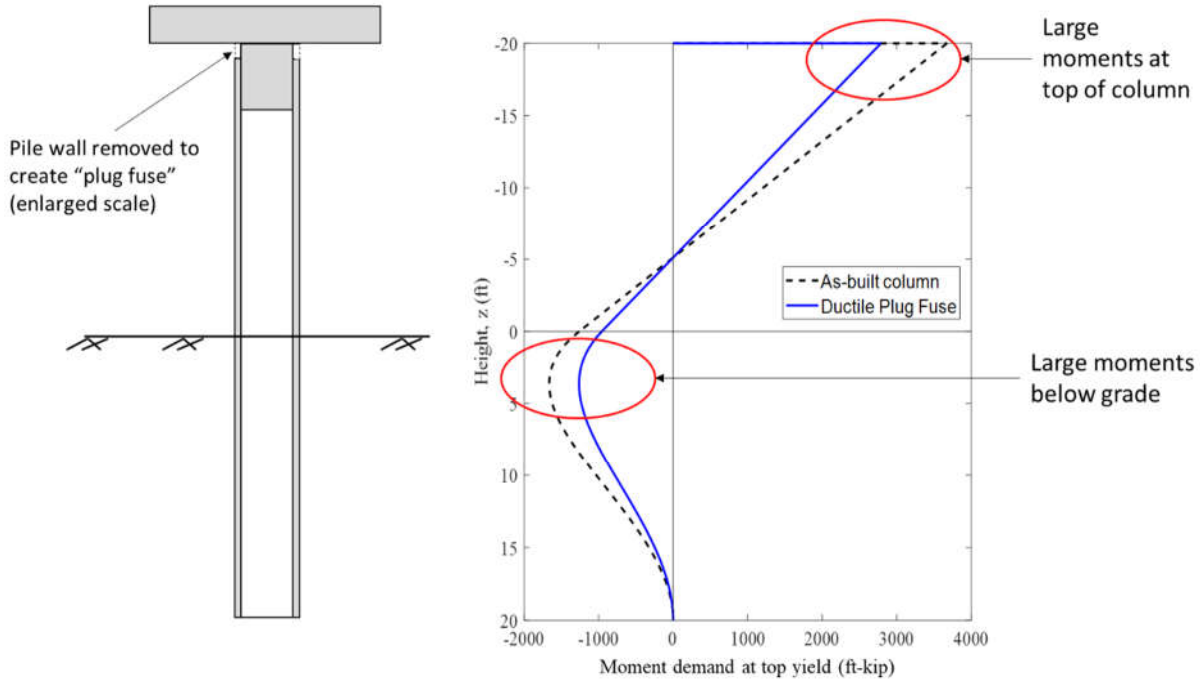

Figure 1-5. Moment demand for as-built vs. "plug fuse" retrofit conditions.

The below-grade location of high moment demand also poses problems, the largest of which is the lack of accessibility for inspection and/or retrofit implementation. One possible solution to the below-grade insufficiency would be to fill the hollow core with structural material but access for filling is constrained by the small space available between strands and this poses a question of constructability that is beyond the scope of this research program.

Given that there are two possible locations of concern in the column, analysis of the flexural and shear response of the columns under seismic loads was needed to identify the critical section and the conditions that lead to its failure. Experimental programming based on these analyses were

then developed. In this way, the results of both the computer analyses and the experimental testing can help to prioritize any necessary retrofit needs and methods.

1.3 RESEARCH OBJECTIVES

This research project was undertaken in order to determine the behavior of both existing and retrofitted hollow, precast, prestressed concrete columns under static and seismic loadings. In order to provide the most comprehensive findings and achieve the overarching objective at the lowest cost to WSDOT and the lowest impact to the travelling public, this research involves both analytical and experimental work as outlined below:

- A parametric study to understand the most important factors that affect the behavior of the as-built column-pile systems under lateral loading. This will be achieved through a numerical model that explores the effects of various parameters such as length of the column, length of the below ground pile and soil stiffness.
- An analysis to evaluate whether the proposed retrofit will perform as a ductile fuse, and to determine how much safety margin exists with respect to the standard AASHTO 1000-year return period response spectrum for Washington State, before the bridge fails.
- An experimental program to preliminarily assess shear friction interface transfer to support the feasibility of the retrofit concept by exploring the effects of plug length, interface surface roughness, pile wall cracking, eccentric loading and external jacketing.
- An experimental test to evaluate the seismic response of the existing columns through reversed cyclic cantilever bending.
- Recommendations for expected performance, further retrofit testing and future research.

1.4 ORGANIZATION OF THESIS

To achieve the objectives outlined in Section 1.3, this thesis involves the following chapters:

- **Chapter 2**: **Literature Review**, provides an overview on the existing research that relates to the seismic performance of hollow-core prestressed concrete column-piles.

- **Chapter 3**: **Analytical Investigation to inform Experimental Programs**, discusses the implementation of a simple numerical model to analyze the performance of the hollow column-pile system under lateral loading.
- **Chapters 4-6**: **Design, Results and Analysis of Experimental Program** to evaluate the shear friction transfer between the plug and pile wall for the proposed retrofit concept.
- **Chapters 7-9**: **Design, Results and Analysis of Experimental Program** to evaluate the seismic behavior of an as-built column specimen.
- **Chapter 10**: **Discussion of Research Program**, summarizes the work done and the effects of the results on the columns in the field.
- **Chapter 11**: **Conclusions and Recommendations**, contains the main findings of the research and provides recommendations for future work before field implementation.
- **Appendices**: Details of the reference bridges are given in Appendix A. Details of the equations used in the numerical model for the analytical investigation in Chapter 3 are provided in Appendix B. Appendix C shows the complete analysis procedure used for evaluating the results of the plug shear friction tests.

Chapter 2. LITERATURE REVIEW

This chapter provides a brief overview of previous research involving the key concepts explored throughout this research program. First, it includes results from previous studies that investigated the flexural behavior of both hollow and solid prestressed concrete piles and/or columns. The shear strength of a hollow concrete section is briefly addressed. A summary of the results of an analytical model done for one of the reference bridges, the Ravenna Boulevard Overcrossing, is presented. Previous studies evaluating the basis of the AASHTO equation for shear friction strength at concrete-to-concrete interfaces are also reviewed. Lastly, the effects of external jacketing to improve the seismic performance of concrete columns are outlined.

2.1 PRESTRESSED CONCRETE PILES AND COLUMNS

The majority of previous research has been done on the flexural behavior of solid prestressed concrete piles, especially in the below-grade hinge region. Since below-grade flexural failure is one of the potential modes of failure of the bridge columns, a review of the literature regarding this behavior is included. Hollow prestressed piles were investigated alongside solid piles in a few papers and these are highlighted.

2.1.1 *Flexural Behavior*

Sheppard (1980) provided a summary of embedded pile performance during earthquakes and proposed interim design provisions for the design of prestressed concrete piling pending further testing and analysis as a result of proposed code changes at the time to restrict their use in the United States. A few of his key conclusions regarding the seismic behavior of piles are that

- Deeper portions of the pile will not fail if the soil does not fail, regardless of any structural damage above it
- Large shears may occur at the pile cap interface due to out-of-phase movement of unrestrained pile caps
- Embedded piles will experience curvatures of various radii when soils are layered

- Critical moment-curvature locations in restrained pile foundations are at the pile to pile cap connection and at the point of fixity in the soil mass. Free-standing, cantilevered pile structures have a potential plastic hinge region at a point of high shear and moment at the pile to pile cap interface.

From the existing knowledge at the time, it was concluded that pile design for ductility could be achieved by adding spiral reinforcement equal to that required for ductile moment resisting frame columns at the potential plastic hinge region at the pile to pile cap interface for unrestrained foundations. Other critical locations for confinement steel were given but the author clearly stated that further criteria needed to be developed for application to hollow-core prestressed concrete piling.

Ikeda et al. (1982) tested circular, hollow prestressed piles under monotonic and cyclic lateral loading by varying four main parameters: transverse reinforcement ratio, non-prestressed longitudinal reinforcement ratio, prestressing steel reinforcement ratio, and prestressing force. The prestressed piles showed brittle failure at displacement ductility ranging from 4.0-8.0, shortly after yield due to fracture of the prestressing tendons. However, the researchers found that the failure mode could be made more ductile by using closely spaced transverse reinforcement to confine the core and prevent shear failure or by including non-prestressed longitudinal reinforcement in order to increase ductility after rupture of the prestressing tendons.

Pizzano (1984) conducted a series of tests on prestressed octagonal concrete piles to examine their behavior under combined axial and lateral cyclic deformations. This study was done to establish the requirements for designing and detailing prestressed concrete piles to resist severe earthquakes in terms of the curvature capacity of the piles in two critical locations – at the grade level pile to pile cap connection and at the location along the pile body of maximum curvature induced by relative motion at the interface of soils with different stiffnesses. The tests found that hollow piles were less ductile than solid piles and that hollow piles may fail in the body by internal implosion of the wall rather than by bursting the spiral outward, especially in the case of heavy spiral reinforcement. However, in general the ductility of solid prestressed concrete piles can be improved by increasing the amount of spiral reinforcement and the ductility achieved at the pile

cap is greater than the ductility achieved below grade in the pile body, for solid piles. Furthermore, no improvement in the curvature capacity was obtained from the addition of non-prestressed reinforcement.

Muguruma, Watanabe, and Nishiyama (1987) tested thirteen high-strength spun concrete prestressed hollow piles in order to find practical ways of improving the flexural ductility of these members. The experimental program varied the net volumetric transverse reinforcement ratio from zero to 3% based on the net concrete area using high-strength wire, and the ductility of the steel using prestressing bars with a maximum elongation from 2% to 5.13%. The unconfined specimens failed by concrete crushing in the compression zone at peak load with no plastic behavior exhibited. For the confined specimens, the prestressing bars showed large post-peak deformation before fracture and obtained much higher tensile strains than the unconfined bars but there was no significant difference in the measured flexural strength. The study concluded that the flexural capacity of high-strength spun concrete prestressed hollow piles can improve significantly by using high-uniform-elongation prestressing steel. However, the transverse reinforcement should be carefully designed since its contribution to increased ductility can also cause the attainment of high tensile strains in the prestressing bars that can lead to undesirable bar fracture.

Budek, Benzoni and Priestley (1997) experimentally investigated the ductility of in-ground hinges in both solid and hollow prestressed concrete piles since analytical studies showed that these subgrade plastic hinges had to form in order to develop the full inelastic potential at the pile to pile cap connection. The experiments looked at six solid and four hollow prestressed piles by varying the transverse reinforcement levels and the provision of external confinement through the load fixture configuration. For the solid piles, a glassfiber jacket over the plastic hinge region was also investigated and for the hollow piles, the addition of non-prestressed longitudinal reinforcement in the pile wall was considered. The piles were loaded cyclically with a test fixture that simulated a soil subgrade moment pattern for an in situ pile.

For the solid piles, the results showed that in the absence of external confinement, a higher transverse reinforcement ratio led to a higher displacement ductility capacity but only up to a volumetric ratio of 2%. There was no influence when external confinement was provided though

showing that a low level of transverse reinforcement (~0.5%) is sufficient for an in-ground hinge. However, the presence of external confinement could provide a slightly higher post-yield flexural strength. On the other hand, the hollow piles' flexural behavior was hardly affected by the variation in transverse reinforcement or external confinement. Failure was due to implosion when the strain at the core's inner surface reached a value of 0.005 (See Figure 2-1) and this occurred at a higher displacement ductility for those piles without any non-prestressed longitudinal reinforcement. The authors suggest that the use of hollow prestressed concrete piles should be limited in seismic applications and that they should be designed to remain elastic since they have little ability to dissipate energy by hysteresis.

Figure 2-1. Internal spalling at core face of hollow specimen (Fig. 6.1.2., Budek, Benzoni and Priestley, 1997)

Budek and Benzoni (2009) conducted a parametric study of the inelastic seismic response of a precast, prestressed concrete pile with a grade level cap beam using a project-specific nonlinear, inelastic finite element program. The purpose of the study was to evaluate whether piles with low amounts of transverse reinforcement could act as ductile structural elements since large code-specified minimum amounts of spiral steel have made prestressed concrete piles an uncompetitive design due to congested construction. The program used nonlinear, inelastic constitutive models

for both the pile and soil structure in order to account for the change in flexural stiffness of the pile as inelastic action took place at each load step.

The analysis found that increasing soil stiffness increased the maximum magnitude of the subgrade moment since the stiffening soil reduced the shear span between the two maximums and required a greater flexural resistance of the pile-shaft below grade. Both elastic and inelastic analyses showed similar ultimate moments at the pile head but the below grade pile shaft maximum moment was much larger for the inelastic conditions. Additionally, the redistribution of moment down the pile shaft after formation of the hinge at the pile cap connection created much higher levels of shear in the pile shaft which was not the case in the purely elastic analysis. The depth of the maximum subgrade moment or hinge was strongly influenced by the whole system stiffness but it approached a limiting value as system stiffness increased, with the largest depth seem in softer soils. Lastly, the ductility capacity increased with both axial load and soil stiffness, while also being significantly affected by the presence of mild steel reinforcement.

2.1.2 *Shear Strength*

Ranzo and Priestley (2001) investigated the shear strength of thin-walled circular hollow columns, made of reinforced concrete with one layer of transverse reinforcement. The specimens were subject to a constant compressive axial load and a cyclic lateral load sequence. The specimens had a column outer diameter to wall thickness ratio between 10 and 11. The experimental results showed good agreement with existing shear models (UCSD model, ATC-32 model and Caltrans Memo 20-4 model) and the study concluded that shear strength of hollow columns was not enhanced by axial load as much as solid columns.

Turmo et al (2009) presented an analytical model for evaluating the contribution of transverse reinforcement in solid and hollow circular concrete members. In particular, a formula for calculating the shear strength in hollow core circular columns with both vertical and spiral reinforcement was deduced theoretically and confirmed experimentally. The deduction of the formula to calculate the contribution of spiral reinforcement to shear strength was based on the development of shear cracking in the form of a helix of constant pitch and this was confirmed through shear strength tests of four hollow circular specimens. The researchers found that the steel

contribution to shear strength is more effective in hollow cross-sections as compared to solid cross sections because the geometry of the reinforcement follows the orientation of the shear stresses. As a result, the well-known formula for calculating the shear strength of transverse reinforcement can be used with an efficiency factor of 1.0 for hollow circular sections.

2.2 PREVIOUS STUDIES FOR WASHINGTON STATE BRIDGES

The Washington State Department of Transportation previously sponsored analytical research that evaluated the piles and pile-cap connections in the Ravenna Boulevard Overcrossing Bridge which is one of the reference bridges of this research program. A summary of the relevant findings of this work is presented below.

Greenwood (2008) performed a series of inelastic nonlinear analyses on an individual hollow pile model to understand the failure mechanisms associated with hollow core prestressed concrete piles and the reinforced concrete pile-to-crossbeam connections used in constructing the I-5 Ravenna Bridge near Seattle, Washington. A simplified model using a beam with plastic hinge behavior in SAP2000 was compared alongside a detailed three-dimensional finite element model using ABAQUS/Standard. The models showed good agreement with past experiments that failure occurs once concrete in the compression zone spalls, allowing the exposed reinforcing steel and prestressing tendons to buckle. Additionally, the transverse reinforcement ratio had little effect on load capacity or displacement ductility. The response of the in situ pile is governed by the tensile capacity of the concrete so that tensile cracks forming led to a nearly linear response until compressive failure began at the opposite pile surface. The model also found that confinement of the exterior surface may improve ductility slightly, but eventually the compressive zone would extend and the wall would spall internally and fail. The study suggested that a viable retrofit method may be to pump non-shrink grout into the hollow void while jacketing the exterior with steel or fiber reinforced materials.

El Gawady et al (2009) assessed the inelastic seismic behavior of the I-5 Ravenna Bridge through nonlinear static and dynamic analyses. A three-dimensional finite element analysis of the whole bridge including modelling of the bridge bearings, expansion joints, and nonlinear soil-structure interaction of three different soil types was performed in SAP2000 (2007) using three response

spectra to represent ground motions with different return periods. The study found that dense sand led to piles that are more vulnerable to failure so that even a low-level earthquake induced overall bridge failure. On the other hand, piles in stiff clay performed the best and could withstand higher level earthquakes. In all cases, the ductility of the piles was very low and elastic pile behavior was followed by an immediate and brittle failure that always occurred first for column-piles toward the center of the bridge. However, when a pile-crossbeam connection model was included, the performance of the bridge improved significantly but the nonlinear dynamic analyses found that the bridge is safe only for a 475-year return period earthquake while larger earthquakes would likely cause failure. Higher mode effects made a significant difference in the response of the whole bridge.

An article in ASPIRE Magazine (**Lengyel, 2014**) briefly described a retrofit scheme that was undertaken for hollow precast, prestressed concrete columns of the Murray Morgan Bridge in Tacoma, WA. The bridge columns showed signs of deterioration in terms of concrete cracking and spalling in high stress area and corrosion of prestressing strands. The repair consisted of pouring a two-component, rigid polyurethane structural foam system to support the interior faces of the hollow concrete columns while the top of the exterior faces, directly under the cap beam were encapsulated in steel jackets. The structural foam is also intended to increase the confinement capacity of the columns in the plastic hinge zones. However, no analytical or experimental evidence to support this retrofit were presented.

2.3 SHEAR FRICTION

The proposed retrofit concept for the hollow prestressed concrete piles (See Chapter 1) involves the removal of the pile wall directly below the cap beam. If this is done, the axial load acting on the columns will no longer be supported via direct bearing on the column-pile wall but will have to transfer through the shear friction strength at the interface between the wall and the inner plug. If the shear friction strength is not sufficient there is the potential for plug slip to occur if the retrofit is implemented.

Numerous studies exist in the literature that examine the shear friction strength at concrete-to-concrete interfaces. **Davaadorj (2018)** conducted a thorough literature and database review of the

existing material in order to develop a unifying strength prediction model for shear friction where "sliding shear" failure is critical. **Habouh (2015)** also provides a concise review of the literature regarding shear transfer strength between concrete placed against hardened concrete in both horizontal and vertical configurations.

The 2012 AASHTO LRFD Bridge Design Specifications examines the interface shear transfer across a given plane through a modified shear friction model in Equation 5.8.4.1-3 (shown below).

$$V_{ni} = cA_{cv} + \mu(A_v f_y + P_c) \qquad \text{(AASHTO Eqn. 5.8.4.1-3)}$$

This modified model accounts for a contribution from cohesion and/or aggregate interlock depending on the nature of the interface under consideration. The interface shear strength calculated from the code provisions are based on experimental data available in the literature from Loov and Patnaik (1994); Patnaik (1999); Mattock (2001) and Slapkus and Kahn (2004). It is based on experimental data for normal-weight, monolithic concrete strengths ranging from 2.5 ksi to 18.0 ksi.

2.3.1 *Influence of Epoxy Mortar*

In the case of the reference bridge columns, an epoxy mortar was applied on the inner surface of the column-pile wall before casting the inner concrete plug. This epoxy mortar is believed to have an effect on the concrete-to-concrete bond strength that exists at the interface. **Júlio et al. (2005)** investigated the influence of an epoxy-based bonding agent applied to a roughened substrate surface in terms of tension and shear. Specifically, the effect on bond strength in shear considering different methods of surface roughening was evaluated through slant shear tests. A total of 40 slant shear specimens were prepared and the only parameter that was varied was the method used to roughen the substrate surface. Ten specimens were used for each roughening technique which included (i.) surface cast against steel formwork; (ii.) surface prepared with a steel brush; (iii.) surface partially chipped; and (iv.) surface treated with sandblasting. The substrate surface preparation was followed by the application of a commercial epoxy resin bonding agent immediately before casting the second layer of concrete for half of the specimens.

For all tests, the observed rupture mode was an adhesive failure at the interface. Furthermore, the bond strength in shear was found to be approximately constant with the results indicating that there is no influence of surface roughness on this value when an epoxy resin is used as a bonding agent. Lastly, comparing the tests with and without epoxy resin showed that the application of the resin did not improve bond strength if the surface preparation method already adequately increases its roughness.

2.4 External Jacketing of Concrete Columns

Concrete columns are known to be deficient in flexural ductility, shear strength, and flexural strength when affected by lap splices in critical regions or by premature termination of longitudinal reinforcement (**Priestley et al, 1996**). Jacketing of concrete columns has been shown in many studies to be an effective retrofit to improve the seismic performance of concrete columns. The jackets can be made of different materials including steel, reinforced concrete and composite materials such as carbon fiber or fiberglass. **Wu et al. (2005)** published a state-of-the-art review of concrete column retrofitting using steel and fiber reinforced polymer jackets. This report summarized the following advantages of the increased confinement provided by external jacketing:

- The external confinement prevents concrete spalling and the buckling of longitudinal reinforcement which enhances the concrete strength and ultimate strain capacity, leading to enhanced flexural ductility.
- The shear strength is improved by the additional hoop confinement that adds to shear reinforcement of the member.
- The jacket confinement provides greater clamping pressure on the longitudinal reinforcing bars that increases their bond and prevents slipping.

Steel jacketing has long been the most common retrofit technique for concrete columns in seismic regions and has been shown to be effective for all three deficiencies of flexural ductility, shear strength and flexural strength. **Priestley et al. (1996)** provided a brief summary of the method and reason for steel jacketing. For circular columns, two half shells of steel plate are site-welded at the

vertical seams to form a continuous tube with a diameter that is typically 1.0 to 2.0 inches larger than the original concrete column and the gap is typically filled with cement grout. The steel jacket adds to passive confinement of the concrete column and is equivalent to continuous hoop reinforcement. The confining hoop stress from the steel jacket is induced in the concrete when the concrete attempts to expand laterally in the compression zone under high axial compression strains, or in the tension zone due to dilation of lap splices near splice failure. The level of confinement depends on the hoop strength and stiffness of the steel jacket.

Riahi and Faridafshin (2008) reported on the use of fiber-reinforced polymer (FRP) composites in the seismic retrofit of concrete bridges. The authors state that FRP composites alter the stiffness of the bridge component only in the direction of the fiber orientation, which gives it an advantage over the conventional use of isotropic steel sheets. Altogether, high strength and stiffness in one direction, low density, high corrosion resistance, minimal disruption to traffic and low maintenance cost make fiber wrapping an ideal retrofit method. However, the fabrication procedure along with the curing conditions and installation process have a big influence on the functionality of the retrofit and these should be monitored carefully. Additionally, these jackets depend on the formation of large strains in the layers during seismic events, therefore FRP jacketing will only be effective for severe earthquake events when structures undergo substantial nonlinear behavior. Lastly, when FRP wraps are used for the retrofit of columns and piers, two things need to be checked to confirm their suitability:

- FRP wraps on the members may induce additional shear stresses in the joints so the shear capacity of these regions should be checked for adequacy after retrofitting.
- The stiffness of the FRP wrap and the concrete substrate should be compatible so that the hinge location does not shift and cause premature shear failure in the unwrapped potions of piers.

Chapter 3. ANALYTICAL INVESTIGATION TO INFORM EXPERIMENTAL PROGRAM

3.1 INTRODUCTION

The first step in the research program was to analytically investigate the structural response of the hollow core precast prestressed concrete column-pile system under lateral loading. Particularly, the objective was to understand the structural mechanics and determine the geometries and soil conditions that would result in the worst system performance. First, this was done to assess the possibility of damage and/or failure of existing bridges based on various conditions. After obtaining those results, the analysis was used to evaluate whether a proposed retrofit of cutting back the pile wall below the cap beam to create a ductile fuse would improve the column performance, and to find out the safety margin that exists.

An Excel program was developed to analyze the system by modelling the column as a simple 2-node beam-column element and then discretizing the element based on conventional shape functions. The connection to the cap beam at the top of the column was modelled as an elasto-plastic rotational spring to allow for post-yield ductility. The pile was modelled as a beam on an elastic foundation following the Winkler beam formulation and the soil was defined as a continuous elastic spring with a constant stiffness value.

Parametric studies were conducted to assess the moment response of the pile and column based on the following variables:

- the soil stiffness, β_{soil} defined by the modulus of subgrade reaction,
- the length of the column L_{col},
- the length of the pile L_{pile},
- the added stiffness of a bridge deck, including the effects of different span lengths and deck widths and,
- the axial load acting per column.

3.2 GOALS

The initial goal of the analytical investigation was to understand the effects of various parameters on the behavior of the hollow, prestressed column-piles through a simple numerical model and to assess what further information was needed from experimental testing. Specifically, the model investigated how much the standard 1000-year, 5% damped, AASHTO design spectrum for site class B conditions in Seattle, WA must be scaled, up or down, in order to achieve failure of the as-built column.

The analysis of the as-built condition considered failure to occur when the first of the moment capacity of the filled section at the top of the column (that is, in the region of the plug) or the moment capacity of the hollow section, above or below ground, was reached. Both of these failure modes were assumed to be non-ductile based on the literature.

- The typical volumetric spiral ratio, ρ_s for the field columns in the region of the plug was found to be 0.08 – 0.22% with respect to the confined concrete area (See Appendix A). The minimum transverse reinforcement area to provide effective confinement to a reinforced concrete column so that it exhibits ductility under seismic loading is given by Equation 1 according to Article 5.10.11.4.1d of the 2012 AASHTO LRFD Bridge Design Specifications.

$$\rho_s \geq 0.12 \frac{f'_c}{f_y} \qquad (1)$$

  f'_c = specified compressive strength of concrete at 28 days (ksi)
  f_y = yield strength of reinforcing bars (ksi)

  This corresponds to $\rho_s \geq 1.2\%$ for Grade 60 rebar and a concrete strength of 6000 psi. Therefore, the amount of spiral steel provided in the existing bridge columns would not guarantee ductile behavior.

- A previous study done by Priestley et al. (1997) suggests that failure of an in-ground hinge on a hollow-core prestressed concrete pile would be brittle due to implosion of the pile wall. Other studies have reported similar behavior for these types of members.

3.3 STRUCTURAL MODEL

The structural model used for the parametric study is shown in Figure 3-1. The model consists of a three-span bridge, with two abutments and two interior bents supported on hollow piles. Reference dimensions are believed to be representative of typical field conditions. The two pile bents provide the interior supports. The abutments and pile bents provide essentially rigid vertical support to the deck. Horizontally, the deck is treated as pinned at the abutments and continuous over the bents, which provide some spring support, based on frame action.

The bridge deck is modelled so as to always contribute to the seismic mass acting on the column. However, the deck stiffness may or may not be continuous at the joints of the existing bridges so its contribution to the stiffness of the system was modelled as a variable. If the deck is continuous so that its stiffness is considered, then it is analyzed as a beam with its depth in the transverse direction of the bridge since the lateral load is applied transverse to the bridge span.

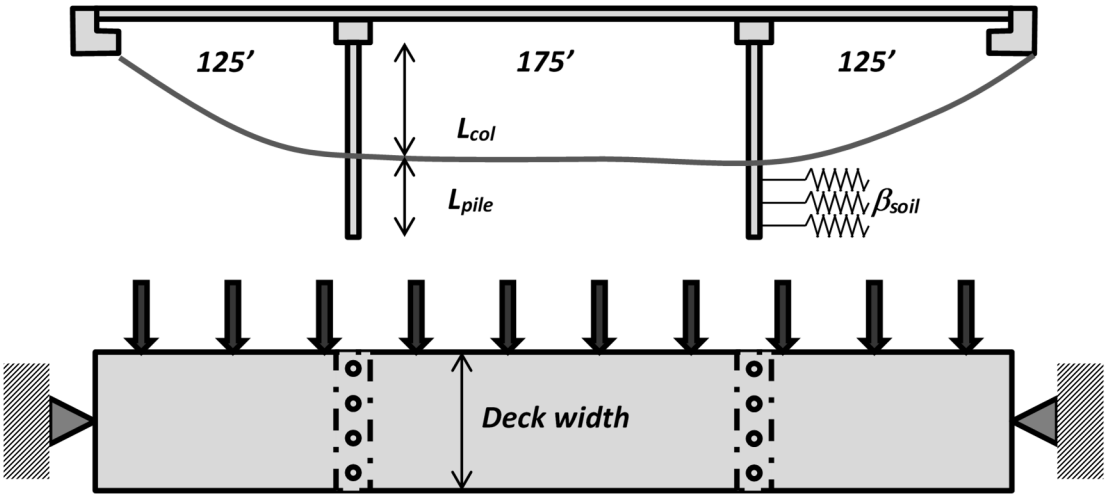

Figure 3-1. Structural Model used for Parametric Studies

In the numerical model, all elements except for the rotational spring at the top of the column are linear elastic. The system is reduced to a Single Degree-of-Freedom (SDOF) system by static condensation of all of the degrees of freedom except the horizontal displacement of the cap beam, where the load is applied. This allows a response spectrum single-mode analysis to be used for the earthquake loading to obtain the results of the parametric studies. The reference response spectrum is the AASHTO LRFD 1000-yr return period design spectrum for Seattle, WA for site class B, with 5% damping (See Figure 3-2). The AASHTO spectrum does not allow for the constant ground displacement region, at periods greater than T_{long}, that the ASCE spectra do.

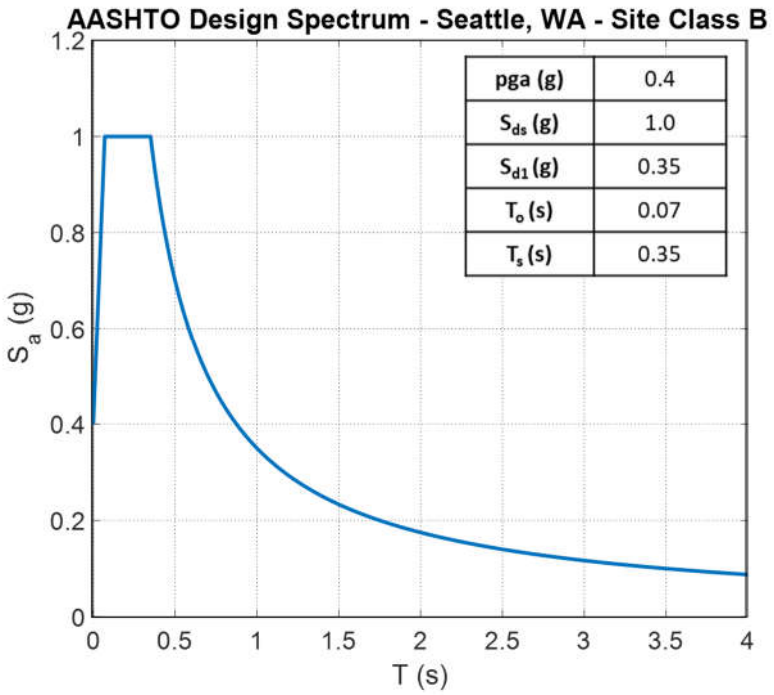

Figure 3-2. Reference Design Spectrum for Parametric Study

3.3.1 *Analysis Model of Pile and Column*

The analysis model consisted of a 2-node beam column element to represent the above-ground column of length L_{col}, and another to represent the below-ground column of length, $L_{pile.}$ Figure 4 shows the model considered for the linear elastic analysis of the column-pile. The mass of the system acted as an axial point load at the top of the column and was comprised of the estimated mass of the superstructure elements, including the deck, girders and cap beam. Based on a user-specified number of columns per cap beam bent, only the mass acting per column was considered.

Also, a rotational spring of stiffness $\alpha EI/L_{col}$ was included at the top node of the column in the element formulation in order to model the cap connection stiffness as either fixed (before yield) or free (after yield). The in-ground pile section was modelled as a beam on an elastic foundation following Winkler's formulation. The soil stiffness was calculated using the modulus of subgrade reaction β_{soil} and this was assumed constant along the length of the pile as a continuous spring support to the pile (See Figure 3-3). A lateral load, Q was applied at the cap beam level, transverse to the traffic direction, to displace the system and obtain a system stiffness as well as to act as an equivalent lateral force compared to the design earthquake load.

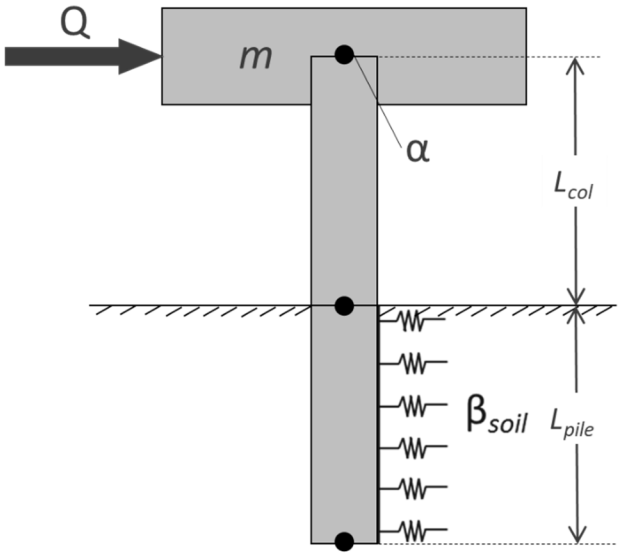

Figure 3-3. Column Model illustration with significant parameters

3.3.2 *Assumptions*

The assumptions governing the numerical model are summarized in the following subsections.

3.3.2.1 Finite Beam on Elastic Foundation

The pile was modelled as a finite beam on an elastic foundation according to Hetenyi's (1946) derivation, shown in Appendix B.

3.3.2.2 Dimensions and Material properties

The dimensions and material properties that were based on typical field conditions and were kept constant throughout the parametric studies are listed below.

- The column-pile cross-section was kept constant at D_o = 54 inches and t_{wall} = 5 inches.
- The plug length was 4.5 feet into the column, from the bottom of the cap beam.
- Elastic column-pile behavior with a concrete modulus of elasticity of E_c = 5000 ksi.
- An elasto-plastic connection between the column and the (rigid) cap beam, controlled by a variable α.
- The weight of the superstructure applied to the column-pile was estimated to be 561 kip per column, with an 8-inch thick deck, girder lines at 8 ft. centers, a cap beam cross-section area of 20 ft^2, and columns at approximately 15 ft. centers.

These bridge properties were based on the drawings of one of the reference bridges for the project, L^E Line Slide Bridge (See Appendix A). The moment capacity of the column-pile was evaluated for two different conditions, defined in Figure 3-4, using a nonlinear moment-curvature program for prestressed members developed by Professor John Stanton (University of Washington). For constitutive laws, it uses the Popovicz (1973) curve for concrete, the Raynor (2002) law for rebar steel and the Menegotto-Pinto (1973) curve for strand. The concrete law did not include any effects of confinement.

The two conditions are described below and their capacities were calculated using f'_c = 9.1 ksi and 44 -0.5" diameter, Grade 250 ksi strands, stressed at jacking to 200 ksi for the hollow column-pile and f'_c = 5.2 ksi with 18-#11 rebar for the inner plug.

- *Hollow pile only*: The geometry was that of the hollow pile, the concrete strength was that of the pile, and the reinforcement consisted of the strand, assumed to be fully bonded.
- *Combined pile and plug*: The geometry was taken as a circular section with diameter equal to that of the pile, because the pile concrete could resist compression by direct bearing. The concrete strength was taken as that of the pile, because the program has provision for

only one strength. The great majority of the compression force occurs in the pile wall, and not in the plug. The reinforcement consisted of the plug bars alone; the strand was not included because, at the column-cap beam interface, the strands terminate and carry no stress there.

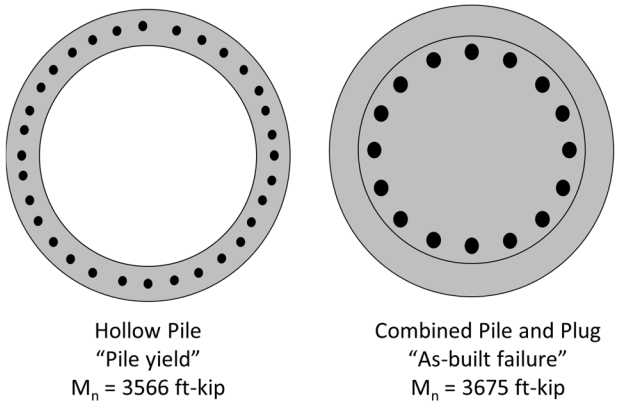

Figure 3-4. Moment Capacities used in Analysis Model for As-built Conditions
** Cross-section geometry used for calculation shown for different sections along the column-pile*

3.3.2.3 Parameter Range

The parameters considered in the model are listed in Table 3-1 along with the reference values for each parameter and the ranges considered.

Table 3-1. Parameter Range considered in Analytical Investigation

Parameter	**Variable (Units)**	**Reference Value**	**Range of Values**
Soil stiffness	β_{soil} (kcf)	1000	20 – 2000
Column Length (above-ground)	L_{col} (ft)	20	10 – 60
Pile Length (below-ground)	L_{pile} (ft)	20	10 – 60
Deck Stiffness		No	Yes/No
*** Deck Length**	L_{deck} (ft)	Span 1: 125 Span 2: 175 Span 3: 125	Scale Factor: 0.6 – 1.4
*** Deck Width**	B_{deck} (ft)	60	Scale Factor: 0.6 – 1.4
Axial Load	P_{axial} (kip)	561	Scale Factor: 0.6 – 1.4

**Only considered when deck stiffness added (Deck Stiffness = Yes)*

The range of soil stiffness was chosen to represent a wide variety of soil types since the sites where these bridges were built are expected to have a range of different soil conditions. Table 3-2 shows a table of values taken from Bowles (1997) for the modulus of subgrade reaction of various soils:

Table 3-2. Representative range of lateral modulus of subgrade reaction (adapted from Bowles, 1997)

Soil*	**k_s, kcf**	**k_s, MN/m^3**
Dense sandy gravel	1400-2500	220-400
Medium dense coarse sand	1000-2000	157-300
Medium sand	700-1800	110-280
Fine or silty, fine sand	500-1200	80-200
Stiff clay (wet)	350-1400	60-220
Stiff clay (saturated)	175-700	30-100
Medium clay (wet)	250-900	39-140
Medium clay (saturated)	75-500	10-80
Soft clay	10-250	2-40
* Either wet or dry unless otherwise indicated		

The reference soil stiffness β_{soil} = 1000 kcf was chosen to correspond with the reference site class B which represents "rock" type soils according to USGS, and these are typically soils with a higher stiffness.

When the deck length and deck width were varied according to the scale factors in Table 3-1, the number of columns per bent was also adjusted so that the axial load acting per column remained constant and equal to the reference value for that parameter. The axial load per column was scaled artificially by changing the moment capacities defined in Figure 3-4 to those that would be found for the new axial load.

3.3.3 *Procedure*

Given the above assumptions, the steps in the calculation procedure are outlined below for elastic behavior of the as-built column.

- The rotational spring at the top of the column was given a stiffness, α = 1000 (an arbitrarily high value) in order to model a rotationally fixed connection at the cap beam.

- An arbitrary point load, Q was applied at the top of the column.
- This load was used to find the displacement of the cap beam, from which the single-degree-of-freedom equivalent linear system stiffness, K_{lat}, was calculated.
- Using this equivalent stiffness and the mass, m, of the system, the fundamental period T_n of the system was found

$$T_n = 2\pi\sqrt{\frac{m}{K_{lat}}} \qquad (1)$$

- Lateral load, Q was applied at the cap beam-column DOF, and increased until the load needed to just cause a particular damage state (e.g. yielding at the top of the column) was calculated.
- The Capacity Response Spectrum method was used with the SDOF system stiffness and period to calculate the ground motion needed to achieve this failure based on the 5% damped spectrum. This was done by plotting the intersection of the linearized force-displacement response of the column with the Acceleration-Displacement response spectrum curve of the reference ground motion (See Figure 3-2). An earthquake amplification factor F_{EQ} was found to describe how much the response spectrum must be scaled so that the motion just causes failure. The 5% damped spectrum was used because the true damping, based on hysteretic behavior, was unknown.
    - If, for example, the peak ground acceleration (pga) corresponding to as-built failure is reported as 0.20g, this means that the reference spectrum (for which AASHTO gives a pga of 0.40g) has to be scaled down by an earthquake amplification factor, F_{EQ} = 0.5 to just cause the corresponding failure moment. In that case, the implication is that the existing column would fail in an earthquake with a return period of less than 1000 years.

$$F_{EQ} = \frac{PGA\ of\ response\ spectrum\ at\ failure}{PGA\ of\ reference\ design\ spectrum} \qquad (2)$$

- The moments and shears at other locations in the column-pile were then evaluated for each set of parameter values.

3.3.4 *Model Limitations*

The model does a good job of presenting overall trends in the flexural behavior of the column when considered as a linear elastic system with an elasto-plastic connection at the cap beam. However, the following limitations should be noted.

- The soil is modelled with a constant elastic stiffness along the length of the pile. A more robust analysis should consider the effects of nonlinearity and layering through the use of p-y curves for different types of soil.
- The analysis only evaluated the effects of the parameters for site class B conditions but it is believed that the same trends would hold in other site classes although the absolute values will change.
- The Capacity Spectrum Method was only used with the 5% damped response spectrum. This remains valid for conditions up to yielding of the linear elastic system. However, if inelastic conditions are considered prior to the ultimate failure of the column-pile, the equivalent hysteretic damping should be used to find the appropriate earthquake amplification factor that will cause failure. This was not done because the hysteretic behavior (which would determine the system damping) of hollow prestressed concrete columns is unknown. The use of the 5% damped response spectrum in the absence of this information gives a conservative estimate for F_{EQ}.
- The parametric study did not consider limitations on the strength or allowable drift and stresses in the deck when investigating the effect of deck stiffness.
- The model did not explicitly account for P-delta effects on the column.

3.4 RESULTS FOR AS-BUILT CONDITIONS

This section presents the results of the parametric studies for the as-built condition. The system was analyzed first with the assumption that the column fails when the "combined plug and pile" moment strength is reached at the top of the column so the lateral load, Q needed to cause this was determined. A check of the moment distribution at this stage of loading showed that in all cases the maximum moment was indeed located at the top of the column, corresponding to the combined

strength and that the moment along the length of the column, below the plug, never reached the moment strength of the hollow pile. These two conclusions are illustrated in Figure 3-5 which shows the moment demand along the length of the column for the reference conditions, and Figure 3-6 which shows the ratio of the maximum moment demand above ground at the cap beam (M_{col}) to the maximum moment demand below grade (M_{pile}) with respect to the parameter, β_{soil}.

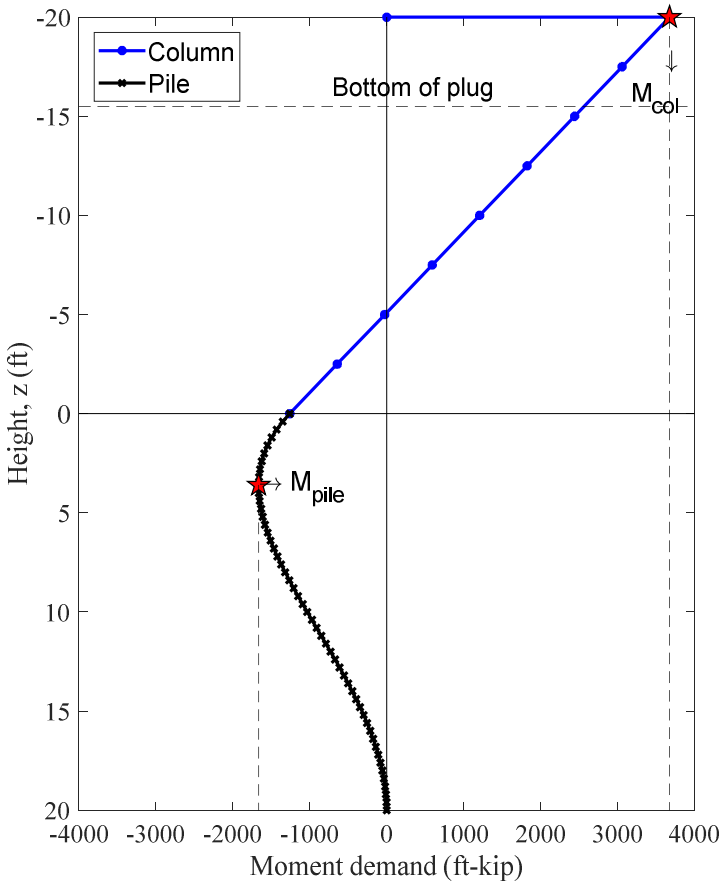

Figure 3-5. Moment Demand for As-built Column-Pile using Reference Conditions

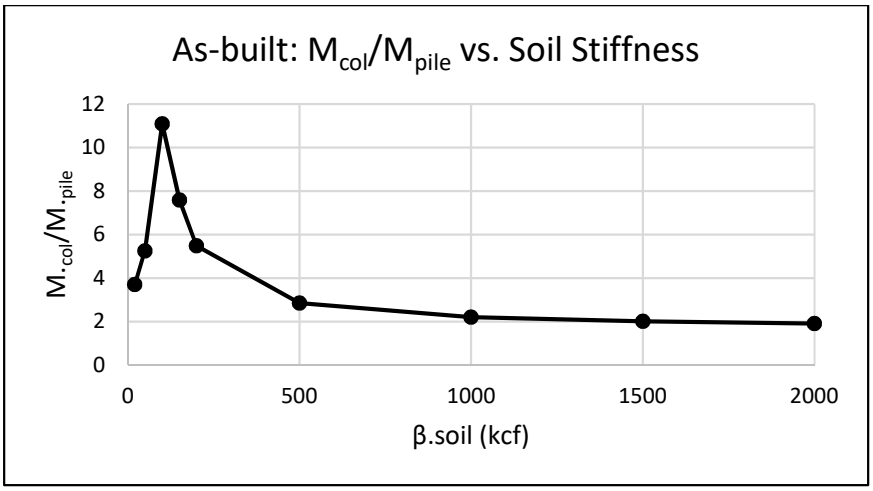

Figure 3-6. Relationship between column moment and pile moment against soil stiffness, for an as-built failure

As can be seen in Figure 3-5 for the reference parameter values, the maximum moment of the hollow section below-grade when the top moment is at its capacity is 1664 ft-kip. This demand is less than half of the predicted moment strength of the hollow pile so failure will invariably occur when the column yields at the top.

In Figure 3-6, the M_{col}/M_{pile} ratio is always greater than 2 which indicates that under elastic conditions, the column moment is always greater than the pile moment. Similar trends were observed when the length of column and length of pile were varied. However, changing the deck properties and the column axial load did not affect this outcome compared to the reference conditions.

Figure 3-7 and Figure 3-8 show the demand to capacity ratio (DCR) of the hollow section just below the plug when the maximum moment in the column is reached. For all parameters studied, the DCR is always below 1.0 which indicates that failure will, theoretically, not occur in the hollow section of the column above ground. The capacity was based on a flexural strength computed theoretically using moment curvature analysis. In practice, the capacity might differ somewhat from this value, in which case some margin of safety, manifested as a DCR much less than 1.0, is desirable. Causes of such differences include the fact that the region experiences shear as well as moment, the moment at which internal spalling occurs is not known precisely, and field conditions

may introduce further unknowns. The range of predicted DCR values lies between 0.70 and 0.90, the higher end of which leaves little room for uncertainties. Long columns pose problems because they are long compared with the length of the plug. Then the reduction in moment between the top of the column and the end of the plug is quite small. Soft soil leads to higher moment demands at the plug end because the moment below grade is small, thereby decreasing the moment gradient and increasing the moment at the end of the plug.

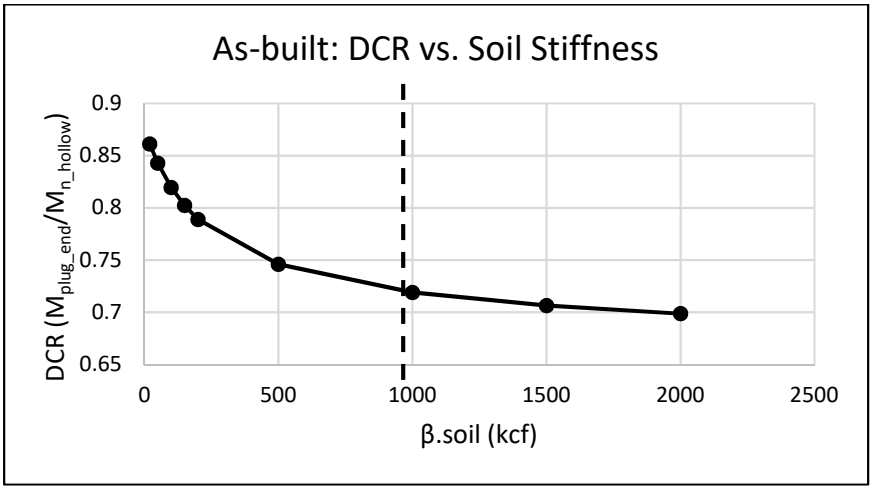

Figure 3-7. Demand to Capacity ratio vs soil stiffness, for hollow section below the plug at maximum moment for as-built conditions

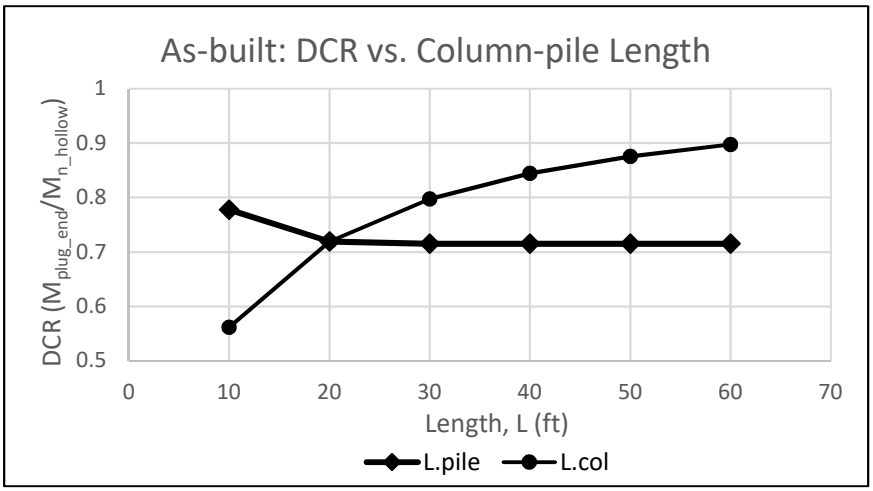

Figure 3-8. Demand to Capacity ratio vs. length of column and length of pile, for hollow section below the plug at maximum moment for as-built conditions

Figure 3-9 shows the scaled response spectrum that would be expected to cause failure of the as-built column reference condition. The scale factor indicates that a smaller earthquake, or an earthquake with a smaller return period than the 1000-year design earthquake could cause failure of the existing columns. The failure considered here is at the top of the column, where the plug is present, and not in the hollow region. The column is assumed to be non-ductile, based on the low proportion of spiral steel, in which case it is assumed to fail when it reaches first yield.

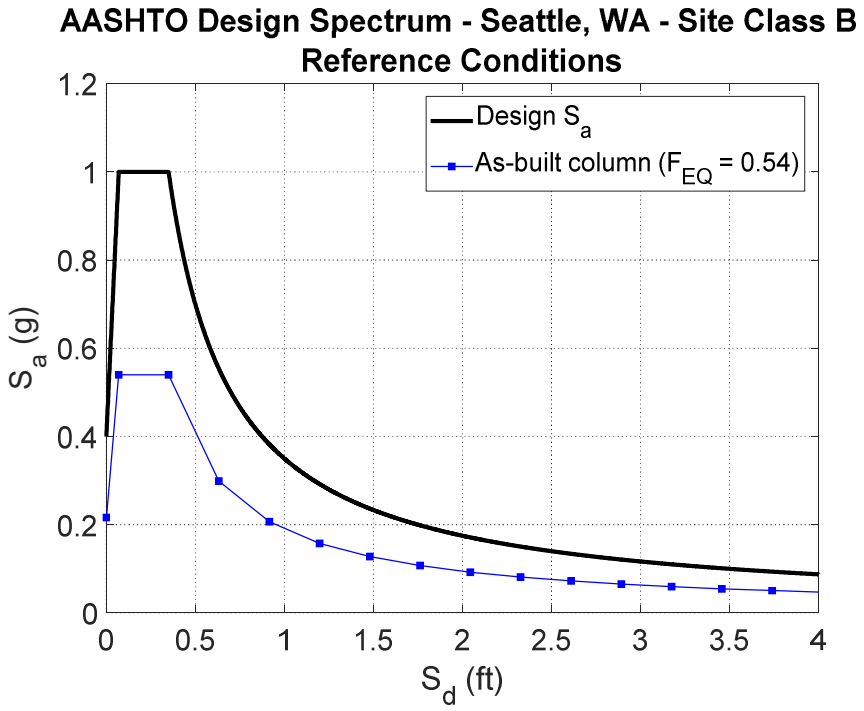

Figure 3-9. Scaled AASHTO Response Spectrum for As-built conditions

From the results of the linear elastic model, a few conclusions can be made about the existing columns. The first and most important conclusion is that, under elastic conditions, the column moment is always greater than the pile moment. This can be understood by viewing the column as being supported at its ends by rotational springs. The stiffness of the bottom spring (the soil) is finite, while that of the top one is infinite. The higher moment occurs at the stiffer end. This indicates that the column will reach failure due to yielding in the cap beam-plug-column connection before the in-ground pile sees any damage.

Combining this with the result shown in Figure 3-9 and the DCR ratios in Figure 3-7 and Figure 3-8, it can be concluded that the first efforts of the research program should be focused on developing a retrofit at the cap beam-column connection that improves the ductility of these hollow bridge columns and lowers the chances of hollow section failure below the plug where the DCR is high. Yielding was assumed to result in failure of the system due to a lack of ductility but the exact nature of the failure that will take place in the plug region when the maximum moment is reached is uncertain.

3.5 RETROFIT CONCEPT: "PLUG FUSE"

The results of the as-built condition led to the development of the retrofit concept that is illustrated in Figure 3-10 below.

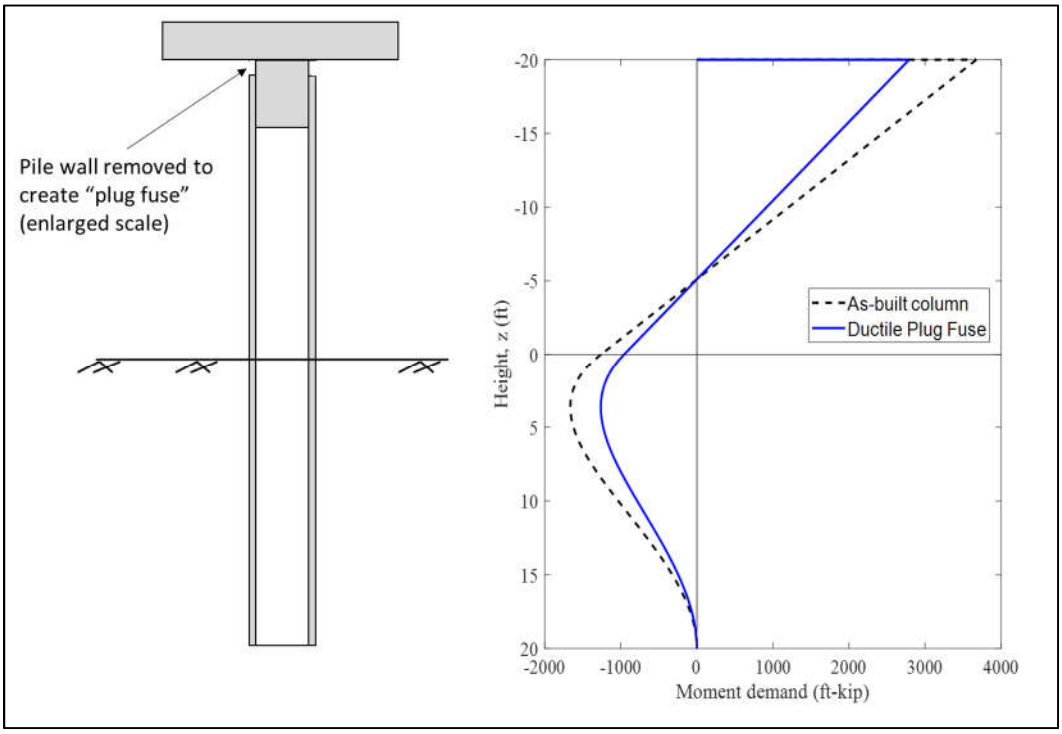

Figure 3-10. Illustration of "plug fuse" retrofit concept

As shown in Figure 3-10, the retrofit is centered on the idea of removing the pile wall over a short distance right below the cap beam (the length of cutback is exaggerated in the figure) so that only the inner plug is able to resist the moment demand at that location. Under elastic conditions if the

rotational stiffness at the top of the column is very high, the maximum moment always occurs at the top of the column when it is subjected to lateral load, as shown in the previous section. If the plug alone is to resist the moment, then the demand is limited by its smaller strength compared to the full cross-section and so the demand in the hollow section also diminishes (i.e. the DCR decreases). This reduces the risk of reaching the flexural strength of the hollow pile below the plug.

In addition to the cutback, the exposed plug and the filled region of the column should be jacketed to provide ductility through external confinement. Therefore, when the plug bars yield at the maximum moment, the plug can act as a ductile "fuse" under increasing lateral loads, until the column fails elsewhere in the hollow section but under a higher lateral load, corresponding to a larger earthquake.

The parametric study via numerical analysis done above for the as-built conditions was repeated to account for the retrofitted condition. The model and procedure were modified as described in the following section.

3.5.1 *Modified Model*

The modified model includes inelastic action, after the plug yields. The moment capacities considered for the retrofitted conditions are as described below and shown in Figure 3-11.

- *Plug only:* The concrete geometry was for the plug alone, and the reinforcement was only the plug bars. The concrete strength used was that of the plug. It was assumed that this capacity could be maintained through the required rotations.
- *Hollow pile only*: Same as before (See Section 3.3.2.2). Pile failure, and hence system failure, was assumed to occur as soon as the hollow pile capacity was reached.

The model was not modified in any other way. However, the elasto-plastic behavior of the rotational spring at the top of the column was invoked to account for the ductility of the jacketed plug after it yields (See Section 3.5.2).

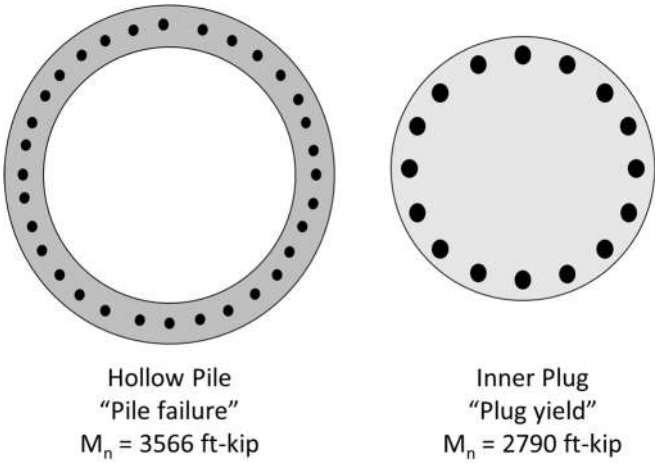

Figure 3-11. Moment Capacities used in Analysis Model for Retrofitted Conditions

3.5.2 *Modified Procedure*

The procedure as outlined in Section 3.3.3 was repeated, considering yielding of the inner plug only (at the top of the column) as the damage state of interest. This is referred to as the "plug fuse retrofit yield" condition since the plug acts as a ductile flexural "fuse" and allows the column-pile to carry increasing load until the moment capacity at another location along the pile is reached. After the yielding analysis, the procedure was modified as follows to account for ultimate failure of the retrofitted hollow column.

- The rotational spring stiffness, α at the cap beam-column connection was set to 0.0 and a moment equal to the plug moment strength was applied to the top node of the column. The combination of these two settings was done to simulate the conditions of "plug yield".
- The lateral load, Q was then increased until the moment demand somewhere in the pile reached the calculated capacity of the hollow section, referred to as "pile failure" in Figure 12. This invariably occurred below grade.
- The static load needed to achieve "pile failure" was converted to a PGA using the Capacity Response Spectrum approach, as before, except that in this case, the secant stiffness was used to define the period, instead of the initial elastic stiffness. The earthquake amplification factor F_{EQ} was recorded
- Column-pile moments and shears were recorded for each set of parameter values.

3.6 RESULTS FOR RETROFITTED CONDITIONS

The retrofitted bridge column analysis consisted of two parts, yielding at the plug, and ultimate failure due to hollow pile failure, henceforth referred to as "plug fuse retrofit yield" and "plug fuse retrofit ultimate".

At first yield of the plug, the moment demand in the hollow column, both at the bottom end of the plug and in the region below grade, is always below the predicted hollow capacity, in the same way as for the as-built condition. Therefore, at this loading stage, there is no danger of the hollow column failing in flexure. At the top of the column, the flexural strength of the plug is less than that of the hollow section, and the moment demand diminishes with distance from the top (as shown in Figure 3-10). The DCR of the hollow pile is given in the plots below and is generally in the range 0.40 to 0.70. This is lower than what is found for the as-built conditions which shows that the retrofit would significantly reduce the risk of failure in the region just below the plug. On the other hand, an earthquake with a smaller PGA is required to cause "plug fuse retrofit yield" than is required to cause the "as-built failure" (See Figure 3-12), but first yield of a ductile element is of little concern; it is expected under the design earthquake in all modern bridges with solid circular columns. The demand below grade is even smaller, essentially because the fixity at the soil surface is less than the fixity at the cap beam.

After the plug yields, any further load must be taken by the pile acting as a cantilever, increasing the moments in the pile below grade (while the moment at the cap beam remains constant as a result of the assumed elasto-plastic behavior). Eventually, at a large enough load, the moment demand below grade reaches the hollow pile capacity. The load, and the corresponding earthquake level, in terms of the earthquake amplification factor, F_{EQ} (See Equation 2) are reported for each condition. The moment demand at the bottom end of the plug remains capacity-protected by the plug, which acts as a fuse. As can be seen in Figure 3-12, the ultimate failure of the retrofitted column-pile still occurs at an earthquake with a lower PGA than the design spectrum for the reference conditions chosen. While this is an unfavorable outcome, it is (at 0.945) only slightly below 1.0, and therefore renders the system able to resist 94.5% of the 1000-year earthquake. This outcome should be compared with the F_{EQ} of 0.54 for the non-ductile as-built condition, which

confirms that the "plug fuse" retrofit would improve the performance of the column-piles. Other combinations of parameters should be explored (e.g. different site classes and column lengths), but it is believed that the same trends would hold (i.e. the "plug fuse" retrofit would improve the performance of the "as-built" columns).

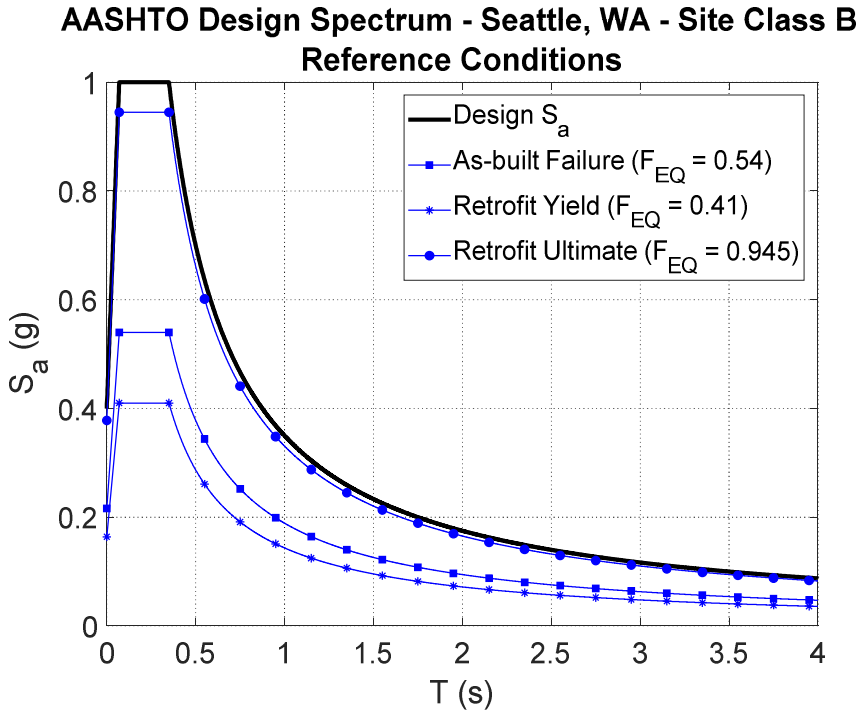

Figure 3-12. Scaled Response Spectrum to cause failure modes for reference conditions (Note: Retrofit refers to "Plug Fuse Retrofit")

The parameters investigated for the retrofitted condition are as given in Table 3-1. In the following sections, the effects of each parameter are investigated by keeping all others constant at the reference value. The results are presented in terms of the DCR at the bottom of the plug for the "plug fuse retrofit yield" condition and in terms of the earthquake factor, F_{EQ} for the "plug fuse retrofit ultimate" condition. Furthermore, inelastic pushover curves are shown for each parameter which shows the critical lateral load that causes the moment capacity to be reached in both locations.

In all parameter studies, an overall trend is that the DCR of the hollow pile at the bottom of the plug decreases from the as-built condition to the "plug fuse retrofit yield" retrofit condition, showing that the plug "capacity protects" the hollow column.

3.6.1 *Effect of Soil Stiffness*

The effect of the soil stiffness is shown in Figure 3-13. Changing the soil stiffness has very little effect on the DCR of the hollow column since a large range of soil stiffness between 20 and 2000 kcf resulted in a DCR range of less than 0.1 between the two conditions. The soil stiffness has a significant effect on the F_{EQ} factor such that higher stiffness soils reduce the ground motion level needed to yield the pile below grade. However, a practical range of soil stiffness for site class B would lie to the right of the dashed line and the PGA required for "plug fuse retrofit ultimate" at all of these values is essentially constant and equal to that of the AASHTO 1000-year return period earthquake.

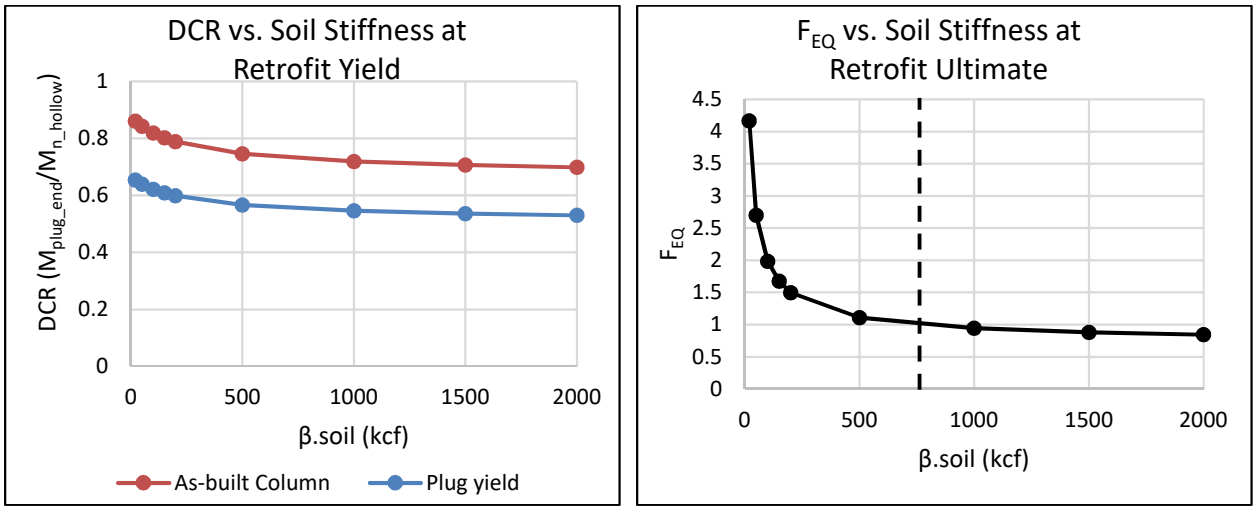

Figure 3-13. Effect of Soil Stiffness, β_{soil}

Figure 3-14 shows a series of pushover curves developed for the reference column-pile for different soil stiffness values. It confirms the limit of practical soil stiffness values since the pile yield for softer soils e.g. β_{soil} = 20 kcf is associated with very large and unrealistic cap beam displacements. This is because the soil is too flexible to allow a moment to develop that is large

enough to jeopardize the pile and this results in the very large PGA needed to reach pile yield (400% of the AASHTO design spectrum).

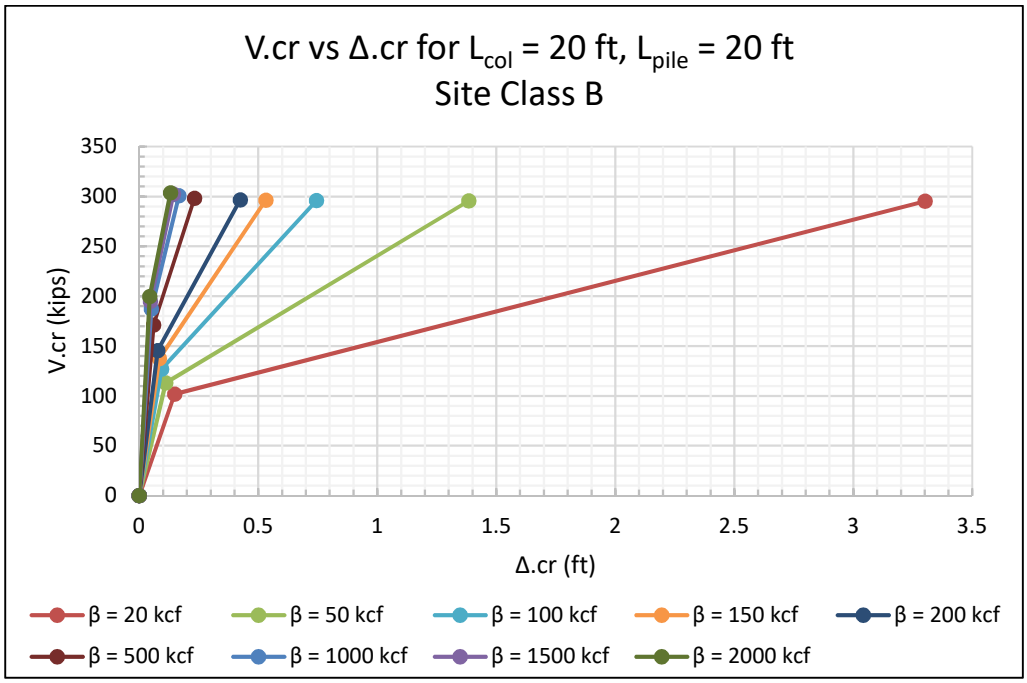

Figure 3-14. Inelastic pushover curves for varying soil stiffness

3.6.2 *Effect of Pile Length*

The effects of the below-grade pile length are similar to those for the soil stiffness since a short pile, like a low-stiffness soil, generates small moment resistance at grade level. There is little effect on the DCR of the hollow column below the plug when the pile length is changed but shorter piles require a PGA that is 50% more than the 1000-year return period earthquake to cause pile yield while longer piles, especially in stiff soil, may require further investigation since the study suggests ultimate failure at a smaller earthquake. That combination is, however, improbable in practice, because stiff soil could develop the vertical capacity, the primary design requirement in the 1960s, within a short pile length.

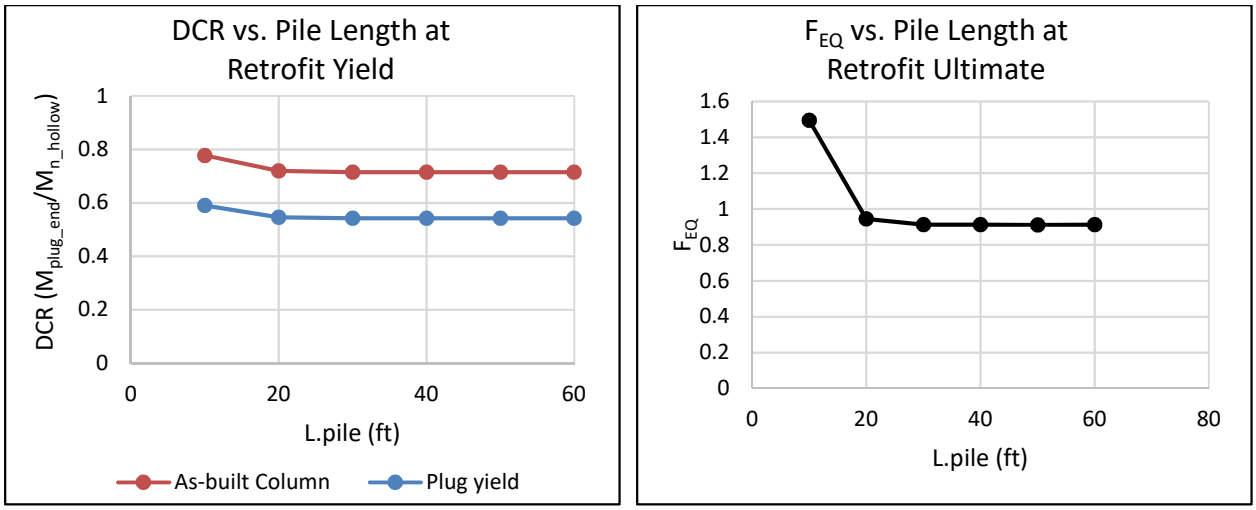

Figure 3-15. Effect of Pile Length, L_{pile}

The series of pushover curves in Figure 3-16 suggest that the length of pile does not have any effect on the critical loads to reach plug yield and pile failure, except for the case of a very short pile (10 ft in this case). The results from this parameter study suggest that piles embedded to a shallower depth below ground, in a stiff soil would not fail during a 1000-year earthquake.

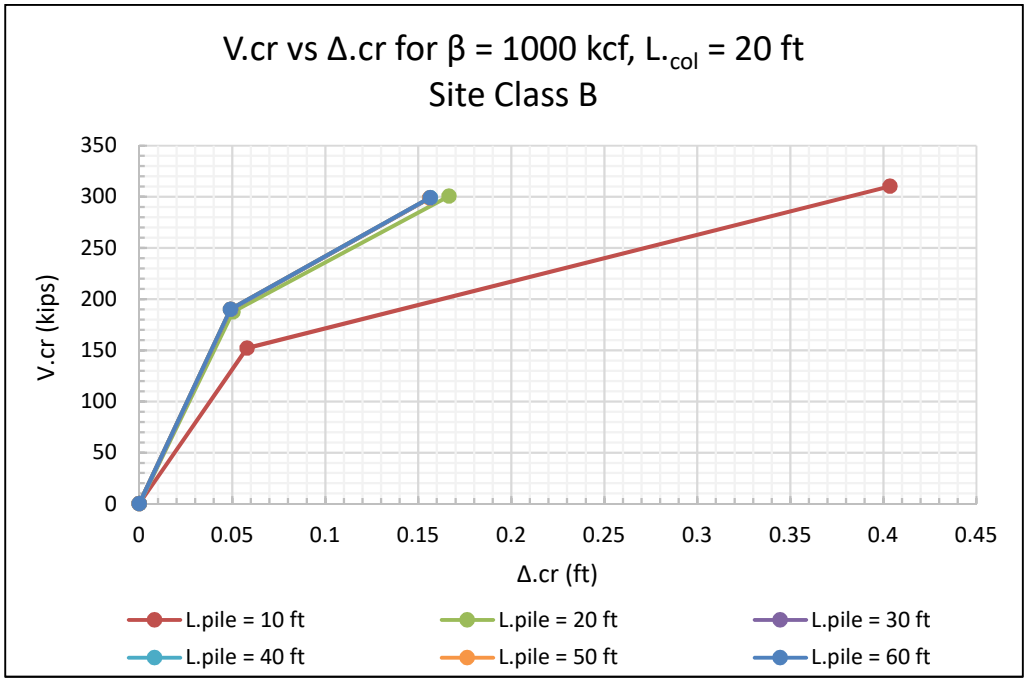

Figure 3-16. Inelastic pushover curves for varying below-grade pile length

3.6.3 *Effect of Column Length*

Figure 3-17 shows that the DCR at plug yield increases for longer columns but still remains well below 1.0 for the practical range of lengths studied. The hollow section remains capacity protected by the plug acting as a ductile fuse. Furthermore, the PGA needed to cause pile failure below grade is typically the design PGA (F_{EQ} = 1.0) at all column lengths investigated.

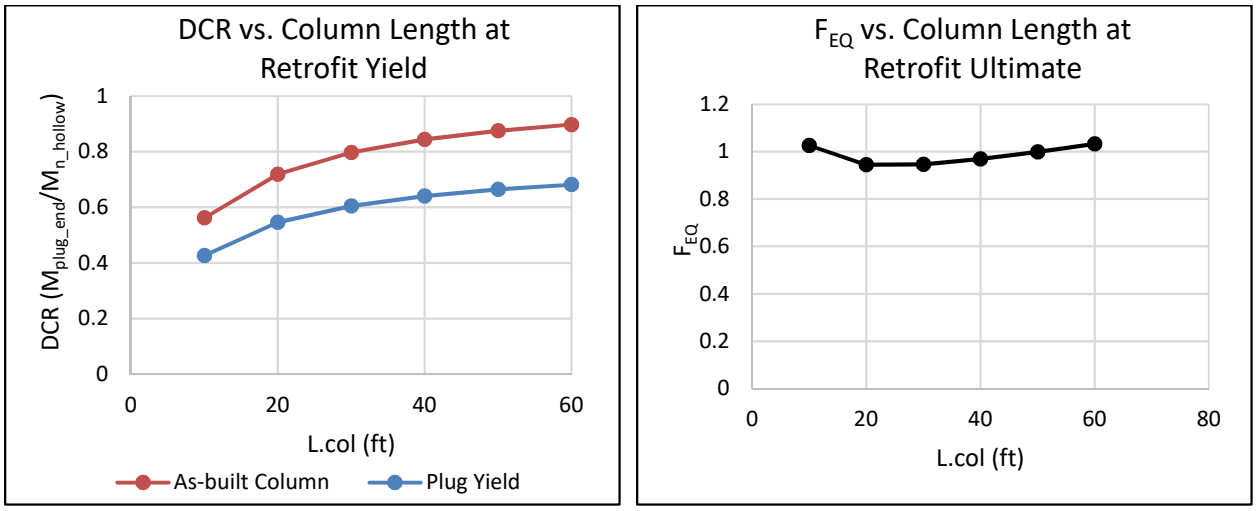

Figure 3-17. Effect of below grade column length, L_{col}

From Figure 3-18, it can be seen that, as expected, longer columns are also associated with high drift levels (> 5%) which may not be realistic in the field.

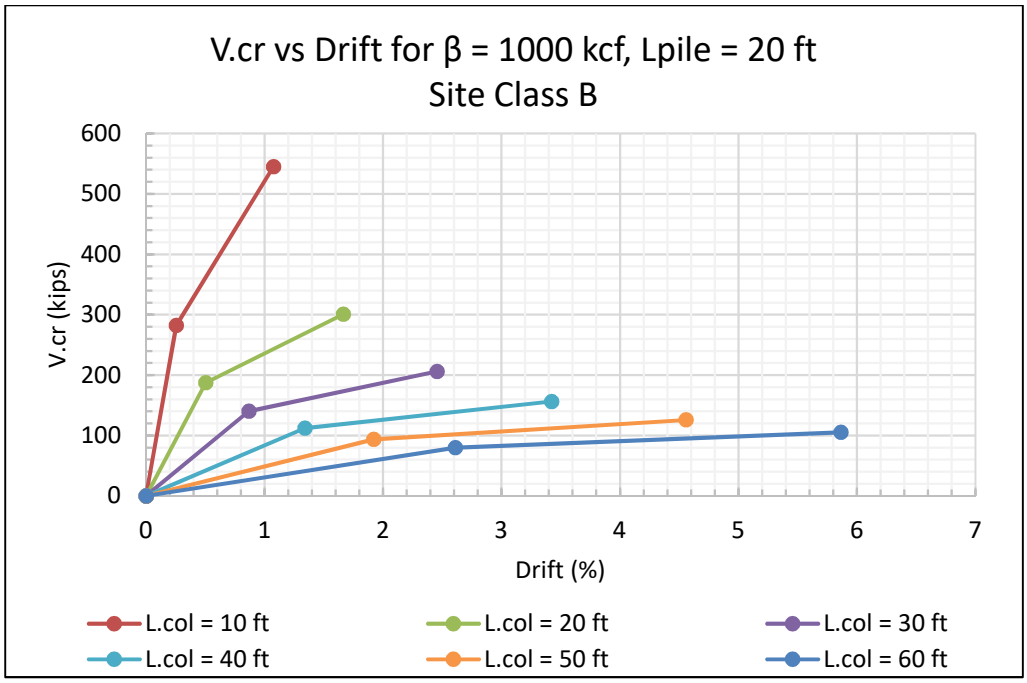

Figure 3-18. Inelastic pushover curves for varying above-ground column length

3.6.4 *Effect of Deck Stiffness*

The presence of a deck could provide additional resistance to lateral loads if there are girder stops at the abutments and no joints over the bents. If this is the case, the deck's stiffness significantly improves the system performance. The effect of the deck stiffness was evaluated in two ways by changing the overall deck length and keeping the same outer to inner span ratio or, by changing the deck width. However, while the deck was considered continuous, the girders were not, since this is expected to be typical for bridges constructed in the 1960's. In the reference condition, used in all the previous parameter variations, the deck was assumed to contribute to the seismic mass, but not to the lateral stiffness or strength.

Figure 3-19 shows that the presence of the deck considerably reduces the DCR of the hollow column to 55% at plug yield which is the largest absolute reduction seen among all parameters. This makes it clear that the deck is much stiffer than the pile bent, regardless of the combination of deck dimensions used. This finding is based on the reference column length of 20 ft. The benefits would be expected to be even greater for longer columns.

Increasing the deck width or decreasing the deck length have, as expected, the same positive effect on the earthquake amplitude factor F_{EQ}, but to different extents. Of particular importance, the presence of the deck increases the value of the PGA at which the pile reaches its flexural capacity below-grade to be at or above the PGA of the 1000-year return period design earthquake. It should be noted that these analyses presuppose checking the strength of the deck and the abutments which may limit the practical behavior of the deck. Also, the Maximum Considered Earthquake (MCE) would occur at an F_{EQ} factor of 1.5 so any values above this are theoretical only.

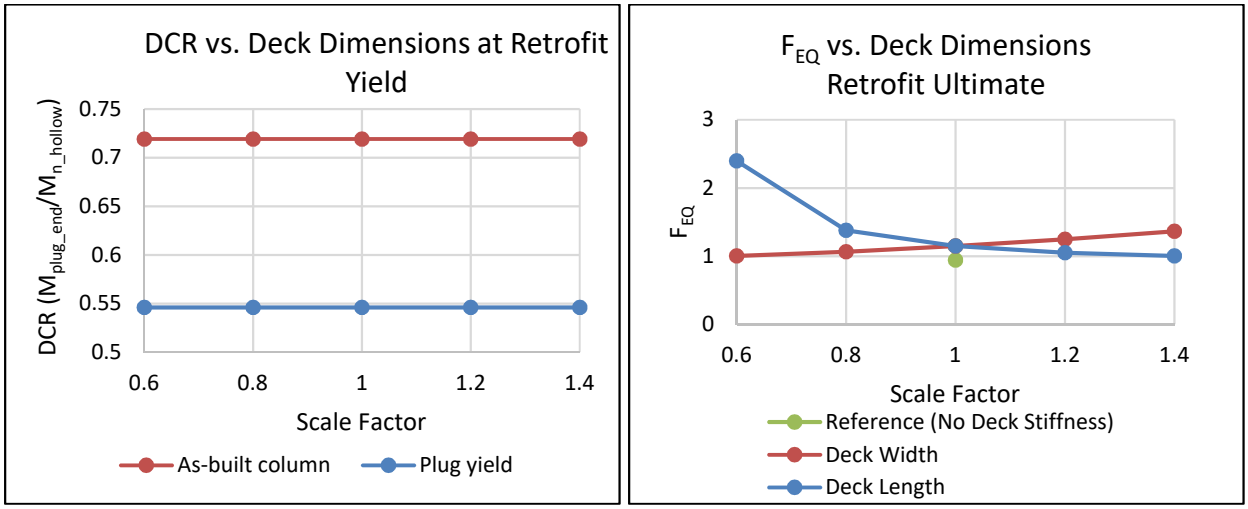

Figure 3-19. Effect of Scaling Deck Dimensions

The series of inelastic pushover curves in Figure 3-20 and Figure 3-21 show that the lateral load needed to cause ultimate failure of the pile below grade significantly increases when the deck stiffness is considered.

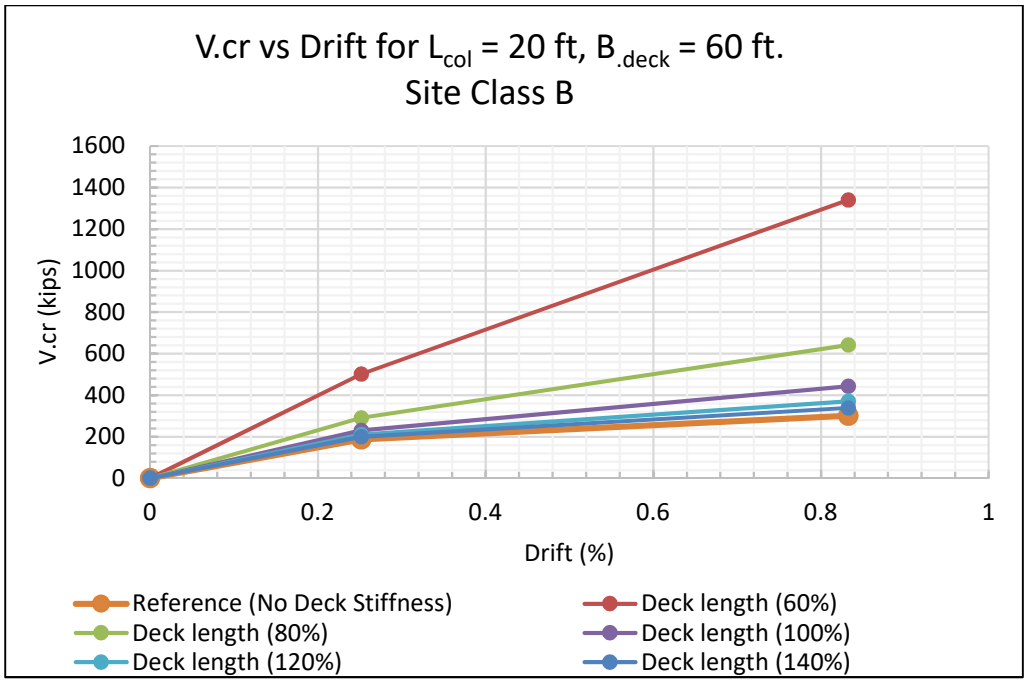

Figure 3-20. Inelastic pushover curves for varying deck length to consider deck stiffness

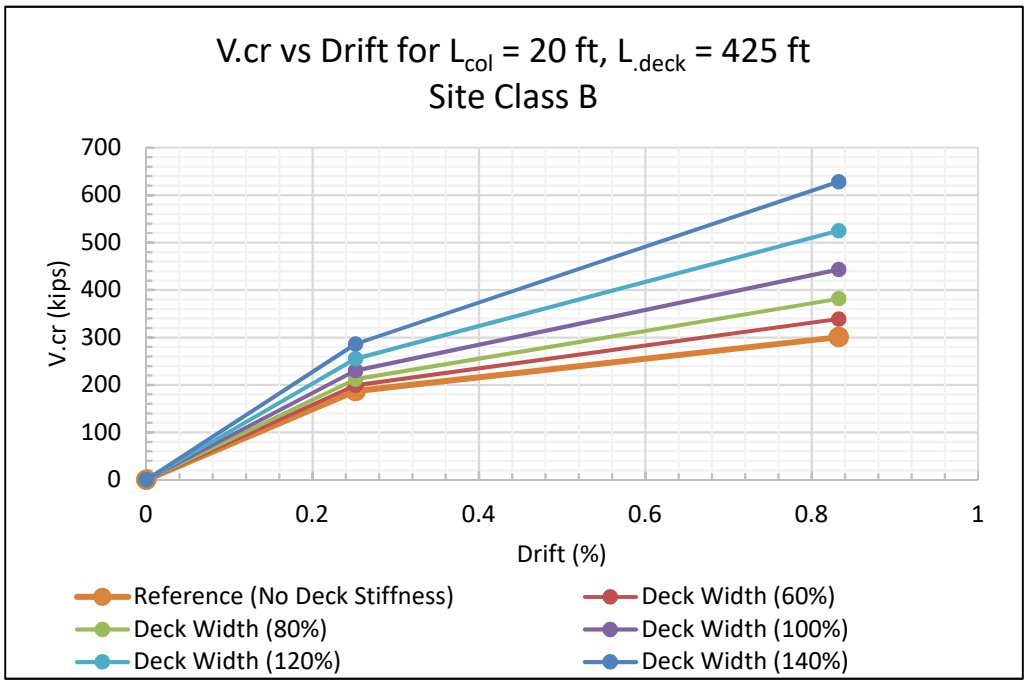

Figure 3-21. Inelastic pushover curves for varying deck width to consider deck stiffness

3.6.5 *Effect of Axial Load*

As shown in Figure 3-22, at the expected reference axial load, the moment capacity for all three failure conditions lies on the ascending branch of the interaction diagram. Therefore, a higher vertical stress on the column will also increase its moment capacity. Furthermore, since the slope of the "plug only" interaction is steeper than that of the hollow pile, the DCR of the hollow section at plug yield should remain below 1.0 at higher axial loads, even with the increased moment demand.

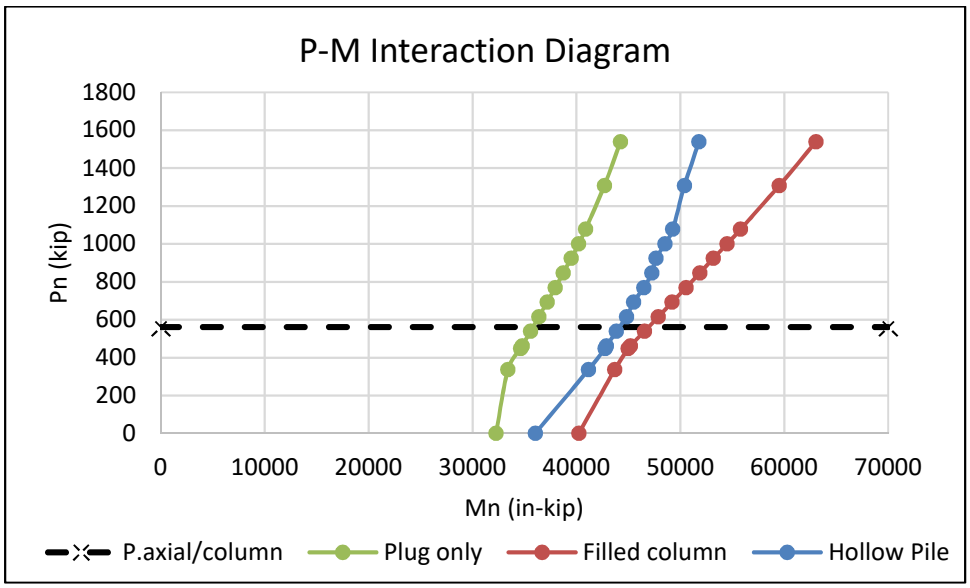

Figure 3-22. P-M Interaction Diagram for the different failure modes

3.7 SHEAR CRITICAL COLUMNS

The parametric studies investigated the performance of the columns assuming flexure-critical behavior. This is the predominant failure mode expected for the majority of the field columns based on the above-ground column lengths. However, a critical length is needed to define which columns should be considered shear-critical.

The critical length can be taken as the length to the point of inflection of the moment distribution from the top of the column. To find this critical length L_{cr} the shear capacity, V_n of the hollow column can be compared to the shear demand at the peak moment. The shear capacity of the hollow

column includes the shear strength of the concrete and the spiral reinforcement. Assuming a principal tensile stress of $f_1 = 4\sqrt{f'_c}$ at the centroidal axis if the walls of the column in the direction of load are treated as the web of the member (ACI 318-11 Provision 11.3.3.2), a Mohr's circle analysis gives the maximum shear stress τ as

$$\tau^2 = \left(f_1 + \frac{f_c}{2}\right)^2 - \left(\frac{f_c}{2}\right)^2 \quad (3)$$

$$f_c = f_{PS} + f_{axial} \quad (4)$$

$$f_{PS} = \frac{N_{str} A_{str} f_{pj}}{A_c} \quad (5)$$

$$f_{axial} = \frac{P_{axial}}{A_c} \quad (6)$$

The shear capacity of the concrete V_c can be taken as

$$V_c = \tau A_{shear} \quad (7)$$

where $A_{shear} = ½A_c$ for a hollow cylindrical section.

Using Equations 3-7, the shear capacity contribution of the hollow pile concrete was found to be 402 kips. The shear capacity contribution from the spiral reinforcement V_s can be found from Equation 8 as follows

$$V_s = \frac{A_{sp} f_y d_{sp}}{s} \quad (8)$$

where A_{sp} = cross-section area of spiral reinforcement, which was #2 gage for the reference bridge
f_y = yield strength of spiral reinforcement, taken as 70 ksi
d_{sp} = diameter of spiral hoop, taken as 49.5 inches
s = max pitch of spiral wire, which was found to be 4 inches for the reference bridge

The shear capacity of the spiral was found to be 46.7 kips so that the total shear capacity of the hollow pile is 449 kips.

The critical length can be found by setting the shear demand at peak moment M_n of the hollow pile to the shear capacity and finding the corresponding shear span. An assumption of fixed end conditions gives the following relationship:

$$L_{cr} = \frac{M_n}{V_n} \quad (9)$$

Taking M_n = 3566 ft-kip Figure 3-4, the critical shear span for the hollow column is found to be 7.9 ft. This shear span is the distance between points of fixity which would be at the cap beam and some distance below grade. Therefore the column-piles can be said to be shear-critical if the above-ground clear height is some length less than the critical length, which is about 1.75 pile diameters.

This finding is necessarily approximate, because no experiments were conducted to verify the shear strength of a hollow prestressed column. Only one study was found, world-wide, that addressed that question and, while it supports the approximate values found here, the experiments were conducted on non-prestressed RC pipes (Turmo et al. 2009). Nonetheless, the approximate values are encouraging. Even if the shear strength is over-predicted by a factor of 2.0, the critical distance to the inflection point would still be only 3.5 pile diameters, or about 16 ft. Many of the piles in the field would then not be shear-critical.

3.8 CONCLUSIONS

The following conclusions can be made from the preceding analysis.

1. Under lateral loads, the as-built hollow column-pile will always fail at the cap beam connection before any below grade damage occurs. This suggests two things:
2. An experiment that investigates and confirms the actual mode of failure and damage state of the as-built column should be conducted and,
3. A primary retrofit should be undertaken to address the cap beam connection.
4. The proposed retrofit of removing the pile wall in the location of maximum moment capacity protects the hollow section directly below the plug by reducing the overall demand before it yields, so that the DCR is less than 0.7 in all cases.
5. After plug yield, the ductile behavior of the retrofit allows the hollow column-pile to withstand a much larger earthquake than the as-built condition before ultimate failure which invariably occurs when the below grade pile reaches peak moment strength – F_{EQ} increases from 0.54 to 0.945 for the reference conditions.

6. For the reference conditions considered, the PGA of the earthquake at ultimate failure (below grade) of the retrofitted column is only 94.5% of the AASHTO 1000-year design spectrum earthquake PGA of 0.4g for site class B, which is unfavorable. However, this outcome is only representative of one specific combination of parameters and does not account for possible damping due to hysteretic behavior.
7. The presence of a continuous deck improves the performance of the retrofitted column-pile so that it would be able to withstand a larger earthquake than the AASHTO 1000-year design spectrum earthquake ($F_{EQ} = 1.2$). This suggests that if there are joints over the bents on the existing bridges, a retrofit approach that eliminated the discontinuity may be a practical and economical way of improving the bridge performance, in addition to the proposed "plug fuse" retrofit.
8. The critical length for shear failure, defined as the length to the point of contraflexure of the moment distribution along the column, was found to be 1.75 column-pile diameters. This corresponds to a length of 7 feet for the 48-inches outer diameter column-piles or 8 feet for the 54-inches outer diameter column-piles. Few columns in the field bridges have shorter above-ground spans so shear-critical behavior was considered a low priority for retrofit.

3.9 Recommendations for Experimental Programming

Based on the conclusions, two experimental programs were formed in order to validate the results of the analytical investigation and promote the implementation of the "plug fuse retrofit" concept.

1. The first experimental program explores the feasibility of the "plug fuse retrofit" concept as its execution would change the axial load transfer mechanism between the bridge superstructure and the column-piles. Instead of a direct transfer of the axial load by bearing, the gravity loads would be supported by the inner plug which would then have to transfer the load to the hollow column wall through shear friction at the interface between the plug and the wall. A parametric experimental study to understand how various factors affect the shear friction strength at the interface will be useful in assessing the practicality of cutting back the column-pile wall to create the "plug fuse".

2. The second experimental program investigates the failure mode of the as-built column in the region of maximum moment at the column-cap beam connection. This is important because the connection is uniquely composite consisting of the cast-in-place concrete cap beam and the precast, prestressed column-pile surrounding the cast-in-place reinforced concrete plug. A system like this has not been tested previously.

Chapter 4. PLUG SHEAR FRICTION TEST DESIGN

4.1 MOTIVATION FOR EXPERIMENTAL PROGRAM

Based on the results of the linear and non-linear analyses described in Chapter 3, it was concluded that a plastic hinge is possible at the top of the column where it meets the cap beam. From this, the research team decided to explore the "plug fuse" retrofit option whereby a small length of the outer wall of each column is removed right below the cap beam. This should decrease the moment capacity of the column in that region to the flexural strength of the plug alone. That is expected to confer two benefits. First, the stiffness of the bent drops, so the period elongates and the seismic base shear decreases. Second, the moment in the critical region of the column (just below the plug) will also be reduced, because it is capacity protected by the plastic hinge at the plug. Preliminary calculations show that the column moment is likely to be low enough to avoid damage to the column wall.

The removal of the outer wall of the column would change the load transfer mechanism from the bridge superstructure to the bridge columns. Instead of a direct transfer of axial loads to the column by bearing, the dead and live loads would be directly applied to the inner plug and then transferred to the hollow column through shear friction at the interface between the plug and column wall. That load transfer is critical.

As a result, an experimental program was developed to be able to determine the shear friction capacity of the interface between the plug and column wall when an axial load is applied to the inner plug only. The following sections describe the variables that were used, the experimental setup and the results of the program.

4.2 TESTING CONSIDERATIONS

To fully investigate the shear friction capacity of the column-plug interface, several variables were considered. These were

- the surface roughness of the interface between the column wall and plug concrete,
- the length of the plug,
- the eccentricity of applied load,
- the effect of cracking in the pipe wall, and
- the effect of jacketing.

4.2.1 *Specimen Description*

The testing program consisted of twelve (12) concrete pipe specimens each of length 36 inches with an outer diameter of 30 inches and a wall thickness of 3 inches (See Figure 4-2). The pipes were reinforced circumferentially with D2.1 Grade 65 wire at a 2-inch pitch, with an 11 inch splice, and longitudinally with W1.7 Grade 65 wire at an 8-inch spacing. The concrete nominal 28-day strength for the pipe wall was 6,000 psi. The circumferential reinforcement area and spacing was designed so that the hoop force equilibrium would be the same as in the field (See Figure 4-1, Equations 1-3).

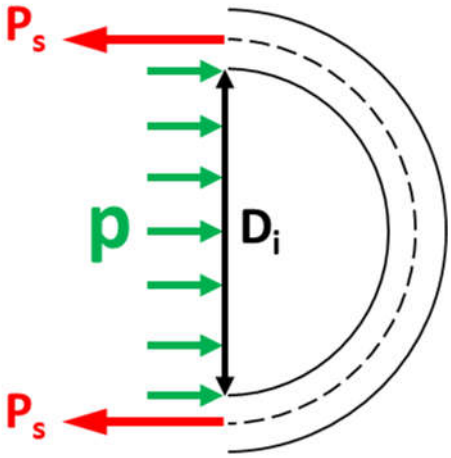

Figure 4-1. Hoop force equilibrium for hoop reinforcement

$$2A_s f_y = psD_i \quad (1)$$

$$p = \frac{2A_s f_y}{sD_i} \quad (2)$$

$$p_{test} = p_{field} \quad (3)$$

These pipes were produced for the research program by Oldcastle Precast in Auburn, WA. It should be noted that these pipes are not the same as the column used for the larger scale column bending test in the second experimental program, which was produced by Concrete Technology Corporation in Tacoma, WA. Since larger columns would have required custom manufacturing,

their production was both too expensive and time-consuming to be used for this part of the experimental program. As such, the concrete pipes from Oldcastle Precast were chosen as a commercially available product that was dimensionally similar, and the reinforcement was adjusted to match that in the existing bridge columns at laboratory scale.

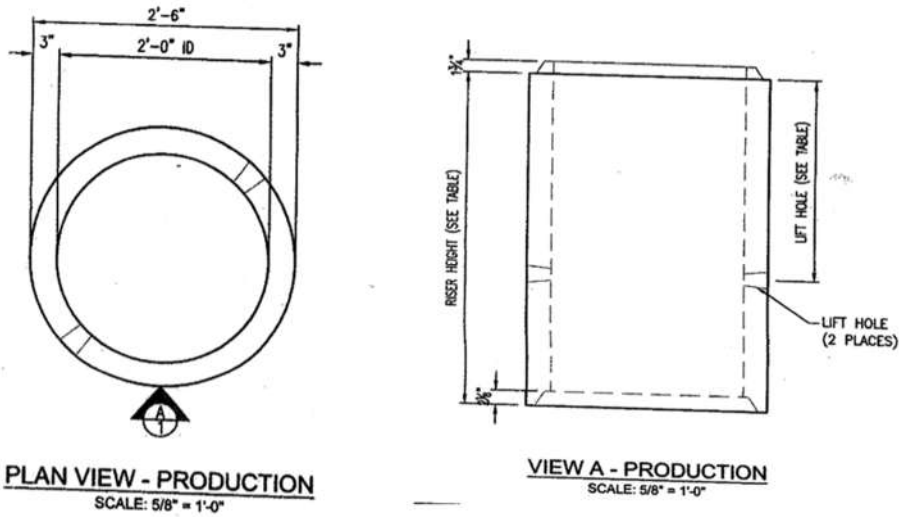

Figure 4-2. Cross-section of Concrete Pipes; b.) Elevation of Concrete Pipes (Courtesy of Oldcastle Precast)

4.2.2 *Test Matrix*

Table 1 shows the testing matrix that was developed for this experimental program. The "Test ID" represents the following:

- 'ep24' means an epoxy coated length of 24 inches on the inside surface of the pipe wall; typically the number also represents the length of the plug except for the case of the specimens without an epoxy-roughened surface ('ep0') wherein the length of the plug was 24 inches
- 'f1' means that the specimen was jacketed in a carbon fiber reinforced wrap and the number indicates the number of layers of the wrap used to form the jacket
- 's1' means that the specimen was jacketed in steel while the number indicates the thickness of the steel jacket in 1⁄16 increments
- '-1' and '-2' indicates whether a second test was done for the particular specimen

- '-cr' and '-ecc' indicates the pre-cracked specimen and the eccentrically loaded specimen, respectively

Table 4-1. Test Matrix for Experimental Program 1 - Plug Shear Friction

Test ID	Surface Type	Length of Plug	Load Eccentricity	Condition	Retrofit Options
ep24-1	Epoxy Mortar	24 inches	Concentric	Uncracked	None
ep24-2	Epoxy Mortar	24 inches	Concentric	Uncracked	None
ep0-1	*Concrete*	24 inches	Concentric	Uncracked	None
ep0-2	*Concrete*	24 inches	Concentric	Uncracked	None
ep18-1	Epoxy Mortar	*18 inches*	Concentric	Uncracked	None
ep14-1	Epoxy Mortar	*12 inches*	Concentric	Uncracked	None
ep24-cr	Epoxy Mortar	24 inches	Concentric	*Cracked*	None
ep24-ecc	Epoxy Mortar	24 inches	*Eccentric at e = 4.5 in*	Uncracked	None
ep24f1-1	Epoxy Mortar	24 inches	Concentric	Uncracked	*Thin FRP Jacket*
ep24f6-1	Epoxy Mortar	24 inches	Concentric	Uncracked	*Thick FRP Jacket*
ep24s1-1	Epoxy Mortar	24 inches	Concentric	Uncracked	*Sheet Metal Jacket*
ep24s4-1	Epoxy Mortar	24 inches	Concentric	Uncracked	*Thick Steel jacket*

4.2.2.1 Baseline Conditions

The baseline test condition (See Figure 4-3) for the program was an uncracked concrete pipe with its inner wall surface coated with an epoxy mortar paste (Section 4.2.2.2) and filled to a depth of 24 inches with a concrete plug. No external jacket reinforcement was used and during the baseline

testing, the axial load was applied concentrically over the inner concrete plug. Two specimens were tested under these conditions (ep24-1 and ep24-2).

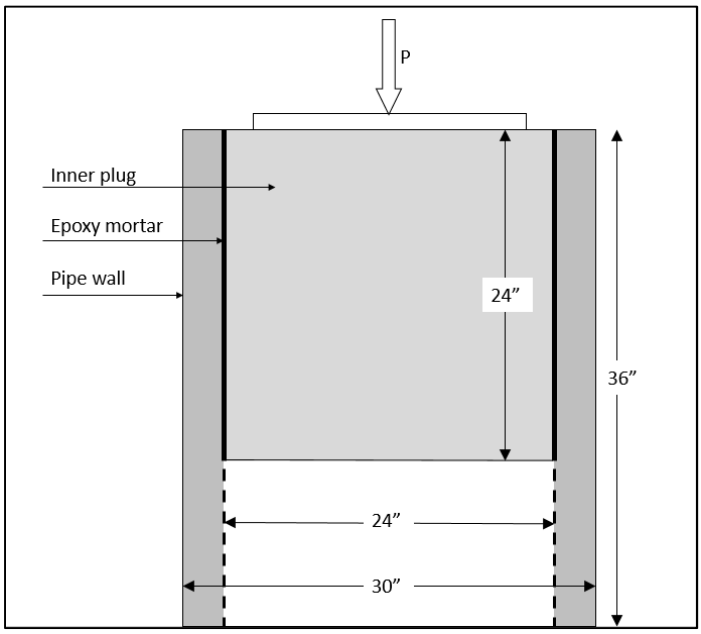

Figure 4-3. Schematic of Baseline Test Condition

4.2.2.2 Surface Roughness

Surface roughness was used as a variable because the original construction records were unclear about the surface details. On the drawings of the bridges that were constructed in this manner, it is stated to “roughen the inside surface of column with an approved epoxy mortar”. Since there is no record of what was considered an “approved epoxy mortar”, upon consultation with WSDOT and Concrete Technology Corporation a sand and liquid epoxy mix was used to imitate these existing conditions based on specifications found from the 1980s.

The sand was typically Sakrete Multi-Purpose fine sand. The epoxy was MasterEmaco® ADH 326 liquid epoxy concrete bonding adhesive with a long pot life. The liquid epoxy to sand ratio was 1:3 by volume and a thick grey paste was formed. This was applied to the inner surface of the pipe wall in an even ¾” layer and ridges were formed using a grout float (See Figure 4-4). The epoxy mortar mix was applied to ten of the specimens while two of the specimens were tested without

this surface roughening. For reference, the pipes were fabricated using steel forms and a dry self-consolidating mix as would be used to manufacture drain risers (See Figure 4-5).

Figure 4-4. Epoxy mortar layer on inner surface of pipe wall

Figure 4-5. Inner surface of pipe wall without epoxy mortar

4.2.2.3 Length of Plug

A typical plug to pipe length ratio of 2:3 was chosen for the test program since the plugs are approximately four to five feet in length on the existing bridges while the typical length of the above-ground column is 15-20 feet. Two of the plugs were cast at shorter lengths of 18 inches and 14 inches to determine how this affects the load transfer between the plug and column wall.

4.2.2.4 Load Eccentricity

Load eccentricity was chosen as a variable in order to simulate what may happen when a moment is applied to the column as would be expected during a seismic event.

The axial load was typically applied over the center of the specimen. However, for specimen ep24-ecc, the load was applied at an eccentricity of 4.5 inches (See Figure 4-6). The eccentricity was determined based on the limitations of the test setup since the plate that was used to apply and

spread the load could only be shifted by that distance and still apply the load to the inner plug only (See Figure 4-7).

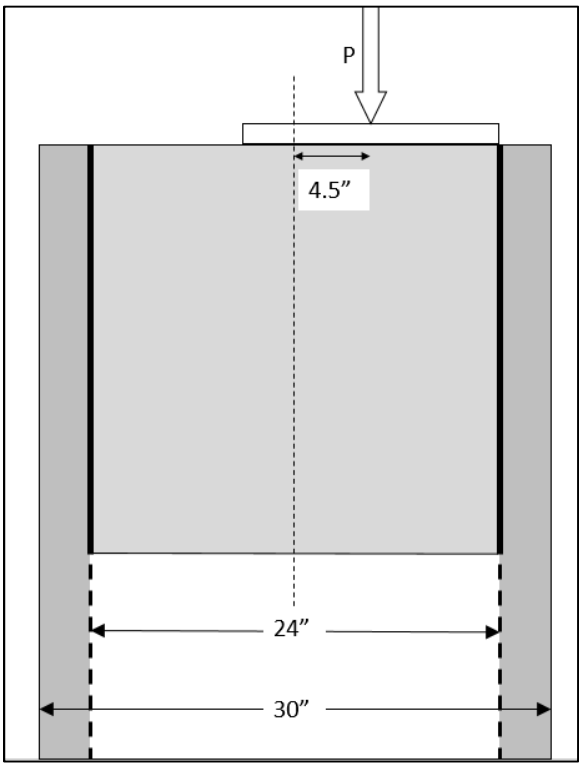

Figure 4-6. Schematic of Eccentric Load Test Set-up


Figure 4-7. Load Bearing Plate shifted off-center for Eccentric Load Test

4.2.2.5 Concrete Condition

One column was cracked prior to casting the inner plug and experimental testing. A radial compressive force was applied to the wall of the pipe as shown in Figure 4-8.

Figure 4-8. Axial Load applied to wall of concrete pipe

It caused bending in the wall of the pipe, and cracks initiated on the inside, at top and bottom as shown in Figure 4-9, and on the outside at the two sides (See Figure 4-9). This “cracked” specimen was included in the experimental program to represent the existing bridge columns that have longitudinal cracks along the column wall. For example, there are many columns on the Ravenna Boulevard Overcrossing Bridge that have longitudinal cracks that are visible today, as shown in Figure 1-2. These are known to have existed since the time of construction, based on archived field notes. The researchers wanted to evaluate whether the existing cracks would result in a lower shear friction transfer capacity on the basis that the cracked section would be less stiff than the uncracked one. The cracks observed in the field are believed to have been caused by bursting stresses under the post-tensioning anchors, and they probably penetrate through the full thickness. The cracks formed in the laboratory were caused by bending and so presumably do not quite penetrate through the full wall thickness. The method was adopted because it was simple, and led to cracks nearly the same as those in the field.

Figure 4-9. Longitudinal cracks - Specimen ep24-cr

4.2.2.6 Retrofit Jackets

Jackets are used to confine the core in solid columns, and that confinement might be expected to increase the shear friction resistance at the plug-column interface in hollow columns as well. The shear friction equations for plane surfaces in the AASHTO specifications (2012) imply that the reinforcement will be stressed to yield, but it is not clear that that would be true in this case. Test evidence was therefore considered essential.

Four retrofit options were examined – two carbon fiber reinforced polymer (CFRP) jackets of different number of layers, and two steel jackets of different thicknesses. The CFRP jackets were made of Tyfo® SCH-41 Composite using Tyfo® S Epoxy and were applied to the specimens following standard wet layup procedures developed by FYFE® Co. LLC (http://www.aegion.com/about/our-brands/fyfe). One specimen (ep24f1-1) was jacketed using one layer of the composite fabric while another (ep24f6-1) was jacketed using two layers of composite fabric and two layers of Tyfo® SCH-41-2X Composite material which is the same material but twice as thick in each layer (See Figure 4-10a and b). It was therefore equivalent to six layers of Tyfo® SCH-41 . The CFRP jackets were applied directly to the pipe wall.

The first steel jacket was a fully seam-welded cylinder made of ¼" thick, A36 plate steel (ep24s4-1) while the second was a rolled sheet of 16 gage galvanized steel (ep24s1-1) with a 20 inch overlap that was sealed using PC-7® Paste Epoxy, a high-strength epoxy adhesive (See Figure 4-10c and d). Both steel jackets were made with a 32 inch inner diameter. The steel jackets were applied to the concrete pipe using Dayton Superior Sure-Grip® High Performance Grout, a high strength cement grout, to fill the one-inch gap between the steel and the concrete. The grout was poured into the gap while the specimen was upside-down and then rodded to reduce air bubbles. The specimen was then flipped a few days later for testing.

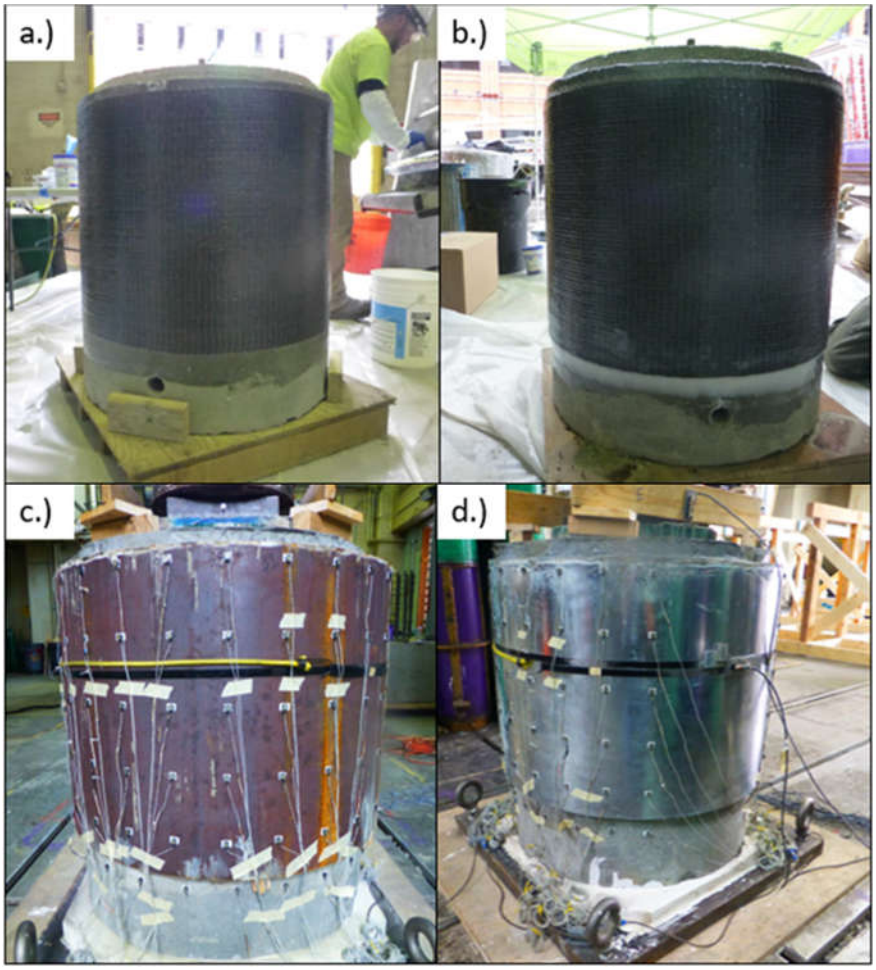

Figure 4-10. Jacketed Specimens - a.) 1-layer CFRP (ep24f1-1); b.) 6-layer CFRP (ep24f6-1); c.) ¼"-thick steel jacket (ep24s4-1); d.) 1/16"-thin steel jacket (ep24s1-1)

4.3 TEST SETUP AND IMPLEMENTATION

The specimens were tested using a Baldwin Universal Testing Machine, with a compressive load capacity of 2400-kips, to apply the axial load (See Figure 4-11). The base of the test setup consisted of a 2-inch thick steel plate that would not deform under the weight of the specimen and the maximum expected load. Each specimen was levelled and grouted in place using hydrostone, which was considered secure anchorage under the compressive load.

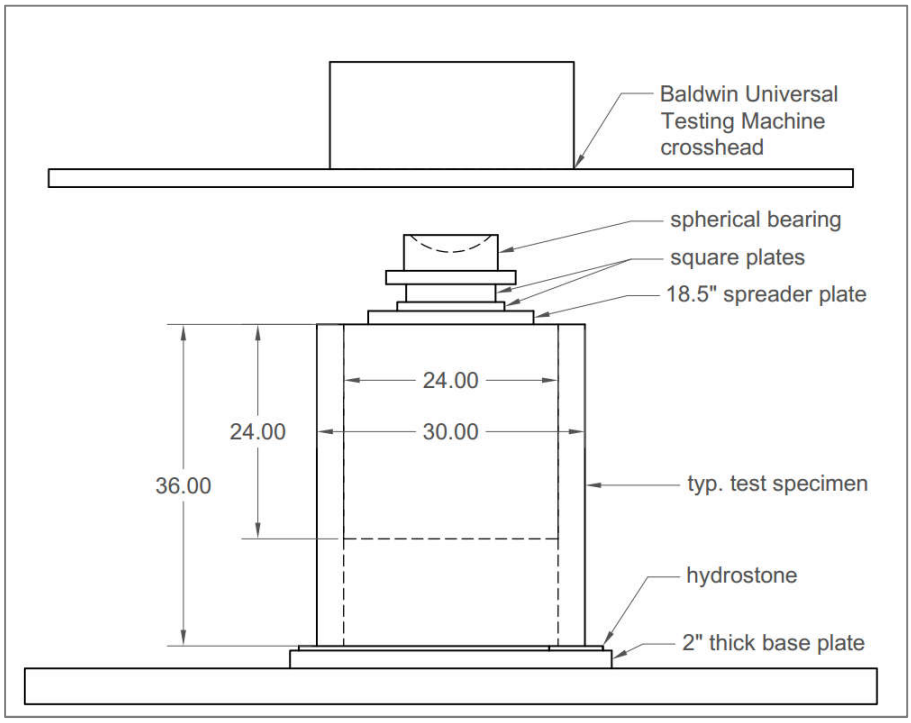

Figure 4-11. Typical Test Setup

The load was applied to the plug by the test machine through a spherical bearing in order to accommodate any differences in level (See Figure 4-11). The bearing was smaller than the plug, so spreader plates were used to distribute the load. Ideally, the loading plate would be the same diameter as the inner plug, that is, 24 inches. However, due to limitations in existing material an 18.5-inch diameter steel plate of 1.5-inch thickness was used (See Figure 4-11). Two square plates were then stacked on top of this plate (See Figure 4-11). All the plates had central holes to allow them to be placed over the lifting rod that was cast into the specimens. The one exception to this overall setup was for the eccentrically loaded specimen (ep24-ecc) where only the spherical

bearing was used to transfer and spread the load. In this case the bearing plate was placed as far to the edge of the plug as possible allowing for an eccentricity of 4.5 inches.

Each specimen was tested under load-controlled conditions up to the maximum load, when the wall cracked and the load dropped suddenly. At that point, testing was paused with no further load or displacement applied while the researchers marked any cracks that had formed around the specimen. Testing was resumed using a displacement-controlled protocol until the plug displaced at least an additional two inches. For load control, the specimen was subject to 25 kips per minute while for displacement control, the specimen was subject to 0.2 inches per minute.

4.4 INSTRUMENTATION

Linear potentiometers and an Optotrak motion capture system were used for each test. These instruments were electronically recorded using computer-controlled data acquisition systems. The applied axial load was directly measured using the Baldwin machine's internal load cell and recorded on the data acquisition system.

The linear potentiometers were used to measure the vertical displacement of the plug as well as the circumferential displacement around the pipe wall (See Figure 4-12).

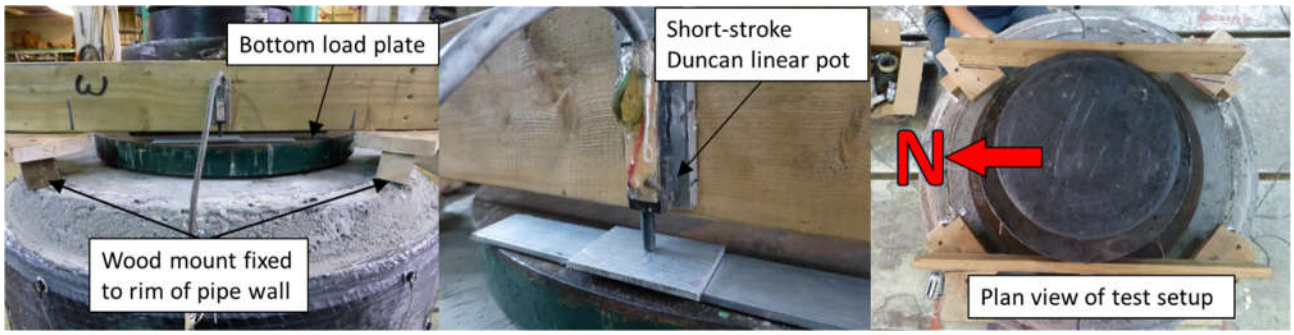

Figure 4-12. Linear Potentiometers used to measure vertical displacement of plug

Two short-stroke Duncan potentiometers were mounted on wooden stands that were fixed to the rim of the pipe wall, on the east and west side of the specimen. The piston of each potentiometer was in contact with a flat aluminum plate fixed to the surface of the last loading plate so that the measured displacement was that of the loading plate relative to the pipe wall. This was taken as

being equal to the displacement of the plug. Any differences would be due to slight deformations of the plate on the top of the plug, and these were expected to be very small. The vertical displacement of the test machine head was also recorded, but it was not used during the data analysis, because it included displacements, such as deformations of the test machine and spherical bearing, other than the plug slip relative to the pipe wall.

To measure the circumferential expansion of the pipe wall, a thin steel strap which was double-wrapped around the perimeter of the pipe and kept tight using a short bungee cord (See Figure 4-13). Relative displacements of the ends of the strap were measured using a short-stroke Duncan potentiometer and L-shaped bracket attached to the strap. This displacement, divided by the pipe circumference, gave the average circumferential strain.

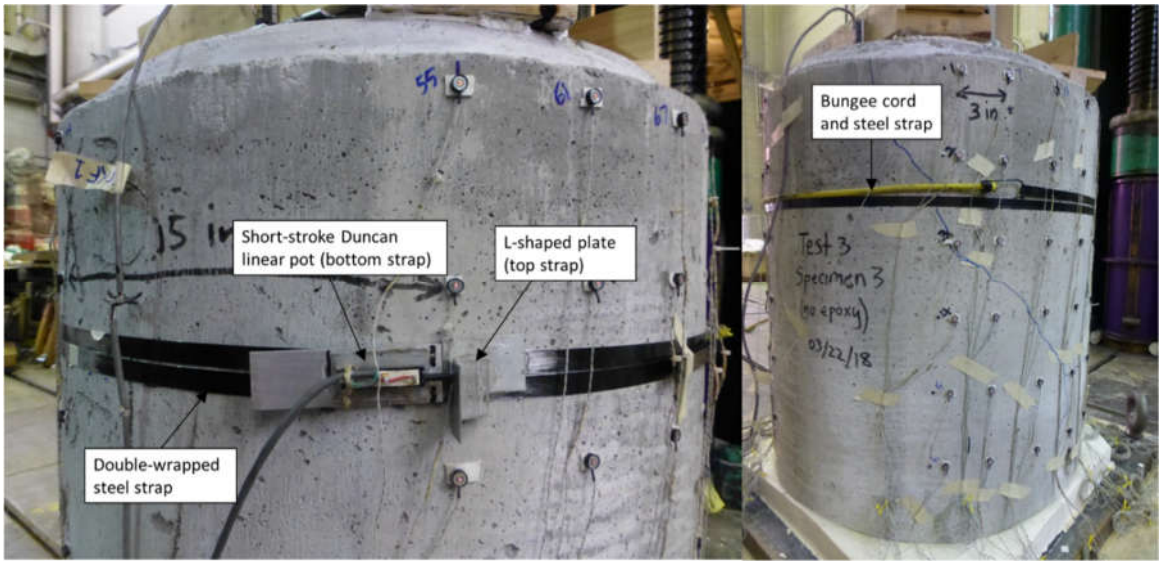

Figure 4-13. Instrumentation design to measure circumferential displacement

Unfortunately, this instrument proved to be insufficiently sensitive to give useful results prior to cracking and the results were typically discarded. Nonetheless, it was used for all tests because it gave an indication of imminent crack formation as the load approached its maximum.

An Optotrak Certus motion capture system was used to monitor the deformation of the pipe wall. The Optotrak system consists of two 3-dimensional optical camera arrays and a series of LED markers, which were attached to the specimen using adhesive foam pads. These markers emit an electronic signal that is photographed by the pair of sensors, each of which consists of 3 precision

cameras that locate the position of each LED marker in 3-dimensional space by triangulation of the relative positions. The cameras and markers were placed around the specimen as shown in Figure 4-14. Two additional markers (not shown) were placed on the north and south sides of one of the loading plates to measure the vertical displacement of the plug in order to corroborate the displacements recorded by the potentiometers.

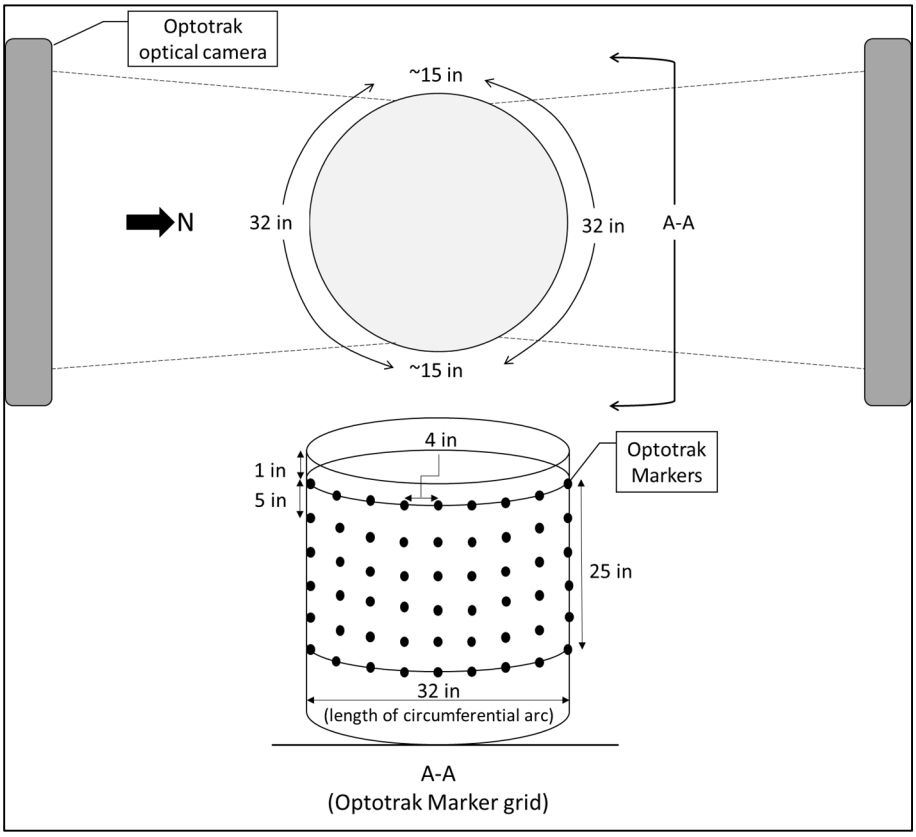

Figure 4-14. Placement of Optotrak motion capture system during testing

For the jacketed specimens, strain gages were also used on the pipe walls. Circumferential strains were measured with the gages for the CFRP specimens (ep24f1-1 and ep24f6-1) while both circumferential and vertical strains were measured on the steel jackets (ep24s4-1 and ep24s1-1). These strain gages were primarily used to measure elastic strains in the jackets for evaluation of the strain distribution in the pipe wall, but also to corroborate the strains calculated from the Optotrak displacement data. Strain gages were set up on each specimen as shown in Figure 4-15. Of note, the number and location of strain gages for ep24f6-1 were informed by the results of ep24f1-1 which is why it is noticeably different. Additionally, the results of the strain gages on the

CFRP specimens, which were tested first, showed that the strains were approximately equal on opposite sides of the specimen so gages were only attached to two faces on the steel-jacketed specimens (See Figure 4-15).

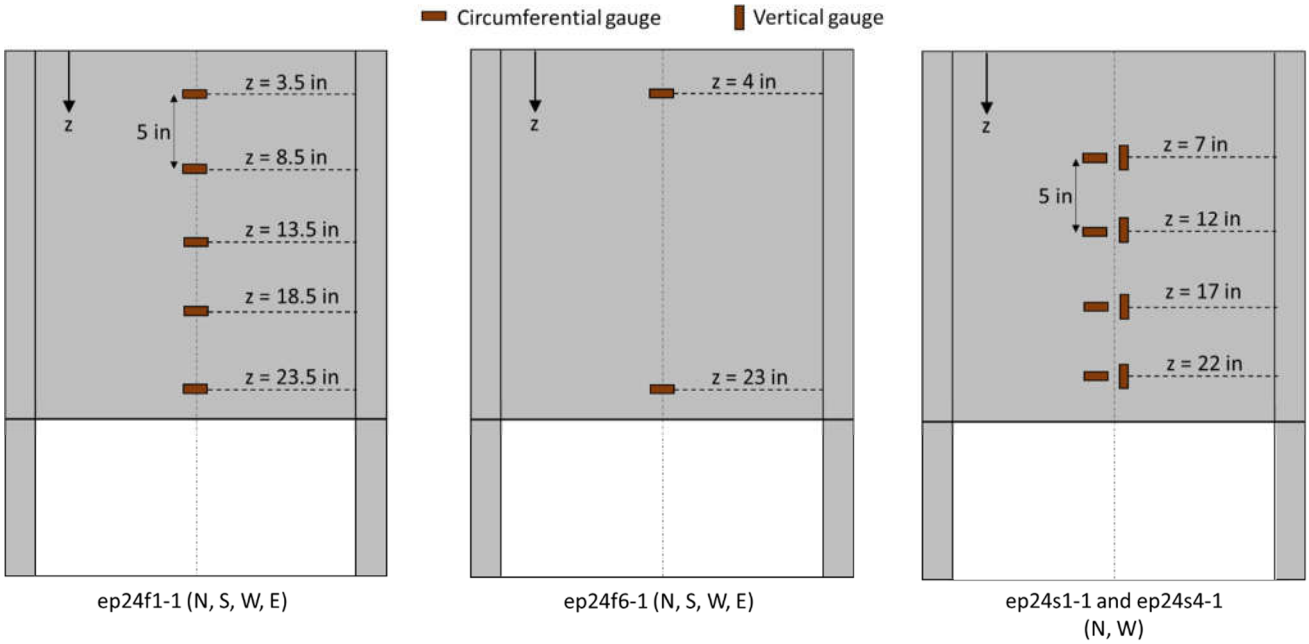

Figure 4-15. Location of strain gauges on jacketed specimens

Chapter 5. PLUG SHEAR FRICTION TEST RESULTS

5.1 INTRODUCTION

The results of the series of plug push-through tests are summarized in this chapter. Table 5-1 provides a quick summary of key results from the experiments, and Figure 5-1 shows the load data in a bar chart. In the table, the peak load is the maximum load reached during each test, and the residual load is the load after the plug was pushed through an additional 0.75 inches vertically. This displacement was chosen since inspection showed that in all tests, the data was much cleaner in the second phase of testing by this point. The test-day strengths for the plug concrete were approximated from a graph of the compressive strength of the concrete based on cylinder tests done at 7 days, 14 days, 28 days, and the last day of testing. For the tests done between 28 days and the last day of cylinder testing, a linear approximation was used.

Table 5-1. Key Experimental Results

Test ID	Peak Strength (kips)	Plug Displacement at Peak Strength (in)	Residual Strength (kips)	$f'c_{plug}$ (psi)
ep24-1	430.65	0.323	116.56	7915
ep24-2	319.51	0.198	45.54	8286
ep0-1	161.35	0.134	61.47	7975
ep0-2	147.72	0.160	59.37	8085
ep18-1	364.33	0.168	65.94	8124
ep14-1	284.83	0.146	106.6	8162
ep24-cr	306.69	0.208	76.89	6998
ep24-ecc	260.19	0.184	53.11	8043
ep24f1-1	806.17	0.230	259.28	8256
ep24f6-1	1046	0.181	478.74	8295
ep24s1-1	476.63	0.234	281.00	8570
ep24s4-1	748.42	0.226	302.66	8548

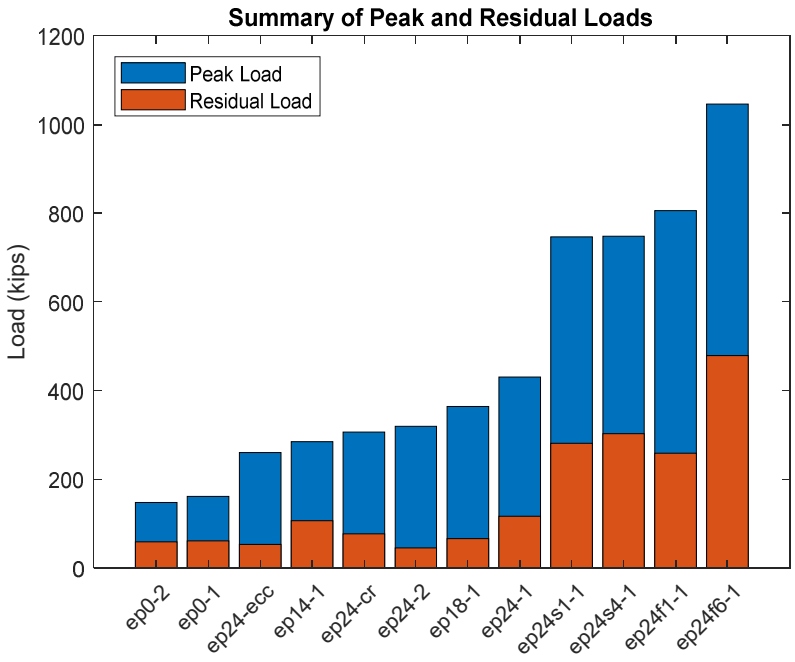

Figure 5-1. Summary of Peak and Residual Loads obtained during plug tests

Figure 5-2 shows that specimens can be grouped into three categories according to the peak load obtained during testing.

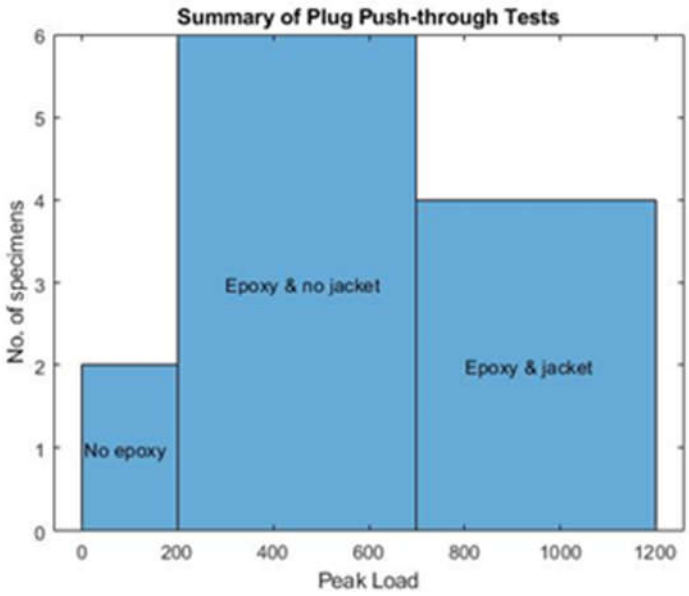

Figure 5-2. Summary of plug tests according to peak loads

The displacements obtained from the Optotrak markers were used to evaluate the crack patterns around the pipe wall, as well as to calculate circumferential (hoop) and vertical strains in the wall as the plug was pushed through. Since the linear pots that were used on the top of the specimen ran out of stroke before the test ended, the two markers that were placed on the loading plates were averaged to produce the load-displacement curve for each test as shown in Figure 5-3.

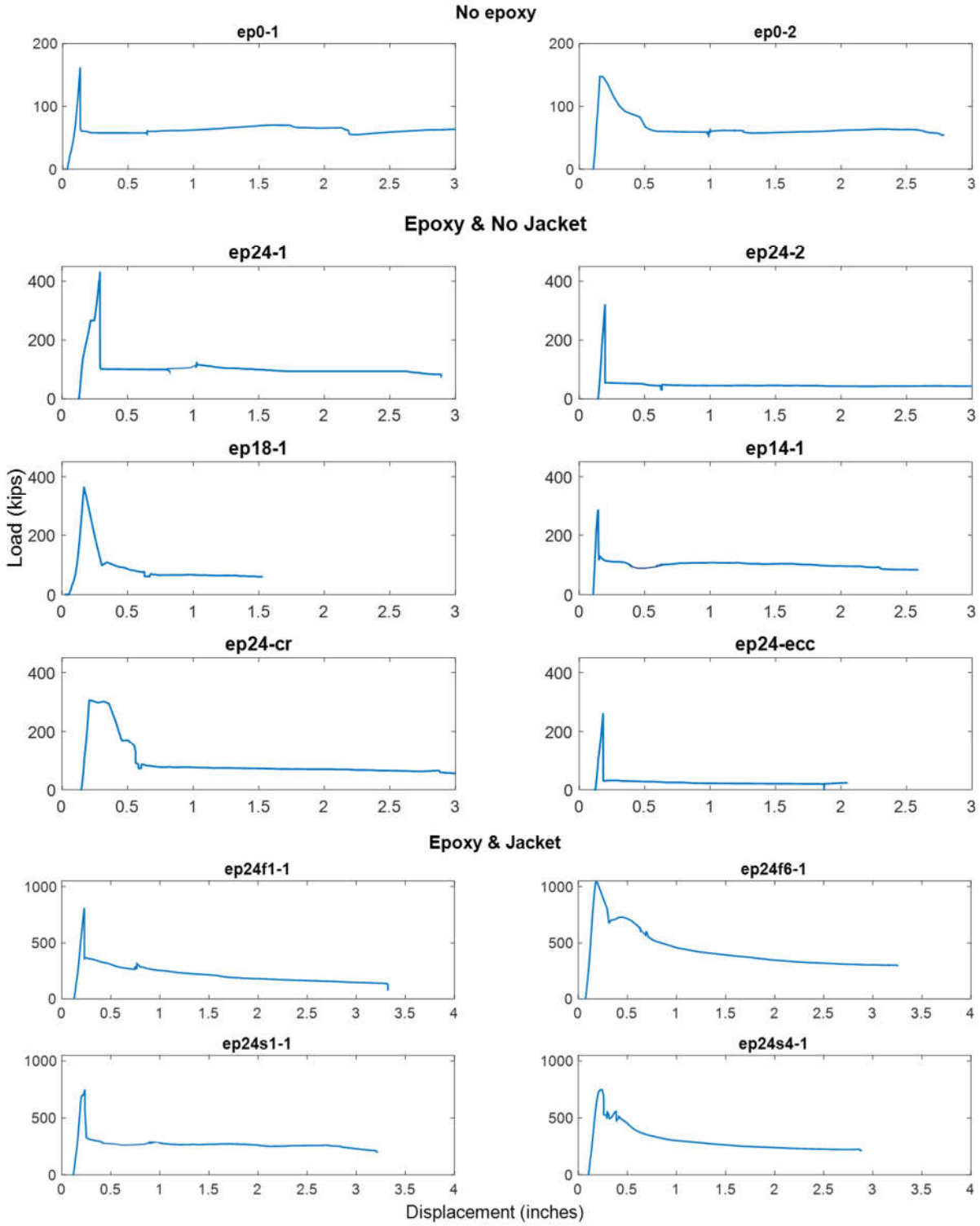

Figure 5-3. Load-displacement curves for all tests

5.2 GENERAL

For all tests, no signs of damage were visible prior to reaching the maximum load, and in particular no cracks. Once the peak load was reached, usually a loud cracking sound was heard, and visible vertical cracks formed around the outer wall of the pipe; the plug and loading plates displaced vertically downward through the pipe; the linear pots and strain gages recorded a significant jump in their measurements. At this stage, loading was paused, cracks were outlined with a marker and pictures of the damage state were taken. In all cases, the longitudinal cracks that formed at the peak load were widest at the top of the specimen and narrowed, sometimes to nothing, down to the bottom.

After cracks were marked at the peak load, loading was resumed using displacement control. Typically, some more cracking sounds were heard during this stage of testing. At the end of testing, any new cracks that formed during the second stage of testing were marked and more pictures taken. Once the machine cross head was raised, the top of the specimen was accessed, and the plug displacement recorded. In most cases, the plug did not displace solely by sliding along the interface but by a combination of punching under the loading plates and sliding along the wall (See Figure 5-4). Typically, when punching occurred, the plug would break at an angle from the top surface to approximately 4-8 inches below, forming a cone-shaped “failure surface” in that top region and then slide along the pipe wall after that (See Figure 5-4).

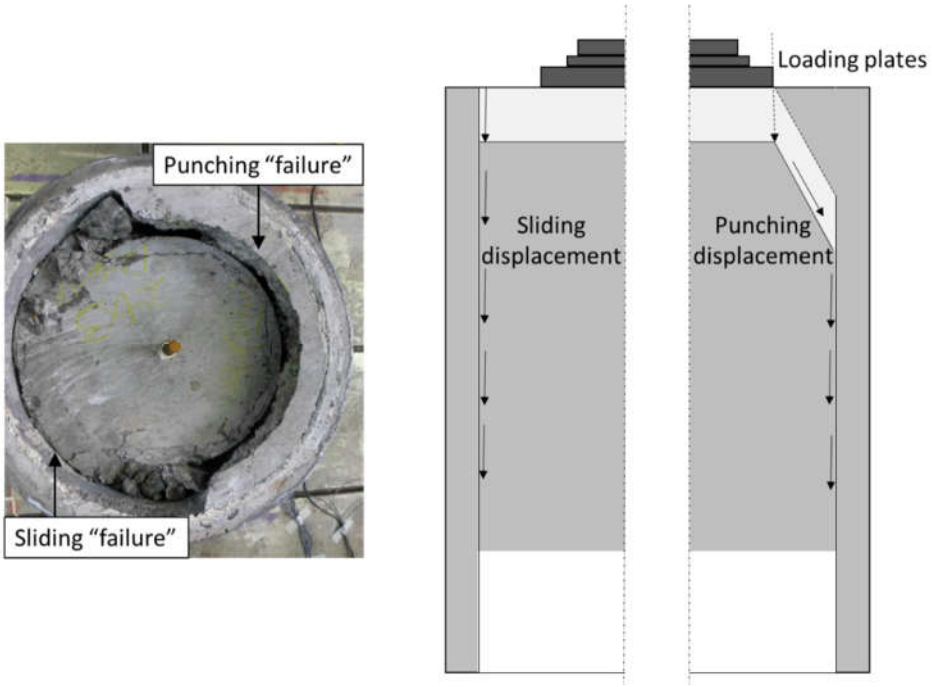

Figure 5-4. Typical final displacement of plug showing both "punching" and "sliding" (Taken from Test ep24f1-1), with sketch of specimen in section to show each type of displacement along wall

5.3 VISUAL OBSERVATIONS

This section summarizes the visual observations of each test. Pictures of the crack formation at peak load are compared as well as any damage that was specific to a particular test.

5.3.1 *Test ep24-1*

Test ep24-1 was intended to be the baseline test for comparison of all others (See Chapter 7, Table 4-1). This specimen was roughened with the epoxy mortar, had a 24-inches long plug, no jacket and was uncracked and concentrically loaded. It showed a combination of punching and sliding failure, similar to what is shown in Figure 5-4. A peak load of 430 kips was recorded, at which point vertical cracks formed around the specimen (See Figure 5-5). There were also some smaller horizontal and diagonal cracks on the eastern side of the specimen. The largest cracks measured approximately 0.25 inches at peak load. During the second stage of testing, the number and width of cracks did not increase very much. The load remained nearly constant during the second displacement-controlled stage of loading (See Figure 5-3).

In the sliding region, the failure occurred between the pipe wall and the epoxy, which remained firmly attached to the plug concrete. This was observed for all tests where epoxy mortar was applied.

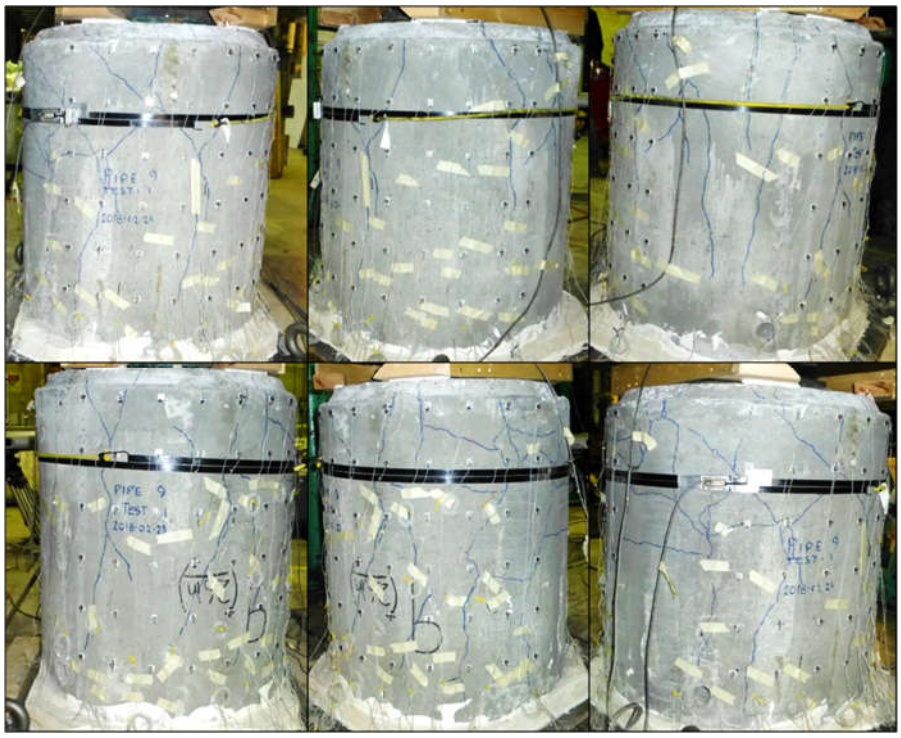

Figure 5-5. Crack formation at peak load for Test ep24-1 (L-R: N-NW-SW; S-SE-NE)

5.3.2 *Test ep24-2*

This test was done as a repeat of the first test that is, keeping all of the variable conditions the same in order to corroborate the results being used for the baseline condition. The peak load for this test was 320 kips, which is approximately 75% of that of test ep24-1, and the number of vertical cracks that formed around the specimen was less than that of the first test. Additionally, there was not a similar cluster of horizontal or diagonal cracks (See Figure 5-6). Unlike test ep21-1, all of the plug displacement was a result of sliding at the interface.

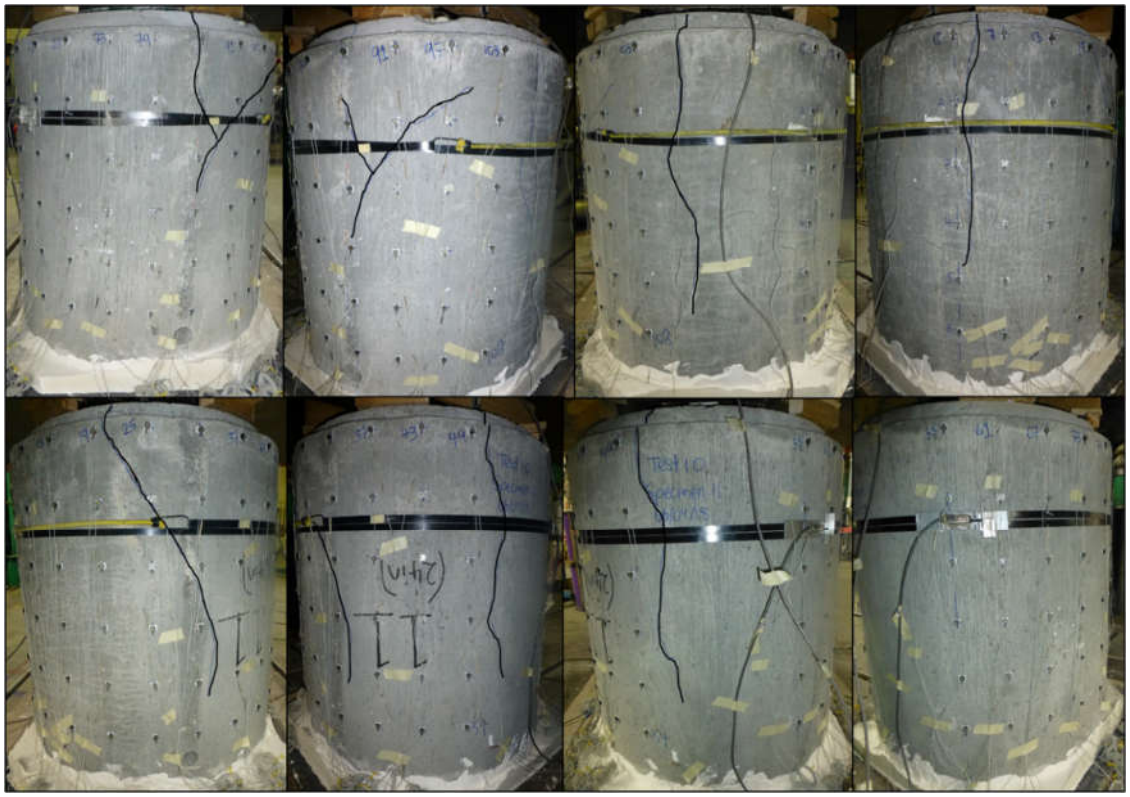
Figure 5-6. Crack formation at peak load for Test ep24-2 (L-R: N-NW-W-SW; S-SE-E-NE)

5.3.3 *Test ep0-1*

Test ep0-1 had a 24-inches long plug and the surface was not intentionally roughened with the epoxy mortar. It was amongst the few tests that showed a pure sliding displacement of the plug. The peak load recorded was 161 kips, much smaller than the baseline tests. At peak load, there were only 3 longitudinal cracks around the specimen (See Figure 5-7). The small number of vertical cracks, and the correspondingly low circumferential strain, suggested that the sliding surfaces were quite smooth, so little radial expansion was needed to allow the slip to occur. The low circumferential strain also suggests that the hoop force was relatively low, and hence, the normal force across the plug-wall interface must have been low as well.

Figure 5-7. Crack formation at peak load for Test ep0-1 (L-R: N-SW-SE-NE)

At the end of the test more cracks had formed around the specimen. In particular, a "horizontal" crack that spanned half of the circumference from the northeast to northwest side formed at approximately 20 inches from the top of the specimen, which is almost to the base of the plug (See Figure 5-8). The formation of these horizontal cracks is discussed in Section 5.5.

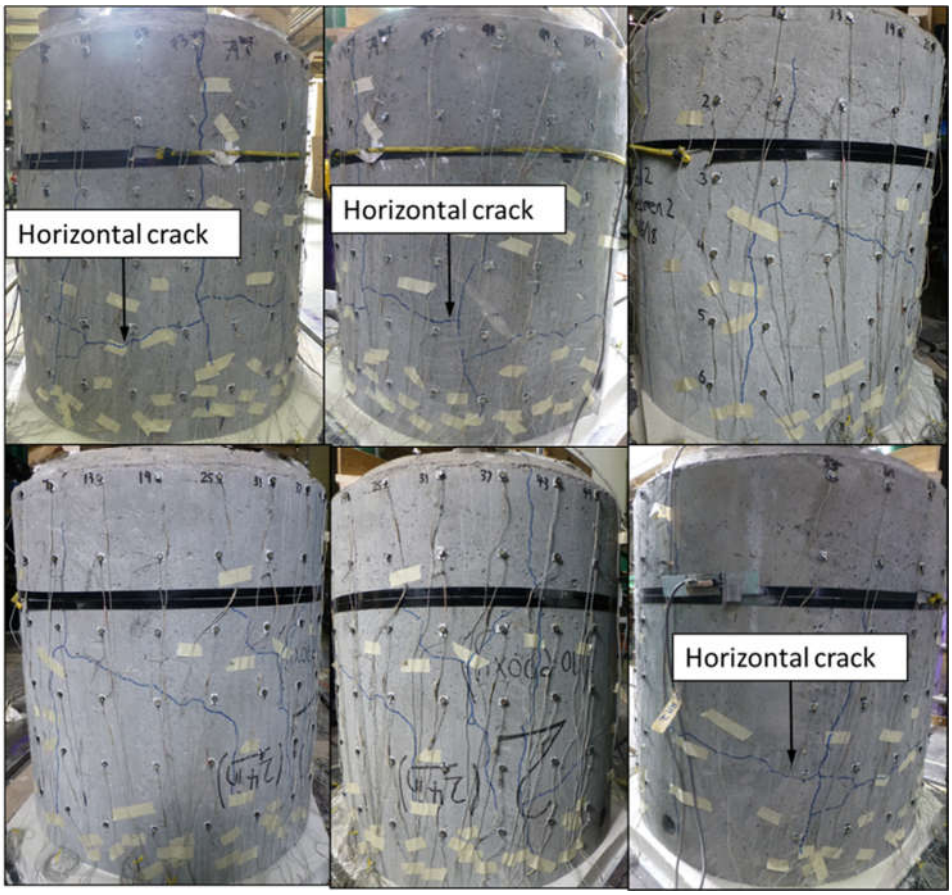

Figure 5-8. Crack formation at end of testing for Test ep0-1 (L-R: N-NW-SW; S-SE-NE)

5.3.4 *Test ep0-2*

This was a repeat of the previous test and similar results were observed. The peak load was recorded at 147 kips, less than 10% different from the companion test, and only 3 longitudinal cracks formed at this load (See Figure 5-9). Additionally, the plug displacement was only due to sliding along the interface (See Figure 5-10). At the end of testing some additional cracks had formed except there was no large-scale horizontal crack as in the former test.

Figure 5-9. Crack formation at peak load for Test ep0-2 (L-R: N-W-S-E)

Figure 5-10. Plan view of Test ep0-2 at end of test showing no "punching" displacement (Similar for tests ep0-1 and ep24-2)

From Sections 8.3.3 and 8.3.4 it can be said that the peak load which can be transferred through shear friction at the plug-column wall interface is significantly less (approximately 50%) when no epoxy mortar is present.

5.3.5 *Test ep18-1*

For this test, the inner plug was cast 18 inches deep instead of 24 inches deep, and the pipe wall was treated with epoxy mortar. The peak load was 364 kips at which point, many longitudinal cracks formed as well as a small number of little horizontal cracks. However, at the end of testing a large horizontal crack that spanned about 75% of the circumference was marked at approximately 18 inches from the top of the specimen (i.e. at the bottom of the plug) (See Figure 5-11).

Figure 5-11. Crack formation at end of testing for Test ep18-1 (L-R: N-NW-SW; S-SE-NE)

5.3.6 *Test ep14-1*

Similar to the previous test, this plug was cast at 14 inches deep, instead of the typical 24 inches. The peak load was 284 kips, which is less than that for the 24 inches and the 18 inches plug specimens. As observed for the previous experiment, at the end of testing a large horizontal crack was marked around the circumference at approximately 14 inches from the top of the specimen, that is, at the base of the plug (See Figure 5-12). For both tests with the shorter plug length, the large horizontal cracks appeared sometime during the second phase of testing.

Figure 5-12. Crack formation at end of testing for Test ep14-1 (L-R: N-NW-SW; S-SE-NE)

From the observations outlined in Sections 8.3.5 and 8.3.6, it can be concluded that the shorter plug length reduces the maximum load that can be transferred through shear friction. Additionally, the smaller plug-to-pipe length ratio appears to increase the effect of bending in the wall, as illustrated by the extent of horizontal cracking observed at the bottom of the plug in both tests compared to the baseline tests. This is further explained in Section 5.5.

5.3.7 *Test ep24-cr*

Test ep24-cr was done on the specimen that was previously cracked longitudinally (See Chapter 7, Section 4.2.2.5). The peak load for this test was surprisingly high at 306 kips, despite the cracks already present in the wall of the pipe. During testing, the existing cracks widened slightly and additional cracks formed around the specimen as seen in Figure 5-13. The plug displaced mainly due to interface sliding, however, some punching failure occurred on the east side of the specimen which also corresponds to the region where the most cracks formed (See Figure 5-14).

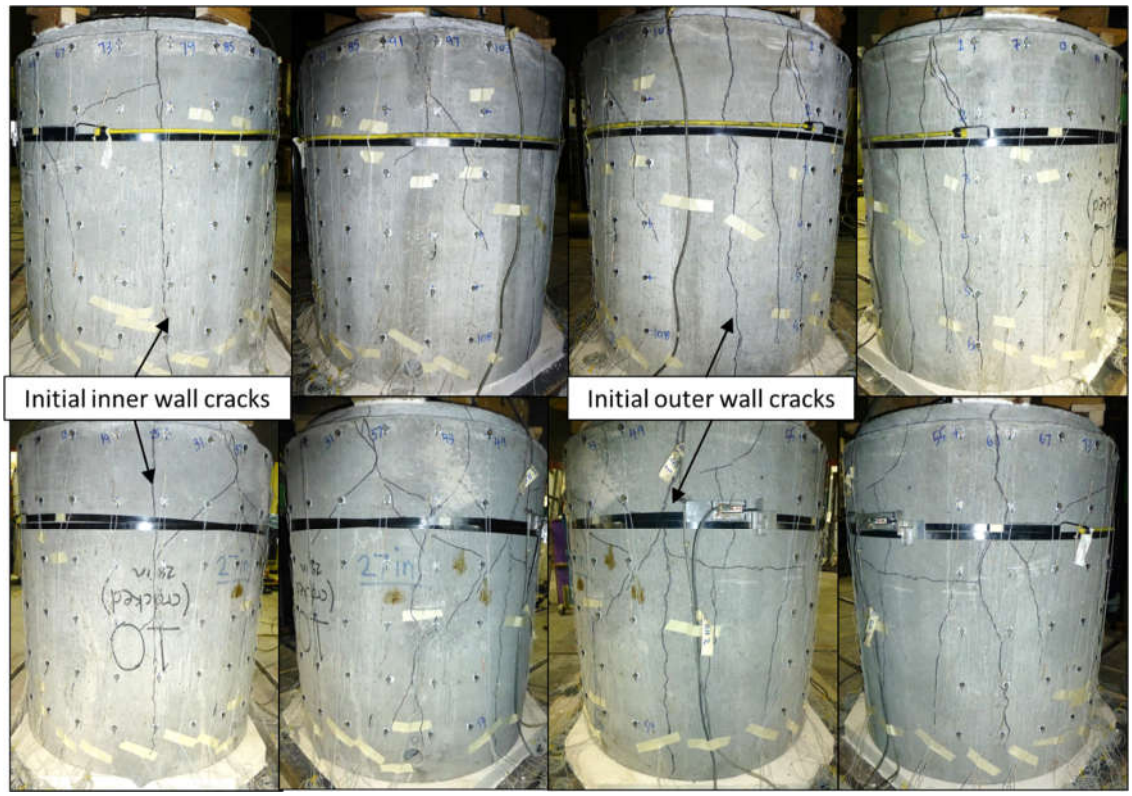

Figure 5-13. Crack Formation at Peak Load for Test 6-ep24-cr (L-R: N-NW-W-SW; S-SE-E-NE)

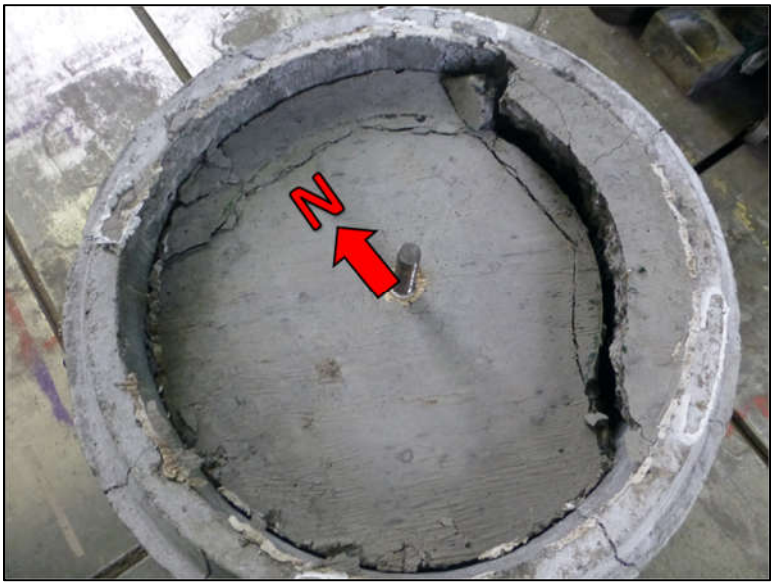

Figure 5-14. Plan View of Test 6-ep24-cr at end of test showing "punching" failure on east side of specimen

The AASHTO Specifications (2012) imply that the resistance to sliding comes from both cohesion and friction at the interface. The cracked pipe must be less stiff than the uncracked specimens, so the friction component was expected to be lower. The relatively high peak load suggests that either the inherent random variations between specimens were large, or that the resistance is in fact dominated by the cohesive component.

5.3.8 *Test ep24-ecc*

This specimen was similar to the baseline specimen, except that it was loaded eccentrically to evaluate the effects of bending moment, in addition to axial load, on the shear friction resistance. As expected, the peak strength under the eccentric load (recorded at 260 kips) was much lower than that achieved by the other specimens with an epoxied surface, but still higher than what was obtained from the smoother interface without any epoxy. A very large crack formed in the wall that measured more than 1 inch in width at the top of the specimen (See Figure 5-15 and Figure 5-16) and the spiral in that region had fractured along half of the wall height.

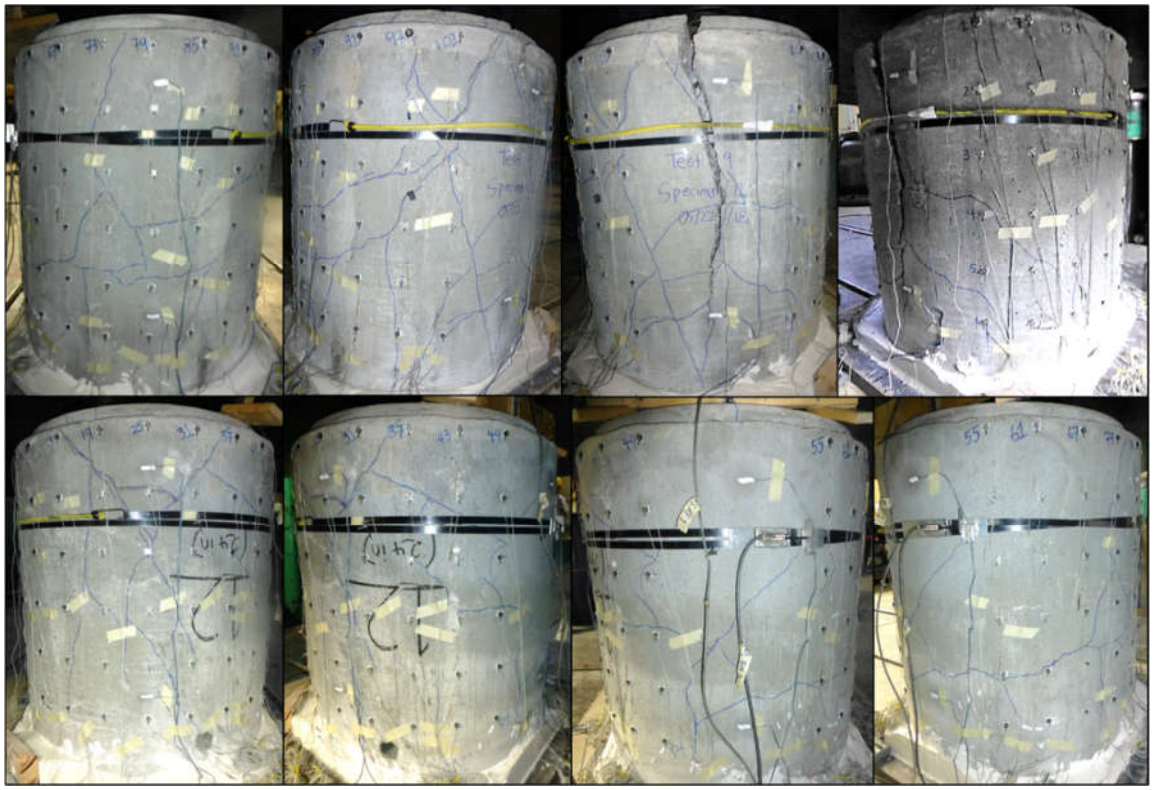

Figure 5-15. Crack formation at Peak Load for Test 9-ep24-ecc showing large crack on west side (L-R: N-NW-W-SW; S-SE-E-NE)

Figure 5-16. Width of large crack on west side of specimen (top to bottom)

5.3.9 *Tests ep24f1-1 and ep24f6-1*

These two tests were performed on the carbon fiber reinforced polymer (CFRP) jacketed specimens. Both tests showed a significant increase in the peak load over the baseline tests ep24-

1 and ep24-2. The 1-layer jacket almost doubled the peak load of ep24-1. The maximum load for ep24f1-1 was 806 kips and the maximum load for ep24f6-1 was 1046 kips.

The behavior after peak load differed significantly from that of the specimens without jackets. During the second stage of both tests, the residual load gradually decreased with increasing displacement whereas in all the previous tests, it had remained almost constant as displacement increased (See Figure 5-3). However, the residual load was still much higher than that of the unjacketed specimens.

5.3.10 *Test ep24s1-1*

Test ep24s4-1 was a "baseline" specimen jacketed in a rolled sheet of 16 gage galvanized steel with a 20 inch overlap that was sealed using PC-7® Paste Epoxy, a high-strength epoxy adhesive. As a result, the formation of cracks during testing could not be observed. However, since the jacket was so thin and sealed using an adhesive it was possible to pry it open and remove it from the concrete pipe at the end of testing, which allowed the observation of cracks that had formed by the end of the test (See Figure 5-17).

A large horizontal crack can be seen at about six inches from the top of the specimen. The overlap joint was also observed to have pulled apart at the top six inches of the jacket over a width of about five inches. The horizontal crack may have formed when the adhesive unstuck in that region thereby releasing the confinement relative to the region below, causing separation to occur.

Figure 5-17. Crack Formation at end of testing for Test ep24s1-1 (L-R: N-NW-W-SW; S-SE-E-NE)

Figure 5-18 shows the typical width of the cracks around the specimen (approximately 0.09 inches) alongside the gap that formed between the two steel faces of the jacket overlap. The gap is assumed to be the cause of the loss of stiffness before the peak load, that is, the small change in the slope near the top of the load-deflection curve, as shown in Figure 5-3.

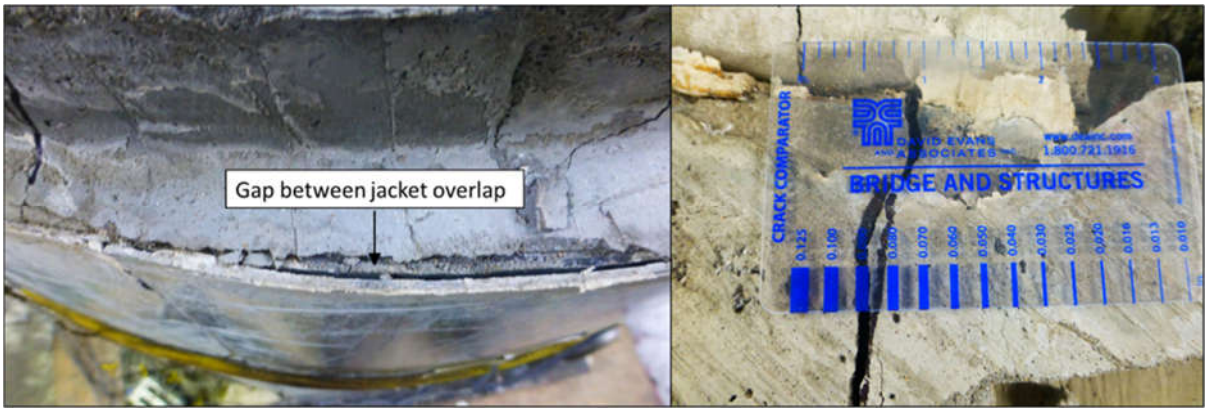

Figure 5-18. Observations at the end of Test 12-ep24s1-1 including gap opening and crack width at the top of the specimen

5.3.11 *Test ep24s4-1*

For this test the specimen was jacketed in ¼-inch thick, grade A36, steel jacket. Due to the steel jacket, the formation of cracks during testing could not be observed. However, at the end of the test, some longitudinal cracks as well as a horizontal crack that spanned 75% of the circumference were marked on the concrete below the jacket as shown in Figure 5-18. Additionally, while the specimen failed by punching under the load plates, the region of punching was much shallower than in other tests where this behavior was observed (See Figure 5-20). The length of plug that remained at the top of the specimen due to the conical punching was approximately two inches instead of the typical four to six inches seen for the other jacketed specimens.

Figure 5-19. Crack formation at end of testing for Test ep24s4-1 (L-R: N-NW-W-SW; S-SE-E-NE)

Figure 5-20. Plan View of Test ep24s4-1 at the end of testing showing "punching" displacement of plug

The steel jackets also appear to increase the peak load that can be obtained through shear friction interface transfer, similar to the CFRP jacketed specimens. However, the extensive horizontal cracking seen below the thicker steel jacket suggests that the sudden change of stiffness at the end of the jacket and plug can lead to higher bending stresses (discussed in Section 5.5) and this may be an issue if combined with a smaller plug-to-pile length ratio (that is, the effects of the shorter plug length).

5.4 Strain Calculations

This section illustrates how the measured data obtained from the Optotrak markers were used to calculate strains in the pipe wall or external jackets. Although strain gages were used on the jacketed specimens, the results from the Optotrak are used exclusively for data processing since the gage data was not always reliable. All measured data were filtered and smoothed for noise but the strains from test ep24-1 were discarded as the results were difficult to interpret even after these attempts were made.

The Optotrak markers were placed on the outside of the pipe wall around the circumference at 18 local points, and along the height of each specimen, in six circumferential layers (See Chapter 4, Figure 4-14). The positions of these markers were tracked in real-time using the Optotrak camera and the Cartesian coordinates of the markers were converted to polar coordinates in Matlab. From these positions (r,ϑ,z), the average hoop and vertical strains were found for the six discrete heights along the specimen.

5.4.1 *Determination of Average Vertical Strain, $\varepsilon_{v,z}$*

The average vertical strain $\varepsilon_{v,z}$ for each height along the specimen was found using the following procedure with reference to Figure 5-21. These strains represent the average strain around the circumference at mid-height between two consecutive rows of Optotrak markers.

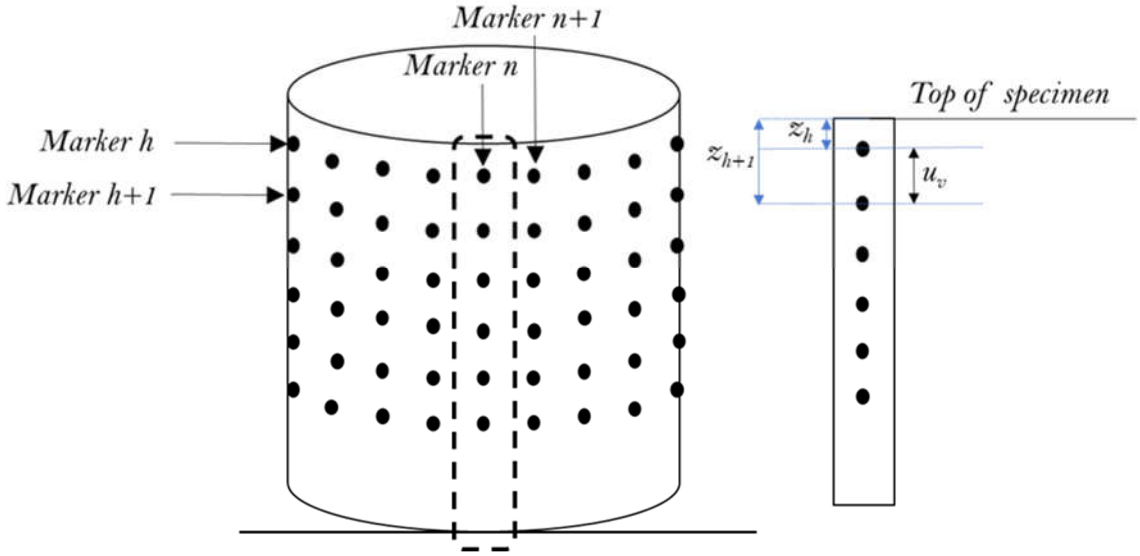

Figure 5-21. Vertical Strain Calculation Details

For each line of markers, *n,* around the circumference:

$$u_{v_i} = z_{h+1_i} - z_{h_i}$$

$$u_{v_{i+1}} = z_{h+1_{i+1}} - z_{h_{i+1}}$$

$$\Delta u_{v_i} = u_{v_{i+1}} - u_{v_i}$$

$$\varepsilon_{v_i} = \frac{\Delta u_{v_i}}{u_{v_i}}$$

$$\varepsilon_{v,z} = \frac{\sum_{n=1}^{N}(\varepsilon_{v_i})_n}{N}$$

$$N = total\ no.of\ markers\ around\ circumfernce\ of\ pipe = 18$$

$$i = time\ increment$$

5.4.2 *Determination of Average Hoop Strain, $\varepsilon_{h,z}$*

The average hoop strain $\varepsilon_{h,z}$ around the pipe was found for the six discrete locations along the height, z, using the following procedure, with reference to Figure 5-22.

$$\varepsilon_{h,z} = \frac{\sum_{n=1}^{N}\left(\frac{s_{i+1} - s_i}{s_i}\right)_n}{N}$$

$$N = total\ no.of\ markers\ around\ the\ pile = 18$$

$$i = time\ increment$$

$$s = r_{avg}d\theta$$

$$s_i = \left(\frac{r_{n+1} + r_n}{2}\right)_i * (\theta_{n+1} - \theta_n)_i$$

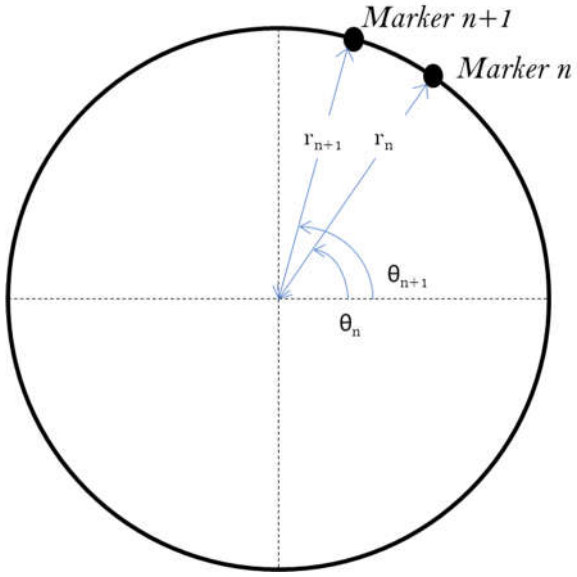

Figure 5-22. Hoop Strain Calculation Details

5.5 VERTICAL STRAINS

The vertical strain data were fairly scattered across all tests and this can be attributed to the differing crack patterns that were observed in that some specimens experienced horizontal and diagonal cracking while others did not. However, for particular tests, the vertical strains confirmed the presence of bending stresses occurring as a result of the normal pressure exerted by the plug on the pipe wall as it is displaced vertically. These are illustrated qualitatively in Figure 5-23.

For the plug to slide downward, it pushes against the pipe wall for it to expand outward. However, below the plug the radial pressure acting in the pipe wall is zero. Also, the base is fixed and cannot move. As a result of this uneven loading and the end condition, the displaced shape of the pipe

wall and the accompanying moments are as shown in Figure 5-23 which is derived from treating the wall as a thin cylindrical shell subject to a radial patch load. As can be seen, near the bottom of the plug, there is a tensile bending moment in the wall as a result of the curvature in the wall. If the bending strain from these moments becomes large enough, the concrete will crack horizontally, as observed.

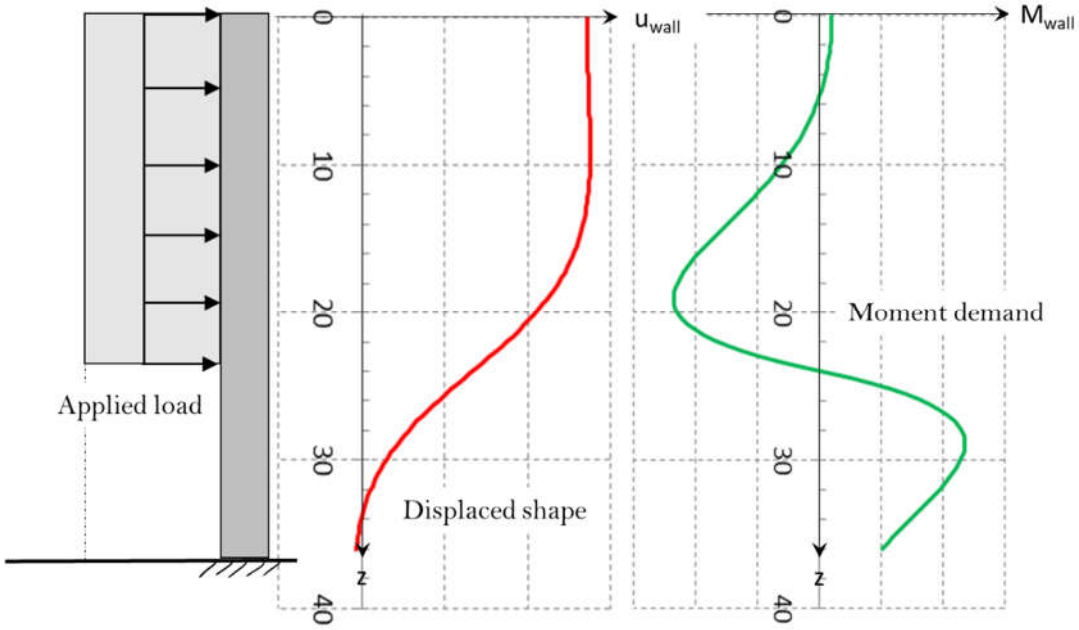

Figure 5-23. Displaced shape and bending moments due to normal pressure from plug

Looking at the vertical strain distributions at the residual load for ep0-1 and ep24s4-1 shown in Figure 5-24, the trend supports the postulation that there is compressive strain in the wall in the region of the plug and tensile strain about where the horizontal cracks were seen. The existence of vertical tensile strains at the height of horizontal cracking was found for all specimens where these cracks were seen.

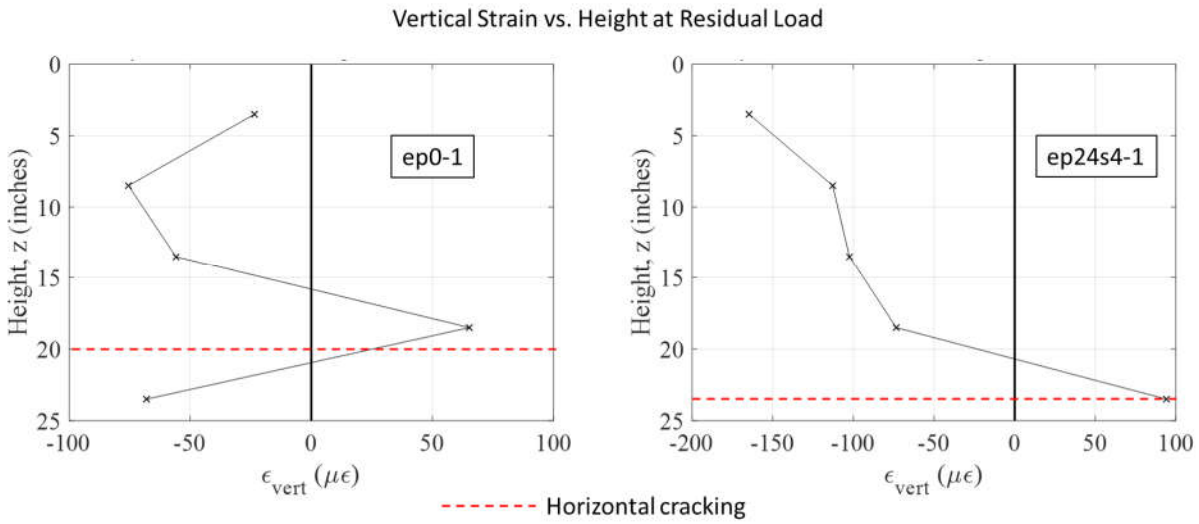

Figure 5-24. Distribution of Vertical strains at Residual Load showing Tensile and Compressive strains

5.6 HOOP STRAINS

The hoop strains provide a measure of the expansion of the pipe wall as the plug displaces vertically. The displacement of the plug is resisted by shear friction at the interface and this arises from the radial pressure of the plug, as described above for the bending stresses in the wall. The hoop strains will be used in Chapter 9 to evaluate the components of the shear friction strength at the interface.

Figure 5-25 shows the average hoop strain at each discrete height of measurement superimposed on the applied axial load, with time for the baseline test ep24-2. Before the peak load is reached, the hoop strains remain very small and relatively constant at each height. At the peak load there is a sudden increase in the hoop strain which corresponds to the formation of longitudinal cracks around the circumference. Additionally, the strains are highest at the top of the specimen and decrease along the height. During the residual phase of testing, the strains at the top of the specimen tend to remain constant or decrease with time (z = 1 inch and z = 6 inches) while the lower strains increase with time. These general trends were typical for all specimens.

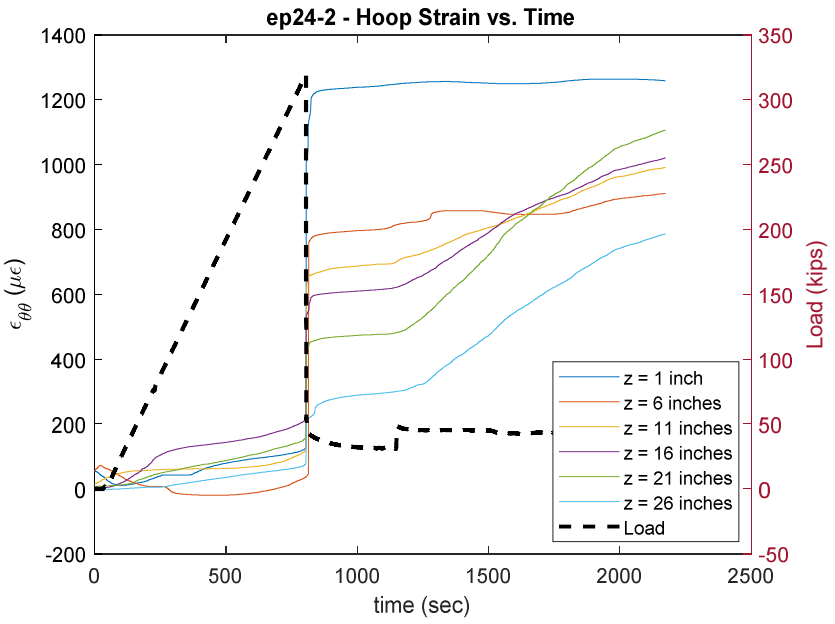

Figure 5-25. Hoop Strain vs. Time, with Axial Load for test ep24-2

The hoop strain distributions with height at peak and residual loads will be used in the following chapter to evaluate a shear friction interface transfer model, expressed in terms of cohesion and friction. Figure 5-26 and Figure 5-27 show the distribution at peak and residual load, respectively, for all tests.

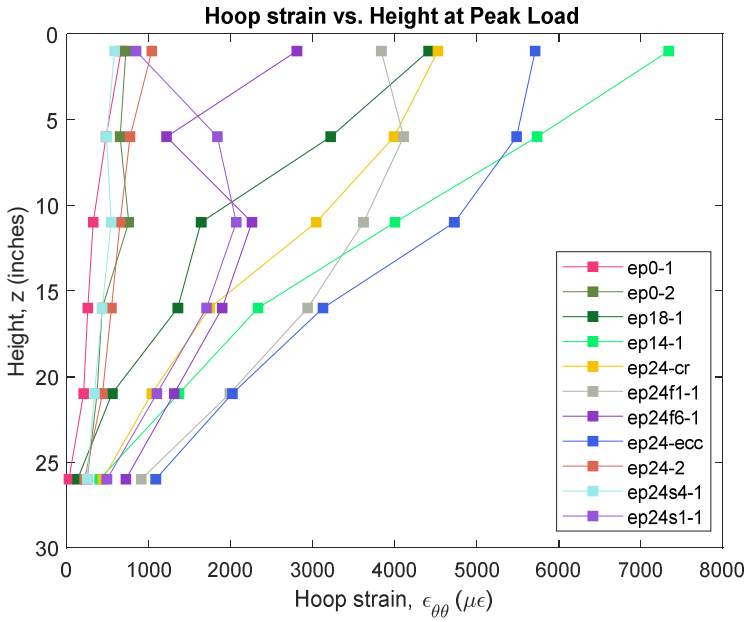

Figure 5-26. Hoop Strain Distribution with Height for all tests at Peak Load

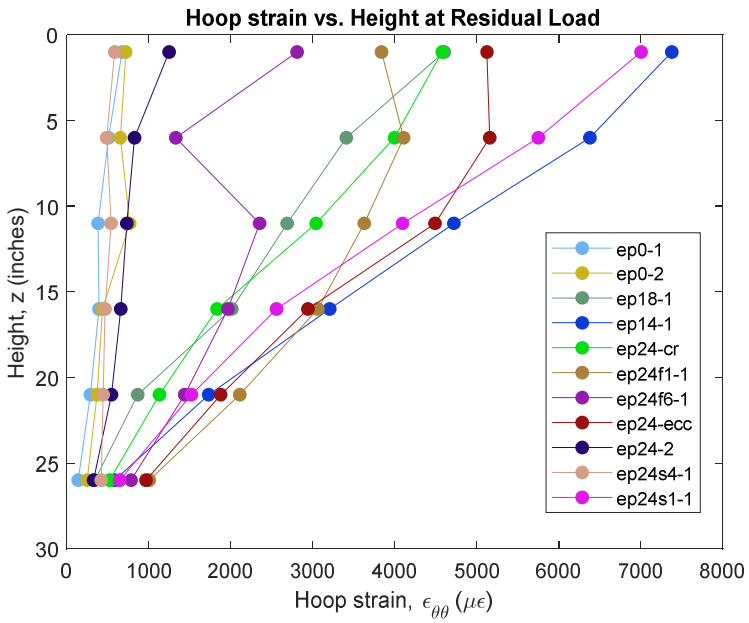

Figure 5-27. Hoop Strain Distribution with Height for all tests at Residual Load

Chapter 6. PLUG SHEAR FRICTION TEST ANALYSIS

6.1 INTRODUCTION

The plug tests were performed to gain insight into the axial behavior of the plug-hollow column assembly. Knowledge of that behavior is needed if the connection is to be retrofitted by cutting away part of the pile wall to create a ductile fuse. The behavior of interest is the potential for the plug to slide down inside the hollow column under gravity load.

The plug-to-column interface resistance to sliding was assumed to come from cohesion and friction, in accordance with the assumptions underlying the model for shear friction in Clause 5.8.4 of the AASHTO Specifications. Two cases were considered and modeled. In the first case, referred to as Model CR (cracked), the assumptions were:

- The plug has slipped through a small distance, so cohesion has been broken and friction alone provides the resistance to sliding.
- The WWF spiral steel has yielded.
- The jacket, if present, acts elastically and the hoop stress can be established from the measured hoop strains.

This model was used to investigate the "Residual Strength" recorded in the tests, that is, after the peak load was reached and slip of the plug had taken place.

For the second model, referred to as Model UN (uncracked), the assumptions were:

- Elastic behavior in the concrete column wall, the spiral, and the jacket where one existed.
- The column wall is treated as uncracked.
- All three materials contribute to the hoop tension force, and resistance to sliding is provided by both cohesion and friction.

The model was used to investigate conditions prior to the peak load, when neither slip nor cracking had been observed.

The major unknowns were the coefficient of friction, μ, the cohesion stress, c, and the hoop stresses to be expected under the two circumstances. The uncertainty in the hoop stresses arises because hoop strain is induced by radial expansion of the column wall which, in turn, is caused by one surface (the plug) riding over the protrusions of the other surface (the column wall). The magnitude of that radial displacement is unknown.

Cracked conditions were addressed first, because the hoop stress could be determined with less uncertainty, and because cohesion stress was assumed to be non-existent. The goal was to establish the friction coefficient from that analysis, and subsequently to treat it as a known quantity in the analysis of the uncracked conditions, from which the cohesion could be established. In the latter analyses, the hoop stresses would be assumed to be derivable from the measured strain data. While the friction coefficient may be different in the two phases of testing before and after peak load, the assumption of a constant coefficient of friction was deemed valid for the analysis using the measured and available data.

This approach is clearly not perfect, but was the best that could be adopted under the circumstances. The greatest limitation is the implied assumption that friction and cohesion both act in the uncracked system. This assumption underlies the shear friction model in the AASHTO specifications, but the literature on shear friction does not definitively support that view (see Davaadorj, 2018).

6.2 MODEL CR: POST-PEAK BEHAVIOR

Figure 6-1 shows the forces acting at the plug-wall interface, and their relationship to the hoop forces. Equilibrium for the half-cylinders requires that:

$$pD_{plug}L_{plug} = 2\{t_{sp}\sigma_{sp} + t_j\sigma_j\}L_{wall} \qquad (1)$$

where

p = radial stress in the plug concrete
D_{plug} = diameter of plug

L_{plug} = length of plug
t_{sp} = effective thickness of spiral reinforcement = A_{sp}/s
A_{sp} = area of spiral reinforcement
s = pitch of spiral reinforcement
σ_{sp} = hoop stress in spiral reinforcement
t_j = thickness of jacket
σ_j = hoop stress in external jacket
L_{wall} = length of wall of column

Because the structure is axisymmetric, the normal stress across the plug-wall interface is the same all around the circumference, in which case the total friction force, F_f is:

$$F_f = \mu p \pi D_{plug} L_{plug} \qquad (2)$$

If the hoop stresses in the spiral and jacket are known, μ can be determined from equations (1) and (2) and the measured friction force, F_f.

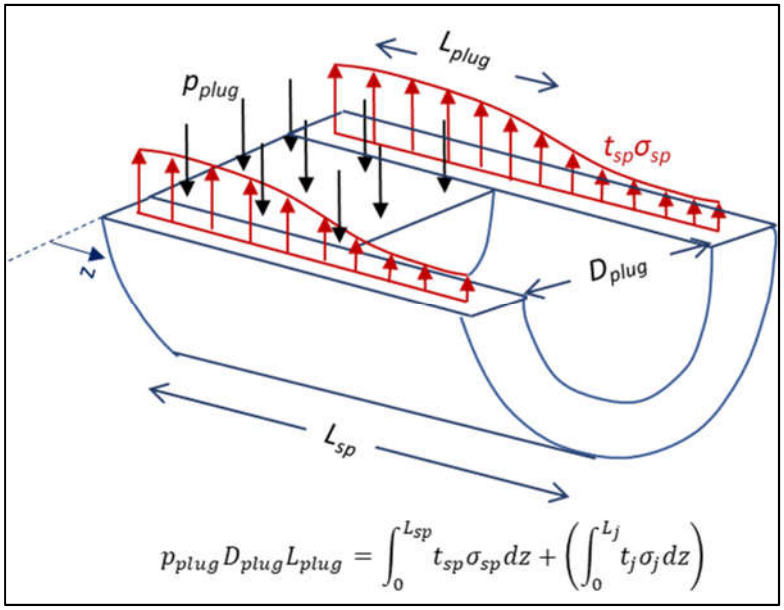

Figure 6-1. Forces acting at the plug wall interface

The hoop stresses in both the jacket and spiral likely varied along the column length, because the plug imposed radial force against the column wall only where it existed. The variation in jacket stress was established from the measured hoop strains in it, which remained elastic. Those hoop strains were obtained from the Optrotrak markers at different heights, $\varepsilon_{h,z}$, as described in Section

5.4.2. The average hoop strain $\varepsilon_{hoop,ave}$ for the specimen at each load increment can then be found by taking the arithmetic mean of the average hoop strains $\varepsilon_{h,z}$ along the height of the specimen. The corresponding stresses, obtained from Hooke's law were used in Equation 1.

The extent of variation in the stress in the spiral steel could be established with less certainty. The column wall was cracked. This was known because, in the specimens without jackets, cracks in the plug region could be seen and, in the jacketed specimens, cracks could be seen below the jacket, where no plug existed, implying cracks existed in the plug region as well.

For an average hoop strain of $\varepsilon_{hoop,ave}$ and n_{cr} cracks in the concrete around the circumference, the average crack width can be calculated as $\pi D_{wall}\,\varepsilon_{hoop,ave}/n_{cr}$. If the spacing around the circumference of the longitudinal wires of the spiral is s_{wire}, and the circumferential wires are assumed to be fully anchored at the wire intersections but not bonded in between, the local strain in the circumferential wires can be calculated as:

$$\epsilon_{sp} = \frac{\pi D_{wall}\varepsilon_{hoop,ave}}{s_{wire}n_{cr}} \qquad (3)$$

Equation 3 represents a lower bound to the strain in the spiral steel, because it ignores any bond to the concrete other than the anchorage provided by the cross-wires. An upper bound estimate of the spiral stress can be obtained by assuming a constant bond stress along the wire, equal to the bond stress implied by code development length equations. This leads to:

$$\epsilon_{sp} = \frac{\pi D_{wall}\varepsilon_{hoop,ave}}{L_d n_{cr}} \qquad (4)$$

For D2.1 wire with f_y = 65 ksi, in concrete with f'_c = 5000 psi, AASHTO LRFD (2012) gives L_d = 4.25 inches and ACI 318 (2014) gives L_d = 3.6 inches. Equations (3) and (4) are identical except for the s_{wire} or L_d term. The wire spacing s_{wire} was 8 inches, so Eqn (4) was used here with L_d taken as 4 inches. If the number of cracks is taken as 8, for example, Eqn (4) gives the spiral strain at a crack as approximately $3\varepsilon_{hoop,ave.}$ The spiral steel will thus yield when $\varepsilon_{hoop,ave}$ exceeds 722 με, assuming a yield strain of ε_y = 2167 με (E_{spiral} = 30000 ksi).

However, the number of longitudinal cracks varied for each specimen as seen in Chapter 8. To this end, Table 6-1 shows measured hoop strains for the non-jacketed specimens and Table 6-2 shows the strain in the spiral along the height of the non-jacketed specimens directly after the peak load, obtained using Equation 4. The average hoop strain, $\varepsilon_{hoop,ave}$ was taken from the strains measured on the jacket or column wall. In most cases, the spiral steel yielded directly after the wall cracked, as shown by the values highlighted in red where the calculated strain is greater than the yield strain.

In Table 6-2, there are some cases where the calculated spiral strains are less than yield strain indicating that the spiral did not yield. However, Equation 4 depends on the number of cracks around the wall to find the strain in the spiral. The number of cracks shown in Table 6-2 for each test was counted at the top of the specimen and they were observed to narrow or disappear along the height of the specimen so that a smaller number of cracks should be used to calculate the spiral strain toward the bottom of the specimen. By using the same number of cracks from z = 1 inch to z = 26 inches, the spiral strain may actually be underestimated at lower heights and lead to conservative values below yielding.

Table 6-1. Measured Hoop Strains at Peak Load for Non-Jacketed Specimens (με)

	ep24-2	**ep0-1**	**ep0-2**	**ep18-1**	**ep14-1**	**ep24-cr**	**ep24-ecc**
z = 1	1246.32	658.995	717.749	4600.049	7339.686	4805.577	5709.952
z = 6	814.430	477.518	648.299	3273.959	5734.052	4184.738	5485.313
z =11	668.268	322.102	755.320	2535.621	4002.08	3169.387	4725.901
z = 16	601.719	255.990	431.014	1853.165	2330.28	1843.386	3123.986
z = 21	456.618	203.451	367.344	842.661	1366.064	1153.692	2018.462
z = 26	262.129	23.741	247.651	285.704	398.396	465.478	1084.265

Table 6-2 Calculated Spiral Strains at Peak Load for Non-Jacketed Specimens (Eqn. 4) (με)

	ep24-2	ep0-1	ep0-2	ep18-1	ep14-1	ep24-cr	ep24-ecc
n_{cr}	3	3	8	9	10	8	5
	ε_sp	ε_sp	ε_sp	ε_sp	ε_sp	ε_sp	ε_sp
z = 1	5873.145	5175.738	5637.1863	13548.26	19215.25	11322.87	16817.2
z = 6	3837.915	3750.418	5091.727	9642.604	15011.71	9860.057	16155.58
z =11	3149.142	2529.785	5932.266	7468.019	10477.42	7467.693	13918.93
z = 16	2835.537	2010.543	3385.1757	5458.022	6100.658	4343.375	9200.898
z = 21	2151.765	1597.9	2885.1114	2481.843	3576.346	2718.322	5944.861
z = 26	1235.254	186.4679	1945.0497	841.47	1043	1096.756	3193.423

6.2.1 *Determination of Friction Coefficient, μ*

The forces acting on the column wall and the plug are shown in Figure 6-2.

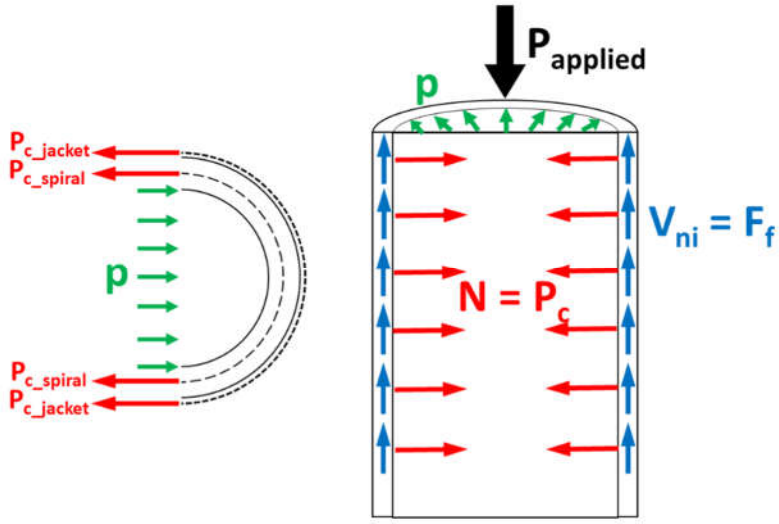

Figure 6-2. Force equilibrium during second phase of plug-push through test

Horizontal force equilibrium requires that:

$$2\left(\sigma_{sp}t_{sp}L_{sp} + \sigma_j t_j L_j\right) = pD_{plug}L_{plug} \qquad (5)$$

Vertical force equilibrium requires that:

$$F_f = \mu p \pi D_{plug} L_{plug} \qquad (6)$$

from which:

$$\mu = \frac{F_f}{p\pi D_{plug} L_{plug}} = \frac{F_f}{2\pi(\sigma_{sp} t_{sp} L_{sp} + \sigma_j t_j L_j)} \qquad (7)$$

In Equations (5) and (7), t_j = 0.0 if no jacket exists.

The spiral and jacket stresses were computed from the strains, accounting for the possibility of yielding. In the great majority of cases the spiral yielded but the jacket remained elastic.

6.2.1.1 Non-jacketed Specimens

For the non-jacketed specimens, Eq (7) reduces to

$$\mu = \frac{P_{residual}}{2\pi t_{sp} f_{sp} L_{sp}} \qquad (8)$$

Because the strain and stress in the spiral vary along the length of the specimen, the product $t_{sp} f_{sp} L_{sp}$ should be evaluated as the integral over the length of the specimen.

Table 6-3. Measured Hoop Strains at Residual Load for Non-Jacketed Specimens (με)

	ep24-2	**ep0-1**	**ep0-2**	**ep18-1**	**ep14-1**	**ep24-cr**	**ep24-ecc**
z = 1	1254.830	664.496	759.825	4685.011	7455.062	4620.864	5123.444
z = 6	832.418	508.292	833.700	3533.075	6382.437	3997.689	4971.672
z =11	725.664	369.178	865.064	2695.360	4730.464	3016.116	4412.646
z = 16	662.861	384.983	664.646	2018.188	3200.767	1836.953	2938.637
z = 21	527.683	272.549	419.106	869.246	1704.621	1145.500	1876.868
z = 26	326.577	130.894	290.275	354.525	564.298	503.103	964.651

Table 6-4. Spiral Strains at Residual Load for Non-Jacketed Specimens (Eqn. 4) (με)

	ep24-2	ep0-1	ep0-2	ep18-1	ep14-1	ep24-cr	ep24-ecc
n_{cr}	5	3	3	8	9	10	8
$P_{residual}$	45.54	61.47	59.37	65.94	106.60	76.89	53.11
	ε_sp	ε_sp	ε_sp	ε_sp	ε_sp	ε_sp	ε_sp
z = 1	5913.247	5218.938	5967.649	13798.5	19517.31	10887.65	15089.79
z = 6	3922.677	3992.116	6547.868	10405.76	16709.18	9419.333	14642.78
z =11	3419.613	2899.519	6794.194	7938.491	12384.33	7106.555	12996.31
z = 16	3123.658	3023.647	5220.12	5944.054	8379.587	4328.218	8655.002
z = 21	2486.649	2140.598	3291.651	2560.141	4462.688	2699.021	5527.833
z = 26	1538.958	1028.037	2279.811	1044.161	1477.33	1185.408	2841.133

At the residual load, the spiral had yielded throughout the specimen for most tests, as calculated by Equation 4 and shown in Table 6-4 in red. However, there are a few specimens where the strain in the spiral is less than the yield strain at z = 26 inches but still greater than half of the yield strain. Given the large scatter and uncertainty inherent in the data, this last value was ignored and the spiral was assumed to have yielded throughout the specimen, so that for all non-jacketed specimens Equation (8) could be simplified to:

$$\mu = \frac{P_{residual}}{2\pi t_{sp} f_y L_{sp}} \qquad (9)$$

This assumption of spiral yield throughout the specimen at the residual load introduces an error of no more than 8% into calculation of the friction coefficient.

Table 6-5 and Figure 6-3 show the friction coefficients obtained for the non-jacketed test specimens following the above analysis. These values are those obtained using a load $P_{residual}$ equal to that which caused the plug to displace an additional 0.75 inches vertically, beyond the initial displacement recorded at the peak load for each test. This value was used because the coefficient of friction remains almost constant in that range for all of these tests (See Figure 6-4).

One exception to this calculation is for the coefficient of friction of test ep24-ecc. The spiral in that test fractured at the peak load along half of its height. As such the length of the spiral in Equation 9 was taken as half of the specimen height or 18 inches.

Table 6-5. Coefficients of Friction, μ for Non-jacketed Specimens

Specimen ID	μ
ep24-2	0.2945
ep0-1	0.3978
ep0-2	0.3847
ep18-1	0.4275
ep14-1	0.6904
ep24-cr	0.4980
ep24-ecc	0.6880

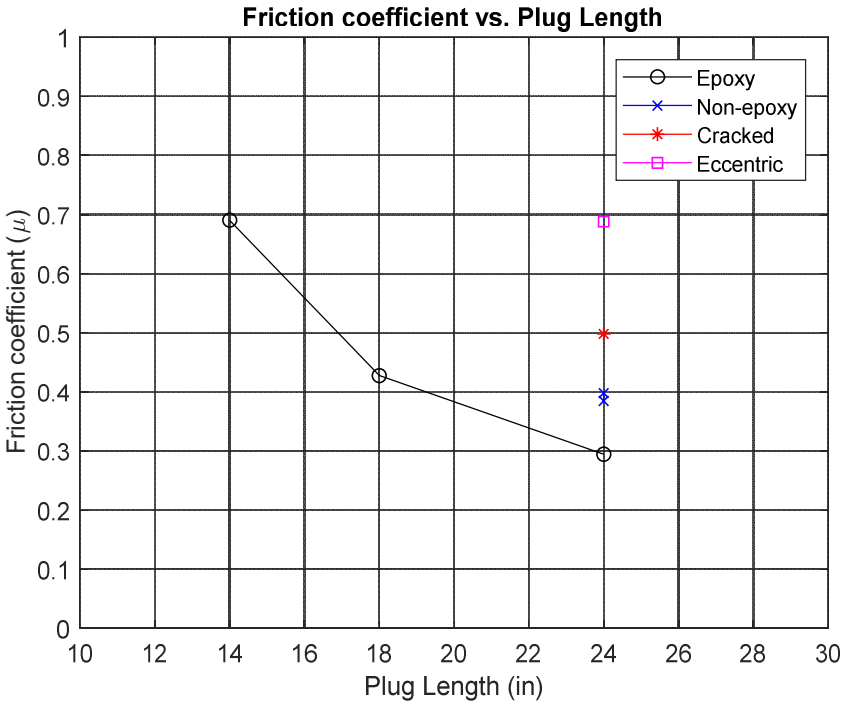

Figure 6-3. Friction coefficient vs. Plug Length for non-jacketed specimens

The results showed considerable scatter. Most were in a plausible range of 0.30 to 0.60 for a clean, smooth concrete-to-concrete interface (CEB-FIB Model 2010). The friction in the non-epoxy surfaces was similar to that of the baseline epoxy-coated surfaces. That finding is consistent with the fact that all the sliding was observed to occur at the inside of the pipe wall, regardless of the interface conditions. The inner surface of the pipe was relatively smooth, and the inner surface of the epoxy was deliberately made much rougher, so the fact that no sliding occurred between the epoxy and the plug was not unexpected.

If the inside surface of the field piles were as smooth as those of the pipes used in the tests, then the process of coating with epoxy mortar provided no benefits. However, it is possible, and even likely, that the surfaces of the field piles were rougher because they are believed to have been made using a different process. The riser pipes used for the plug tests were made (by Oldcastle Precast) in vertical steel models that were opened up for release of the product. The field piles of the 1960s, made by Concrete Technology Corporation, are believed to have been made using a movable mandrel inside a fixed circular cylindrical form. The mandrel moves longitudinally through the form as the concrete is deposited. This process requires a stiff mix to avoid collapse of the top of the annular pile. Experience in other plants that use the mandrel technique has shown that the stiff mix sometimes sticks to the mandrel, which then drags, or tears at, the surface of the concrete and leaves an inner surface rougher than that of the riser pipes. The method of manufacturing, and thus the surface roughness, are not known with certainty, but the outcome is that the surface of the field piles is likely to be as rough as, or rougher than, that of the riser used for testing. This implies that the friction coefficients found here are likely to be lower bounds to the values for the field piles.

The two outliers, ep14-1 and ep24-ecc, are difficult to explain. For ep24-ecc, a possible reason for the anomaly is the fracture of the spiral at peak load which would affect the radial clamping force used to calculate the coefficient of friction and perhaps, the reduction of the spiral length does not fully account for this difference. A reason for the higher coefficient of friction for the shorter plug length could not be given.

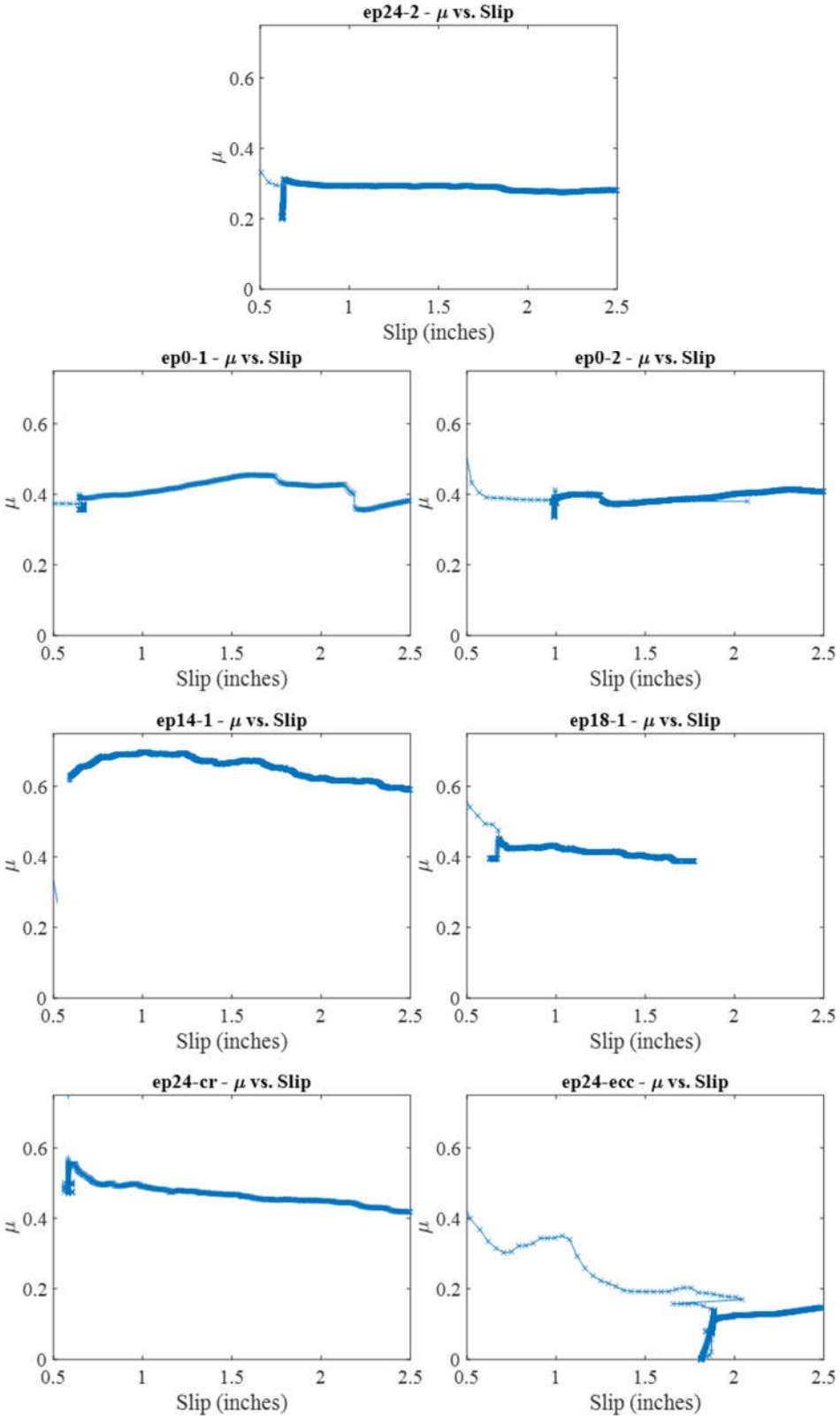

Figure 6-4. Friction coefficient vs. plug vertical slip for Non-jacketed specimens

6.2.1.2 Jacketed Specimens

For the jacketed specimens, both the spiral reinforcement and the jacket contribute to the hoop tension. Eqn. (7) can again be used to determine μ, but this time the jacket thickness is not zero, and the stresses in the spiral and jacket were both in the elastic range, so they must be determined by an elastic analysis that accounts for compatibility between layers. The main complexity is that the concrete was cracked longitudinally, but radially it was in compression and so was presumably not cracked. Therefore, the concrete wall has different elastic moduli in the radial and hoop directions, in which case the conventional thick-walled cylinder analysis is invalid.

The analysis was conducted using the stiffness method, in which the concrete has no stiffness circumferentially. The details are provided in Appendix C. Using this approach, for any measured hoop strain in the jacket, the hoop stresses in the jacket and spiral, and the normal pressure at the interface, p_z, could be computed. The coefficient of friction were then computed after integrating the normal pressure along the height of the specimen in order to get the total normal force acting to cause friction as in Equation 10. The results are summarized in Table 6-6.

$$\mu = \frac{F_f}{p\pi D_{plug} L_{plug}} = \frac{P_{residual}}{\pi D_{plug} \int p_z \, dz} \qquad (10)$$

Table 6-6. Measured Hoop Strains and Calculated Radial Pressures for Jacketed Specimens

	ep24f1-1		**ep24f6-1**		**ep24s4-1**		**ep24s1-1**	
	$\varepsilon_{h,z}$	**p_z (ksi)**	**$\varepsilon_{h,z}$**	**p_z (ksi)**	**$\varepsilon_{h,z}$**	**p_z (ksi)**	**$\varepsilon_{h,z}$**	**p_z (ksi)**
z = 1	4930.019	0.279	2914.913	0.844	689.268	0.453	7002.072	0.317
z = 6	4785.444	0.272	2269.777	0.670	537.962	0.353	5750.808	0.317
z =11	3751.294	0.226	2378.231	0.699	572.678	0.376	4095.416	0.317
z = 16	3069.495	0.195	2003.833	0.598	471.313	0.309	2550.017	0.317
z = 21	2095.596	0.151	1437.938	0.430	443.695	0.291	1506.717	0.282
z = 26	994.392	0.074	780.956	0.234	422.646	0.278	644.763	0.121
$\int p_z \, dz$ (k/in)		5.102		14.679		8.475		7.267

The above analysis was performed considering strain values throughout the residual phase of testing for each of the jacketed specimens. Figure 6-5 shows the coefficients of friction calculated against the vertical slip of the plug. It can be seen that the calculated coefficient of friction

decreases with time for all of the jacketed specimens, which makes sense on account of the interfaces presumably getting smoother as the plug slides downward. On the same figure, the μ values calculated at the residual load from the strains in Table 6-6 and the average μ for the residual phase are plotted for each test. While the two values are typically close to each other, the average values were taken to represent typical coefficients of friction since μ does not remain constant during the residual phase of loading, as was seen for the non-jacketed specimens. The values are all in the plausible range for concrete interfaces.

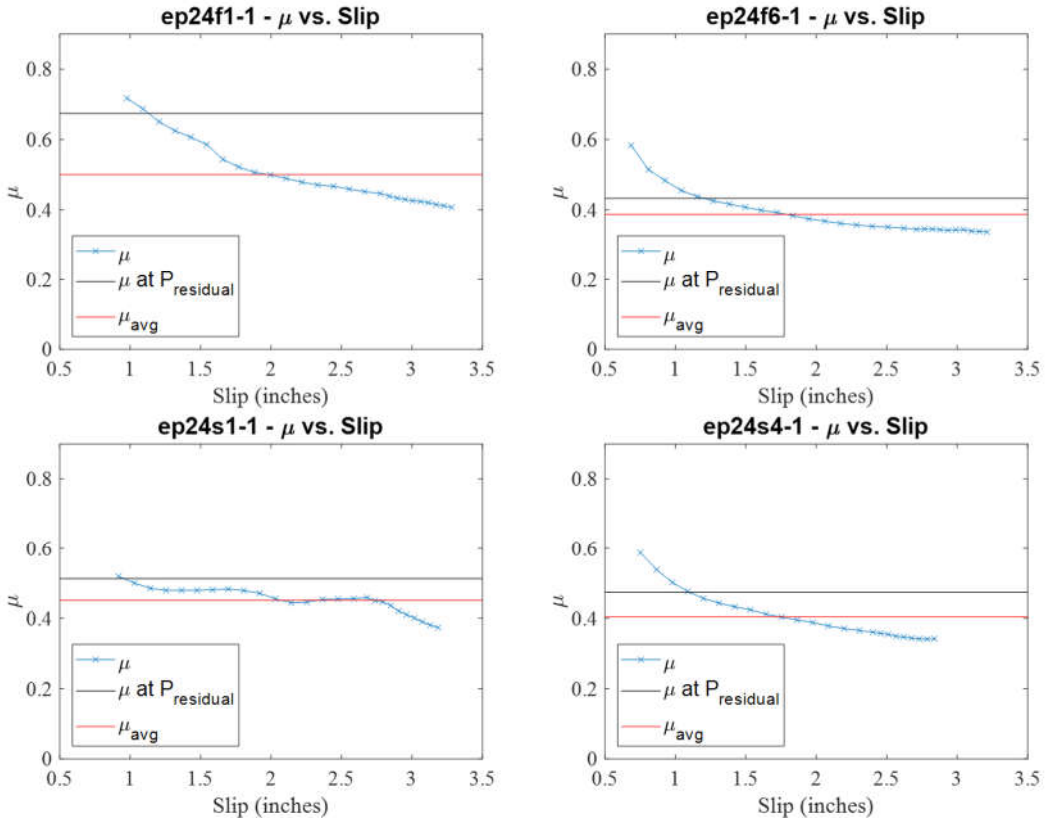

Figure 6-5. Friction coefficient vs. plug vertical slip for jacketed specimens

Table 6-7. Coefficients of Friction, μ for Jacketed Specimens

Specimen ID	μ
ep24f1-1	0.501
ep24f6-1	0.387
ep24s1-1	0.452
ep24s4-1	0.405

6.3 MODEL UN: PRE-PEAK BEHAVIOR

Model UN addresses conditions prior to cracking, and is based on the behavior of concentric thick-walled cylinders. At the interfaces, the radial displacements and stresses are the same for any two adjoining materials, which remain elastic. Plane stress conditions were considered whereby the cylinders undergo zero axial stress but non-zero axial strain from the applied load. Model UN is based on the following equation for the deformation, u, of a thick-walled cylinder subjected to both internal and external pressures (p_i and p_o, respectively).

$$u = \left(\frac{1-\nu}{E}\right)\left(\frac{r_i{}^2 p_i - r_o{}^2 p_o}{r_o{}^2 - r_i{}^2}\right) r + \left(\frac{1+\nu}{E}\right)\left(\frac{r_i{}^2 r_o{}^2 (p_i - p_o)}{(r_o{}^2 - r_i{}^2) r}\right) \tag{9}$$

The model was programmed into Excel whereby the system was divided into four concentric cylinders as shown in Figure 6-6 which were:

1. the concrete wall of the pile between the inner plug and the welded wire fabric reinforcement,
2. the welded wire fabric reinforcement treated as a cylinder of thickness $t_{sp} = A_s/s$,
3. the concrete wall of the pile between the welded wire fabric and the jacket, and
4. the external jacket (in the case of the unjacketed specimens, this cylinder was assigned zero thickness).

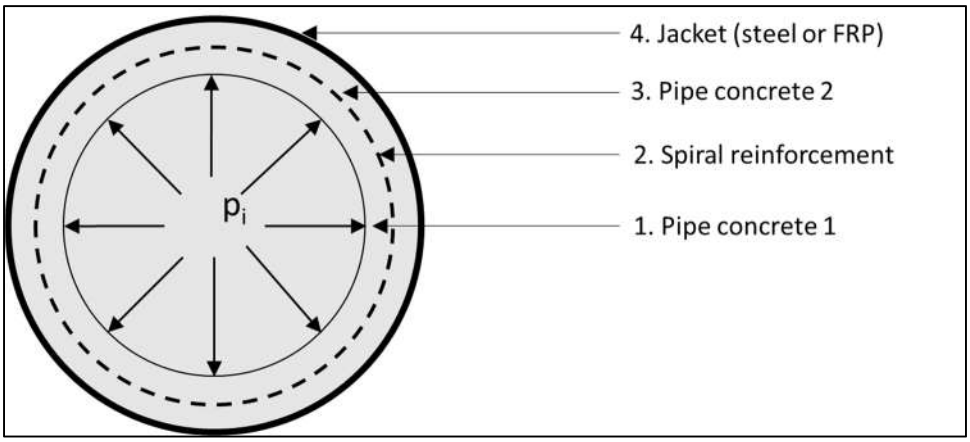

Figure 6-6. Layers of thick-walled concentric cylinders used in Model UN

Using Eqn (9), the radial displacements at the inner and outer surface of each cylinder, treated as an individual element, were related to the pressures acting at those surfaces through a flexibility

matrix. This was then inverted to find the stiffness matrix for each element and assembled to find the stiffness matrix of the concentric cylinder system. An arbitrary internal radial pressure, p_i was applied to the inner surface of the innermost cylinder and the stiffness matrix was used to find the radial displacement at each layer interface. The hoop and radial strains and stresses could then be obtained from the radial displacements. This is fully described in Appendix C.

The innermost surface was programmed as the surface between the plug and the pile wall, treating the epoxy as a part of the plug, and the hoop strain at the outside of the jacket layer was found. This analysis allowed a relationship between the outside hoop strain and the internal radial pressure to be established for the different jacket conditions in the form of an equivalent elastic stiffness value, K_{el} (See Table 6-8).

The one exception to using this analysis was for the pre-cracked specimen, ep24-cr. Since the concrete was cracked prior to testing then the assumption that the concrete remains elastic and has the same moduli in the radial and hoop direction is no longer valid. This case is the same as that of the jacketed specimens in Model CR but with a zero thickness jacket. Therefore the same stiffness method analysis was used to find a relationship between the inner radial pressure and the outer hoop strains, before the spiral yielded. This value is also given in Table 6-8.

Table 6-8. Equivalent Elastic Stiffness for Different Jacket Conditions using Thick-walled Cylinder analysis

Jacket Type	**Jacket thickness, t_j (in)**	**K_{el} (ksi)**
No jacket	0	1430
No jacket, cracked	0	29.167
1-layer Carbon Fiber	0.04	1480
6-layer Carbon Fiber	0.24	1720
1/16" thick steel	0.0625	2130
¼" thick steel	0.25	2630

The material properties used in the thick-walled cylinder analyses are given in Table 6-9.

Table 6-9. Material Properties used in Model UN analysis

Material Property	Concrete	Steel	Carbon Fiber
Young's Modulus, E (ksi)	5000	30000	13500
Poisson's ratio, ν	0.2	0.3	0.1

6.3.1 *Determination of Cohesion Factor, c*

To find the friction coefficient between the plug and the pipe wall, it was assumed that any cohesion was lost after the peak load was reached. However, before the peak load, some cohesion exists at the interface according to the AASHTO specification on shear friction interface transfer. Therefore, the peak load is in equilibrium with both the cohesion and friction that exists at the interface between the plug and pipe wall.

$$P_{peak} = cA_{cv} + \mu P_c \qquad (10)$$

Using the coefficients of friction found in the previous section, the cohesion factor for each test can be calculated using the Equations 11 for the non-jacketed and jacketed specimens, respectively.

$$c = \frac{P_i - \mu * (K_{el}\varepsilon_i \pi D_{plug} L_{plug})}{A_{cv}} \qquad (11)$$

Where

c = cohesion value (ksi)
P_i = load at increment, i in the pre-peak phase of loading
ε_{peak} = the average of the hoop strains along the height of the jacket, measured before peak load, when no cracking was observed
D_{plug} = diameter of plug
L_{plug} = length of plug
A_{cv} = see Eqn. 12

In both cases, A_{cv} is the area of concrete considered to be engaged in interface shear transfer which is the interface between the pipe wall and the inner plug.

$$A_{cv} = L_{plug} \cdot \pi d_i \qquad (12)$$

Table 6-10 shows the resultant cohesion values for all tests. These values represent the maximum cohesion that was calculated for all data in the pre-peak phase of loading. Typically the maximum

value was obtained at the peak load but, for a few tests, the cohesion was seen to drop significantly right before the maximum load was recorded. The researchers attribute this to the beginning of spiral yield or concrete cracking but the exact cause is unknown. Also, the cohesion values obtained for ep0-2 were very noisy and so the value for non-epoxy surfaces will be taken as that of ep0-1.

Table 6-10. Maximum cohesion stress obtained for all tests

Test ID	Cohesion, c (ksi)
Non-jacketed Specimens	
ep24-2	0.1351
ep0-1	0.0775
ep0-2	0.0495
ep18-1	0.2228
ep14-1	0.2139
ep24-cr	0.1678
ep24-ecc	0.1014
Jacketed Specimens	
ep24f1-1	0.3057
ep24f6-1	0.4147
ep24s1-1	0.2232
ep24s4-1	0.2622

The cohesion values are also very scattered and range between 101.4 and 414.7 psi. For the non-epoxy specimens, *c* can be taken as 0.078 ksi which is similar to that used for "*concrete placed against a clean concrete surface, free of laitance, but not intentionally roughened"* which is 0.075 ksi according to the AASHTO specifications. For the epoxy specimens with no jacket, there is considerable scatter in the data so a typical value is difficult to define. For specimens that are jacketed with steel, a cohesion value of 0.240 ksi can be used, regardless of the thickness of the jacket. This value is actually the same as the AASHTO-recommended value for "*concrete placed against a clean concrete surface, free of laitance, and intentionally roughened to an amplitude of 0.25 in"* although AASHTO does not consider external jacketing. For the CFRP-jacketed specimens, the values are considerably different which suggests that the number of layers used can affect the degree of cohesion but requires further investigation. However, these specimens

exhibited a marked increase in the peak load attained which can be attributed to increased cohesion before cracking.

6.4 SUMMARY OF RESULTS

A summary of the results of Model CR giving the coefficients of friction, and Model UN giving the cohesion values, for all considered tests is given in Table 6-11. The recommended values for each test according to the AASHTO LRFD Bridge Design Specification on interface shear friction are also presented.

Table 6-11. Summary of Coefficients of Friction and Cohesion Factors

Test ID	Test Program		AASHTO Specifications	
	Friction, μ	Cohesion, c (ksi)	Friction, μ	Cohesion, c (ksi)
Non-jacketed Specimens				
ep24-2	0.3	0.135	1	0.24
ep0-1	0.4	0.078	0.6	0.075
ep0-2	0.4	0.050	0.6	0.075
ep18-1	0.4	0.223	1	0.24
ep14-1	0.7	0.214	1	0.24
ep24-cr	0.5	0.168	1	0.24
ep24-ecc	0.7	0.101	1	0.24
Jacketed Specimens				
ep24f1-1	0.5	0.306	1	0.24
ep24f6-1	0.4	0.414	1	0.24
ep24s1-1	0.4	0.223	1	0.24
ep24s4-1	0.4	0.262	1	0.24

From these results, the following conclusions can be made:

- The coefficient of friction given by AASHTO is overall unconservative. Smaller values should be adopted and the test results suggest that a value of 0.4 is more appropriate. Two reasons why a lower value compared to AASHTO is plausible are:

    - The AASHTO coefficient of friction is also used to account for friction contributed by dowel action of steel crossing the shear interface of which there was none in these tests.
    - Sliding was observed between the pile wall and epoxy interface for those specimens with epoxy, suggesting that the controlling surface roughness was that of the smooth pile wall. This also explains the similarity between coefficients of friction for the epoxy and non-epoxy surfaces.
- The cohesion component of the shear friction model benefitted from the application of the epoxy mortar since the cohesion values for the non-epoxy surfaces were the lowest of all calculated values.
- The cohesion value calculated for the non-epoxy tests was basically the same as that suggested by AASHTO for surfaces that are "not intentionally roughened", that is, c = 0.075 ksi.
- The cohesion component of the shear friction model also benefitted from the external jacketing as the values obtained for all of the jacketed specimens were higher than those of the non-jacketed specimens. The extent of this benefit cannot be explicitly defined given the scatter in the test results.
- The influence of the epoxy mortar on the cohesion at the pile wall-plug interface cannot be quantified as the results for these specimens are very variable. It would seem that without an accurate and repeatable standard to follow regarding the application of mortar to the surface, a standard μ and c cannot be established.

6.5 Application to Field Conditions

The foregoing results can be used to predict the shear friction capacity of the bridge columns to transfer the expected axial loads from the superstructure to the hollow pile along the interface of the plug and pile wall, if the retrofit involves cutting back the pile wall.

For these predictions, the μ factor was taken as 0.4. Two values of cohesion were evaluated for the following cases:

1. The lower bound case, considering no epoxy or an unroughened surface with c = 75 psi
2. The upper bound case, considering an external fiber jacket with c = 350 psi

The area of cohesion A_{cv} was calculated using the inner diameter of the bridge piles and the typical plug length less 6 inches (representing an arbitrary cut back length for the "plug fuse retrofit") for each bridge. The normal force for friction, P_c was calculated as in Equation 11 with ε_i roughly estimated as the average of all the measured strains just before the peak load for all specimens, as given in Table 6-12. The dimensions and elastic properties for each bridge are given in Table 6-13. The equivalent elastic stiffness values K_{el} were calculated using the thick-walled cylinder analysis from Model UN.

Table 6-12. Measured Hoop Strains before Peak Load (με)

	z = 1	**z = 6**	**z = 11**	**z = 16**	**z = 21**	**z = 26**
ep0-1	-0.001	1.904	3.903	34.204	51.647	18.882
ep0-1	38.666	157.232	98.113	54.472	58.565	49.226
ep18-1	133.588	171.479	76.643	149.198	64.101	33.096
ep14-1	-118.228	198.389	393.294	226.137	129.637	19.621
ep24-cr	146.841	242.138	44.864	98.945	73.170	-65.309
ep24f1-1	1.254	137.631	111.772	165.073	295.039	198.390
ep24f6-1	0.552	145.100	453.228	466.327	554.399	427.037
ep24-ecc	55.912	76.589	46.226	114.492	-16.387	7.762
ep24-2	122.072	34.278	114.222	210.570	153.789	73.082
ep24s4-1	516.096	483.821	539.220	383.955	334.740	301.690
ep24s1-1	494.616	1278.284	1552.814	1384.904	965.424	454.490
Average	230.650					

Table 6-13. Typical Dimensions and Elastic Properties used in Shear Friction Capacity Analysis

Dimension	Ravenna Boulevard	Galer-Lakeview	Le Line/Slide	Green River
D_{plug} (in)	38	38	44	44
L_{plug} (in), typ.	50	51	52	60
A_{sp} (in^2)	0.054	0.054	0.054	0.054
s (in)	3	6	2	2
E_{conc} (ksi)	4000	4000	4000	4000
Lower Bound K_{el} (ksi)	1150	1125	1050	1050
Upper Bound K_{el} (ksi)	1300	1280	1125	1125

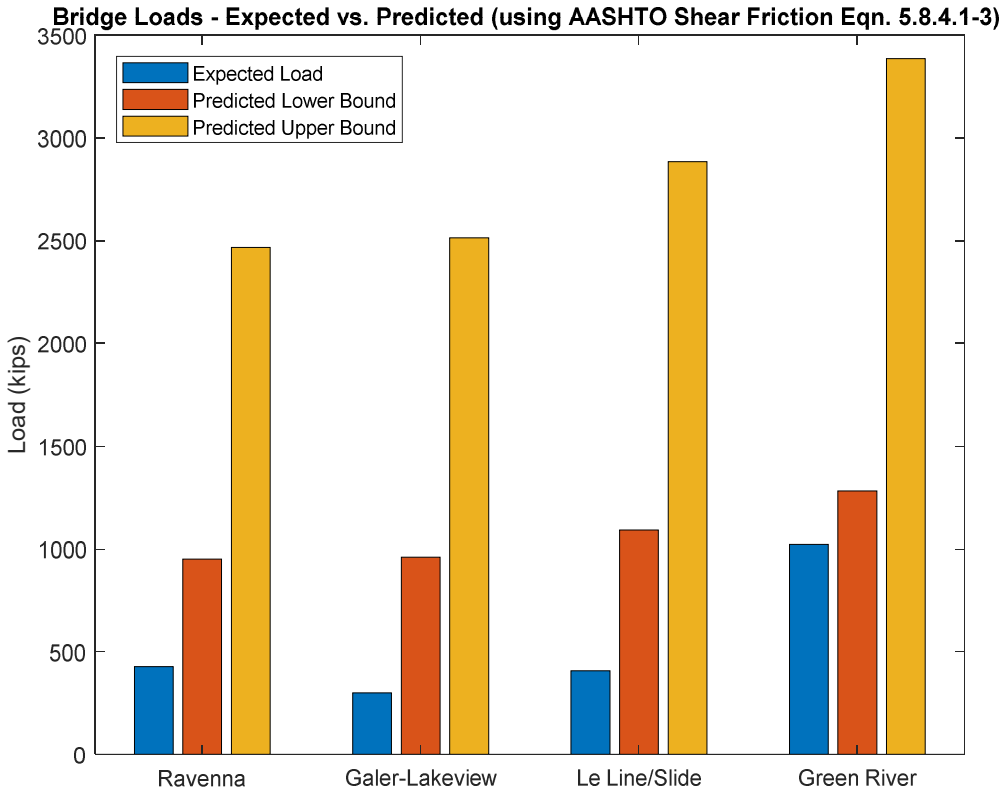

Figure 6-7. Expected Demand vs. Predicted Shear Friction Capacity for Reference Bridges

Figure 6-7 clearly shows that even for the lower bound case, considering no intentional roughening of the pile wall-plug interface, the expected dead load demand is much smaller than the predicted shear friction transfer capacity. This suggests that if the wall of the pile were cut back over a short distance below the cap beam, the columns would be able to transfer the axial load safely without the risk of plug slip occurring.

Chapter 7. COLUMN BENDING DESIGN

7.1 INTRODUCTION

In the past, there have been few studies that investigate the flexural strength of hollow core concrete column-piles. In order to provide an effective seismic retrofit solution to WSDOT, the research team planned to perform a test of a scaled model of an existing column. However, upon inspection of the bridges under investigation it was found that no two bridges were completely alike, making a true scale model of an existing column not possible. Therefore, to evaluate the behavior of the hollow core concrete column-piles themselves, the researchers chose to modify the design of the specimen to mitigate other potential failure modes. This chapter will describe the factors affecting the design of the specimen and the experimental set-up so that a flexural failure in the column itself was produced.

7.1.1 *Design Prototype*

Based on the differences between all the bridges that were found and described in previous chapters, the researchers consulted with WSDOT regarding how to proceed with testing a model of the as-built conditions (See Figure 7-1). After discussions with WSDOT and review of the construction drawings, it was decided to test a pre-tensioned hollow pile to accommodate the state's retrofit schedule.

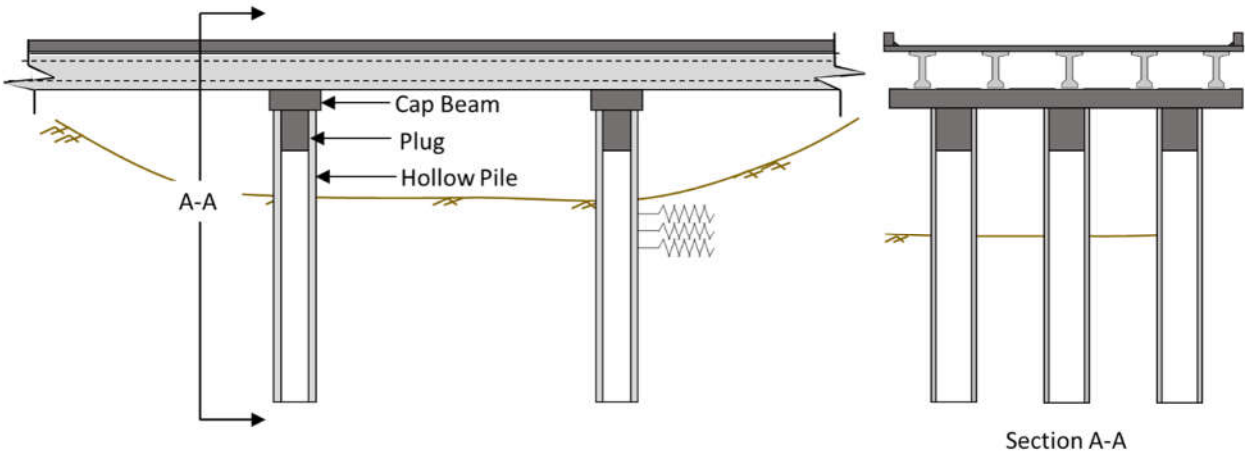

Figure 7-1. Sketch of Field Prototype Conditions

7.2 TESTING CONSIDERATIONS

When designing a model specimen to study the behavior of larger structures, it is important that it is both an accurate representation of the overall structure and has the greatest research breadth while using the fewest testing resources (A. Jellin, 2008). To understand the behavior of the pile above ground, particularly at the column-cap beam connection under seismic loading, the structure can be modelled by placing a lateral load at the predicted point of inflection along the length of the pile. However, it should be noted that since the lengths of piles varied greatly among the bents of all bridges, the length from the cap beam-column interface to the point of inflection L_{inf} also varies. For this reason, L_{inf} was chosen based on the scale factor of the model and the limitations of the test rig.

The column-pile specimens were manufactured by Concrete Technology Corporation in Tacoma, Washington who were also the manufacturers of the post-tensioned piles on the Ravenna Bridge and the pre-tensioned piles on the Slide Bridge and the Green River Bridge. Concrete Technology already had a circular column form of diameter 36 inches so, in order to save time and cost, this was chosen as the outer diameter of the test column. This diameter gives a 3/4 scale ratio to the 48" post-tensioned piles in the Ravenna Bridge and a 2/3 scale ratio to the 54" pre-tensioned piles used elsewhere. Originally, the team was tasked with investigating the post-tensioned piles and had designed the whole specimen based on a 3/4 scale linear factor. When the decision was made to evaluate the pre-tensioned piles of Green River and Slide bridges, the design ratio for the column and reinforcement was changed to accommodate the new appropriate 2/3 scale factor but all other dimensions remained the same, based on the Ravenna and Galer-Lakeview.

Some minor adjustments had to be made to the aforementioned scale to account for the equipment being used. Firstly, due to the capacity of the lifting crane in the lab, the length of the cap beam had to be restricted to 8 feet between supports which is only a 0.44 scale of the prototype between columns. As a result of this, the shear reinforcement in the cap beam was also increased by using a tighter spacing to deal with the higher shear force caused by the shorter shear span. Secondly, the length to the inflection point L_{inf} was determined by the maximum height of the horizontal actuator on the test rig and was taken as approximately 108 inches, or 3.0 column diameters, above

the cap beam. This choice constrains the moment that can be generated in the hollow section beyond the plug. There were, however, no other viable options that would fit within the time, resources and budget of the project.

7.3 SPECIMEN DESIGN

The overall dimensions of the test specimens used in this study are shown in Figure 7-2.

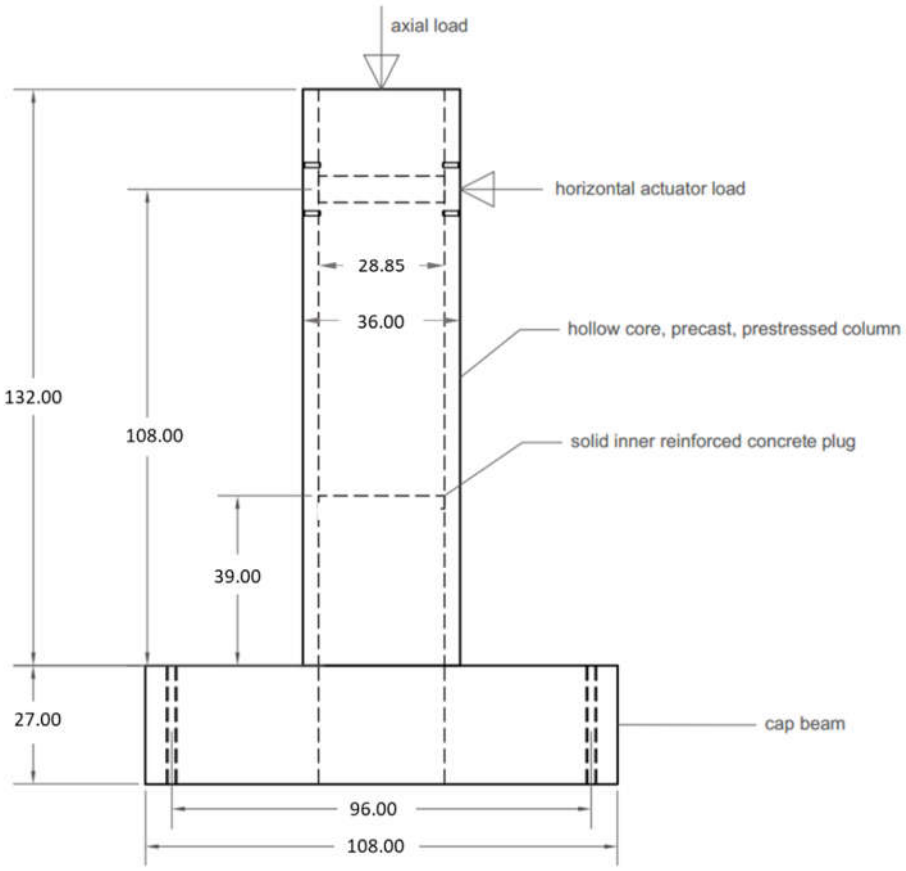

Figure 7-2. Overall Specimen Dimensions (all dimensions given in inches)

As described in the previous section, most of the dimensions related to the column specimen are based on a 2/3 scale factor to the pre-tensioned 54-inch diameter piles. The column dimensions are shown in Figure 7-3 and Figure 7-4. It was 11 feet tall with a 36-inches outer diameter and a 28.85-inches inner diameter, leaving a wall thickness of 3.575 inches. The internal diameter was constrained by the sizes of sonotube form commercially available. The column prestressing was achieved using thirty-two ⅜-inch diameter, 270 ksi, low-relaxation strands pre-tensioned to 16

kips each. The column had spiral reinforcing of #7 gage cold-drawn wire, at a center to center pitch of 3.5 inches along the length except at the very top where there were 5 turns of wire at a 1.25-inch pitch.

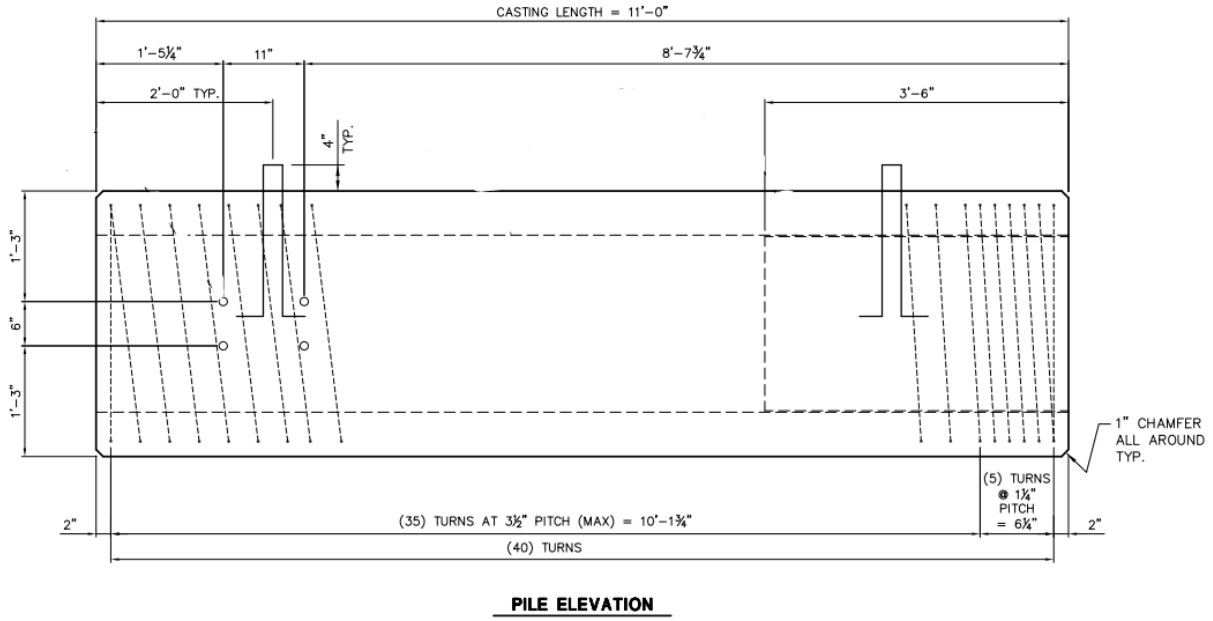

Figure 7-3. Elevation of Column, showing dimensions (courtesy of Concrete Technology Corporation)

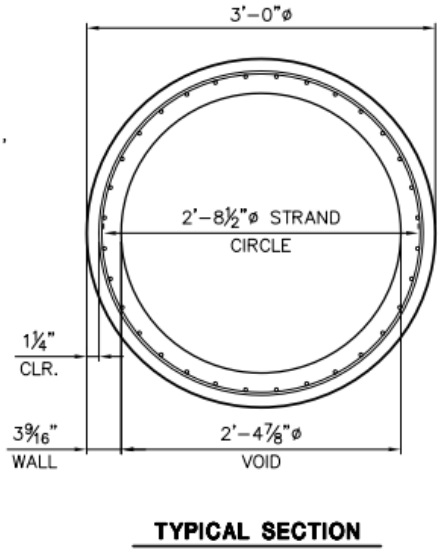

Figure 7-4. Cross-section view of test pile, showing dimensions (courtesy of Concrete Technology Corporation)

On the existing bridges, there is a solid concrete plug that extends between four and five feet into the core of each column from the cap beam-column interface, and it is reinforced with longitudinal bars that extend into the full depth of the cap beam. For the test, the plug was designed in order to maintain a length of plug to diameter of plug ratio that is similar to what exists on the bridges (See Table 7-1). The average L/D ratio of the plug on the existing bridges was approximately 1.34, ignoring that of Le Line Slide which was much lower than the others. A plug length of 39 inches was chosen for the specimen design (by rounding to the nearest inch), given that the diameter of the plug was nominally 28.85 inches.

Table 7-1. Length to Diameter Ratios of Column Plug

Reference Bridge	Length of plug (typ.) (in)	Diameter of Plug (in)	L/D
Ravenna Overcrossing	50 inches	38 inches	1.32
Galer-Lakeview	51 inches	38 inches	1.34
Le Line Slide	52 inches	44 inches	1.18
Green River	60 inches	44 inches	1.36
Average L/D ratio = 1.34			
Test Specimen	38.66 inches	28.85 inches	1.34

The longitudinal reinforcement for the plug was designed so that the ratio of the moment capacities of the plug to the column were similar to that of the field conditions and the bars were fully developed (See Table 7-2).

Table 7-2. Moment Capacities of Reference Bridge Columns

Reference Bridge	M_{n_plug} (in-kip)	M_{n_hollow} (in-kip)	M_{n_plug}/M_{n_hollow}	M_{n_filled} (in-kip)	M_{n_plug}/M_{n_filled}
Ravenna Overcrossing	17296	25779	0.67	23180	0.75
Galer-Lakeview	16022	26164	0.61	21231	0.75
Le Line Slide	33616	42149	0.80	44039	0.76
Green River	37677	43254	0.87	50670	0.74
Average Ratio			0.74		0.75
Test Specimen	9656	12121	0.80	13253	0.73

The moment capacities in Table 7-2 were calculated as follows:

- M_{n_plug} – The moment capacity of the inner plug, ignoring the outer pile concrete and prestressed strands.
- M_{n_hollow} – The moment capacity of the hollow column only, considering the prestressed strands as the reinforcement.
- M_{n_filled} – The moment capacity of the combined column and plug ("filled") section, using the nominal strength of the hollow column concrete and considering the plug reinforcement only (ignoring the prestressed strands, which are discontinuous at the cap beam).

Since there was high variability in the M_{n_plug}/M_{n_hollow} ratio, the plug reinforcement of the specimen was designed to match the M_{n_plug}/M_{n_filled} ratio as closely as possible. As such, sixteen #8 bars were used with a 180 degree hook on the end that extends into cap beam and a straight end on the other side which imitated the worst-case condition that exists for any of the bridges, particularly the Le Line Slide bridge (See Figure 7-5 and Figure 7-6). Hoop ties made of #3 rebar were spaced at 6.5-inch centers around the plug reinforcement. These were most likely used in the past for construction purposes but were included in the test specimen in case of any contribution to confinement of the plug concrete.

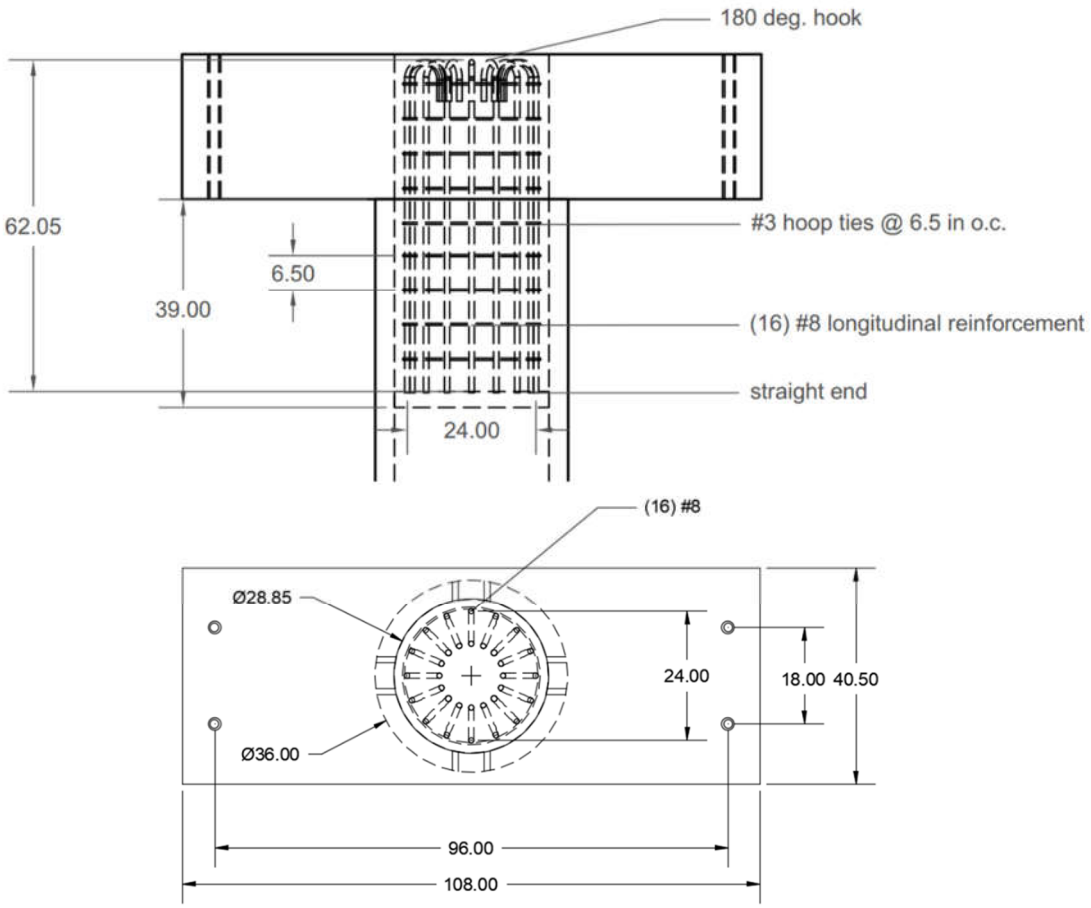

Figure 7-5. Plug Dimensions and Reinforcement

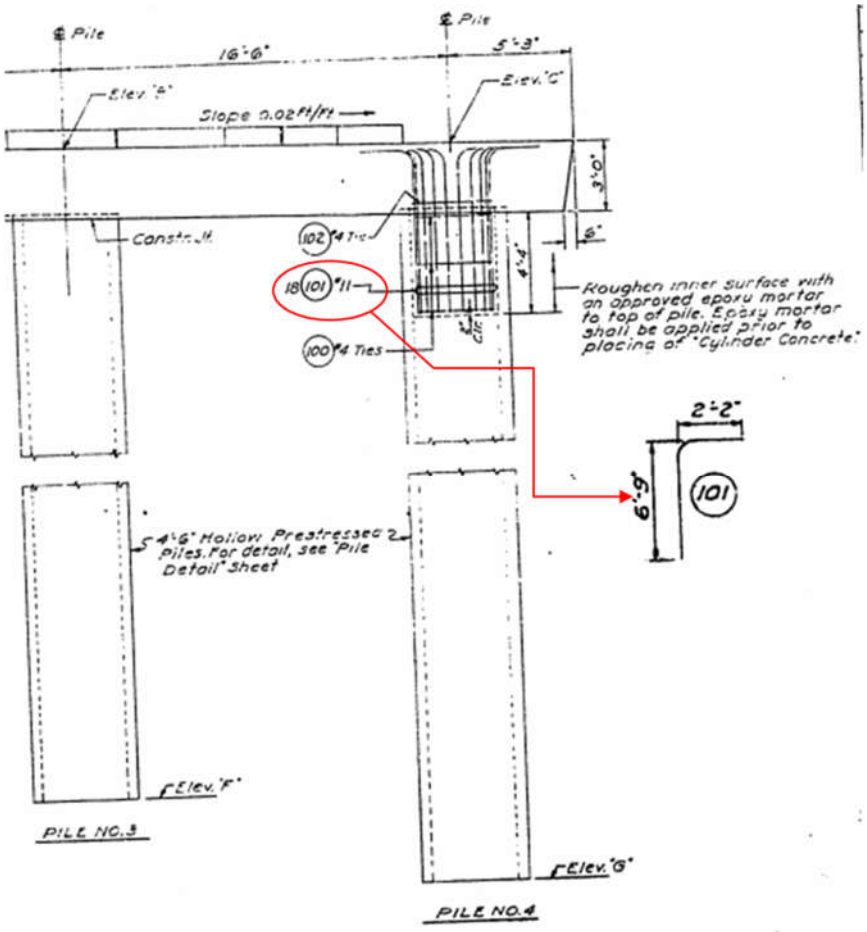

Figure 7-6. Plug Reinforcement Details for Le Line Slide Bridge

The last main component of the specimen design is the cap beam (See Figure 7-7). While all effort was made to design the cap beam to a 2/3 scale like the column and plug, restrictions existed due to the size of the testing equipment. The cross-section area and reinforcement was designed to the same scale but the length of the beam and the amount of shear reinforcement included was changed to accommodate testing conditions. The length of the cap beam was shortened to 8 feet between supports, that is, between points of zero bending moment, and the shear reinforcement spacing remained constant throughout the length of the beam on either side of the column-beam joint instead of increasing, as is shown on plans for the existing bridges. This was to account for the increased shear demand over the shorter span of the cap beam.

The tension reinforcement was designed so that the moment capacity of the cap beam during testing was 25% greater than the expected demand at the face of the column, given the predicted

ultimate moment capacity of the column. This was done to provide capacity protection for the cap beam and ensure failure in the column. The compression reinforcement was designed to be 2/3 of the area of tension reinforcement which was similar to what was used in the cap beams of the prototype bridges. As such, the cap beam cross-sectional rebar consisted of ten #8 bars at the bottom and eight #8 bars at the top. The shear reinforcement was a six-legged stirrup made of #5 bars and implemented via one large outer and two smaller inner rectangles (See Figure 7-7). The rebar layout modeled the current field conditions except for some top and bottom bars which were displaced slightly to avoid congestion and to accommodate hold-down anchor rods for the test. It should be noted that although there is no joint shear reinforcement in any of the existing bridges, this was included in the specimen design in order to capacity-protect the cap beam and ensure a failure in the column. The joint shear reinforcement consisted of two layers of #6 rebar, 30 inches long with 6-inch long 90-degree hooks on either end, placed approximately 7 inches apart along the cross-section of the cap beam within the region defined by the plug reinforcement (See Figure 7-7).

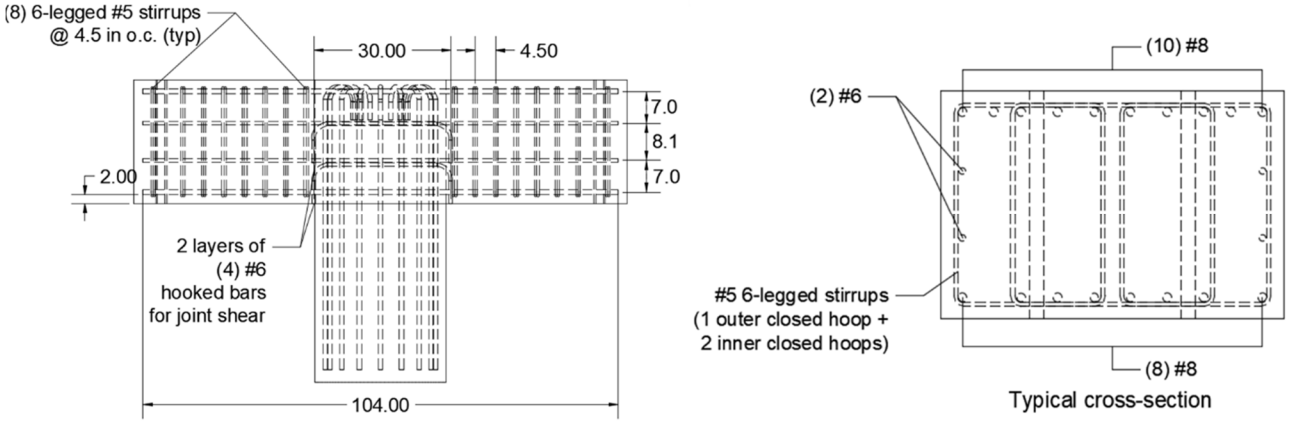

Figure 7-7. Cap Beam Dimensions and Reinforcement

7.3.1 *Materials*

The cap beam and column plug were both cast-in-place on site during construction of the reference bridges with lower strength concrete than that of the piles. The concrete used was Class A concrete with a specified strength of 4000 psi. For the test specimen, concrete with a nominal strength of 5,000 psi was used for these components to simulate the expected present-day strength of the

concrete on the bridges. The rebar for the cap beam and plug were ordered from ASTM A615 Grade 60 stock.

The columns on the existing bridges were typically specified to be constructed using concrete with a 28-day strength of 6,000 psi which suggests that the columns would have an approximate present-day strength of 8,000 psi using a 1.3 factor for increase in strength over time (Caltrans Seismic Design Criteria). Self-consolidating concrete with a 28-day nominal strength of 9,000 psi was used for the columns in order to ensure good consolidation in the narrow walls.

7.4 SPECIMEN CONSTRUCTION

The precast, prestressed hollow core columns were constructed at Concrete Technology Corporation's facility in Tacoma, Washington. At the plant, the column was cast using a 36-inches diameter steel tube for the outer form and a 28.85-inches outside diameter Sonovoid® Round concrete void form (sonotube) capped with plywood to create the hollow core (See Figures 8 and 9). The sonotube was used because a steel inner form was unavailable. The column specimens were line cast so that three were fabricated at the same time (See Figure 7-8).

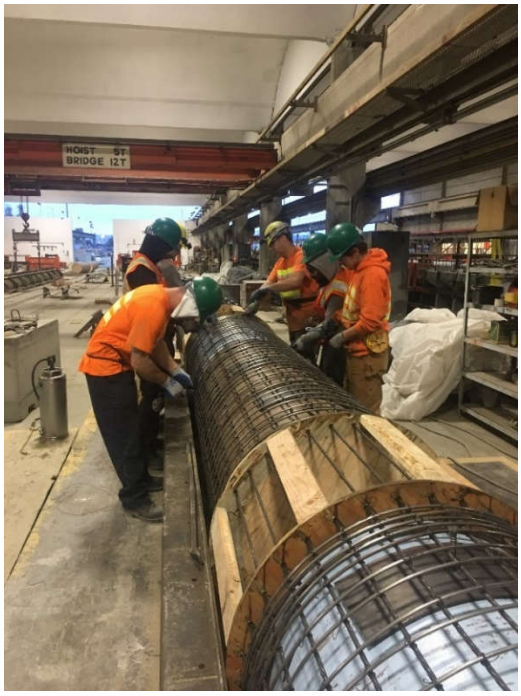

Figure 7-8. Column reinforcement being prepared for casting at Concrete Technology Corporation

Figure 7-9. Sonovoid® Round concrete void forms

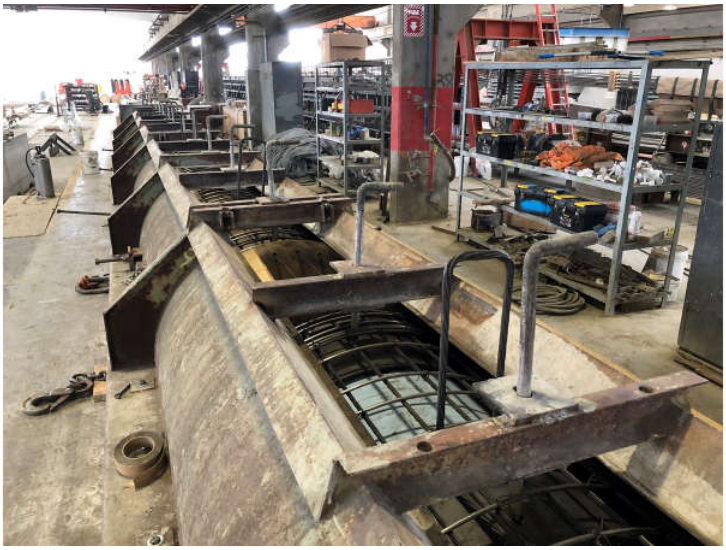

Figure 7-10. Column formwork ready to be line-cast at Concrete Technology Corporation

In order to prevent the sonotube from floating up during the concrete casting, curved steel plates attached with lag screws were used at discrete locations along the top length of the form (See Figure 7-11). The plates were 8" wide oriented along the length of the column by 14" circumferentially and were placed at 1'-3" on center. Some additional spiral was also used around the sonotube at discrete locations for construction purposes. These additions are important to note but are not believed to affect the failure conditions observed later.

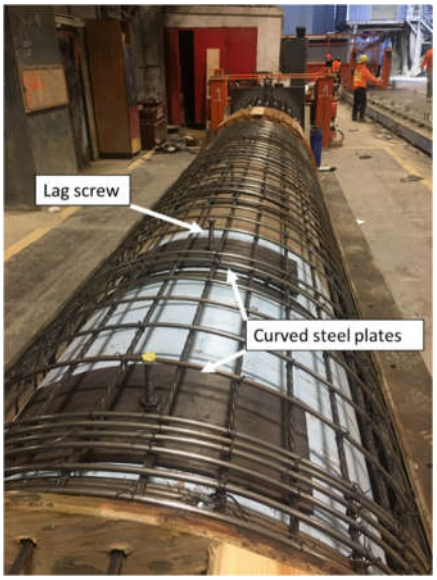

Figure 7-11. Hold-down plates used for sonotube during casting

In order to create an inner surface roughness similar to what may have been caused by mandrel-casting used in the past, especially in the region where the plug would be cast, a retarder (Euro-Tard 05) was applied to the surface of the sonotube before casting. When the sonotube was later removed, this gave the inner surface a sandblasted roughness (See Figure 7-12). After the columns were cast in a line, the strands were cut flush when the concrete had obtained a compressive strength of at least 5,000 psi although cylinder tests indicate strengths greater than 6,500 psi in all cases.

Figure 7-12. Comparison of surface roughness after removal of sonotube, with and without retardant

The remainder of each specimen was constructed in the Structural Research Laboratory at the University of Washington. To remove the need for the construction of temporary shoring in the lab, the specimens were constructed upside down so that the columns were connected to the cap beams while the cap beams rested on the floor. In this regard, the construction sequence did not follow what was done in the field where the cap beam forms were hung from the upright piles and poured after the piles had been placed and driven.

Firstly, the cap beam formwork was constructed using sheets of 0.75-inch thick CDX plywood sheathing and SPF 2x4 Premium #2 & Better Grade Kiln dried studs (See Figure 7-13).

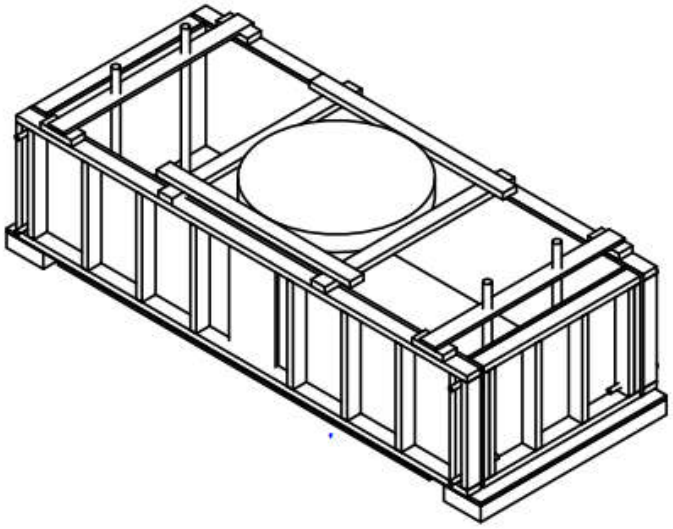

Figure 7-13. Isometric View of Cap Beam Formwork

The cap beam reinforcement cage, including the plug rebar, was fabricated outside of the formwork and then positioned into the beam form (See Figure 7-14).

Figure 7-14. Reinforcement cage for cap beam being lifted into formwork for casting

PVC pipes were then placed to create the necessary voids for 1-1/4 inch diameter threaded anchor rods that would anchor the specimen to the reaction block of the test frame. The cap beam was cast in place, leaving a small 1-inch deep circular recess at the top in order to grout the column into place and model the field conditions where the columns were embedded approximately 2 inches

into the cap beam. This void was achieved using a 5-inch wide plywood ring around the plug reinforcement (See Figure 7-15).

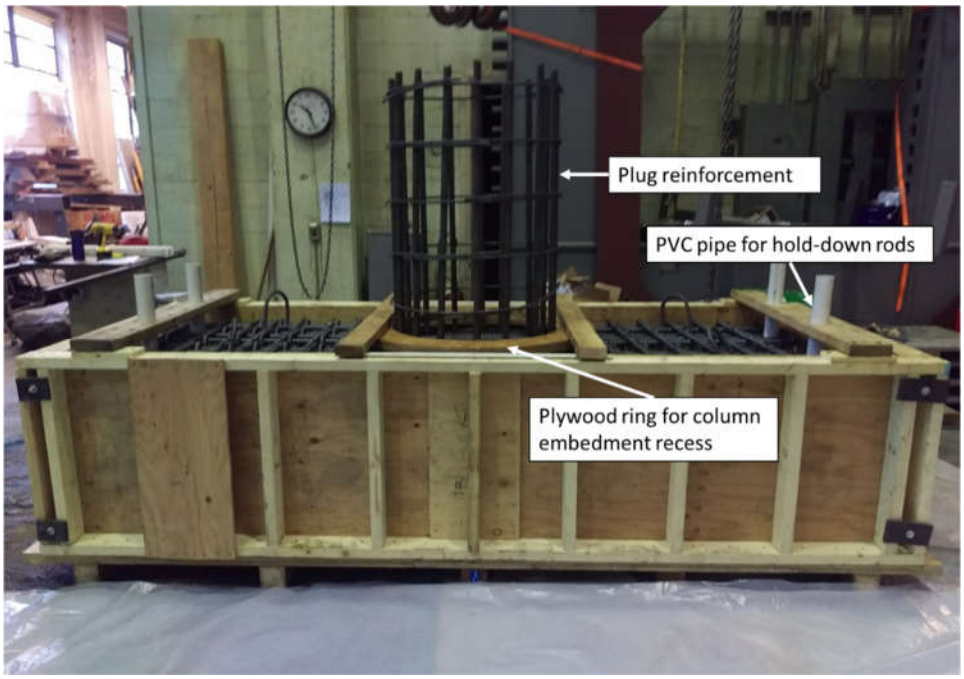

Figure 7-15. Final formwork assembly for cap beam casting

Figure 7-16. Cap beam and plug reinforcement in formwork before casting

In Figure 7-16, it can be observed that there are 10 longitudinal bars at the top of the cap beam which was not as designed (Figure 7-7). This was a mistake during construction, in that the top and bottom longitudinal reinforcement were reversed resulting in a lower moment capacity for the cap beam than intended. To fix this, the cap beam was externally prestressed before testing using two 1-3/4 inch diameter Williams Form Engineering All-Thread high strength steel bars loaded to 90 kips each (See Figure 7-17).

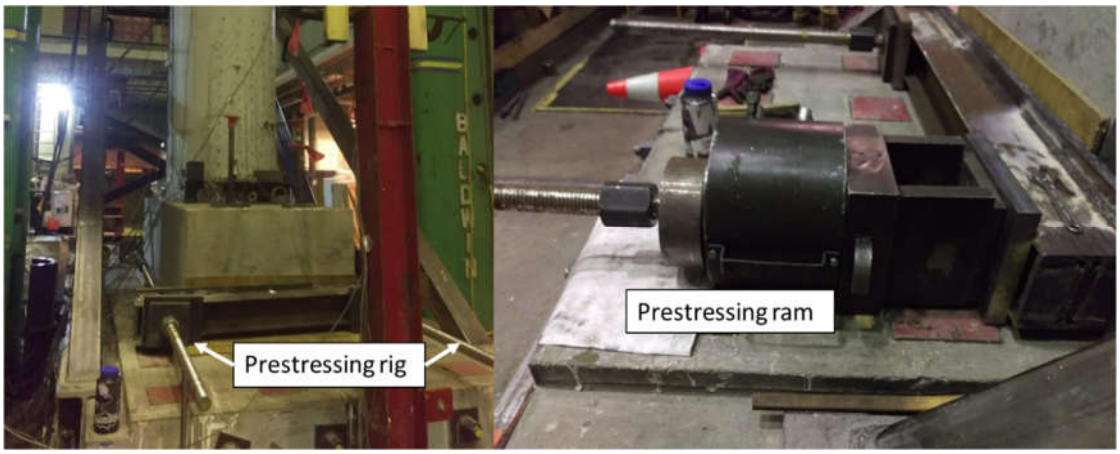

Figure 7-17. External prestressing to increase moment capacity of cap beam

Before casting the column, an epoxy mortar paste as described in Section 4.2.2.2 to once again imitate conditions of the field columns as indicated by the drawings.


Figure 7-18. Inner surface of column roughened with epoxy mortar

When the epoxy mortar was dry, the column was erected on top of the cap beam. To set the column in place, the precast, prestressed hollow column was lifted using a 10-ton capacity crane and lowered over the plug bars and centered on the cap beam. The column was grouted around its base so that it would be seated correctly on the cap beam. A timber bracing system was built to hold the column in place so that the plug could be cast (See Figure 7-19). A concrete truck was brought in to pour the inner plug through the top of the column. Since the plug was cast using a bucket and funnel over the top of the column (See Figure 7-20), it was difficult to ensure that the exact length of plug was poured and as such, the plug ended up being 42 inches long which was a few inches more than the design.

Figure 7-19. Column braced on top of cap beam

Figure 7-20. Casting plug inside of column

7.5 TEST SETUP

A cyclic test was performed on the as-built model specimen using a self-reacting test frame with a 220-kip horizontal actuator. The frame worked in conjunction with a Baldwin Universal Testing Machine to apply both lateral and axial loads to the column. The Baldwin machine applied a 200-

kip gravity load while the 220-kip capacity actuator applied cyclic lateral load to simulate earthquake effects (See Figure 7-21).

To set up the experiment, after the full specimen was constructed as described in the previous section, it was moved and installed under the Baldwin machine on top of the self-reacting base block. It was leveled and grouted into place using a very thin layer of Hydrostone under the base so that the column was vertical under the head of the test machine.

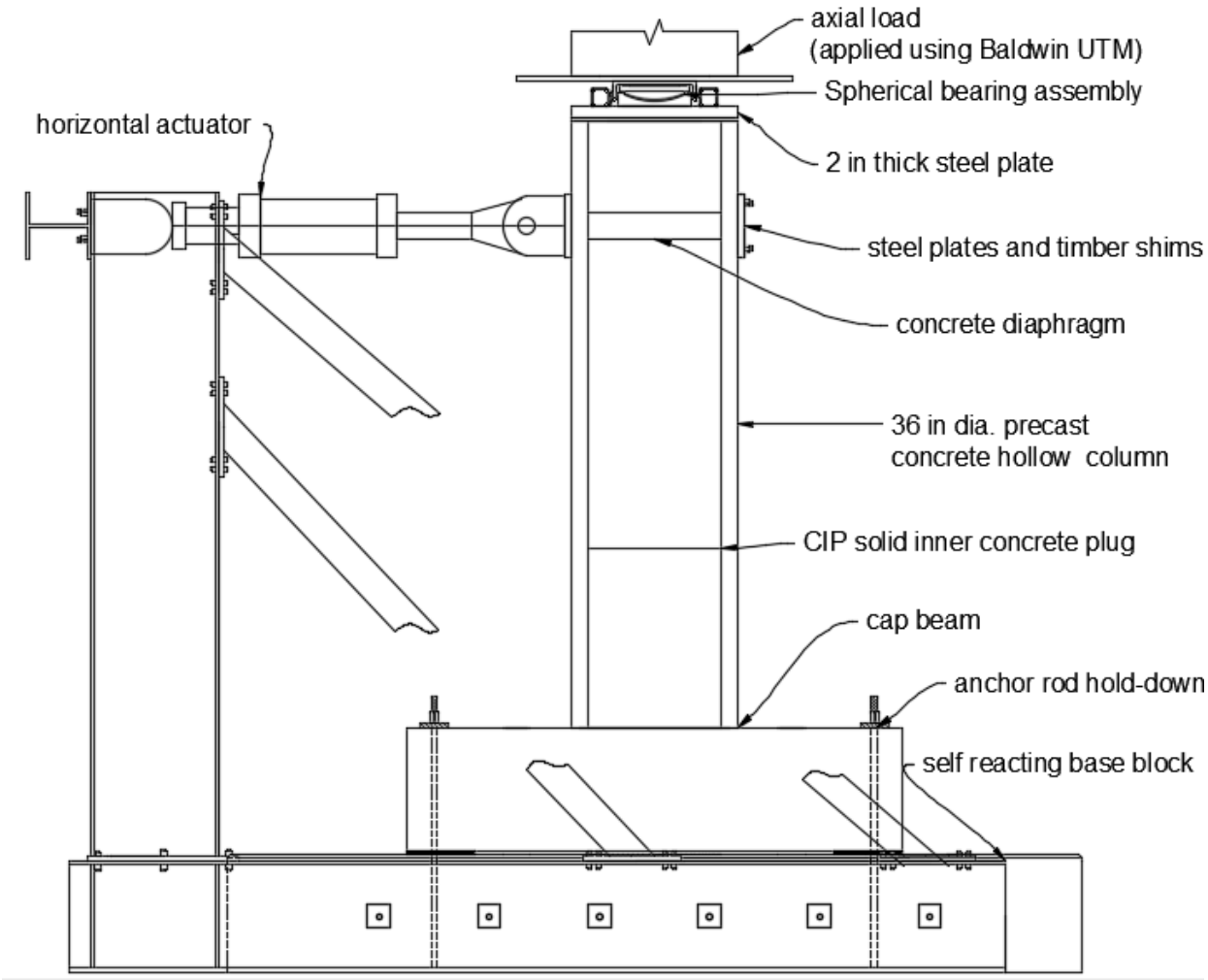

Figure 7-21. Test Setup with Specimen

7.5.1 *Test Equipment*

The specimen was anchored to the self-reacting base block using 1-1/4 inch Williams Form Engineering All-Thread high strength steel bars post-tensioned to 85 kips each, and placed 96 inches apart in the longitudinal direction and 18 inches apart in the transverse direction. This ensured that the specimen was rigidly attached to the concrete anchor block and no sliding or uplift of the cap beam occurred during testing.

The actuator was connected to the specimen using four 1-inch diameter high-strength steel threaded rods and two steel plates (1 inch thick) with timber shims and thin rubber pads to protect the concrete wall. The timber shims were machined to conform to the outside circumference of the column. On the interior of the column, a precast concrete diaphragm was grouted in place between the rods to eliminate the possibility of punching shear through the thin column walls by the applied lateral load (See Figure 7-22).

Figure 7-22. Concrete diaphragm to prevent punching shear (temporary wood formwork)

The column axial load was applied using the Baldwin load head and simulated a pin connection through the use of a spherical bearing, a Teflon surface and a channel track (See Figure 7-23). The spherical bearing allowed for rotation of the column under the lateral load while keeping the axial

load constant. The top surface of the spherical bearing had a recessed Maurer Sliding Material (MSM) pad that bore against the inner web of the channel that was lined with silicon greased stainless steel to create a low friction sliding surface. The outer surface of the channel flanges was also lined with silicone greased stainless steel that bore against rectangular HSS tubes, lined with Teflon strips, to create a low friction sliding track. These HSS pieces were welded to a 2-inch thick steel plate that was placed on top of the column to evenly distribute the load to the column wall. The channel was fixed to the bottom of the Baldwin head using four high strength threaded rods to prevent out-of-plane movement.

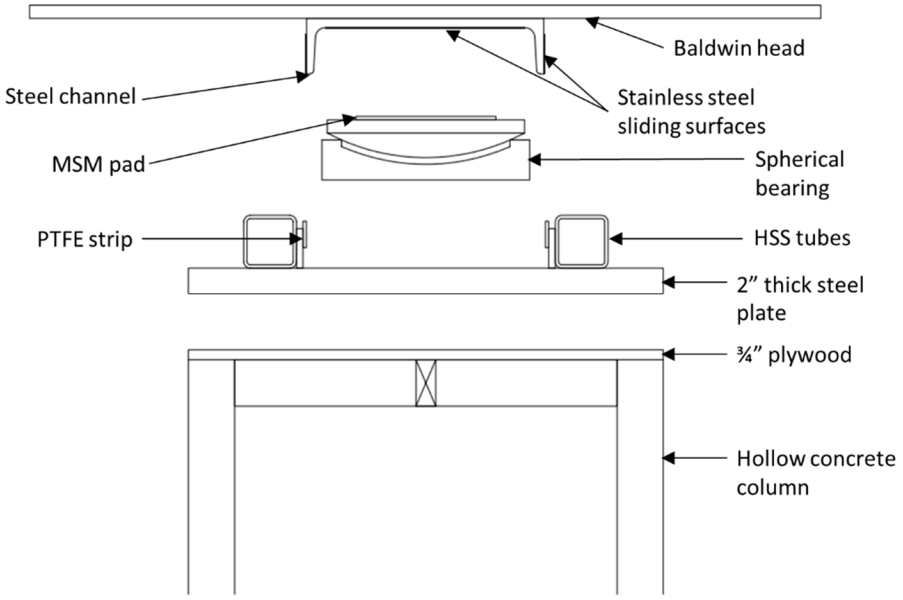

Figure 7-23. Spherical Bearing with Low Friction Sliding Surface

7.5.2 *Testing Protocol*

A 200-kip axial load was applied to the column using the Baldwin Universal Testing Machine. This load represented a scaled axial load per column based on a dead load takedown of the existing bridges (See Table 7-3). The gravity load was calculated from the weight of the superstructure including girders, traffic barriers, cap beam and diaphragms acting over the tributary width of each column. The scaled load was taken as an average of that for four bridges considered.

Table 7-3. Gravity Load Takedown for Reference Bridges

Reference Bridge	Gravity Load (kips)	Linear Scale Factor	Axial Load
Ravenna Bridge	428.15	0.75	240.83
Galer Lakeview	298.97	0.75	168.17
Green River Bridge	632.92	0.667	281.58
Slide Bridge	407.13	0.667	181.13
		Average Axial Load	217.93

A displacement-controlled lateral cyclic history was employed whereby a benchmark first yield deformation was predicted using a moment curvature analysis of the column strength (See Table 7-4). The displacement history was designed according to the nominal displacement of the actuator and the target drifts are calculated using a height of 108 inches. A series of three cycles at an elastic displacement level were chosen, followed by three cycles at the predicted yield displacement. Following this, cycles at post-yield displacements that increased by multiples between 1.25 and 1.5 were chosen until the rotation capacity allowed by the test setup was achieved which is in accordance with ACI ITG/T1.1-99's suggested test method. One exception to this was that the last series was done at an increase of only 15% in order to try to capture the failure drift more accurately at the higher inelastic drifts. The displacement sequence is illustrated in Figure 7-24.

Table 7-4. Displacement History

Series	Purpose	MTS disp (in)	N cycles	Target drift (%)	Ratio Increase
0	instrument	0.25	1	0.2	
1	elastic	0.5	3	0.46	2
2	predicted yield	1.0	3	0.926	2
3	post-yield	1.5	3	1.39	1.5
4		2.0	3	1.85	1.333
5		3.0	3	2.78	1.5
6		4.0	3	3.70	1.333
7		5.0	3	4.63	1.25
8		7.0	3	6.48	1.4
9	rig limit	8.0	1	7.41	1.143

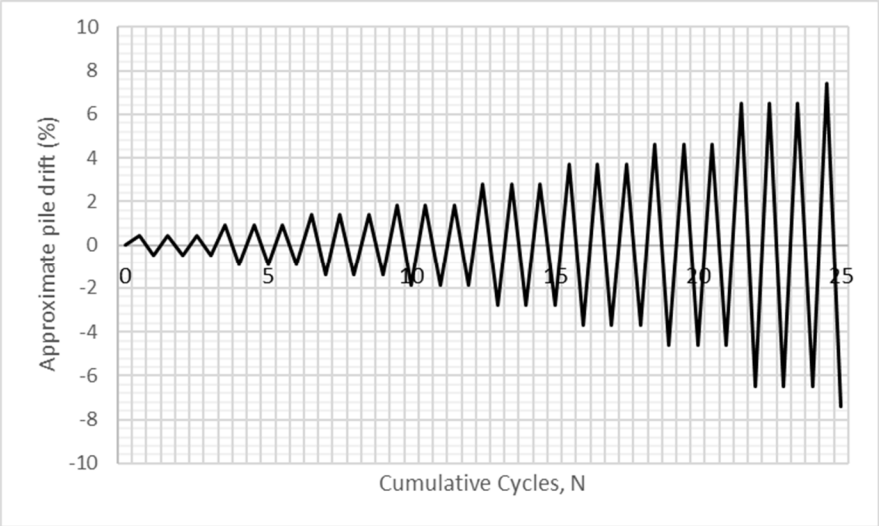

Figure 7-24. Displacement History

7.5.3 *Testing Procedure*

During testing the axial load was first applied with the specimen in the neutral position and then this load was held "constant" throughout the remainder of the experiment. Because the top of the column rises and falls during the lateral motion, the load had to be adjusted continuously. This was done automatically by the control software of the Baldwin Testing Machine. The load was thus maintained constant within ±8 kips. Following this, the displacement history as shown in Figure 7-24 was implemented.

The lateral load sequence consisted of 9 series, typically consisting of 3 cycles each at a nominal displacement. The nominal displacement for each series was defined as the maximum absolute displacement of the horizontal actuator during each cycle. This displacement was always greater than that of the specimen because of the flexibility of the beam to which the actuator was connected to the reaction block as well as the compression of the timber shims used to connect the actuator to the column. A single cycle was defined as moving from zero displacement, travelling to the nominal displacement in both the positive and negative directions (south then north) and then returning to zero displacement.

The first two cycles of each series were typically performed without stopping in order to collect instrument data without interruption. During the third cycle, the specimen was pulled to the south

(positive direction) to the desired nominal displacement and testing was paused in order to inspect for cracks, mark them in a blue color on the specimen and take photographs. The specimen was then pushed to the north (negative direction), testing paused and the crack inspection and documentation repeated, this time in a red color. The specimen was then returned to zero displacement and the next series started.

7.6 INSTRUMENTATION

Instrumentation for the test comprised strain gages, linear potentiometers, string potentiometers, inclinometers and an Optotrak motion capture system (See Figure 7-25 - Figure 7-29). All instruments were recorded using computer-controlled data acquisition systems.

Loads were measured using the internal load cells of the Baldwin machine and the MTS horizontal actuator. Additionally, the displacement stroke of the horizontal actuator was measured by its own LVDT and this was used to track the nominal displacement for each series.

Strain gages were used to measure the strains of the plug rebar (See Figure 7-25). They were placed on the east and west sides of four separate bars (one each in the north, south, east and west direction of the specimen) in order to only measure axial bar strains. Gages were placed at 3 inches and 9 inches above the cap beam on all four bars, and at 15 inches above the cap beam on the north and south bars. This meant that the strain gages were placed in the region that would allow understanding of the behavior within the expected plastic hinge.

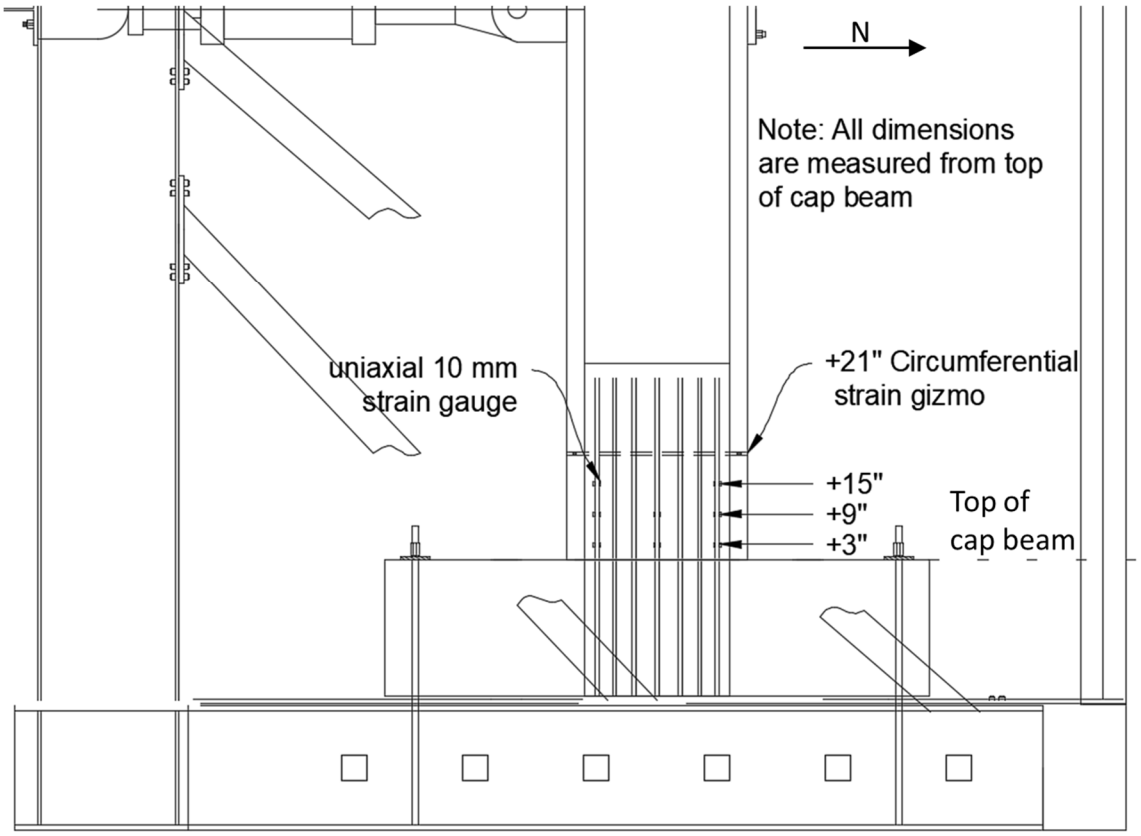

Figure 7-25. Strain gage locations on specimen

Four additional strain gages were used as part of a gizmo to measure any circumferential strain in the column wall (See Figure 7-26). These strain gages were placed on the northeast, northwest, southeast and southwest sides of the column at 21 inches above the cap beam which corresponds to about half of the as-built plug length. Two layers of clear packaging tape were stuck together and the gages were glued to one side of the tape which was then wrapped around the column and fixed with sticky tape (See Figure 7-26). The tape was used as a material that would stretch open if the column expanded outward but not break or yield on its own thereby acting as a circumferential extensometer.

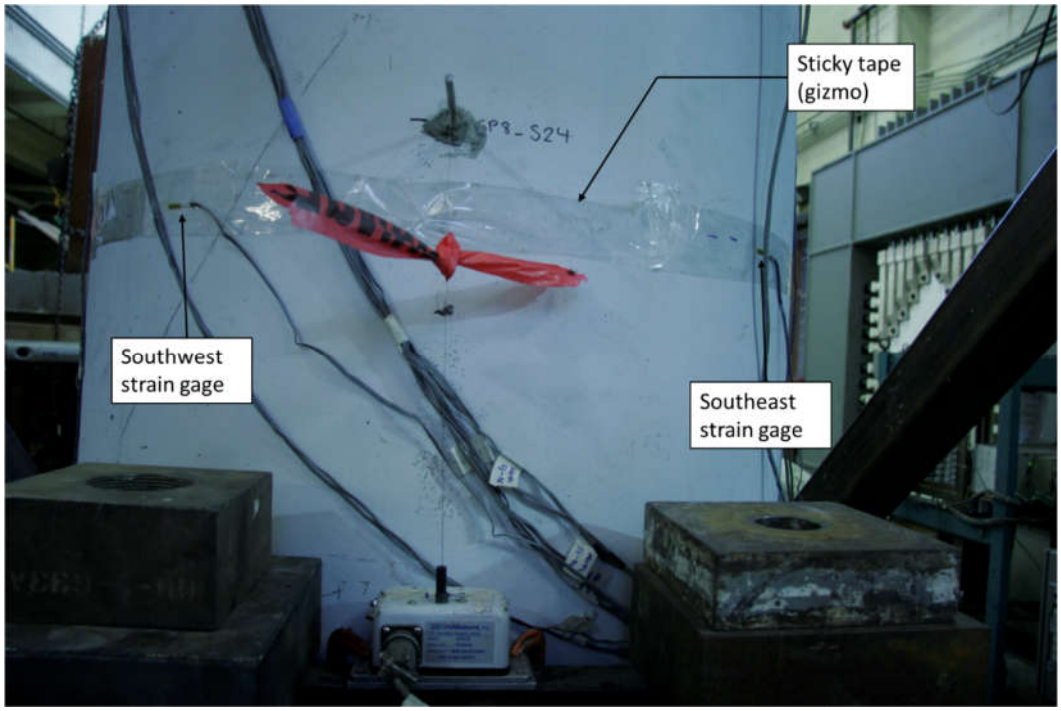

Figure 7-26. Circumferential Strain Gage "Extensometer", South face

Displacements were measured using two types of potentiometers (See Figure 7-27). Short-stroke linear Duncan potentiometers were used to monitor any uplift or slip of the specimen cap beam. String potentiometers are capable of measuring a large range of displacements (typically 10 – 20 inches maximum) and as such these were used to measure the lateral displacement of the column at five discrete locations along its height, including at the height of the actuator where the load was directly applied (See Figure 7-27). The string potentiometers were attached using piano wire to a fixed reference tower at the north of the test rig in order to ensure independent, global measurements were recorded. The displacements measured using the string potentiometers allow for the development of a displaced profile of the column and to determine the rigid body rotation of the column.

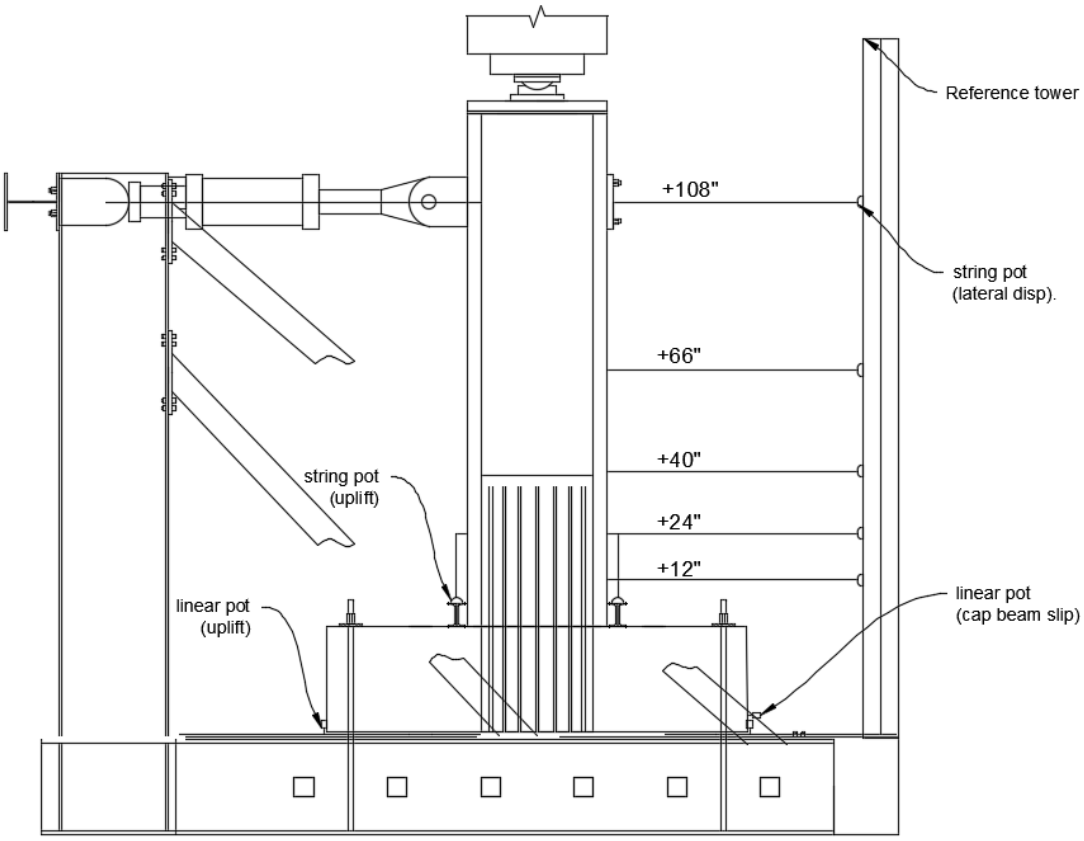

Figure 7-27. String pot and linear pot instrumentation for testing

These rotations were also measured by inclinometers along the height of the column on its east and west sides as shown in Figure 7-28. String pots were also used to measure the vertical displacement of the pile in the case of any crushing or uplift at the base and these were placed on the north and south side of the column using heavy steel pieces to set them on the base (See Figure 7-27, string pot (uplift)).

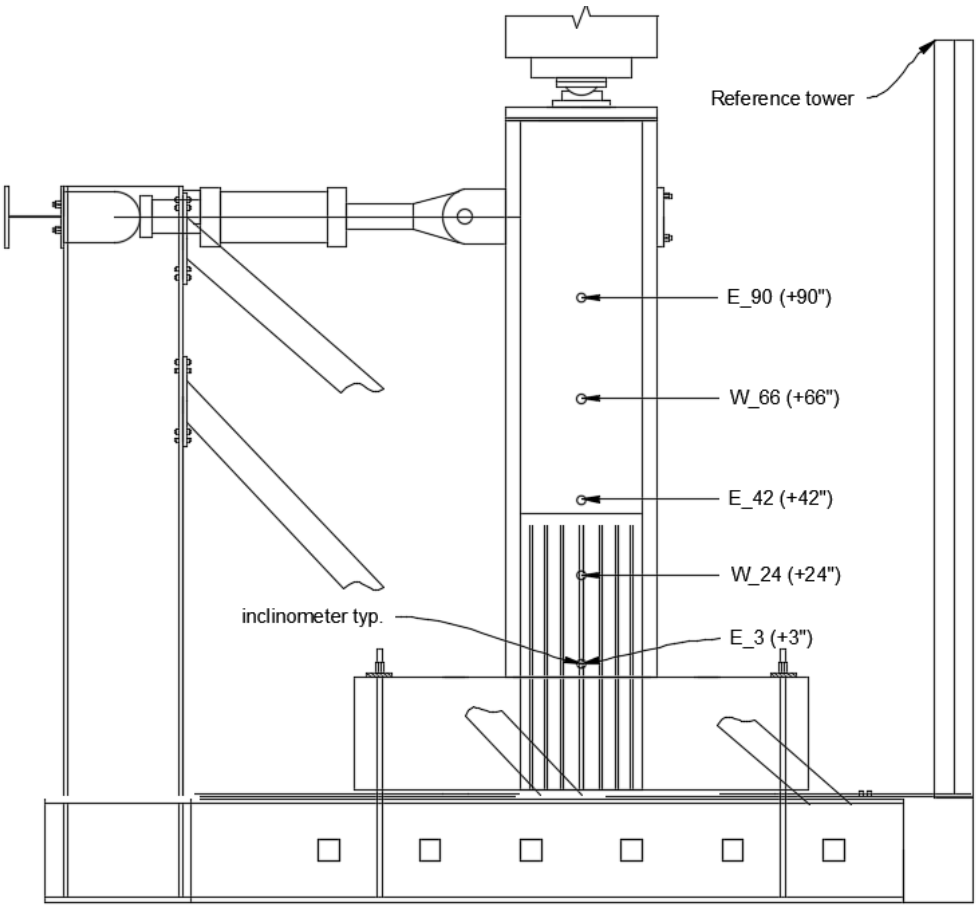

Figure 7-28. Location of inclinometers to measure rotation (E-East face, W-West face)

Lastly, an Optotrak Certus motion capture system was used to measure the deformations in the north-west quadrant of the specimen in the region of the inner plug (See Figure 7-29). The Optotrak system consists of a 3-dimensional optical sensor (camera) and a series of LED markers arranged in a pre-determined grid system. The system records the 3-dimensional position of each marker with respect to the camera's own coordinate system. From these position measurements, deformations of the column wall can be calculated, in particular, shear and vertical deformations.

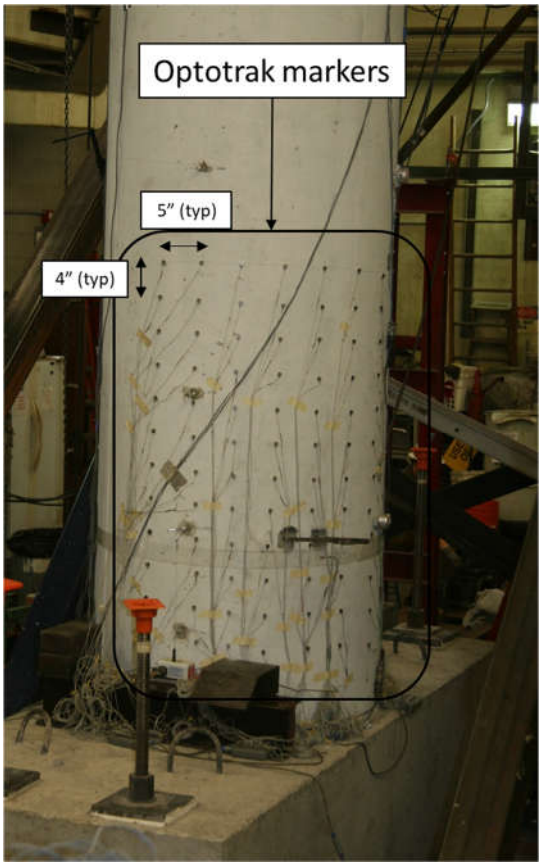

Figure 7-29. Optotrak Marker Grid on Northwest face of column

Chapter 8. COLUMN BENDING RESULTS

This section will discuss the results observed during the test that was conducted on December 7th, 2018 at the University of Washington Structural Research Laboratory. It contains descriptions of the visual damage that was observed and a summary of the local and global behavior that was recorded from the instrumentation.

8.1 GENERAL

Table 8-1 compares the target drift values for each series of cycles and the actual drift levels that were achieved during testing. The results are reported in terms of the actual values. The drift ratio is calculated as the ratio between the horizontal displacement at the level of the actuator to the distance between the top (in lab orientation) of the cap beam and the actuator which was 108 inches. It should be noted that the actual drift levels were lower than the target drift levels in all cases and, in all cases the actual drift when the specimen was pushed to the north is higher than when it was pulled to the south. The reference coordinate system is defined in Figure 8-1.

Table 8-1. Target Drift Levels and Actual Drift Levels Achieved

Series	Target Actuator Displacement (in)	Nominal Target Drift	Actual Average Drift	
			South	North
1	0.5	0.0046	0.0023	-0.0025
2	1.0	0.0093	0.0047	-0.0060
3	1.5	0.0139	0.0075	-0.0097
4	2.0	0.0185	0.0100	-0.0136
5	3.0	0.0278	0.0172	-0.0221
6	4.0	0.0370	0.0259	-0.0305
7	5.0	0.0463	0.0347	-0.0391
8	7.0	0.0648	0.0526	-0.0551
9	8.0	0.0741	0.0633	-0.0656

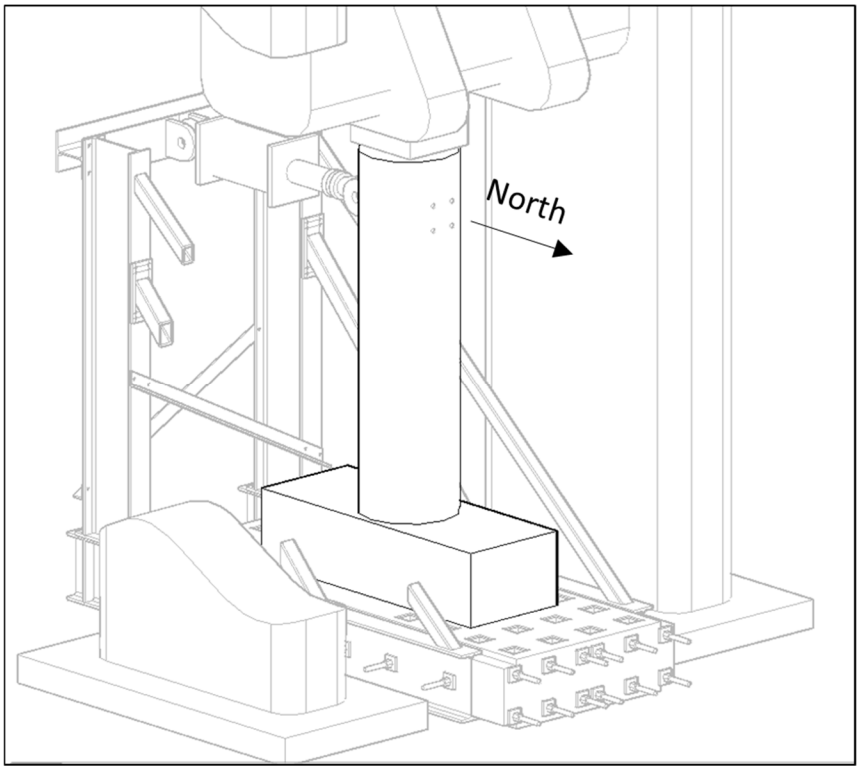

Figure 8-1. Coordinate System for Results

The two differences in drift values were both due to the flexibility of the beam on which the actuator is supported and how it is connected to the reaction frame in the test setup (See Figure 8-2). The overall difference between target drift and actual drift was due to the deflection of the actuator beam and its connections to the columns. The north-south inconsistency occurred because the connections were less stiff in tension (column moving north) than in compression (column moving south) (See Figure 8-2 and Figure 8-3).

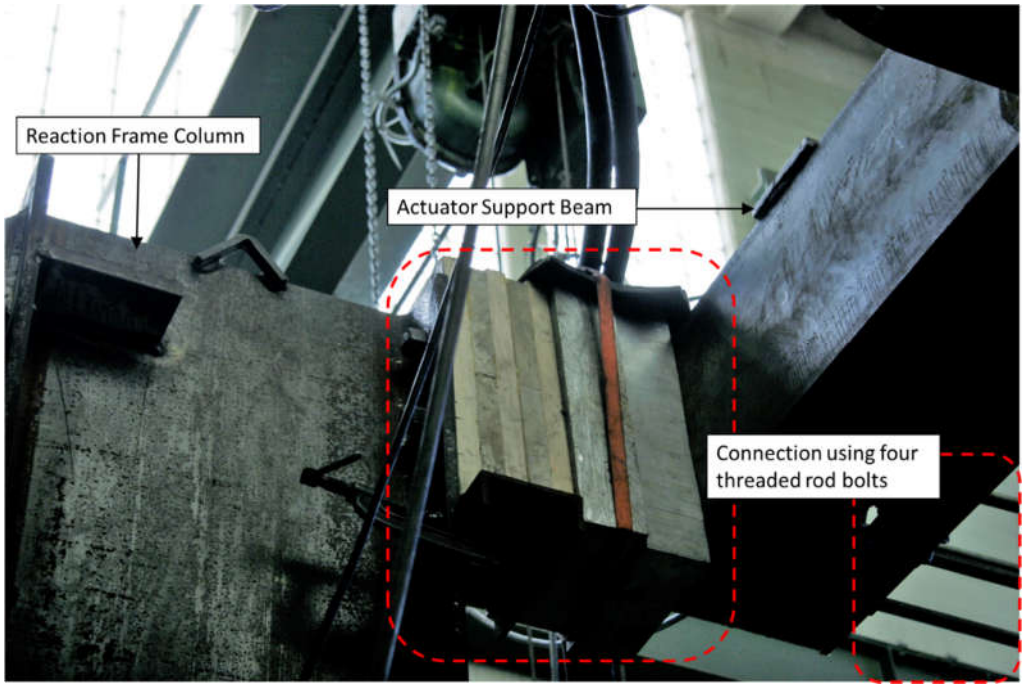

Figure 8-2. Connection between actuator beam and reaction frame

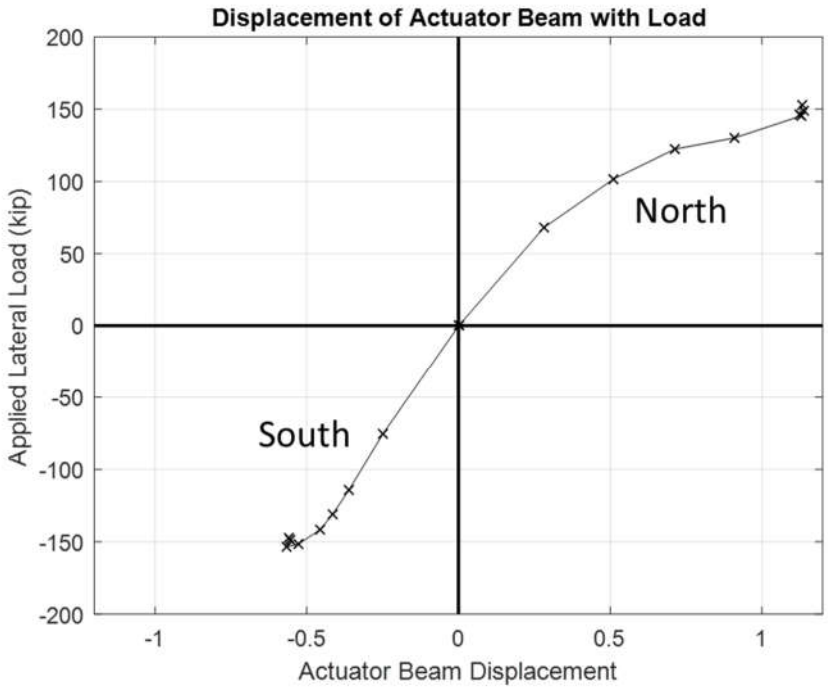

$$\Delta_{beam} = \Delta_{actuator} - \Delta_{column}$$

Figure 8-3. Load-Displacement curve of actuator beam at peak loads, showing different stiffnesses (Direction corresponds to column displacement)

The damage observed during the test is mostly described in terms of observed concrete spalling and concrete cracking. Table 8-2 defines cracks in terms of the measured width and Table 8-3 categorizes the spalling states of the concrete. In the pictures that follow, cracks were marked in blue when the column was pulled to the south and in red when the column was pushed to the north.

Table 8-2. Crack Descriptions

Crack Description	Crack Width Range
Narrow	< 0.013 in
Medium	0.013 – 0.040 in
Wide	> 0.040 in

Table 8-3. Spalling Descriptions

Minimal Spalling	Initial spalling of concrete cover
Moderate Spalling	Partial cover spalling
Substantial Spalling	Exposure of spiral reinforcement

8.2 VISUAL OBSERVATIONS

The first short, narrow cracks were observed on the northeast and northwest sides of the column, at the base right above the cap beam during loading series 2 (drift ratio +0.47%/-0.6%) (See Figure 8-4).

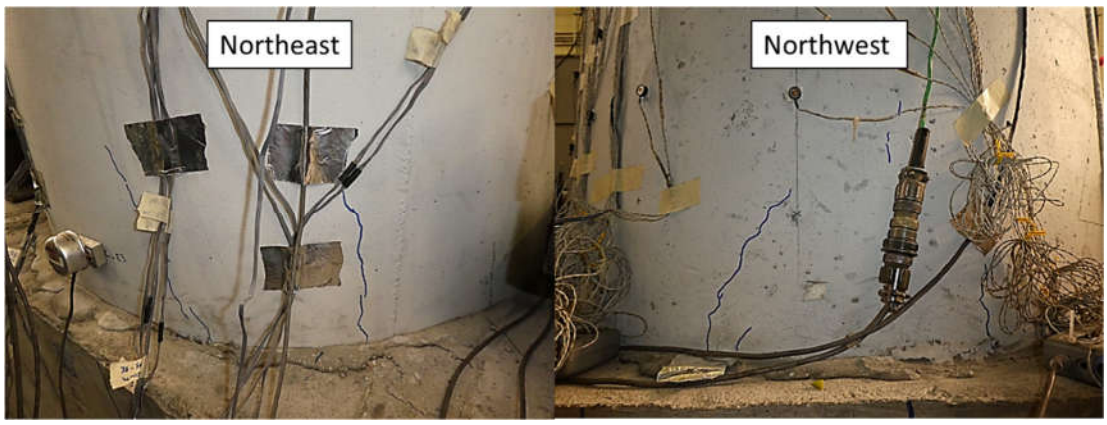

Figure 8-4. Short, fine cracks, Series 2

During series 3 (drift ratio +0.75%/-0.97%), significant cracking was observed on both the north and south faces. The majority of the cracks were horizontal medium-sized (see definition in Table

8-2) cracks, located between 24 inches and 40 inches above the cap beam (See Figure 8-5). Additionally, a narrow vertical crack formed on the north face of the column that measured about 38 inches in length, and a couple of diagonal cracks extending from the south face to the east and west sides were noted (See Figure 8-5).

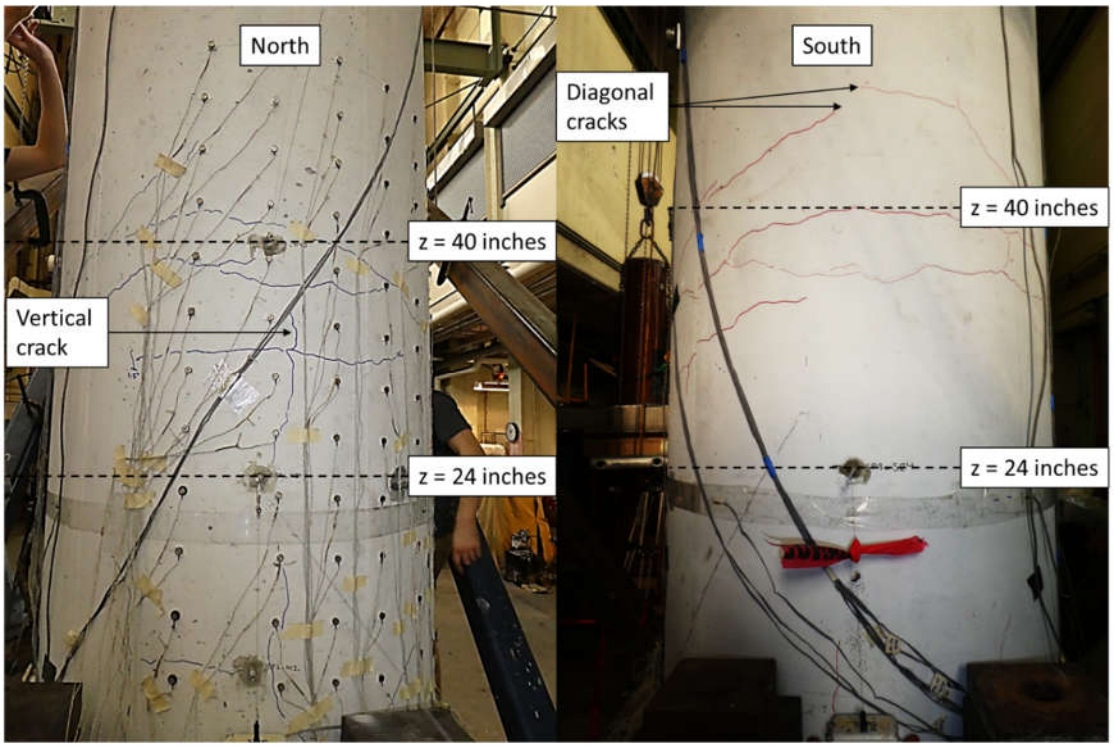

Figure 8-5. Significant crack formation on North and South faces, Series 3

During series 4 (drift ratio +1.00%/-1.36%) the existing cracks widened, particularly the diagonal cracks that were previously measured and marked as 0.04 inches wide. Additionally, minor spalling was observed at the base on the north and south sides of the column, behind the channels that were used for the vertical string potentiometer setup (See Figure 8-6).

Figure 8-6. Minimal Spalling at base of column, Series 4

A drift ratio of +2.59%/-3.05% was reached during series 6. At this stage, moderate spalling was observed at the base of the column in addition to some uplift between the column and the cap beam (See Figure 8-7). Upon noticing the uplift, a piece of wire was inserted into the void and used to measure the extent to which the column was experiencing uplift. From this crude measurement, it was found the uplift was affecting a column depth of approximately 3.5 inches (i.e. the thickness of the hollow pile wall), indicating that only the hollow pile was rising up but no crack had propagated into the inner solid plug. This also suggests that the hollow pile wall was slipping relative to the inner plug.

Additionally, during this loading series a long, narrow, vertical crack formed on the south face of the column that extended from the base of the column, to about 38 inches above the cap beam (See Figure 8-8). The existing cracks also widened significantly, with some of the horizontal cracks on the south side reaching a width of 0.05 inches. Lastly, new horizontal cracks were detected about 12 inches above the cap beam, on both the north and the south sides of the column.

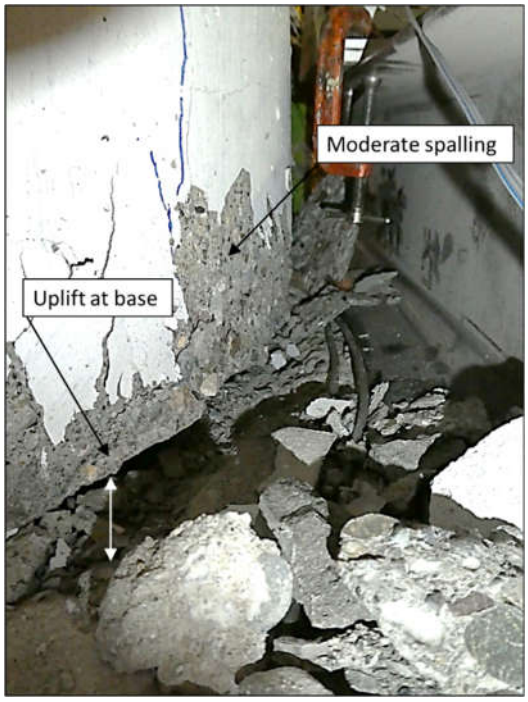

Figure 8-7. Moderate spalling and uplift on north side of column, Series 6

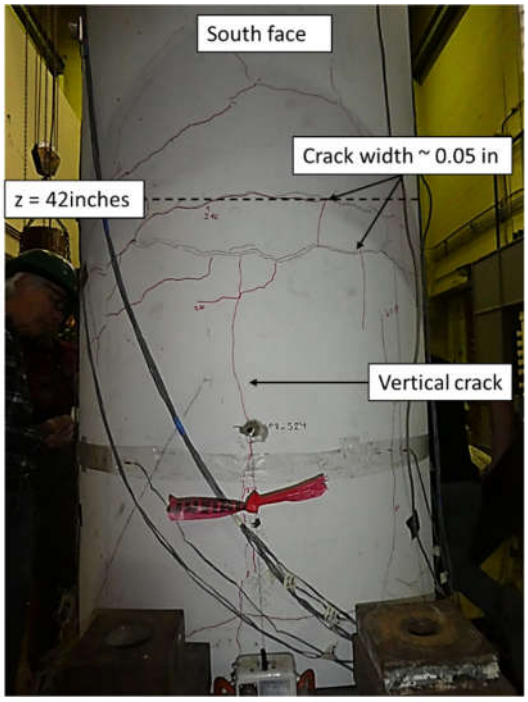

Figure 8-8. Horizontal and vertical cracks on south face, Series 6

Substantial spalling at the base of the column was observed at a drift level of approximately +3.47%/-3.91%. In addition, the end of the spiral reinforcement was exposed on the north side of the column (See Figure 8-9). The gap between the top of the cap beam and the bottom of the

column wall (See Figure 8-10) due to column uplift reached a width of approximately 0.5 inches on either side when that side was in tension.

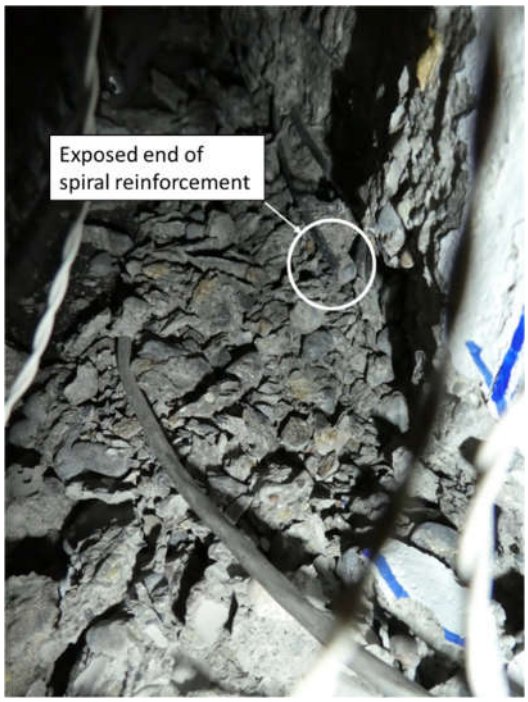

Figure 8-9. Substantial spalling at base of column, Series 7

Figure 8-10. Gap from uplift at base of column measures 0.5 inches, Series 7

During series 7, the cracks propagated to form an extensive network around the column (See Figure 8-11). However, it is important to note that these cracks were confined mostly to the region

between the base of the column and 42 inches above the cap beam, which corresponds to the top of the solid plug.

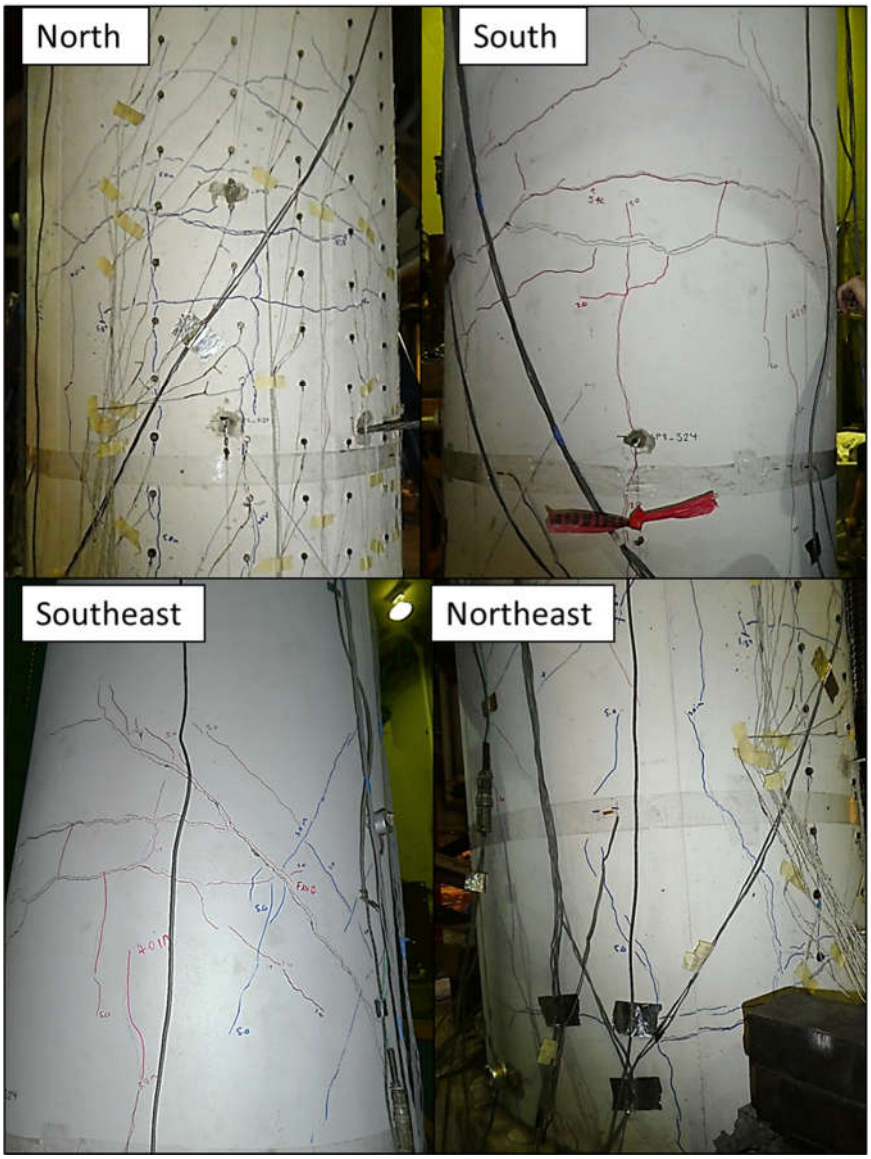

Figure 8-11. Extensive network of cracks formed during Series 7

During the next series, at a drift of approximately +5.26%/-5.51%, a very wide horizontal crack formed on the north face of the column as it was pulled it to the south (See Figure 8-12). This crack was located 34 inches above the cap beam and measured 3/8 inches in width. Substantial spalling was observed in the bottom 12 inches of the column wall, exposing multiple turns of spiral reinforcement (See Figure 8-13) on both the north and south faces.

Figure 8-12. Very wide crack on north face, Series 8

Figure 8-13. Substantial spalling and exposed spiral reinforcement, Series 8

During the next series (series 9), only one loading cycle was executed as significant concrete degradation was observed that would have created dangerous conditions under further testing. At this stage, the column was considered to have failed. The maximum drift obtained was +6.33%/-6.56% as the column was pushed to the north. Figure 8-14 shows the propagation of spalling that occurred on the north face where a very wide crack had progressively widened over the previous series. Looking closely, it can be seen that the prestressed strands had also buckled. The concrete spalled just above the top of one of the hold-down steel plates used during construction of the column by Concrete Tech (Refer to Figure 7-11).

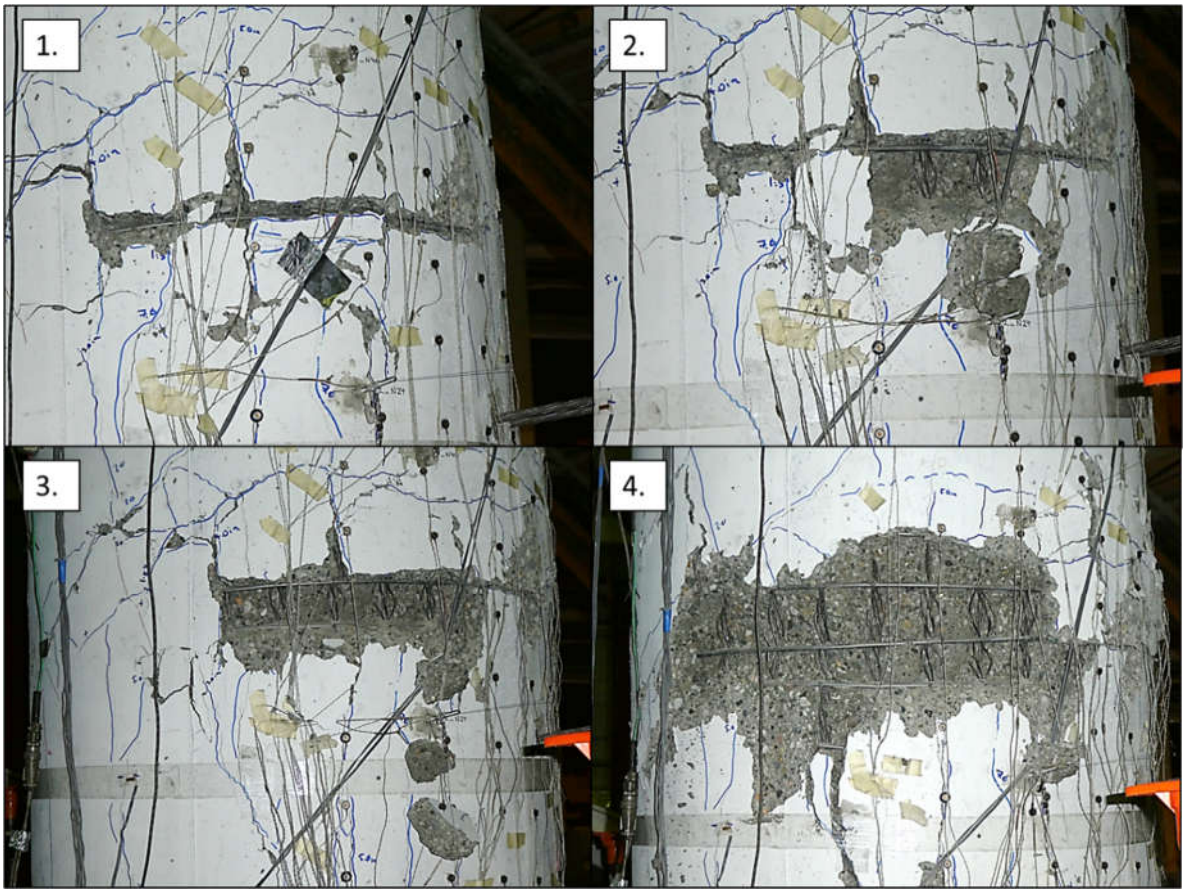

Figure 8-14. Degradation of concrete during series 9

In Figure 8-15, fracture of the spiral reinforcement is shown around the buckled strands, while Figure 8-16 shows the final position of the specimen before the axial load was removed at the end of testing.

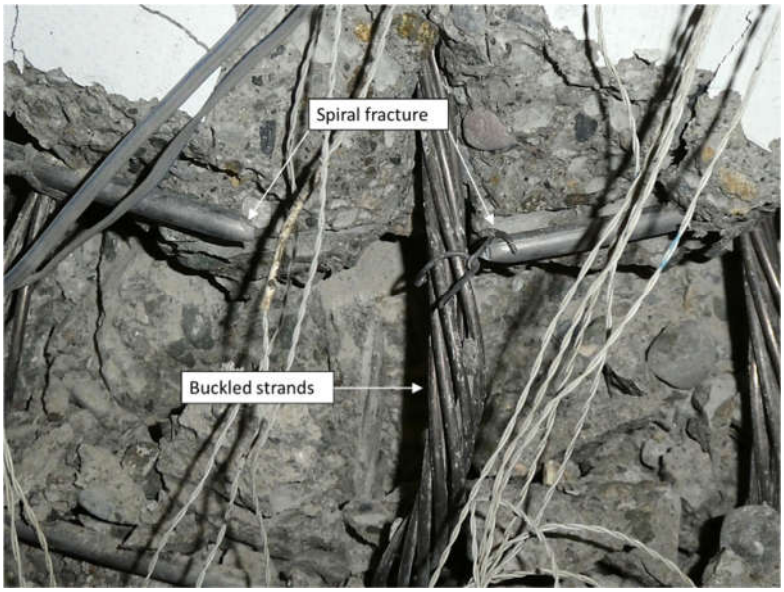

Figure 8-15. Spiral reinforcement fractured at failure, Series 9


Figure 8-16. Final position of specimen at failure

8.3 MATERIAL PROPERTIES

The material properties of the specimen are provided in Table 8-4 and Figure 8-17 and Figure 8-18. The average concrete compressive strength of the cap beam, plug and hollow pile were obtained in accordance with the ASTM 39 *Standard Test Method for Compressive Strength of Cylindrical Concrete Specimens*. The tensile stress-strain relationship for the rebar steel used as longitudinal plug reinforcement was obtained in conformance with ASTM A370-15 *Standard Test Methods and Definition for Mechanical Testing of Steel Products* and ASTM A615-16 *Standard Specification for Deformed and Plain Carbon-Steel Bars for Concrete Reinforcement.*

Table 8-4. Concrete Compressive Strength at Different Ages for Specimen Components (psi)

	7 days	**14 days**	**28 days (f'_c)**	**Test day (age in days indicated in parentheses)**
Hollow pile	-	-	13140	14840 (105)
Plug	5355	6261	7106	7590 (84)
Cap Beam	4566	-	5779	6464 (386)

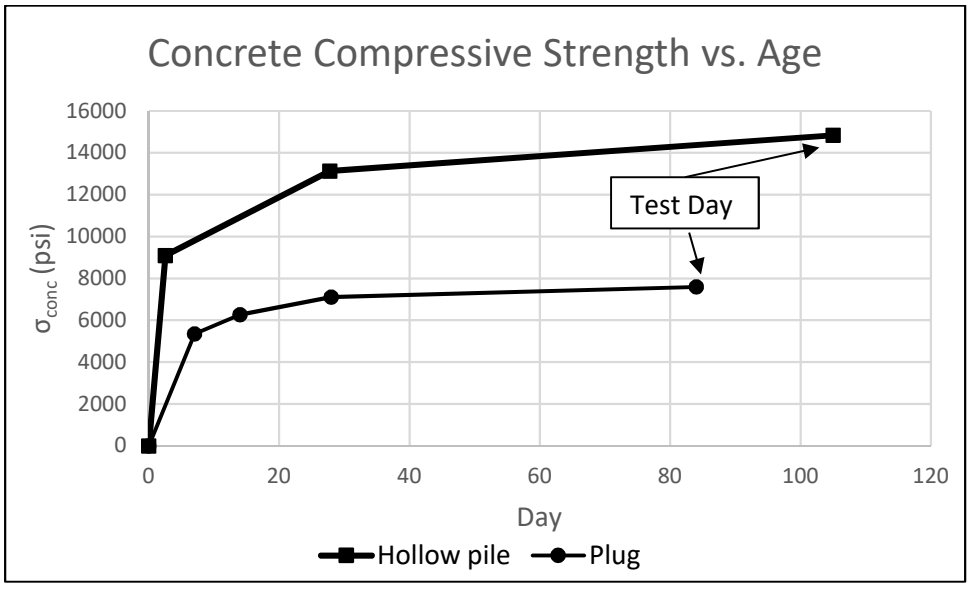

Figure 8-17. Concrete Compressive Strength for Column

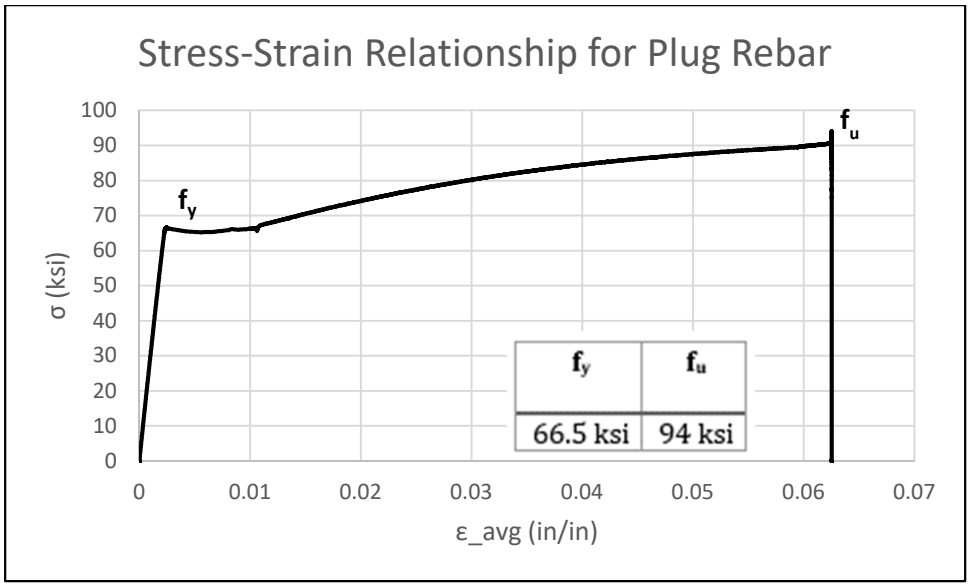

Figure 8-18. Stress-Strain Relationship for Plug Rebar

8.4 COLUMN BEHAVIOR

The behavior of the column can be evaluated on a local and a global level. On a global scale, the hysteretic base moment vs. drift behavior and the hysteretic effective force vs. drift behavior is examined. On a local scale, the strains, deformations and rotations of various components are computed and analyzed. For all plots shown, positive behavior is defined as the column moving south and negative behavior is defined as the column moving north.

The effective force and base moment calculations are shown in Equations 1 and 2, with reference to Figure 8-19.

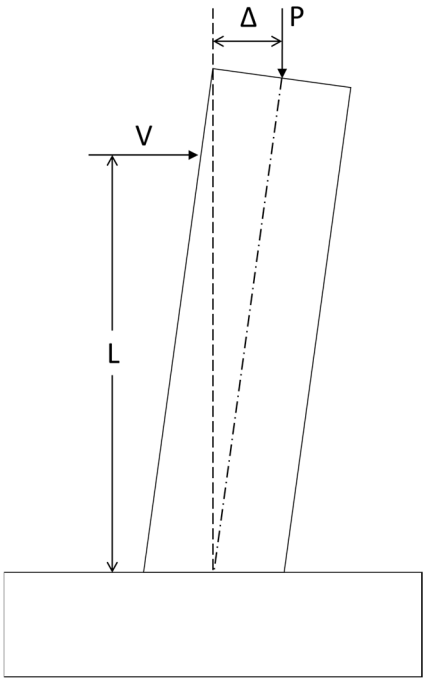

Figure 8-19. Effective force and Base moment Calculation Details

$$M_b = V * L + P * \Delta \quad (1)$$

$$F_{eff} = \frac{M_b}{L} \quad (2)$$

M_b = Base moment (at column-cap beam interface)
V = Horizontal Load applied by the Actuator
L = Height from cap beam interface to horizontal load application point (108 inches)
P = Axial load applied by the Baldwin machine (Nominal Load = 200 kips)
Δ = Horizontal displacement of column, taken as the average of two string potentiometers at the horizontal load application point
F_{eff} = Effective Lateral Force

8.4.1 *Global Behavior*

The base moment vs. drift ratio hysteretic response is shown in Figure 8-20, with the key damage points identified in the graph. The maximum base moment of 16,500 in-kip was achieved at a drift ratio of +5.2%, during the first cycle of series 8.

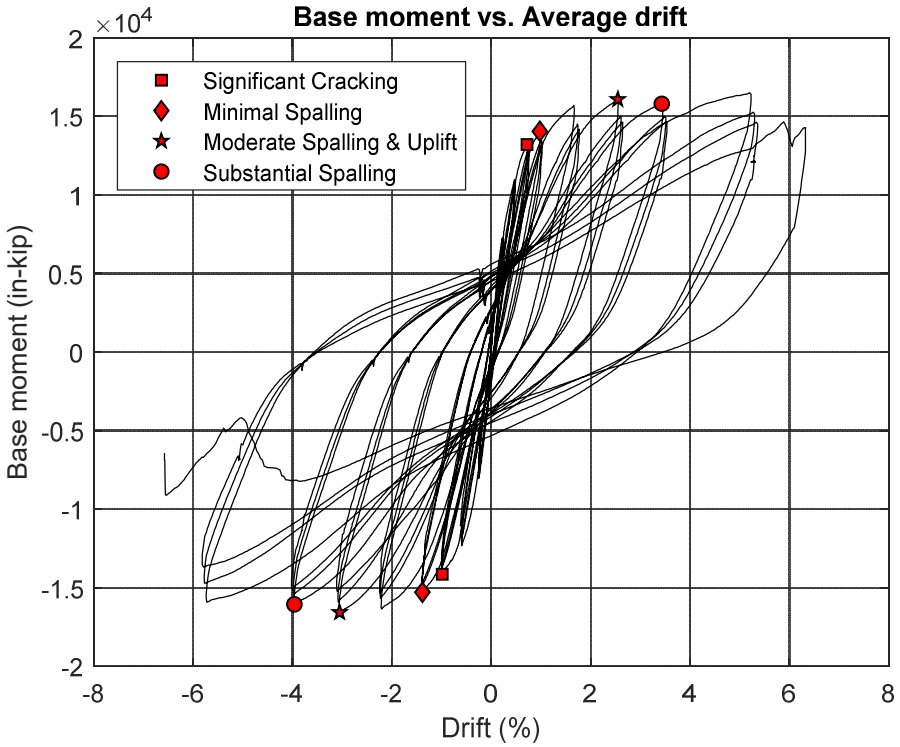

Figure 8-20. Base moment vs first peak drift with key damage states identified

Figure 8-21 shows the effective horizontal force vs. drift ratio, along with the backbone curve identifying the peak forces associated to each loading series. From the backbone curve, it can be seen that past a drift ratio of about 2%, the peak force remained roughly constant throughout the test at about 150 kips, indicating very little strength degradation until failure.

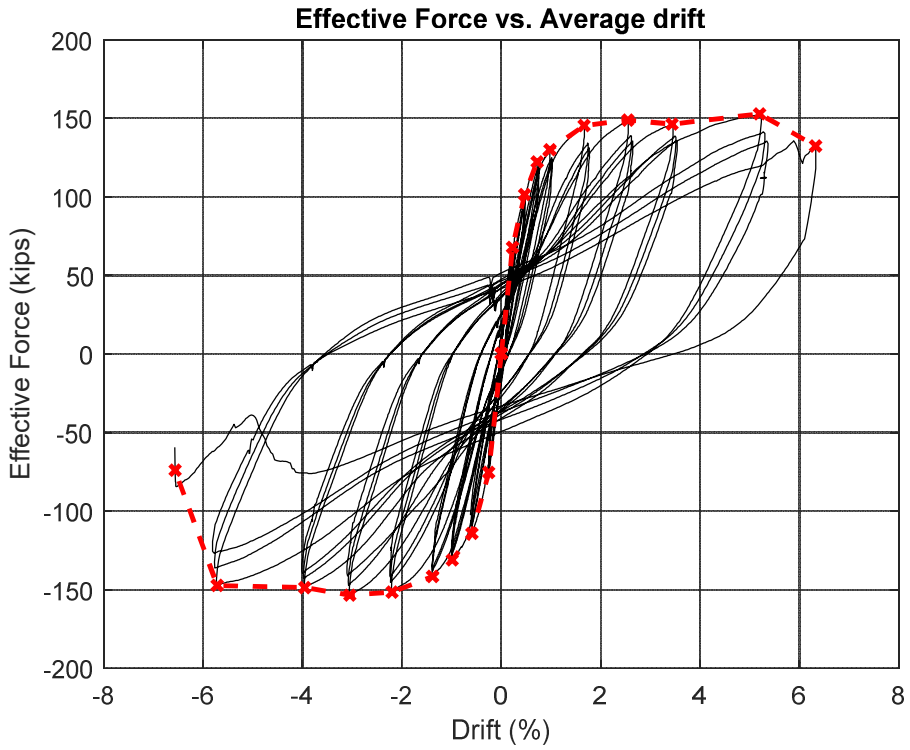

Figure 8-21. Effective force vs. Average drift with cycle 1 backbone behavior

8.4.2 *Local Behavior*

As stated in Chapter 4, strain gages were used to monitor the status of the longitudinal plug reinforcement. Figure 8-22 shows the longitudinal reinforcement strains recorded at the peak displacement during the first cycle of each loading series, for the four bars that were monitored. The strains shown are the average of the measurements acquired from the pair of gages at the various locations along each bar.

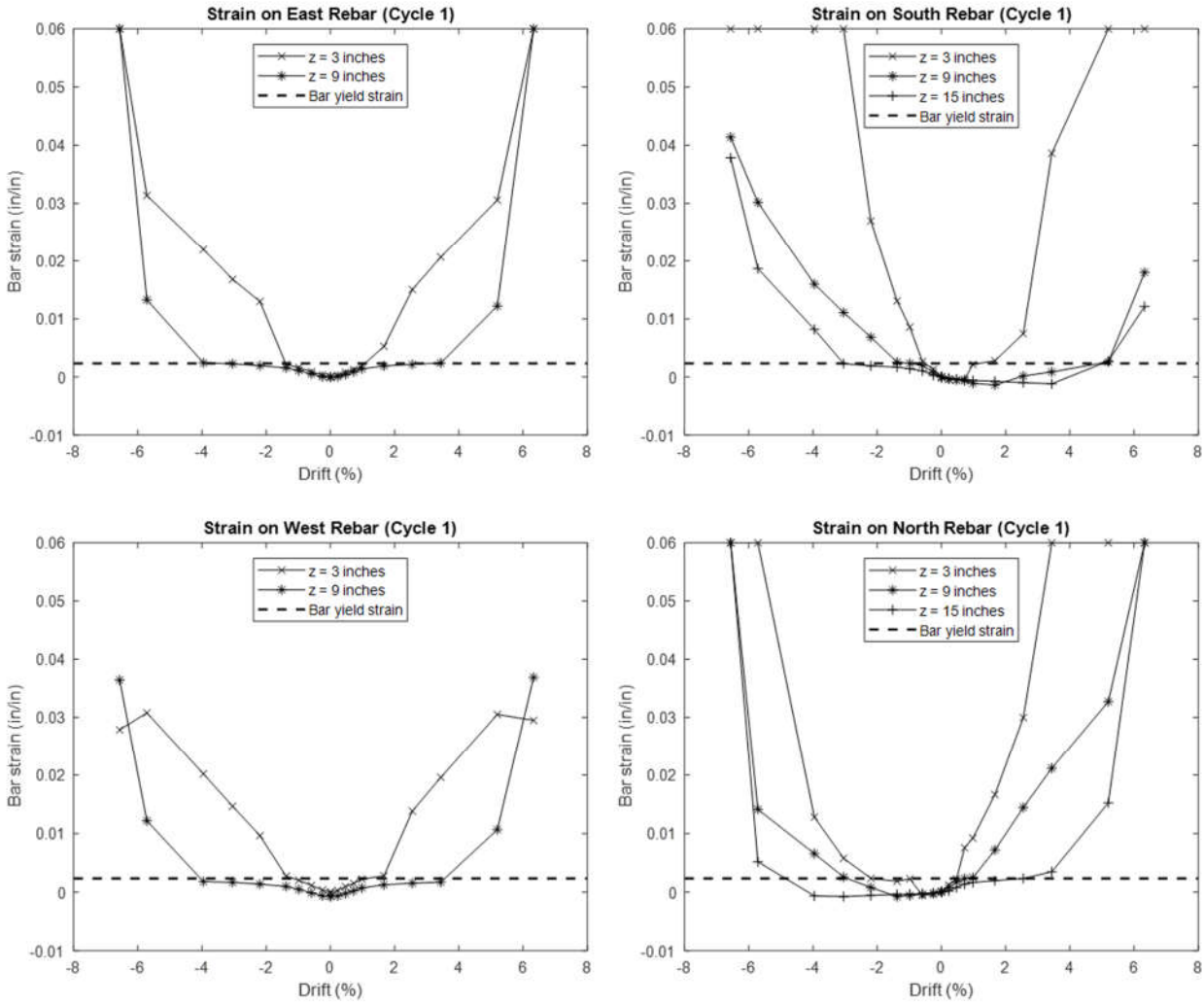

Figure 8-22. Plug rebar strains at peak drifts for cycle 1 for all series

From the graphs, it can be seen that the plug reinforcing bars experienced progressive yielding along their length (beginning at the base of the column). Both the east and west reinforcing bars reached yield strain at 3 inches above the base of the column, at a drift level of approximately +1%. At this drift level, significant pile cracking was also observed (See Figure 8-20). Consistently, a marked change in slope (i.e. a loss in stiffness) can be observed with reference to the force-displacement backbone curve (See Figure 8-21). As the column underwent increasing horizontal displacement, the reinforcing bars yielded more extensively. Yield strain values were recorded up to 9 inches away from the base of the column, once the drift ratio was about 4%. The north and south reinforcing bars followed a similar trend, with early yielding at the base followed by strain hardening and progressive yielding along the length of the bars.

Strain gages were also used to measure circumferential strain in the column wall (See Figure 7-26). Figure 8-23 shows the hoop strain vs. drift, measured at 3 locations around the circumference of the column and corresponding to the peak drifts pertaining to the first cycle of each loading series. This graph indicates that the measured hoop strains did not exceed the cracking strain of concrete (taken as 100με) until series 6, which is when vertical cracks had formed on both the north and south faces of the column. Furthermore, assuming the spiral strain is the same as the measured strain on the outside wall is a lower bound estimate of the average strain in the spiral, especially after cracking occurs. Therefore, if the yield strength of the steel spiral is taken as 70 ksi, the hoop strain readings suggest that the spiral reinforcement yielded and that the column failed soon after. This is consistent with the fact that the spiral reinforcement was made from cold drawn steel wire, which typically reaches its ultimate strength soon after yielding. Fractured spirals were found in different locations at the end of testing.

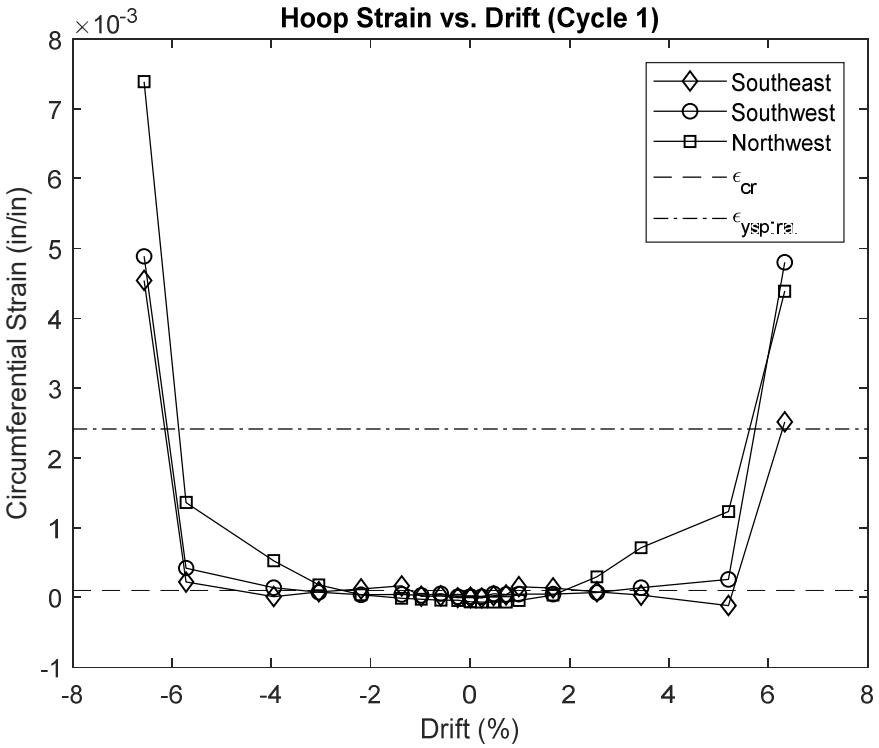

Figure 8-23. Hoop Strain at 21 inches above the base vs. Drift

In addition to the strains, the local behavior can be assessed in terms of the column displacements and rotations. Figure 8-25 shows secant drift ratios (SDR) vs. drift, based on the horizontal

displacements measured by the string pots at various heights along the column. The ratio is calculated as shown in Figure 8-24 and Equation 3. From Figure 8-25, it can be seen that at higher drift levels the SDR calculated from string pots located at different heights along the column tend to diverge. More specifically, lower secant drift ratios are obtained from string pots located closer to the column base and vice versa. This outcome is consistent with the visual damage seen in the test whereby significant cracking was concentrated in the plug region which would cause a loss of stiffness in that region compared to above the plug where there was no damage.

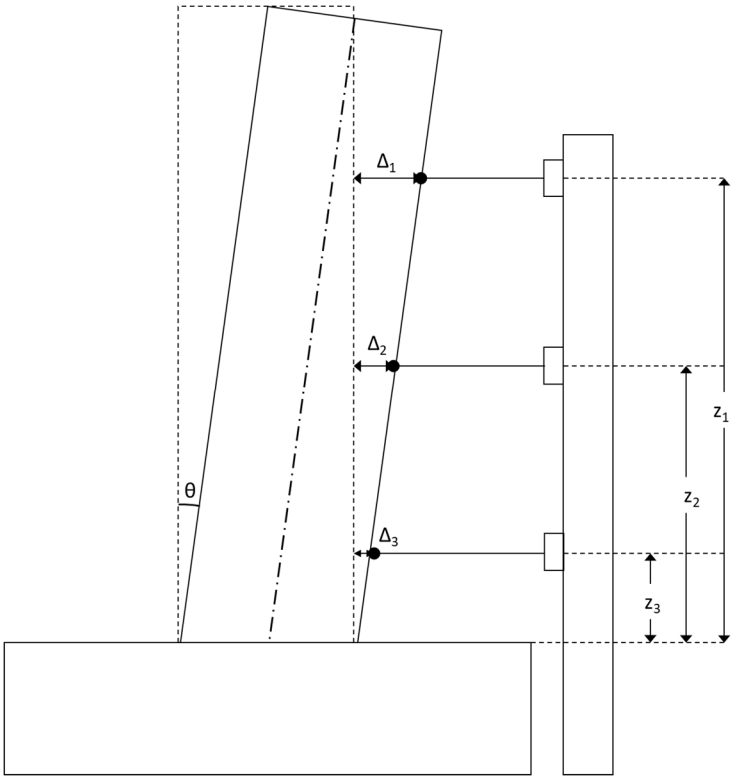

Figure 8-24. Base rotation Calculation Details

$$SDR = {\Delta_i}/{z_i} \quad (3)$$

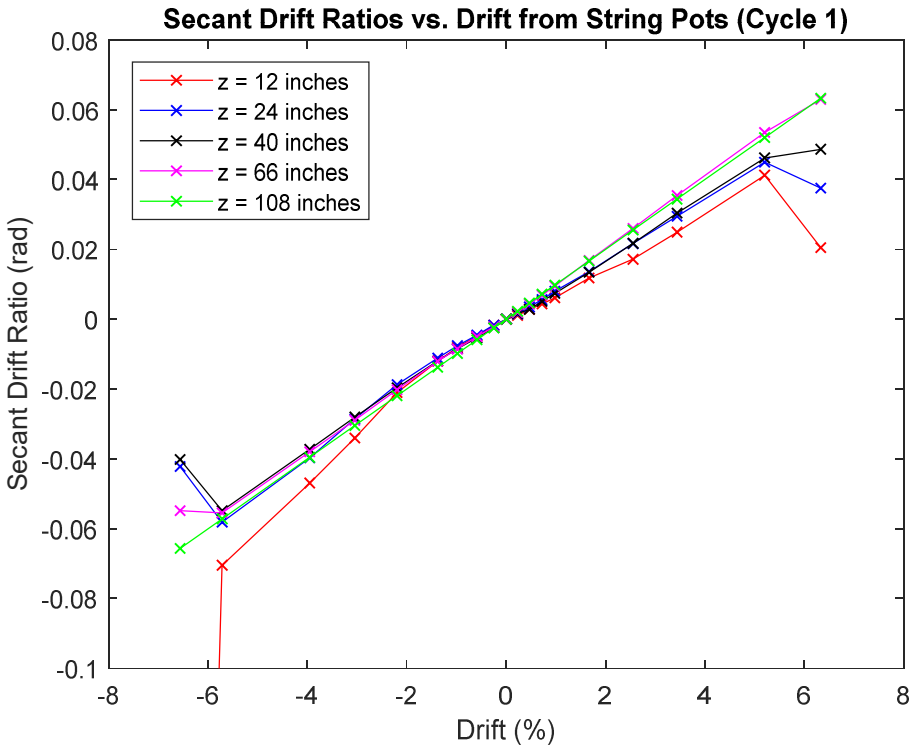

Figure 8-25. Secant drift ratio vs. drift calculated from horizontal string pot displacements

Figure 8-26 shows the total displacement measured at the top of the column by the string pots and the displacement from rotation, as measured by the vertical string pots which were attached at 24 inches above the cap beam (Eqns. 4 and 5).

$$\theta_{base} = \frac{\Delta_{vnorth} - \Delta_{vsouth}}{B} \quad (4)$$

$$\Delta_{rot} = \theta_{base} * L \quad (5)$$

θ_{base} = rotation at base
Δ_{vnorth} = vertical displacement on north side of column
Δ_{vsouth} = vertical displacement on south side of column
B = distance between point of measurements of string pots
Δ_{rot} = displacement from rotation
L = Height from cap beam interface to horizontal load application point (108 inches)

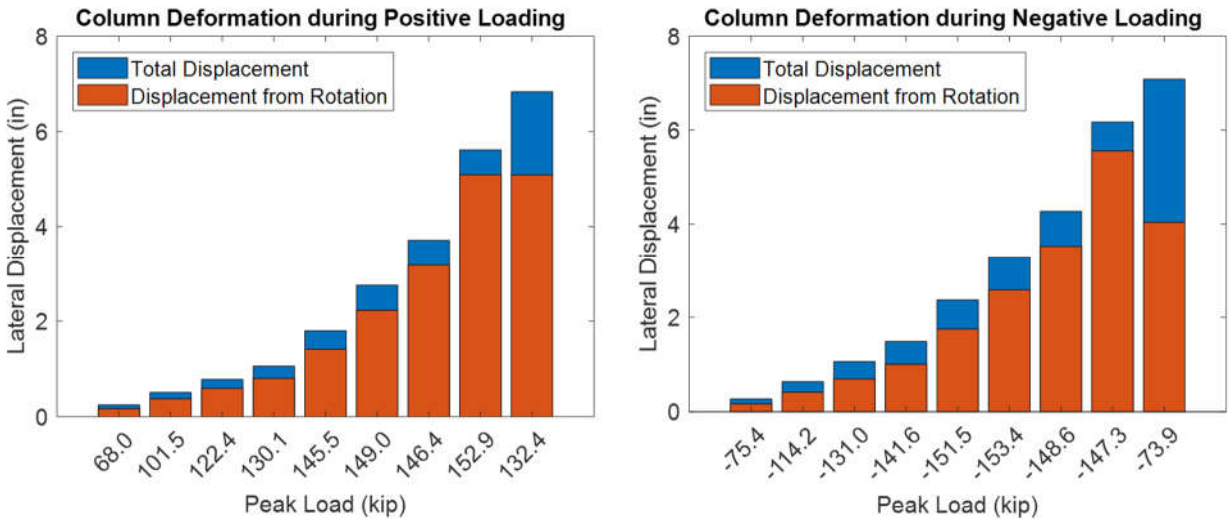

Figure 8-26. Difference between Total Displacement and Rigid Body Displacement

The displacement from rotation is a measure of the rigid body motion of the column while the difference indicates any column bending deformations. From Figure 8-26, it can be seen that the majority of the column displacement is due to rigid body motion throughout the experiment with bending deformations accounting for 9% of the total displacement at the maximum load. This is emphasized in Figure 8-27 which shows the slope of the displaced shape vs. height at several peak drift values in the positive and negative load directions. The local slope is measured directly by the inclinometers and also calculated for the mid-height between horizontal string pots using the secant stiffness as follows

$$Local\ Slope = \frac{\Delta_{z_i} - \Delta_{z_{i-1}}}{z_i - z_{i-1}} \qquad (6)$$

$$z_i = height\ of\ horizontal\ string\ pot, i$$
$$\Delta_{z_i} = measured\ displacement\ of\ horizontal\ string\ pot, i\ located\ at\ height, z$$

The difference between the local slope and the rotation at the base is another indication of any column bending deformations. As shown, the difference is very small except at the -5.7% drift which is after the tensile crack opened up on the north face of the column, precipitating failure and confirms the results in Figure 8-26. Also, the values shown for the horizontal string pots at a height of 53 inches are considered outliers due to measurement errors.

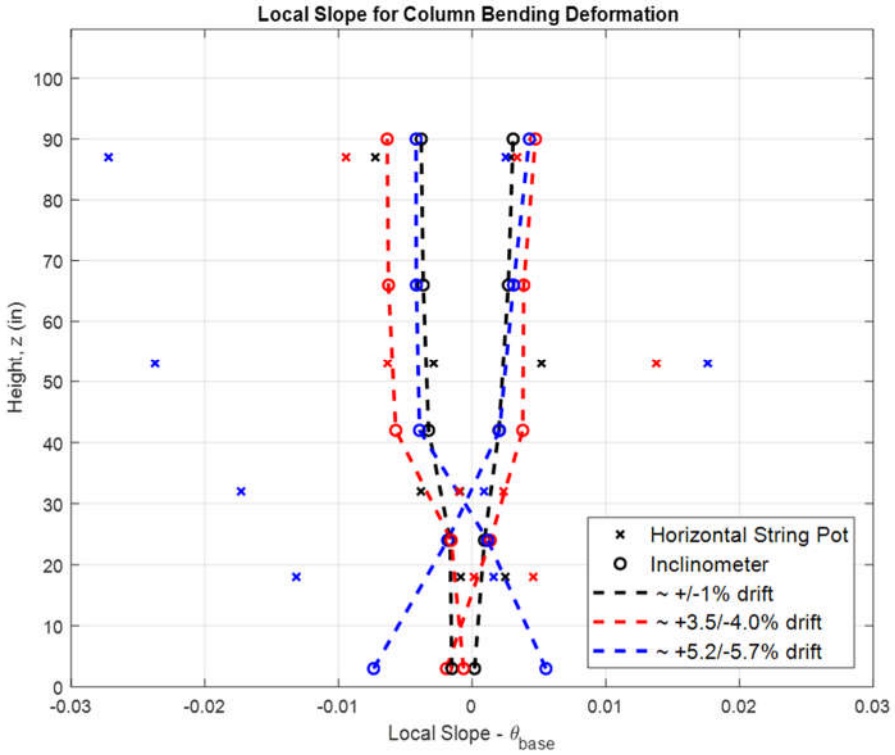

Figure 8-27. Extent of Column Bending Deformation in terms of Local Slope

Figure 8-28 shows the column bending deformation up the height of the column as compared to only at the top of the column shown in Figure 8-25. Again, the difference in total displacement and displacement from rotation is very small (<10%) throughout testing until failure is reached at +5.2% drift. This confirms that mostly rigid body deformations due to column rocking at the base occurred during testing.

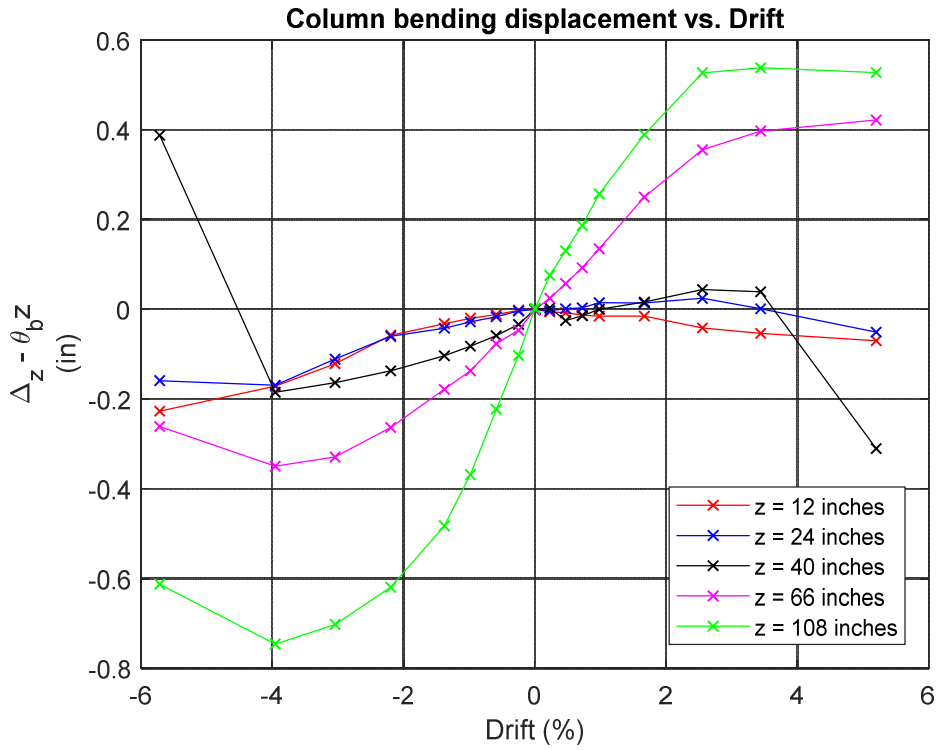

Figure 8-28. Extent of Column Bending Deformation in terms of Local Lateral Displacements

One final measure of the local behavior of the column is to assess whether the column experienced any shear deformations. This can be determined by comparing the rotations measured due to horizontal displacement to those due to vertical displacements. If the column underwent shear deformations then there would be no difference between the vertical displacements measured on either side of the column, and therefore zero rotation, since the horizontal displacement would be due to pure sliding (See Figure 8-29). On the other hand, if there are no shear deformations the horizontal displacement would be a result of rotation at the base and both rotations measured from horizontal and vertical displacements would be equal (See Figure 8-29).

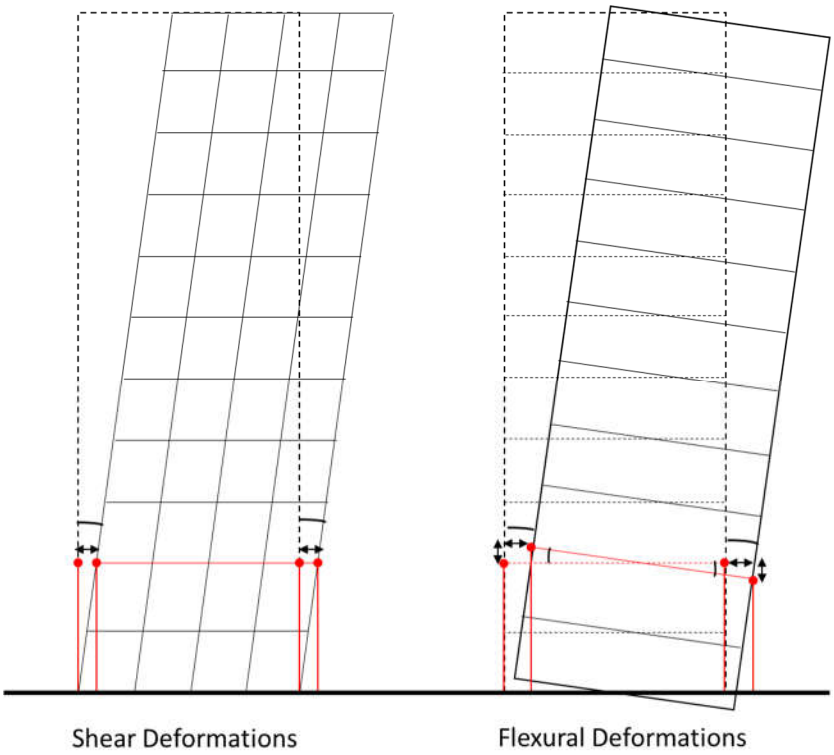

Figure 8-29. Shear vs. Flexural Deformations due to Column Displacement

Figure 8-30 shows the rotations measured from 3 different instruments at the same height along the column (24 inches). As can be seen, the rotations measured and calculated from each instrument are very similar at the peak loads of all series indicating that the column did not deform in shear and confirming a flexural failure. The readings for the final series of testing are very different due to the loss of the instruments when concrete began to fall off at failure.

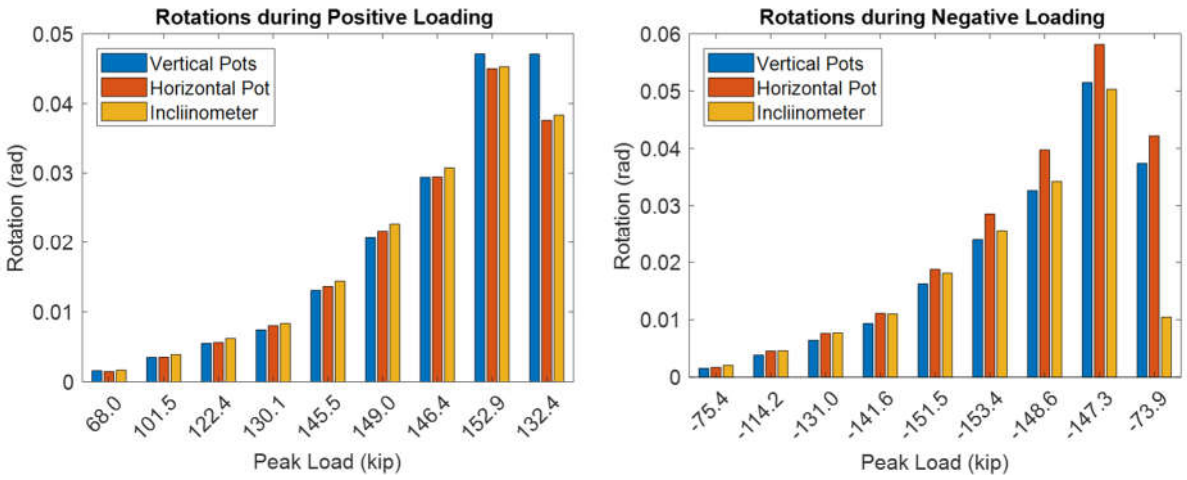

Figure 8-30. Rotations due to Vertical and Horizontal Displacement of Column

Chapter 9. COLUMN BENDING ANALYSIS

The cantilever column bending test described in Chapter 7 was done to understand the response of an as-built specimen to seismic loads. A reversed cyclic load history was applied to simulate the effects of lateral earthquake loads on the structure. The results of that test were presented in Chapter 8 and this chapter will discuss the implications of those results in predicting the behavior of the field columns.

9.1 MOMENT CAPACITY

The maximum moment at the base of the column during the test was measured as 16,500 in-kip at a drift ratio of +5.2%, during the first cycle of the series before failure. At end of test, the base moment was calculated as 14,300 in-kip.

The expected moment capacities of the hollow pile, the inner plug and the combined pile and plug (defined in Figure 9-1) were calculated with an in-house moment-curvature program used in the undergraduate reinforced concrete class and developed by Professor John Stanton. For constitutive laws, it uses the Popovicz curve (1973) for concrete, the Raynor (2002) law for rebar steel and the Menegotto-Pinto curve (1973) for strand. The concrete law did not include any effects of confinement. The moments were found using the material properties from Section 8.3 and the maximum moment and cracking moment are presented in Table 9-1 for each case. The assumed conditions, illustrated in Figure 9-1, were:

- *Plug only:* The concrete geometry was for the plug alone, and the reinforcement was only the plug bars. The concrete strength used was that of the plug.
- *Hollow pile only*: The geometry was that of the hollow pile alone, the concrete strength was that of the pile, and the reinforcement consisted of the strand, assumed to be fully bonded.
- *Combined pile and plug*: The geometry was taken as a circular section with diameter equal to that of the pile, because the pile concrete could resist compression by direct bearing. The concrete strength was taken as that of the pile, because the program has provision for

only one strength. The great majority of the compression force occurs in the pile wall, and not in the plug. The reinforcement consisted of the plug bars alone; the strand was not included because, at the column-cap beam interface, the strands terminate and carry no stress.

Table 9-1. Moment Capacities for Column Components

	Hollow Pile	Inner Plug	Combined Pile and Plug
Moment Capacity (in-kip)	13276	10860	15494
Cracking Moment (in-kip)	7844	3150	4327

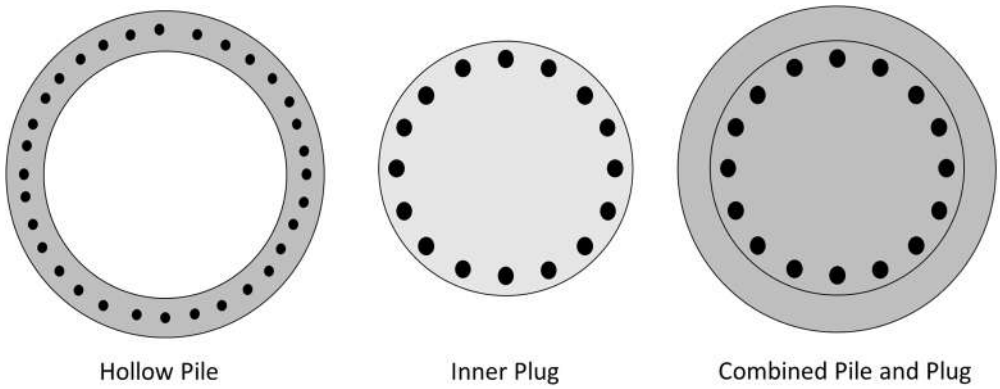

Figure 9-1. Reference for cross-section used to calculate moment capacities

Figure 9-2 shows the conditions at failure and the results demonstrate that the behavior in the plug region is complicated. Significant damage occurred both at the base and in the region between 30 and 38 inches up from the base (cap beam soffit) in the shaded “Damaged Area”.

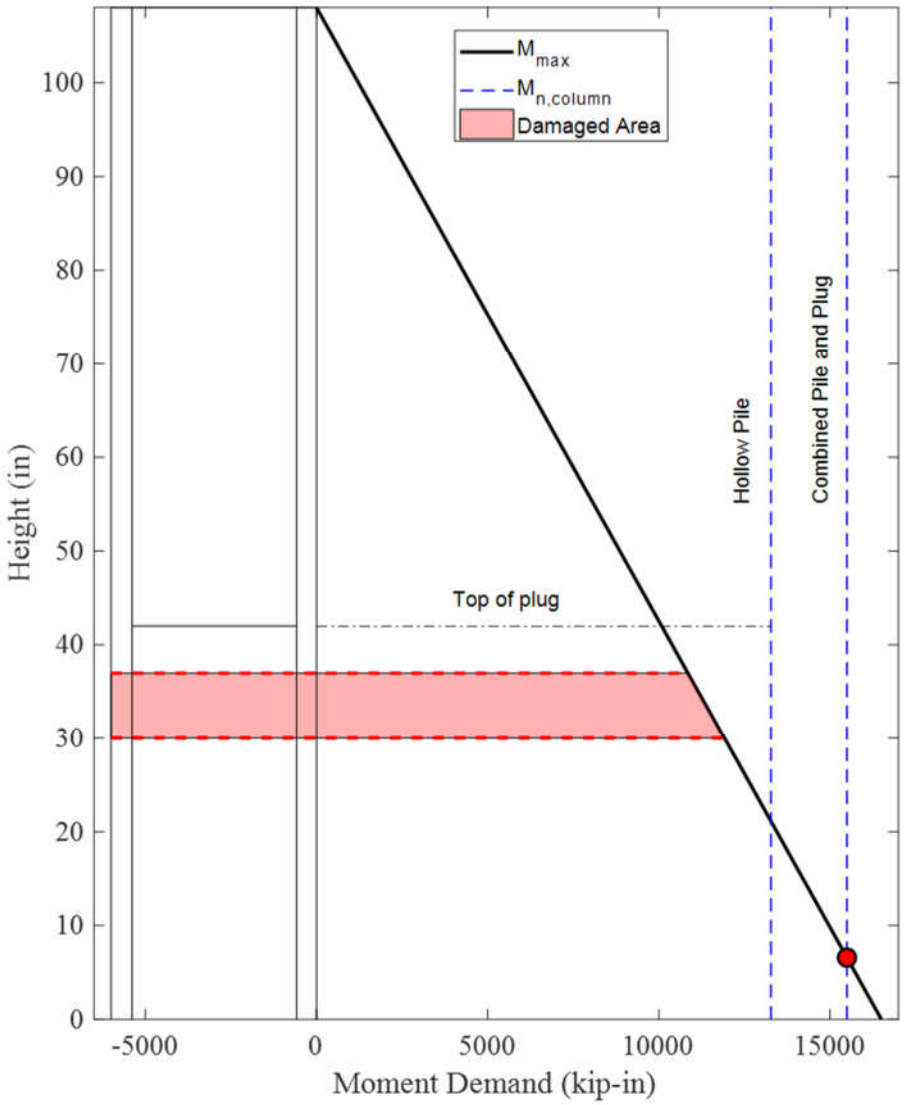

Figure 9-2. Conditions at Maximum Moment

The measured moment at the cap beam, where the plug bars yielded and the pile wall crushed, was 16,500 in-kip which is 6.5% larger than the predicted 15,500 in-kip for the combined cross section. This difference between the measured and predicted moment strength could be because the moment curvature program does not account for the added confinement of the concrete provided by the spiral reinforcement in the pile wall. However, only half of the column wall thickness lies inside the spiral.

In the second region of failure, near the end of the plug, large pieces of concrete spalled off the pile wall, the spiral fractured and the prestressing strands buckled (See Figure 9-3). This location

was well within the plug region, so the column wall could not spall inwards, in which case the section might be expected to behave like a solid one. However, the moment demand at mid height of the region was 11,350 in-kips, which is less than either the predicted hollow capacity (13,276 in-kips, assuming the strands can reach full strength), or the filled capacity of 15,500 in-kips (based on the plug bars providing the tension capacity).

Figure 9-3. "Damaged Area" at end of testing showing concrete spalling, buckled strands and spiral deformation

The reason for this location of the observed damage in compression is less clear. A possible explanation is as follows:

- *Strand bond*: The development length of the 3/8" diameter strands if taken as $150d_b$ is approximately 56 inches according to ACI318, assuming that it is fully stressed initially. That assumption is likely not valid, because the location is close to the free end of the pile. Consequently, the development length was probably longer than 56 inches, in which case the strands were not fully developed at that location. The crack formed when the north face of the column was in tension, and its width suggests some debonding. It is possible that the

strand slipped, allowing the crack to open but, on the next half cycle, the remaining bond stress was high enough to prevent the strand slipping back before it buckled. The buckling strand pushed radially outwards on the spiral, which kinked and fractured.

The highest moment demand in a hollow region (at the end of the plug) was 10,000 in-kips. This is 75% of the predicted hollow capacity, and largely explains why the column did not fail in the hollow region. This is in the lower region of the demand to capacity ratios predicted for the field piles under as-built conditions in Chapter 3. Thus, while it was logistically impossible to simulate all of the field conditions, the outcome of the test still provides useful insights into this question.

It is likely that a jacket would have improved the performance of the splice in the plug region, and that would have changed some of the moment demands and capacities. For example, if the strand had remained fully bonded, all the inelastic behavior would have been forced into the region at the column-cap beam interface. However, the behavior measured in the test shows that the load transfers in the plug region are sufficiently complex, and contain enough uncertainties, that further testing, and modeling, will be necessary to develop a reliable retrofit based on the use of the as-built section.

The region resembles the one investigated by Tran (2015). In that research, a precast column was embedded in the top of a larger diameter cast-in-place drilled shaft, and the connection was subjected to bending and shear. The load transfer mechanism identified were complicated, and the outcome depended on the depth of embedment and on the quantity of spiral in the shaft.

9.2 SHEAR CAPACITY

The shear capacity of the hollow column can theoretically be calculated using ACI's criterion of a principal tension stress of $4\sqrt{f'_c}$ at the centroidal axis if the walls of the column in the direction of load are treated as the web of the member (ACI 318-11 Provision 11.3.3.2). If this value is used and following a Mohr's circle analysis, a value for the shear strength of the column concrete can be found, as in Chapter 3.5, Equations 3-7. The shear strength of the test column concrete was calculated as 214 kips, based on the compression strength of 14,500 psi (day of test), and a

maximum shear stress of $2V/A_c$, where A_c is the net cross-sectional area of 364 in^2. The factor of $A_{shear}/A_c = 0.5$ was derived theoretically for a thin-walled hollow cylinder.

The spiral reinforcement will also add some shear strength to the column and this is simply given by

$$V_{n_{spiral}} = \frac{2A_{spiral}f_y d}{s} \qquad (1)$$

where
V_{n_spiral} = shear capacity of spiral reinforcement
A_{spiral} = cross-section area of spiral (W7 wire) = 0.07 in^2
f_y = yield strength of spiral steel, taken as 70 ksi
d = center to center diameter of spiral = 32.5 inches
s = spacing of spiral reinforcement along the length of the column = 3.5 inches

The shear strength added by the steel is 91 kips therefore the total shear capacity of the hollow column is 305 kips. The maximum shear demand on the column under test conditions was 152 kips which is half of the theoretical value for the shear capacity and 75% of the shear strength of the concrete alone. This is consistent with the fact that no shear cracks or deformations were observed or measured in the pile wall during testing.

This demand to capacity ratio of the shear strength in the column confirms the purely flexural failure that was observed during testing. In the field, the dominance of shear or flexural failure is dependent on the critical shear span of less than 3 column diameters as shown in Chapter 3.7 for a fixed-fixed column subject to sidesway loading. While this is re-assuring, because it appears to remove one potential failure mode from consideration, the research should include experimental investigation of the shear strength of a hollow column, because so little previous work has focused on this behavior and the validity of the method used to find the shear strength of the concrete is uncertain.

9.3 Capacity Spectrum Method

The drift at maximum moment was +5.2% which was much higher than expected based on previous analysis. Also, the column showed very little strength degradation over many cycles of

increasing displacement before ultimate failure, exhibiting surprisingly more ductile behavior than was predicted.

The ductility of the system warrants a second evaluation of the peak ground acceleration (PGA) required to cause failure of the column, as well as other preceding damage states. The PGA is a measure of the earthquake intensity level that would be needed to cause the particular failure mode investigated. This can be done using the Capacity Spectrum Method (Freeman, 2004).

The Capacity Spectrum Method (CSM) estimates the peak response of a system by comparing demand and capacity of a nonlinear system. The demand is expressed by plotting the pseudo-spectral acceleration, S_a, vs the spectral displacement, S_d. These spectral values are computed in the conventional way for a linear system. The capacity curve is obtained from a "pushover" force-displacement curve, in which the force is divided by the mass of the system to give acceleration. The two curves are superimposed and the point where they intersect gives the displacement of the system. This response point is defined by the damage state being investigated and can be related to any point along the force-displacement pushover curve.

The approach is convenient in that it allows a linear response spectrum to be used, even though the response is nonlinear. It avoids the need for time-consuming non-linear modeling in the time domain. It is necessarily approximate, because it assumes that a nonlinear system can be represented by a linear one with the same secant stiffness to peak response, and a viscous damping value derived from the EDC (Energy dissipated per cycle) of the real nonlinear system. These are the same assumptions that underlie the Direct Displacement Based Design method (Priestley et al. 2007).

For the test column, three main damage states (DS) were identified for evaluation:

- *DS1*: Yielding of plug reinforcement, corresponding to the start of inelastic behavior. This was determined by the results obtained from the strain gages on the plug rebar and was taken as the point of first yield at any location along the bars, typically 3 inches above the base of the cap beam (at approximately 0.72% drift).

- *DS2*: Substantial spalling and exposure of spiral reinforcement. This was determined by visual observations noted during the test.
- *DS3*: Ultimate failure, corresponding to the point of maximum base moment and this was determined from the results of the calculated base moment.

The three damage states are identified on the graph of effective horizontal force vs. drift ratio (See Figure 9-4). The backbone curve identifying the peak forces associated to each loading series will be used as the pushover curve in the capacity spectrum method. For simplicity, the analysis will only be shown for the positive force-displacement results.

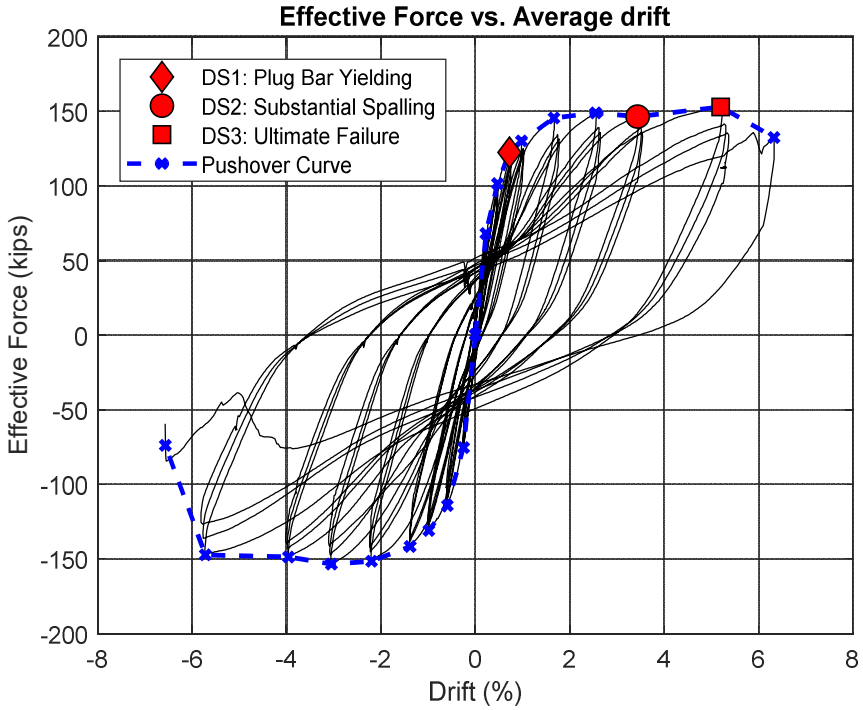

Figure 9-4. Force-displacement curve with key damage states (DS) identified for CSM

9.3.1 *Capacity Curve*

The first step in the capacity spectrum method is to convert the pushover curve to an equivalent capacity curve. For a single degree of freedom system, like the cantilever test column, this is simple. The equivalent spectral displacement S_d is the measured displacement while the equivalent

spectral acceleration S_a (in terms of the gravity constant, g) is the ratio of the applied lateral force to the total weight acting on the system, which in this case was the applied axial load of 200 kips.

$$S_d = \Delta \; ; \; S_a = \frac{V}{W} \qquad \text{(2) and (3)}$$

The capacity curve for the test column response is shown in Figure 9-5.

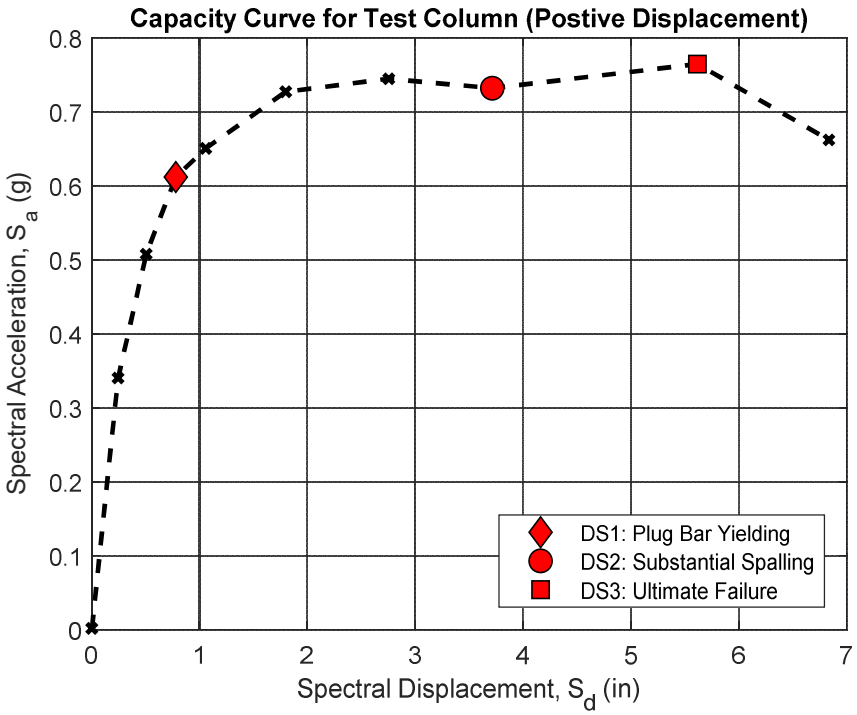

Figure 9-5. Capacity curve from pushover conversion

9.3.2 *Demand Curve*

The second step in the capacity spectrum method is to develop the demand curve for the particular damage state of interest. As stated before, the demand curve is derived from the 5% damped design spectrum. For this analysis, the design spectrum was taken as the 1000-year return period AASHTO LRFD spectrum for site class B in Seattle, WA (See Chapter 3, Figure 3-2). The actual demand spectrum for each damage state should be calculated from a damping reduction factor that is a function of the effective damping associated with the capacity curve at that displacement, which is defined by equivalent viscous damping or the idealized area under the hysteresis curve.

However, to remain consistent with the analysis done in Chapter 3, the hysteretic damping that can be calculated from the test results will be ignored here and the 5% damping assumed.

For the three damage states identified, the measured lateral force and displacement, and displacement ductility, are given in Table 9-2.

Table 9-2. Characteristics used for Demand Spectra at Damage State Levels

	Damage State 1	Damage State 2	Damage State 3
Force, V_{DS} (kip)	122.4	146	153
Displacement, Δ_{DS} (in)	0.781	3.71	5.61
Displacement Ductility, μ	1.0	4.75	7.19

The normalized spectrum can be used to find the PGA of the earthquake that would be needed to induce the damage state of interest. From an analytical point of view, the PGA_{DS} associated with a given damage state can be determined as the ratio between its spectral acceleration corresponding to the force level on the pushover curve, and the normalized spectral acceleration at the effective period of the system, T_{eff} on the equivalent damped response spectra (in this case the 5% spectrum). The demand spectrum for each damage state can then be plotted against the capacity curve by using an earthquake magnitude factor, F_{EQ} given by the ratio of PGA_{DS} to the PGA of the reference spectrum.

The procedure is outlined below:

- Find the spectral acceleration corresponding to the particular damage state, Sa_{DS}

$$S_{a_{DS}} = \frac{V_{DS}}{M} \qquad (6)$$

- where M = seismic mass on the column, taken as the mass calculated from the applied axial load of 200 kips
- Find the effective period of the system corresponding to the particular damage state, T_{eff_DS}

$$T_{eff_{DS}} = 2\pi\sqrt{\frac{M}{K_{eff_{DS}}}} = 2\pi\sqrt{\frac{M}{V_{DS}/\Delta_{DS}}} \quad (7)$$

- Find the spectral acceleration at the effective period of the system using the normalized 5% damped spectrum for the damage state, Sa_ξ.
- Find PGA_{DS} and F_{EQ} for the damage state, then plot the demand spectrum. The PGA_{ref} is 0.4g for the reference spectrum used

$$PGA_{DS} = \frac{S_{aDS}}{S_{a\xi}} \quad (8)$$

$$F_{EQ} = \frac{PGA_{DS}}{PGA_{ref}} \quad (9)$$

The results of the analysis are summarized in Table 9-3.

Table 9-3. Capacity Spectrum Method Results for Damage States

	Damage State 1	**Damage State 2**	**Damage State 3**
Effective Period, T_{eff_DS} (s)	0.361	0.718	0.866
Spectral Acceleration, Sa_{DS} (g)	0.612	0.73	0.765
Sa_ξ (T_{eff}, ξ_{eff}) (g) - normalized	2.424	1.219	1.01
PGA_{DS} (g)	0.252	0.599	0.757
EQ Magnitude Factor, F_{EQ}	0.63	1.50	1.89

9.3.3 *Results*

The Capacity Spectrum Method was employed to describe the results of the cantilever bending test for a scaled as-built column in terms of the seismic hazard. The PGA values obtained from the above analysis represent an estimate of the median threshold value of the peak ground acceleration related to the selected damage state (Cardone et al, 2011) and can be used as a reasonable first estimate of the ground motion required to cause damage to a similar column in the field. The key takeaways from the analysis are discussed below and the main limitations are presented.

Damage State 1 in which the plug reinforcing bars begin to yield will occur during an earthquake with a lower PGA than the 1000-year AASHTO design earthquake for site class B in Washington State (F_{EQ} = 0.63). As observed during the test, this damage state is associated with significant cracking on the pile wall in the plug region but no concrete spalling. Damage State 2 which corresponds to substantial spalling of the unconfined concrete in the pile wall at the cap beam-column and Damage State 3 that corresponds to the maximum strength of the column before ultimate failure both require an earthquake with a much larger PGA than the 1000-year design earthquake and even the 2500-year maximum considered earthquake (for DS3), typically given as 1.5 times the design earthquake (F_{EQ} = 1.5 and 1.89, respectively). These results stem from the highly ductile performance of the filled plug region, which appears to have acted as a plastic hinge where all the damage was concentrated.

While the results are favorable, there are limits to their application. Firstly, the reference response spectrum is general and may not be applicable to the site conditions in the field. Secondly the test specimen was designed to be a general and scaled model of a hollow column with a reinforced plug at the cap beam-column connection but some aspects such as the length of the span were limited by the available test equipment (See Chapter 7). Furthermore, the test only evaluated the failure associated with the aboveground column that is an isolated component of the field columns, and did not account for any possible failure of other regions below ground. Lastly, the effects of damping are not accounted for even though there is some damping due to energy dissipation as indicated by the hysteresis curve. However, the use of the 5% damped reference response spectrum gives a conservative estimate of the ground motion needed for damage and provides results consistent with the previous analyses. A brief analysis using the numerical model of Chapter 3 was done to incorporate the test results into the full system and this is shown in the next section.

9.4 Numerical Simulation of Test Conditions for Field Application

A trial and error approach was used to find the combination of column length and pile length that would result in the moment strength of the test column (M_n = 16,500 in-kip) being achieved over the same span length used in the test (L_{span} = 108 inches), under the same column axial load (P = 200 kips). This was confirmed by checking the M/V ratio such that it was 9 feet as was the case in the test. This was evaluated using the site class B response spectrum, a soil stiffness of 1000 kcf

and assuming deck weight but no deck stiffness, as was done for the reference condition in Chapter 3. The approach led to L_{col} = 11 feet and L_{pile} = 22 feet. For these values, an earthquake amplification factor F_{EQ} = 0.76 was found to cause yielding at the top. However, this corresponds to a cap beam displacement of 0.552 inches and therefore no ductility demand, as observed in the lab.

To capture the ductility seen in the lab, the analysis was set up as in Chapter 3 for "pile yield" whereby the rotational spring stiffness, α at the cap beam-column connection was set to 0.0 but a moment equal to the moment strength of the test column was applied at the top node of the column. When this was done, the system failed at a location below ground when the predicted moment strength of the hollow pile was reached. This corresponded to an F_{EQ} = 1.00 and a cap beam displacement of 1.2 inches. However, this analysis used the 5% damped spectrum and so is somewhat conservative since the ductility demand in the lab implied bigger damping for higher damage states.

For the purpose of evaluating the merit of the proposed retrofit given the ductile response of the as-built column, an analysis was also performed as in Chapter 3 assuming the removal of the pile wall directly below the cap beam so that the "plug only" moment strength governs first yield at the cap beam, followed by the "pile yield" below grade. The results for these analyses using the numerical model are summarized in
Table 9-4 and shown in Figure 9-6 in the acceleration-displacement response domain.

Table 9-4. Summary of Results from Numerical Analysis using Test Conditions

	F_{EQ}	Δ_{cap_beam} (in)	DCR_{col}	DCR_{pile}
As-built first yield	0.76	0.552	0.76	0.51
As-built ultimate	1.00	1.194	0.61	1.0
"Plug Fuse Retrofit" first yield	0.50	0.360	0.50	0.34
"Plug Fuse Retrofit" ultimate	0.92	1.224	0.30	1.0

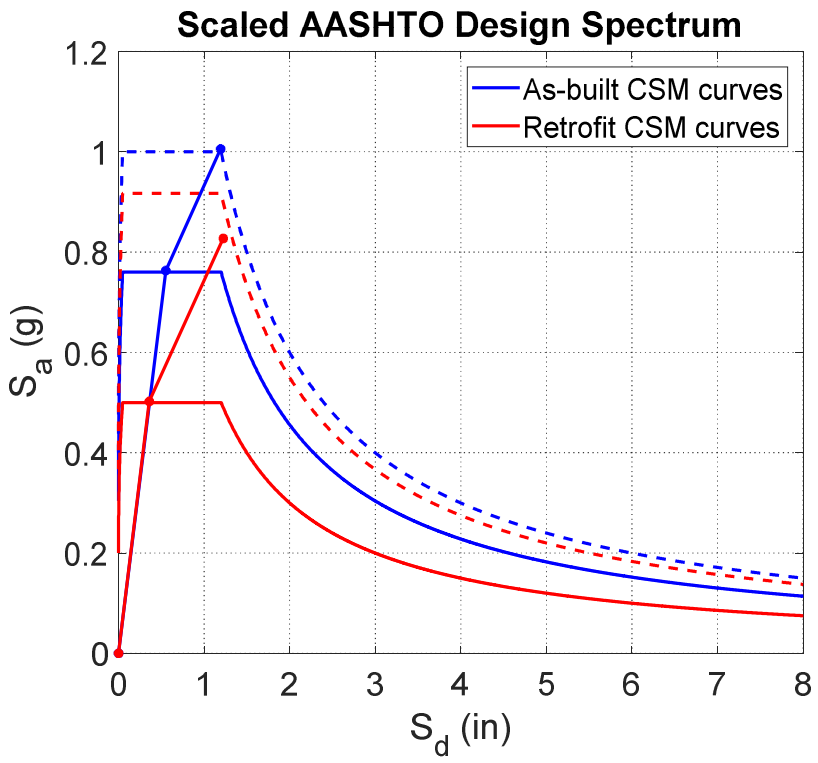

Figure 9-6. Demand and Capacity curves for Numerical Analysis of As-built and Retrofit Test Conditions

There are two main outcomes to be noted:

- The as-built column test displayed much greater ductility than can be expected when considering the whole system since the hollow pile below grade will control the ultimate failure, as evidenced by the results in Table 9-4. When considering the column-pile together, the hollow section below grade reaches its peak flexural strength at a cap beam displacement of 1.2 inches which relates to a displacement ductility of 2.2. This is much less than what was considered for Damage State 2 in the CSM, indicating that, in the field, below-ground failure will precede the DS2 and DS3 performance levels at the cap beam. However, this below grade failure occurs at an F_{EQ} of 1.0.

- A comparison of the as-built and retrofitted projections shows that each has advantages at different damage states. At first yield of the plug, the retrofitted column reaches that state at a lower FEQ, in other words, it yields under a less severe earthquake. However, yielding

of the ductile element is not a critical event. Perhaps more important, the hollow column just below the plug experiences a 33% lower DCR when retrofitted than as-built (DCR of 0.50 vs 0.76). That means that the section of hollow column just below the plug is better protected against damage at this stage. However, under larger ground motions, i.e. those that cause enough displacement and plastic rotation at the cap beam that the pile reaches its capacity below grade, the as-built system has an 8% advantage (FEQ = 1.0 vs 0.92)

9.5 Application to Field Conditions

In this chapter, an attempt was made to project the behavior seen in one test out to field conditions. That process is uncertain for several reasons:

- Ultimate failure is expected to occur below grade in all cases, but the test was conducted on a column to cap beam connection. Extrapolating from one to the other requires assumptions about the other parts of the system that connect them, including the pile bending and soil deformations.
- The proportions of the laboratory test specimen differed somewhat from those to be expected in the field, for reasons controlled by available pile sizes and test equipment.

Despite these uncertainties, several outcomes can be seen:

- The damage that occurred in the test was located in the plug region, and no internal spalling was seen in the hollow section. (The moment in the hollow column reached only 75% of its predicted nominal moment capacity, so it could be argued that damage should not be expected. However, it is useful to have such a lower bound value for the spalling threshold). The finding suggests that the plug-column-cap beam connection should be retrofitted first, because otherwise the lateral load could not increase enough to cause failure below ground.
- The as-built column-to-cap beam connection was more ductile than expected, and a retrofit option that involves simply jacketing the column in that region may be feasible.

- Retrofitting the column-to-cap beam connection alone, without any changes to the hollow regions of the column, offers good prospects for making the system able to resist a 1000-year earthquake motion.

Chapter 10. DISCUSSION

10.1 REVIEW OF RESEARCH PLAN

The seismic performance of bridges built with hollow, precast, prestressed concrete column-piles was relatively unknown at the start of the research program. Previous studies suggested brittle flexural failure of the hollow prestressed concrete columns due to internal implosion of the wall. Two locations in the column-pile are particularly susceptible to large moments which can trigger this mode of failure. These are (1) just below a solid reinforced concrete plug at the cap beam-column connection and (2) below grade. The reinforcement in the plug extended into the cap beam, where it was developed, with the goal of creating a moment connection between them. The plug extended a short distance into the hollow column directly below the cap beam so its presence prevents the inward implosion of the hollow section in that critical region. However, depending on the length of the plug and the moment gradient along the length of the column, there exists the risk of a hollow section flexural failure just after the plug ends, where there is a sudden change in the column's flexural capacity. This motivated the evaluation of the following retrofit concept, termed a "plug fuse", to reduce the risk of hollow column failure in that region.

The retrofit is centered on the idea of removing the pile wall over a short distance right below the cap beam so that only the inner plug is able to resist the moment demand at that location. Then the moment demand at the cap beam level is reduced to the value of the plug flexural capacity, and so the demand along the length of the hollow column-pile also diminishes. Additionally, the plug would be jacketed as to improve its ductility. Therefore, when the plug yields at its maximum moment, it can act as a ductile "fuse" under increasing lateral loads, until the column fails elsewhere.

However, cutting back the pile wall directly below the cap beam introduces the issue of indirect transfer of the axial load to the continuous column-pile. The axial load from the bridge superstructure would have to be transferred through shear friction at the interface between the pile wall and the cast-in-place plug rather than by direct bearing, as is the case in the as-built structure. The available models for shear friction interface strength are limited in their applicability to this

situation due to the difficulty in predicting the normal force acting in the radial direction. Additionally, the surfaces of the pile walls were roughened with an epoxy mortar according to the bridge record drawings but the details of the pile surface roughness, mortar mix and its application were unknown and so the effect this would have on the shear friction at the interface was also uncertain. Therefore the issue of shear friction transfer at the epoxied interface also had to be addressed to fully determine the feasibility of the retrofit concept.

The research program was planned to confirm the behavior of the as-built column, and to explore the feasibility of the retrofit scheme through both analytical modelling and experimental work. The analytical investigation was undertaken to inform the scope of the experimental program. The analytical model is described in Chapter 3.3 and was used to perform a parametric study on factors that affect the performance of the column-pile system under lateral loading, accounting for both the as-built and potential retrofit conditions through an elasto-plastic spring at the cap beam-column connection. A summary of the findings from the analysis is given in Section 10.2.

Motivated by those findings, two separate experimental programs were developed. The first experimental program was conducted as a parametric study to explore the shear friction interface strength between the column wall and the cast-in-place plug since the analysis showed that the plug fuse concept is a viable retrofit to improve the column-pile response to seismic loads. The second program sought to understand the type of failure that would be expected of the existing bridge columns at the cap beam-column connection as a result of the complicated composite system that is formed by the presence of the cast-in-place reinforced concrete plug in the hollow, prestressed concrete pile.

10.2 Research Findings

The results of both the analytical modelling and the experimental programs are summarized in the following sections.

10.2.1 *Analytical Results*

The analytical investigation undertaken in Chapter 3 addressed both the as-built condition and the retrofitted state in which the wall is cut back and the plug region jacketed. The analysis assumed non-ductile performance for the as-built conditions based on a low confining steel ratio and previous literature on hollow pile failure. The retrofitted conditions assumed two damage states which were yielding at the "plug fuse" section followed, after a further increase in load, by brittle failure of the hollow pile. The analysis suggested that the "plug fuse" concept would be a valid retrofit solution to explore as the parametric studies showed three main outcomes that affect bridge performance:

1. In the as-built condition, the column-pile will always yield at the cap beam-column connection, but in some cases the demand to capacity ratio (DCR) at the hollow section of the column-pile immediately below the plug was as high as 0.9, leading to the possibility of internal spalling there. When the plug is exposed by removing the column wall and the moment capacity at the point of maximum moment decreases, the DCR immediately below the plug was never higher than 0.7. In this regard the "plug fuse" retrofit provides better capacity protection to the hollow section.
2. By allowing the plug to act as a ductile "fuse" for the system, the pile behavior could sustain inelastic rotation after yielding at the cap beam level, to the point at which the pile capacity was reached at some other location, which always proved to be below grade.
3. The hollow section failure below grade always occurred at an earthquake loading significantly greater than that needed to yield the top of the column.

A more detailed summary of the results of the analytical investigation is provided in the following sub-sections.

10.2.1.1 All Columns

The presence of a deck provides considerable resistance to the lateral loads, provided the deck is continuous and has no joints. That condition is found, for example, in the Green River Bridge. The load resisted by the deck reduces the load to be carried by the bents, and thus reduces the

column and pile moments. In all of the analyses where the deck stiffness was considered, the column-pile failure occurred at a peak ground acceleration at or greater than the PGA of the 1000-year return period design earthquake.

Under elastic conditions, the parameters most damaging to flexural strength of the as-built columns are softer soils and longer columns. For both of these conditions, the DCR of the hollow section directly below the plug increases reaching as high as 0.85 for very soft soils (β_{soil} = 20 kcf) and 0.9 for very long columns (L_{col} = 60 ft). Furthermore, these conditions lead to unrealistic drifts at ultimate failure which could jeopardize other components above ground.

The length of pile has no effect on the DCR of the below-plug hollow section or the earthquake amplification factor F_{EQ} for ultimate failure except for very short piles e.g. L_{pile} = 10 ft, with L_{col} = 20 ft. Then for a given moment at the cap beam, the moment gradient is less steep and the DCR at the end of the plug rises.

The analytical model used was relatively simple in order investigate the several parameters in a reasonable time. Its limitations include:

- The soil was modelled as linear elastic with constant stiffness with depth below ground. Use of nonlinear soil springs, and stiffness that varies with depth, may make a difference to the results. However, large differences are not expected, because a wide range of stiffnesses was explored with the elastic stiffness model.
- The ground was assumed level in all cases, so that all column lengths are the same. Sloping ground, which is the case at Galer-Lakeview and L^E Line/Slide bridges, will likely cause larger drift ratios in the shorter columns, and a redistribution of the seismic load among the columns.

While the model considered the flexural failure of the columns, the possibility of shear failure was considered. Little experimental evidence is available for the shear capacity of hollow columns, so the values are open to some doubt. However, the critical shear length, defined as the point to contraflexure in the moment distribution along the column-pile, was found to be 1.5 pile diameters

from the bottom of the cap beam. This critical length implies that columns shorter than this may be susceptible to shear failure. Few columns in the field are likely to meet this criterion, so shear failure was regarded as less important than flexural failure.

10.2.1.2 As-built Columns

For the as-built condition, the column yields at the top first and constitutes system failure under the assumption of no ductility. When this occurs, the DCR of the hollow section directly below the plug is in the range of 0.7-0.9 leaving little room to account for the uncertainties and assumptions in the model. The trends observed for the elastic conditions described in the previous section hold true. The addition of the deck stiffness makes no difference to the DCR but does increase the earthquake amplification factor that causes yielding. The difference is slight with the standard values for all the parameters, but increases for combinations of parameters that increase the ratio of deck stiffness to column stiffness, such as longer columns or a shorter deck. However, the factor remains significantly below 1.0, in the range F_{EQ} = 0.55 - 0.7, indicating that the as-built column will always fail during an earthquake smaller than the AASHTO 1000-year design earthquake.

10.2.1.3 "Plug Fuse" Retrofitted Columns

For the retrofitted conditions, the pile wall directly below the cap beam has been removed over a short distance and the exposed plug is jacketed to improve ductility. First yielding of the exposed plug typically occurred at an F_{EQ} in the range of 0.4 – 0.5. However, even though the plug fuse will yield in an earthquake smaller than the one required to cause first yielding of the as-built condition, the DCR of the hollow section below the plug drops significantly to between 0.55 – 0.65, essentially ruling out failure in the hollow section. System failure is caused by the hollow pile's reaching its flexural capacity below ground. This happens at an F_{EQ} just under or at 1.0, which is favorable.

10.2.2 *Experimental Results*

The measured results of the two experimental programs were used to better understand the behavior of both the as-built column and the potential "plug fuse" retrofit solution. The results were favorable and are reviewed in the following sections.

10.2.2.1 Plug Shear Friction Push-through Tests

The results of the parametric plug shear friction tests were very scattered so that developing a robust model to describe their behavior was difficult. Most of the difficulty lay in the fact that the radial stress at the plug-wall interface is difficult to determine reliably. However, with the approximations made in Chapter 6, the following key findings should be noted.

1. Failure consistently occurred between the epoxy mortar and the wall, and not between the epoxy and the plug concrete. This is not surprising in view of the fact that the wall was much smoother than the deliberately roughened surface of the epoxy mortar. However, it implies that the surface roughness of the inside of the piles in the field is critical, but it is unfortunately not known.
2. The friction coefficient suggested by the AASHTO provisions is much too high for predicting the shear friction interface capacity at the pile wall-plug surface.
3. The cohesion term given by AASHTO provisions appears to be consistent with the measured behavior. The application of the epoxy mortar on the inside of the pile wall before casting the plug, as noted in the reference bridge drawings, seemed to improve the cohesion at the surface.

Due to the uncertainty inherent in the results, further testing for confirming the data can be done. If the shear friction capacity is deemed inadequate and reinforcement, such as radial bars crossing the interface, is planned, that detail should be tested.

10.2.2.2 Column Cantilever Bending Test

The tested cantilever column exhibited more ductility than had been expected, in view of the low spiral ratio. The behavior of the column showed little strength degradation over increased cyclic displacements, out to 5% rotation before failure. Damage accumulated gradually but was concentrated in the plug region of the column, with rotation occurring at the cap beam connection, but failure was initiated by an unexpected mechanism, consisting of a large tension crack near the end of the plug region that appeared to be associated with bond failure of the strand.

The hollow region of the column was not loaded to its predicted moment capacity due to limitations of the test equipment but adjacent to the plug, a DCR of 0.75 was measured (The demand was measured while the capacity was computed from moment curvature analysis). There was no sign of implosive failure as seen in past research studies and this suggests that further testing should be done to determine the actual bending strength of the hollow pile in order to validate the predicted capacity and confirm the mode of failure to be expected in the hollow section.

Additionally, there was no sign of shear deformation or even shear cracking. The length of the specimen made it theoretically not shear-critical, so these findings agree with the predicted flexural failure mode. Since there are some very short columns that exist in the field, further testing to determine the true shear capacity of the hollow columns would be beneficial.

10.3 Research Application to Bridges in the Field

The ductility of the as-built test column raises the question of whether the "plug fuse" retrofit is the best solution to improve the seismic performance of the column-piles. An analysis that relates the scaled test conditions to the field showed that the ductility afforded by the as-built condition is sufficient to permit enough inelastic rotation at the cap beam to allow the column to reach its flexural capacity below ground. Furthermore, the F_{EQ} when it did so was slightly higher (1.00 vs 0.92, see Table 10-1) than the F_{EQ} for below-ground failure with the retrofit scheme (See Table 10-1, taken from Chapter 9). These findings suggest that the bridge would suffer damage, but not quite collapse, in the 1000-year earthquake, even if no retrofit were undertaken. However, this is

risky given the limitations of analytical model used and the fact that it is based on only one test result.

That risk could be significantly reduced by implementing a different retrofit concept, namely jacketing the column in the plug region without cutting back the pile wall. This is referred to herein as the "jacket-only" retrofit. The jacket might be expected to increase the rotational ductility capacity at the top of the pile. The expected benefit would be that the F_{EQ} required to reach final failure (underground) would be about 8% higher than for the original retrofit scheme (F_{EQ} of 1.00 instead of 0.92 as shown in Table 10-1). The drawback would be that the DCR at the end of the plug would be higher (0.76 vs. 0.50), and would risk a premature implosive failure there. Note that the values given in the table are for the reference conditions used in the analyses, superimposed to align with the test results (See Section 9.4) and would change if any of the parameters were to change. If this approach were to be adopted, the configuration should be tested. The force transfer mechanisms in the region are complicated, and it is possible that suppressing one failure mode might promote another unexpected one.

Table 10-1. Summary of Results from Numerical Analysis using Test Conditions

	F_{EQ}	Δ_{cap_beam} (in)	DCR_{col}	DCR_{pile}
As-built first yield	0.76	0.552	0.76	0.51
As-built ultimate	1.00	1.194	0.61	1.0
Retrofit first yield	0.50	0.360	0.50	0.34
Retrofit ultimate	0.92	1.224	0.30	1.0

The initially proposed "plug fuse" retrofit and the "jacket only" retrofit thus offer different benefits. The "plug fuse" approach offers 50% better capacity protection for the hollow section below the plug (DCR of 0.50 vs. 0.76 under reference conditions) under moderate earthquake motion but 8% worse strength for resisting failure below ground in the design earthquake. Tests to determine the bending capacity prior to implosive failure are thus necessary to evaluate relative benefits of the two approaches. However, the "jacket only" retrofit would be simpler to implement.

Additionally, the proposed retrofit method (the "plug fuse") could be viable especially in terms of the shear friction strength at the interface. Applying the more conservative friction coefficient from

the experimental results to the AASHTO shear friction equation still shows that there is sufficient capacity to transfer the axial load from the plug to the pile without any slip occurring at the interface. This is true under static axial loads as tested and as can be expected during and after construction. However, under cyclic loading such as during an earthquake, the plug would be expected to experience prying forces. This would increase the radial forces across the interface in the displaced system which would increase the shear friction resistance but if there are residual deformations when the column returns to vertical, this could cause separation of the plug from the wall and possibly, slip. This requires testing beyond the scope of this work to confirm the behavior.

10.4 Outstanding Research Questions

The research program thus far has provided insight into the behavior of the hollow, prestressed concrete column-piles but there are outstanding questions to be answered before a final recommendation can be presented to the WSDOT. Recommendations for future research include:

- Experimental tests that confirm the flexural and shear strength of a hollow prestressed concrete cylinder member. These are important in order to validate the predictions of the analytical model used in this research, as well as any future analysis of bridges with these column-pile systems. In particular it is necessary to know the relationship between the moment at which implosion starts and the flexural strength predicted by moment-curvature analysis.
- Cantilever column bending test of retrofit scheme to confirm the improved behavior expected from the analytical results. The two possible retrofit schemes that can be tested are:
    - "Plug fuse" retrofit whereby the column wall is cut back directly below the cap beam (to reduce the DCR in the hollow section below the plug) and jacketed (to provide ductility beyond yielding of the exposed plug)
    - "Jacket only" retrofit whereby the column is simply jacketed with a fiber wrap in the region of the plug to guarantee ductility at the connection, similar to what was seen in the as-built bending test.

- A more robust analysis of the hollow column-pile system that accounts for non-linear soil-structure interaction and acceptable stress and drift limits of the superstructure.
- Large-scale global analytical models of the reference bridges to include more site-specific details in order to evaluate a priority level of retrofit needs. For example, the Green River Bridge, which is strategically critical, has a box girder with no deck joints. The deck's stiffness could be harnessed to improve performance, as suggested in the analytical parameter study.
- Further shear friction plug tests that with better instrumentation can i.) Provide more reliable data for the parameters evaluated in this study and ii.) Evaluate the effectiveness of installing radial steel dowels through the column wall and into the plug to prevent slip from occurring.

Chapter 11. CONCLUSIONS AND RECOMMENDATIONS

The main conclusions from the research program are provided below.

1. For the hollow column-pile systems found in bridges across Washington State, there exist three locations of potential vulnerability. These are:
    a. The moment transfer region at the plug, which is the location of maximum moment in the system under lateral loading, when elastic conditions are considered,
    b. The hollow column section directly below the cast-in-place reinforced concrete plug,
    c. The hollow pile section below grade.

    Successful retrofit of the system requires that all three vulnerabilities be addressed.
2. Conditions at the upper and lower vulnerable hollow sections (above and below grade, respectively) differ markedly, and the same solution cannot be reasonably provided for both. First, at the top, the moment demand is accompanied by shear whereas, below grade, no shear exists at the location of the peak moment. Second, the region at the top lies within the development length of the strand and some slip should be expected, while below grade the critical section typically lies far enough from the free end of the pile for the strands to be fully bonded.
3. The initial analytical investigation assumed that the as-built column had no ductility due to the low confining steel ratio in the column-pile and the system would fail when the column-plug-cap beam connection at the top yielded. Consequently, the bent could withstand a ground motion of approximately 50% of the design motion ($F_{EQ} = 0.54$) (The design motion was taken as the 1000-year AASHTO response spectrum for site class B conditions, considering 5% damping).
4. However, the cantilever column bending test in the second experimental program showed that, at least for that one specimen, the plug region exhibited more ductility than expected. The analysis showed that, if comparable ductility were available in the field structures, system failure would be controlled by the below grade hollow pile after inelastic displacement to a ductility of 2.0 and this would occur at 100% of the design

motion (F_{EQ} = 1.00), which is more favorable than expected when no ductility was assumed.

5. The hollow sections can be addressed by increasing the ductility capacity, for example by filling the columns, or by decreasing the ductility demand, for example by capacity protection. Filling the columns poses questions of constructability which lay outside the scope of this study and so this option was not considered here.
6. At the top of the hollow region of the column-pile (below the plug), the analytical investigation indicated that the moment demand could reach as high as 70% - 90% of the predicted flexural capacity, M_n, in the as-built conditions. However, it also showed the moment demand can be kept between 50% and 70% by introducing the "plug fuse" retrofit, in which the column is locally weakened by cutting away the column wall to leave only the plug and jacketing the exposed plug and column wall for ductility. The cyclic bending test that was conducted during this work showed that the hollow column could sustain a moment of $0.75M_n$ without any sign of damage, including internal spalling. This suggests that the "plug fuse" retrofit would be effective with the predicted DCR values. However, the process of cutting back the column wall would require careful construction. Additionally, the connection introduces the need to transfer vertical gravity loads from the plug to the column wall by shear friction rather than the as-built mode of direct bearing.
7. Tests conducted to investigate the shear friction issue raised in (6) above showed considerable scatter, but suggested that the capacity was, on average, sufficient. The capacity could be increased by installing steel dowel bars radially through the column wall into the plug, but this detail would need to be tested.
8. Alternatively, the top hollow section could be capacity protected by jacketing the plug region without cutting back the column wall. This would lead to simpler construction, but it would provide a lower level of protection because the connection strength would be higher, in which case the moment demand on the hollow section would also be higher. Since the moment in the hollow region of the as-built test did not reach higher than $0.75M_n$, the margin of safety that exists at higher DCRs is unknown. This is particularly true since the moment capacity was derived theoretically by a moment curvature analysis, and test evidence to define the criterion for the onset of internal spalling is sparse.

9. The below-grade hollow section experiences, under elastic conditions, moments that are significantly smaller than those at the top so it is not vulnerable under earthquake loading up to about 50% of the design earthquake when connection yielding occurs.
10. At higher earthquake loads, the moments experienced below grade will depend on the retrofit solution chosen for the plug region, and on the particular site conditions (including column length, soil properties, deck stiffness, etc.). For the reference conditions used in the analytical investigation, with the "plug fuse" retrofit detail, the below-grade section would reach its theoretical flexural capacity at an earthquake of 95% of the design earthquake intensity (F_{EQ} = 0.95). However, given the results of the as-built test column, a "jacket-only" retrofit that guarantees the ductility observed in the test would increase the ultimate F_{EQ} to 1.00. Thus, in both cases, the capacity is either theoretically adequate, or very nearly so. In both cases, the earthquake amplification factor could be higher if any of the parameters were more favorable, such as the presence of a continuous deck that adds lateral stiffness. Additionally, the analysis did not consider any damping effects from hysteretic energy dissipation and therefore the F_{EQ} values provided are conservative.

Recommendations for further research include:

1. The performance of the plug transfer region under flexural cyclic test loads was more ductile than previous studies would suggest, but the reserve ductility capacity was insufficient to justify leaving that region of field columns unretrofitted. It is likely that the ductility of the plug transfer region could be improved by some form of jacketing, but that would need to be tested.
2. Further testing, and accounting for site-specific conditions such as the contribution of the bridge deck, may allow some of the restrictions to be relaxed, showing that retrofit of the cap beam region alone may make the bridges able to withstand 100% of the design motion, or possibly more.
3. Pure bending tests should be conducted on a hollow section to determine the conditions under which internal spalling occurs and the ductility capacity, if any. Such tests are important because implementing a below-grade retrofit would be very difficult and, if the choice is made to not retrofit the region because its existing capacity appears to be so

nearly adequate, the supporting evidence for the choice should be based on applicable test data.

4. Shear tests should be conducted on the hollow section. The shear capacity was evaluated theoretically and appears to show that only very short columns (less than 3 column diameters from underside of cap beam to grade) will be shear-critical. The column bending test revealed no signs of shear damage but the shear demand in it reached only approximately half the predicted capacity. Thus, it provided evidence only of a lower bound on capacity. Only three previous studies were found in which hollow columns were tested in shear (Ranzo and Priestley, 1997; Pizzano, 1984; Turmo et al, 2009), and only one case was prestressed (Pizzano, 1984). Thus considerable uncertainty exists over the shear strength of hollow prestressed concrete columns.

BIBLIOGRAPHY

AASHTO (2012). AASHTO LRFD Bridge Design Specifications. 7th Edition. American Association of State Highway and Transportation Officials (AASHTO), Washington, DC.

ACI Committee 318 (2014). Building Code Requirements for Structural Concrete and Commentary (ACI318R-14). Farmington Hills, MI: American Concrete Institute.

ACI (1999). "Acceptance Criteria for Moment Frames Based on Structural Testing," ACI ITG/T1.1-99. Report by ACI Innovation Task Group 1 and Collaborators, ACI.

ASTM A370-15, 2015, "Standard Test Methods and Definition for Mechanical Testing of Steel Products," ASTM International, West Conshohocken, PA, 2015, DOI: 10.1520/ A0370-15, www.astm.org

ASTM A615-16, 2016, "Standard Specification for Deformed and Plain Carbon-Steel Bars for Concrete Reinforcement," ASTM International, West Conshohocken, PA, 2016, DOI: 10.1520/ A615-16, www.astm.org

ASTM C39/C39M-18, 2018, "Standard Test Method for Compressive Strength of Cylindrical Concrete Specimens," ASTM International, West Conshohocken, PA, 2018, DOI: 10.1520/C0039_C0039M-18, www.astm.org

Bowles, J. E. (1996). Foundation Analysis and Design, The McGrawHill Companies. *New York.*

Budek, A. M., Benzoni, G., & Priestley, M. N. (1997). Experimental investigation of ductility of in-ground hinges in solid and hollow prestressed piles. Report no. SSRP, 97, 17.

Budek, A.M., and Benzoni, G. (2009). Obtaining ductile performance from precast, prestressed concrete piles. PCI Journal, 54(3).

Cardone, D., Perrone, G., & Sofia, S. (2011). A performance-based adaptive methodology for the seismic evaluation of multi-span simply supported deck bridges. Bulletin of Earthquake Engineering, 9(5), 1463-1498.

Caltrans (2013). Caltrans Seismic Design Criteria. Version 1.7. California Department of Transportation, Sacramento, CA.

CEB-FIP Model Code 1990. Model code for concrete structures. In: Comité Euro-international du Béton. Secretariat permanent. Case Postale 88, CH-1015 Lausanne, Switzerland; 1990

CEN (Comité Europeen de Normalization) (1998). Eurocode 8: Design of Structures for earthquake resistance – part 1: general rules, seismic actions and rules for buildings. PrEN 1998-1: 1998, CEN, Brussels

Davaadorj, O. (2018). Shear Stress Transfer Across Concrete to Concrete and Steel to Concrete Interfaces (Master's Thesis, University of Washington). Retrieved from https://digital.lib.washington.edu/researchworks/handle/1773/42253

EIGawady, M., Cofer, W. F., & Shafiei-Tehrany, R. (2009). Seismic assessment of WSDOT bridges with prestressed hollow core piles: part II (No. WA-RD 732.2). Washington (State). Dept. of Transportation. Office of Research and Library Services.

Freeman, S. A. (2004). Review of the development of the capacity spectrum method. ISET Journal of Earthquake Technology, 41(1), 1-13.

Greenwood, S. M. (2008). Analytical Performance Evaluation of Hollow Prestressed Piles and Pile-Cap Connections in the I-5 Ravenna Bridge (Master's Thesis, Washington State University).

Gutman, D. (2018, February 12). Here's why I-5 is such a mess in Seattle area, and what keeps us moving at all. Retrieved June 15, 2018, from https://www.seattletimes.com/seattle-news/transportation/heres-why-i-5-is-such-a-mess-in-seattle-area-and-what-keeps-us-moving-at-all/

Habouh, M. I. (2015). Shear Transfer Strength of Concrete Placed Against Hardened Concrete (Master's Thesis, University of Akron).

Hetényi, M. (1971). *Beams on elastic foundation: theory with applications in the fields of civil and mechanical engineering*. University of Michigan.

Ikeda, S., Tsubaki, T., and Yamaguchi, T. (1982). Ductility Improvement of Prestressed Concrete Piles. Transactions of the Japan Concrete Insitute, 113(2), 531-538.

Jacobsen, L. S. (1930). Steady forced vibration as influenced by damping. Trans. ASME-APM, 52(15), 169-181.

Júlio, E. N. B. S., Branco, F. A. B., & Silva, V. D. (2005). Concrete-to-concrete bond strength: influence of an epoxy-based bonding agent on a roughened substrate surface. Magazine of concrete research, 57(8), 463-468.

Kowalsky, M. J., Priestley, M. N., & Macrae, G. A. (1995). Displacement-based design of RC bridge columns in seismic regions. Earthquake engineering & structural dynamics, 24(12), 1623-1643.

Lengyel, M. (2014, June). Morgan Murray Bridge. Aspire The Concrete Bridge Magazine, 42.

Menegotto, M., & Pinto, P. (1973). Method of Analysis for Cyclically Loaded Reinforced Concrete Plane Frames Including Changes in Geometryand Non-elastic Behavior of Elements Under Combined Normal Force and Bending. Proceedings. IABSE Sympoium on Resistance and Ultimate Deformability of Structures Acted on by Well-Defined Repeated Loads.

Muguruma, H. (1987). Improving the flexural ductility of pretensioned high strength spun concrete piles by lateral confining of concrete. In Proceedings of the Pacific Conference on Earthquake Engineering, Wairakei, New Zealand, 1987 (Vol. 1, pp. 385-396).

Pizzano, B. A. (1984). Behavior of prestressed concrete piles under seismic loading (Master's Thesis, University of Washington).

Popovics, S. (1973). A numerical approach to the complete stress-strain curve of concrete. Cement and concrete research, 3(5), 583-599.

Priestley, M. N., Seible, F., & Calvi, G. M. (1996). Seismic design and retrofit of bridges. John Wiley & Sons.

Ranzo, G., & Priestley, M. N. (2001). Seismic performance of circular hollow columns subjected to high shear. Structural Systems Research Project, University of California, San Diego.

Raynor, D. J., Lehman, D. E., & Stanton, J. F. (2002). Bond-slip response of reinforcing bars grouted in ducts. *ACI Structural Journal, 99*(5), 568-576.

Riahi, Z. and Faridafshin, F. (2008). Seismic Retrofit of Reinforced Concrete Bridges with Fiber Reinforced Polymer Composites: State-of-the-Art Review, The 14th World Conference on Earthquake Engineering, Beijing, China, 2008.

Shafiei-Tehrany, R., ElGawady, M., & Coffer, W. (2011). Pushover Analysis of I-5 RAVENNA Bridge. Electronic Journal of Structural Engineering, 11(1), 2011.

Sheppard, D. A. (1983). Seismic design of prestressed concrete piling.

Takeda, T., Sozen, M. A., & Nielsen, N. N. (1970). Reinforced concrete response to simulated earthquakes. Journal of the Structural Division, 96(12), 2557-2573.

Timoshenko, S. (1983). Strength of materials, part 1 and part 2.

Tran, H. V. (2015). *Drilled shaft socket connections for precast columns in seismic regions* (Doctoral dissertation, University of Washington)

Turmo, J., Ramos, G., & Aparicio, A. C. (2009). Shear truss analogy for concrete members of solid and hollow circular cross section. Engineering Structures, 31(2), 455-465.

Wu, Y. F., Liu, T., & Oehlers, D. J. (2006). Fundamental principles that govern retrofitting of reinforced concrete columns by steel and FRP jacketing. Advances in Structural Engineering, 9(4), 507-533.

APPENDIX A: REFERENCE BRIDGE DETAILS

There are 22 bridges throughout Washington State that were founded on hollow-core prestressed concrete column-piles. As part of this research program, the following four bridges were studied and their design details are given in this appendix. All drawing excerpts were provided by the Washington State Department of Transportation.

A.1 LOCATIONS

1. Ravenna Boulevard Overcrossing (Ravenna): 47°40'28.6"N, 122°19'15.1"W
2. East Galer St. to Lakeview Boulevard Viaduct (Galer): 47°38'04.0"N, 122°19'24.7"W
3. L^E Line Bridge over Slide, South 184th Street to South 144th Street (Slide): 47°27'0.60"N, 122°15'48.0"W
4. Green River Bridge (Green River): 47°27'45.4"N, 122°14'56.9"W

A.2 GENERAL DETAILS

Table A-1. Design Details of Reference Bridges

	Ravenna	**Galer**	**Slide**	**Green River**
Overall				
Length (ft)	1372	1671	515	245
No. of spans	20	19	5	3
Superstructure type	Cap beam + girders	Cap beam + girders	Cap beam + girders	Box girder
Prestressing Type	Post-tensioned	-*	Pre-tensioned	Pre-tensioned
Average L_{col} (ft)	20.1	35.4	-*	27.5
Average L_{pile} (ft)	20.6	28.5	-*	22.2
Hollow Column-Pile				
D_o (in)	48	48	54	54
D_i (in)	38	38	44	44
t_w (in)	5	5	5	5
A_{hollow} (in^2)	675.4	675.4	769.7	769.7
f'_c (psi)	6000	6000	7000	6500
Strand Reinforcement				
f_{pu} (ksi)	250	250	270	250

d_{str} (in)	0.6656	0.6656	0.5	0.5
No. of strands	12	14	44	38
A_{str} (in^2)	0.348	0.348	0.153	0.144
A_{ps} (in^2)	4.176	4.872	6.732	5.472
F_i (kip)	61.0	58.9	28.9	25.2
f_{ci} (psi)	1084	1221	1652	1244
Spiral Reinforcement (#2 Gage Spiral Hooping, ASTM 82)				
d_{sp} (in)	0.262	0.262	0.262	0.262
A_{sp} (in^2)	0.054	0.054	0.054	0.054
D_{core} (in)	43	43	49	49
s_{min} (in)	3.0	6.0	2.0	2.0
t_{sp} (in)	0.018	0.009	0.027	0.027
ρ_{hollow} (%)	0.36	0.18	0.54	0.54
ρ_{filled} (%)	0.167	0.084	0.22	0.22
s_{max} (in)	6.0	6.0	4.0	4.0
ρ_{hollow} (%)	0.18	0.18	0.27	0.27
ρ_{filled} (%)	0.084	0.084	0.11	0.11
t_{sp} (in)	0.009	0.009	0.0135	0.0135
Inner Plug				
f'_c (psi)	4000	4000	4000	4000
D_{plug} (in)	38	38	44	44
L_{plug} (ft) – typ.	4.167	4.25	4.33	5.00
A_{plug} (in^2)	1134	1134	1520.5	1520.5
Plug Reinforcement				
d_b (in)	1.0	1.0	1.375	1.375
No. of bars	16	16	18	16
c_{c_plug} (in)	2.0	2.0	2.0	2.0
Loads and Capacities				
P_{axial} per column (kip)	428.15	298.97	407.13	1023.37
M_{n_hollow} (ft-kip)	2260	2305	3565	3700
$M_{n\_combined}$ (ft-kip)	1910	1750	3675	4205
M_{n_plug} (ft-kip)	1385	1260	2790	3235

* Not enough information found

A.3 RAVENNA BRIDGE OVERCROSSING

Hollow column-pile

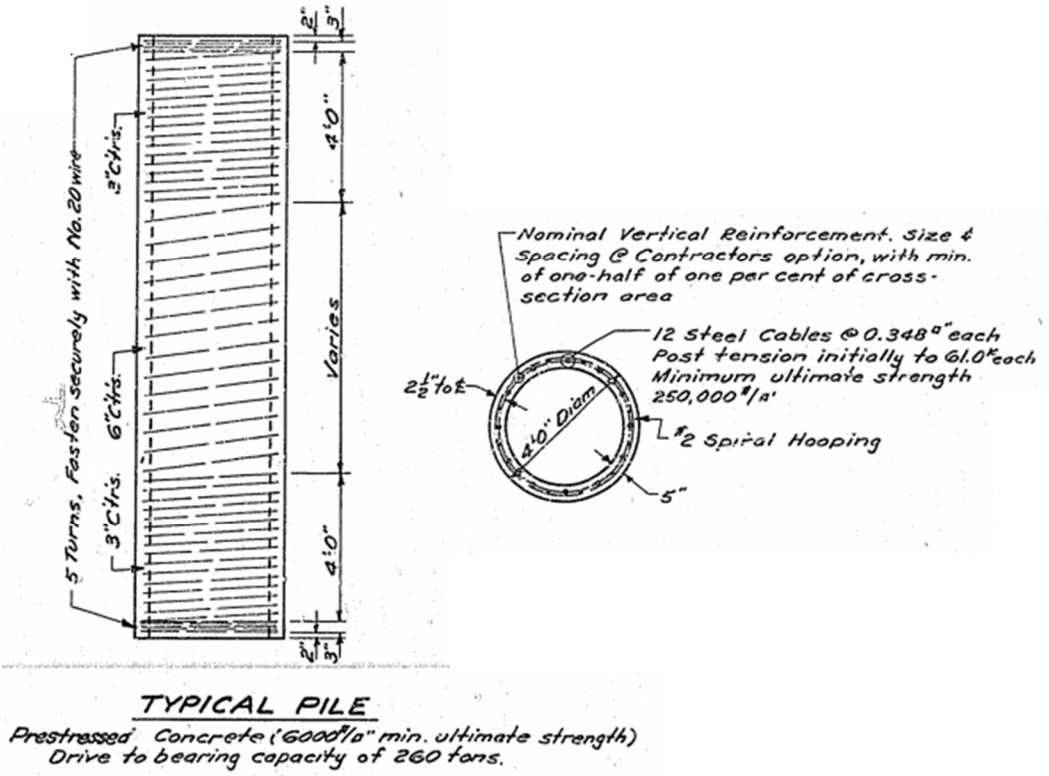

Figure A-1. Details of Hollow Prestressed Concrete Column-Pile (Ravenna)

Inner plug

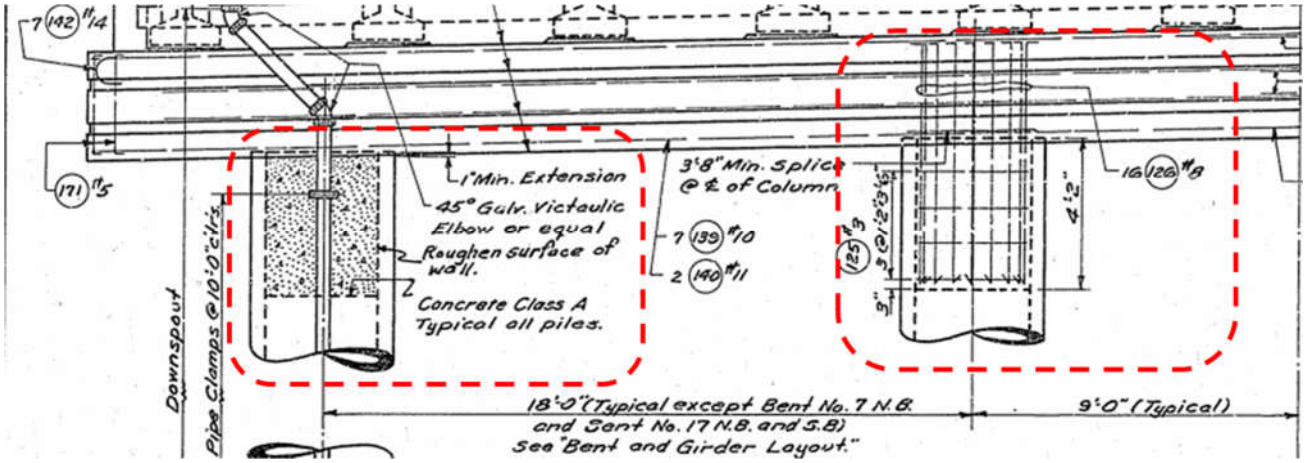

Figure A-2. Details of Inner Plug Reinforcement (Ravenna)

Cap Beam

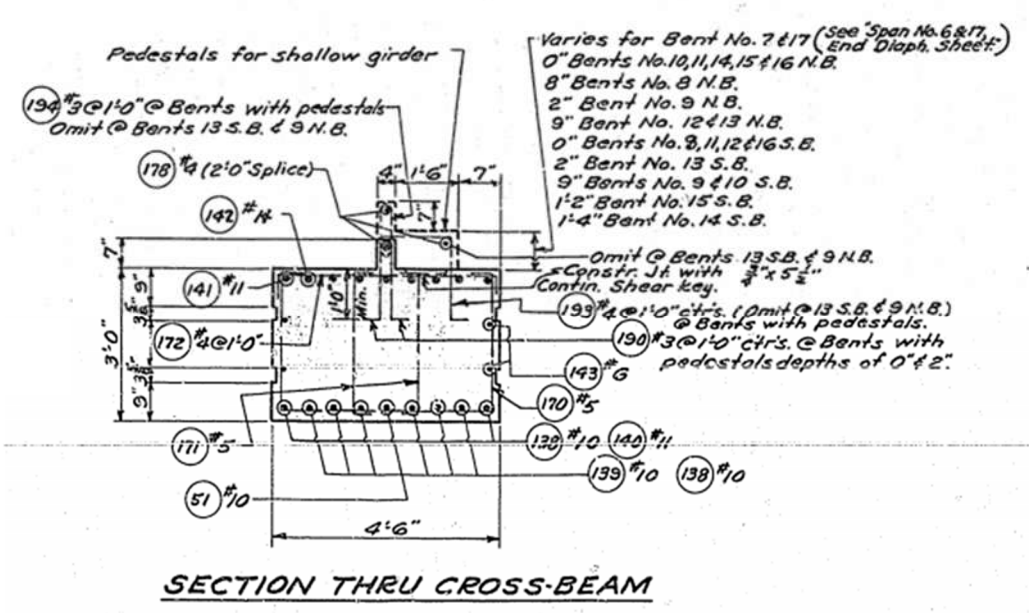

Figure A-3. Cap beam cross-section for Typical Bent (Ravenna)

A.4 East Galer St. to Lakeview Boulevard Viaduct

Hollow Pile

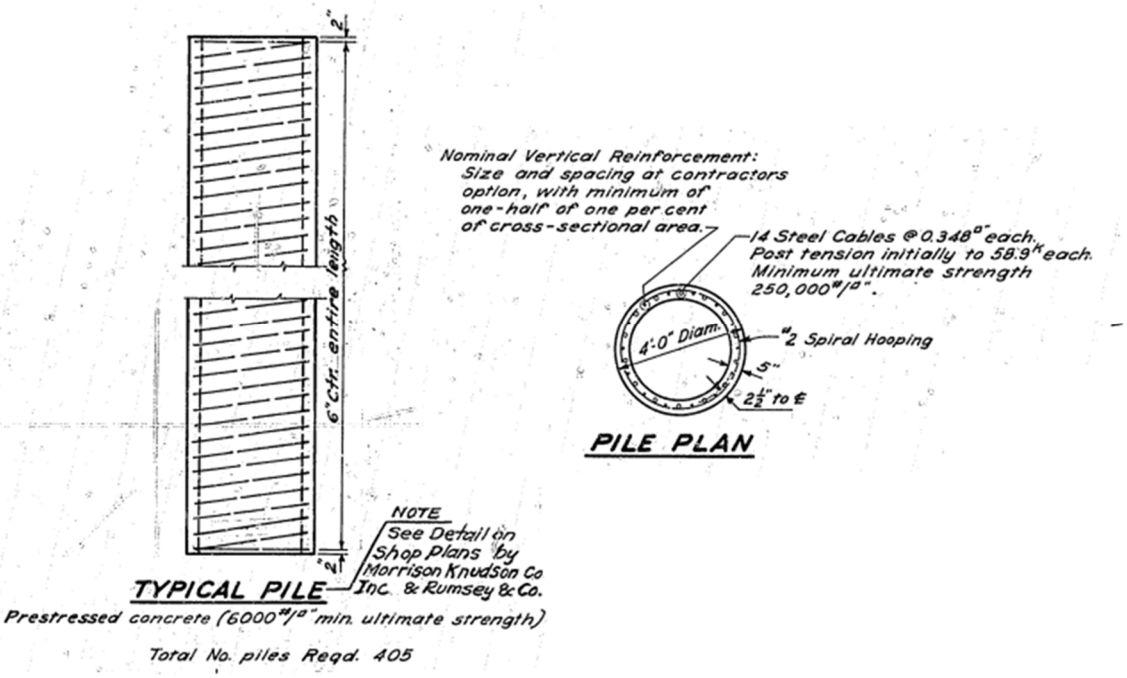

Figure A-4. Details of Hollow Prestressed Concrete Column-Pile (Galer-Lakeview)

Inner Plug

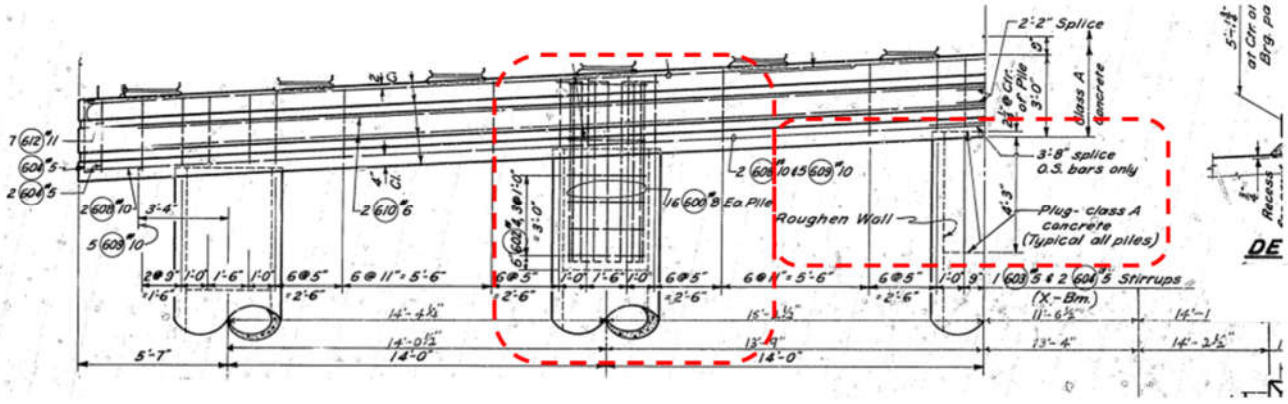

Figure A-5. Details of Inner Plug Reinforcement (Galer-Lakeview)

Cap Beam

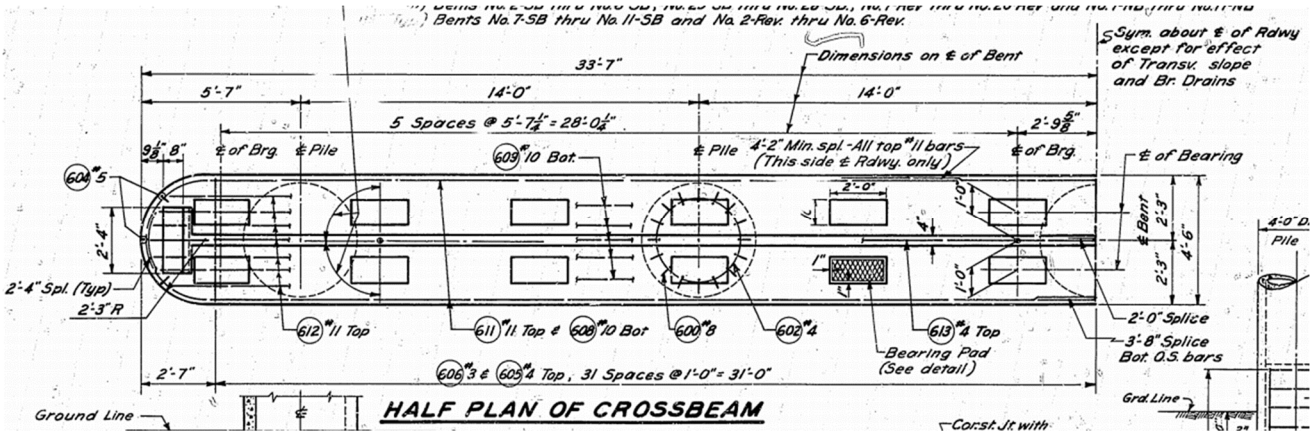

Figure A-6. Plan view of Cap Beam for Typical Bent (Galer-Lakeview)

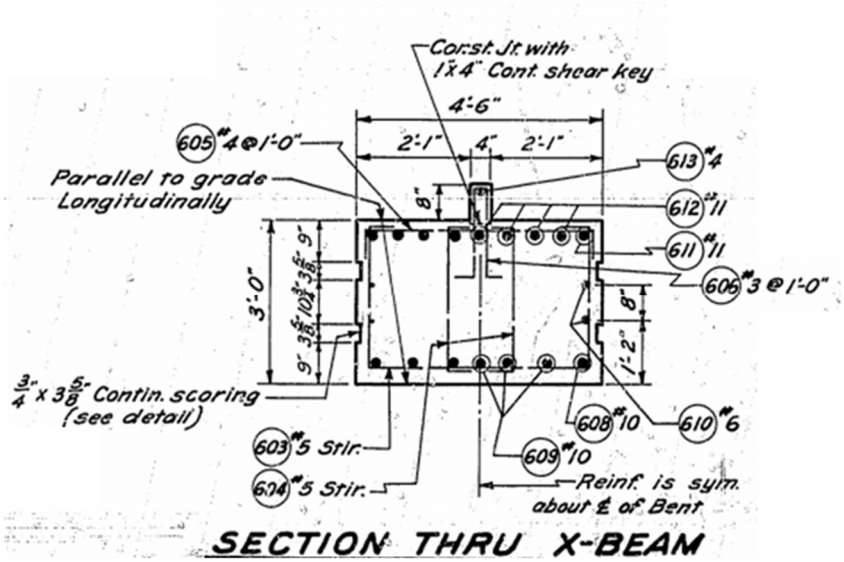

Figure A-7. Cap beam cross-section for Typical Bent (Galer-Lakeview)

Special Details

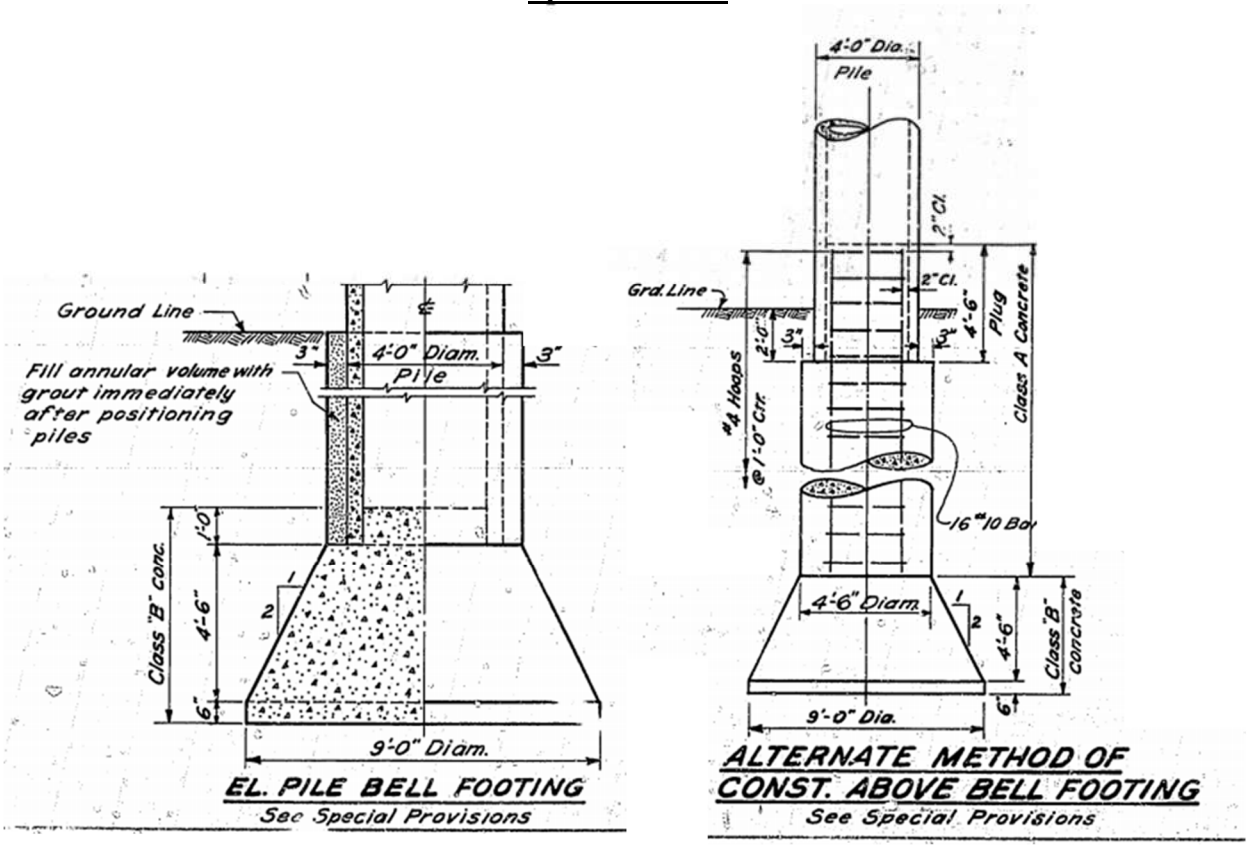

Figure A-8. Alternative Below Grade and Footing Details (Galer-Lakeview)

A.5 L^{E} LINE BRIDGE OVER SLIDE

Hollow Pile

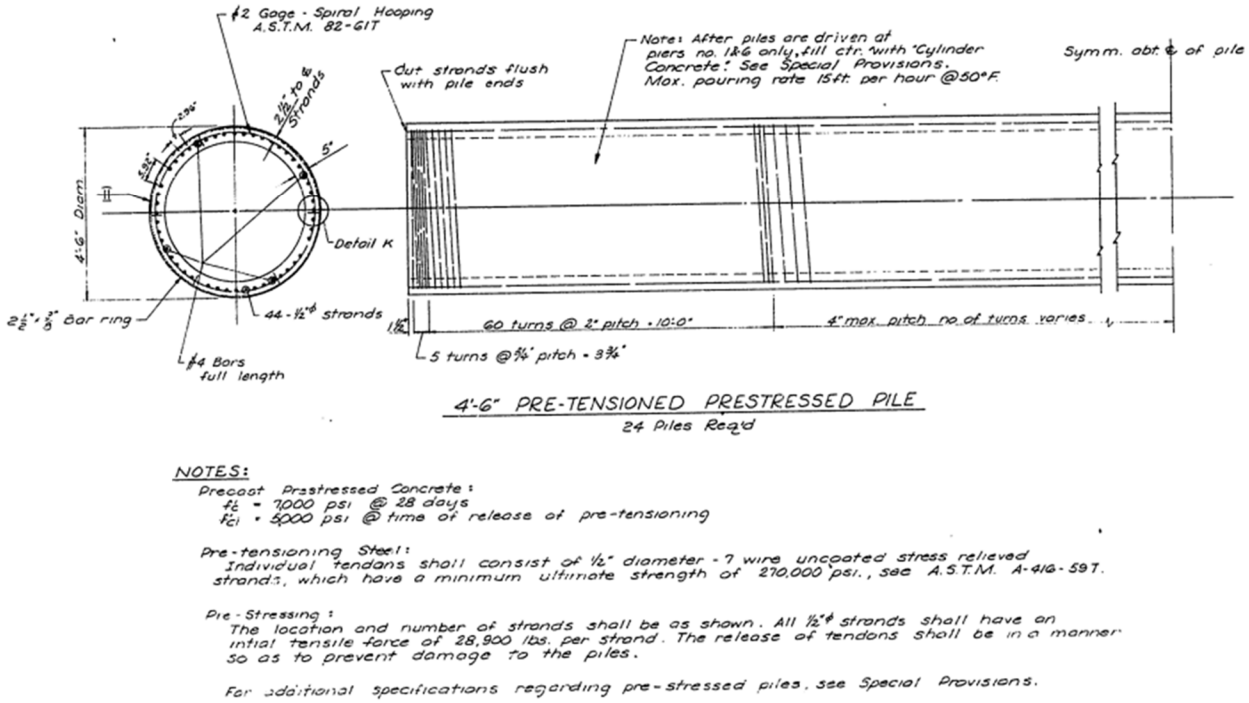

Figure A-9. Details of Hollow Prestressed Concrete Column-Pile (Slide)

Inner Plug

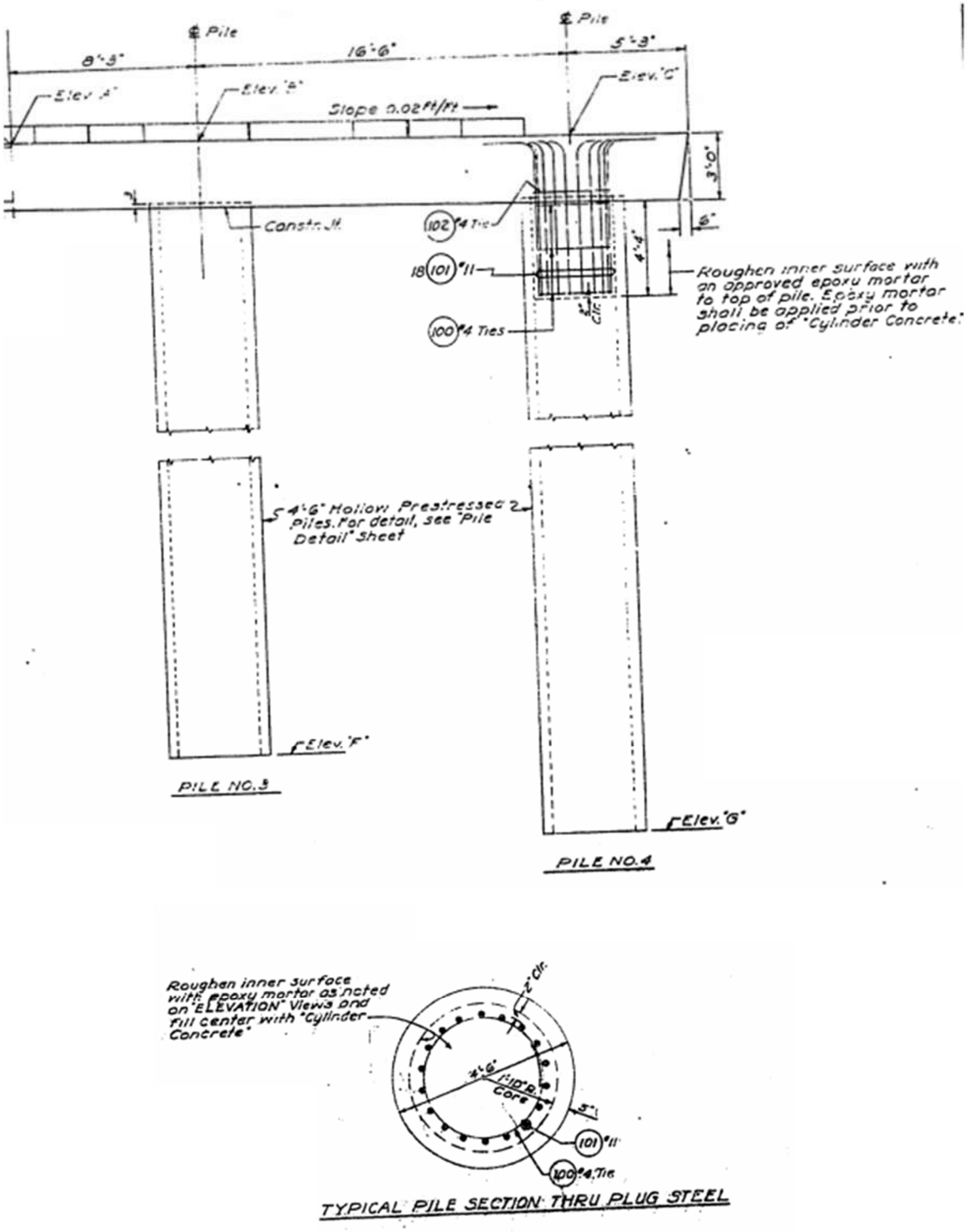

Figure A-10. Details of Inner Plug Reinforcement (Slide)

Cap Beam

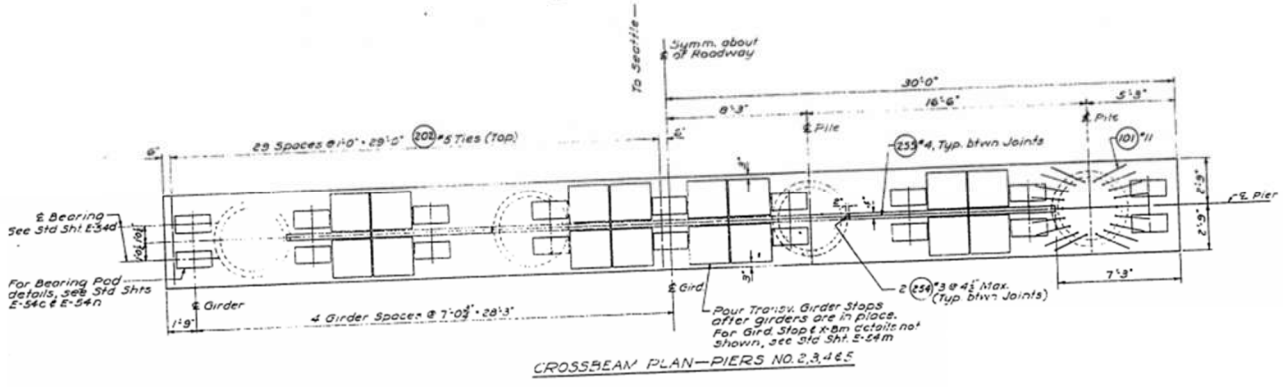

Figure A-11. Plan View of Typical Cap Beam (Slide)

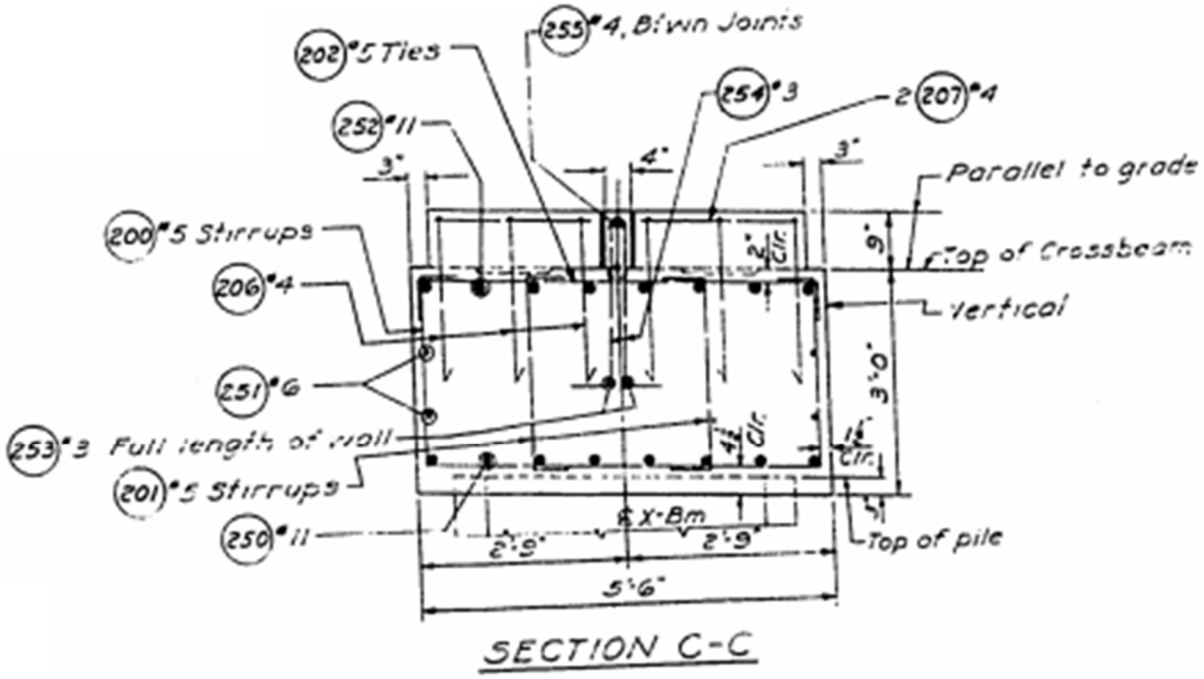

Figure A-12. Cap beam cross-section for Typical Bent (Slide)

A.6 GREEN RIVER BRIDGE

Hollow Pile

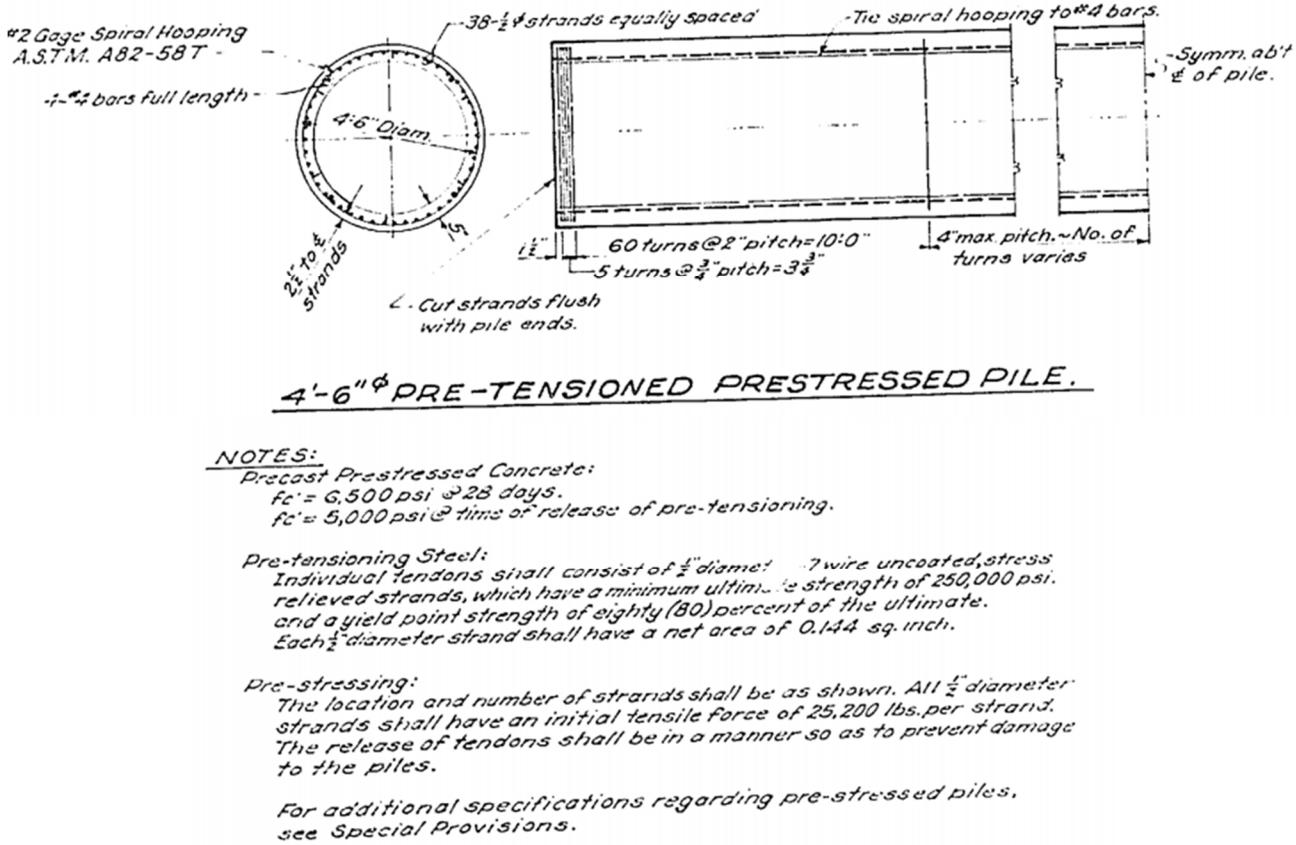

Figure A-13. Details of Hollow Prestressed Concrete Column-Pile (Green River)

Inner Plug

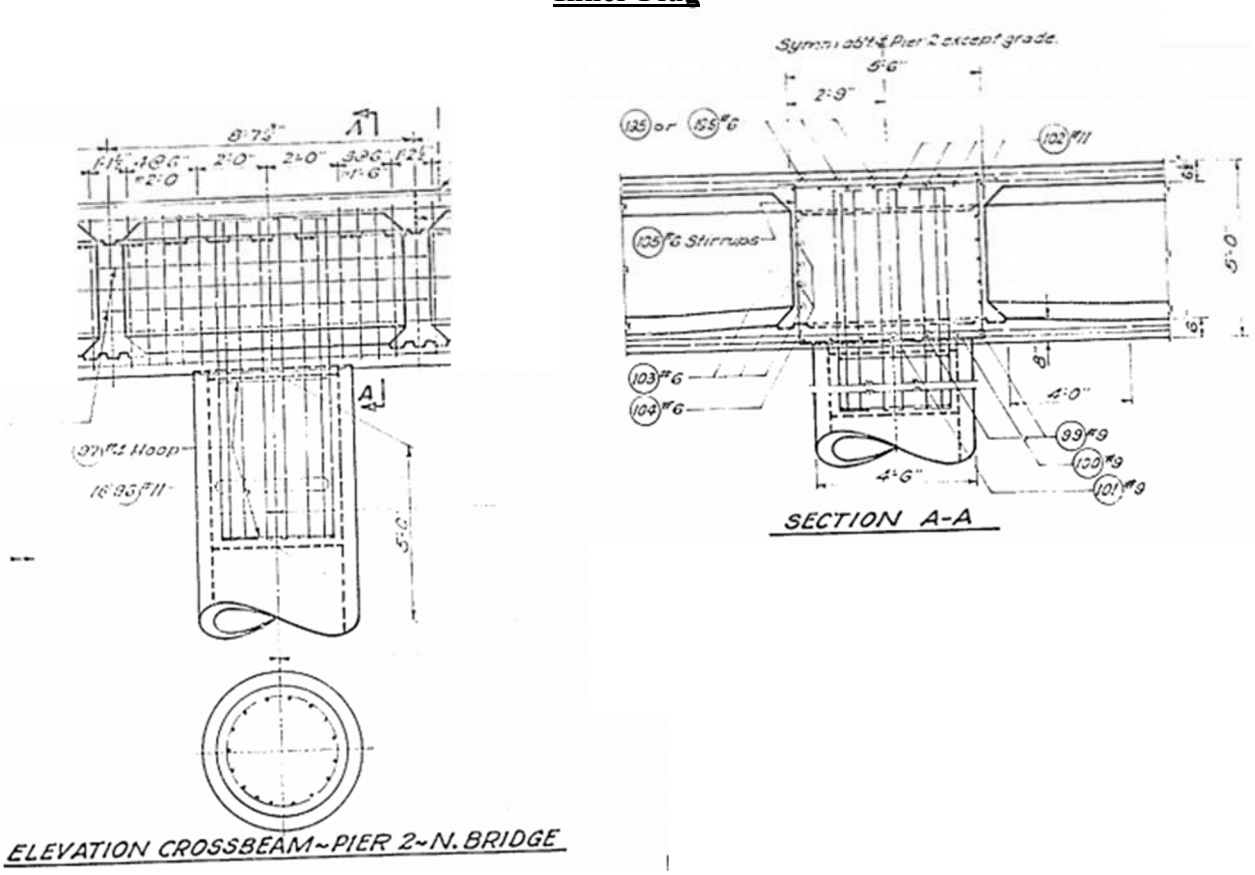

Figure A-14. Details of Inner Plug Reinforcement (Green River)

Special Details – Box Girder

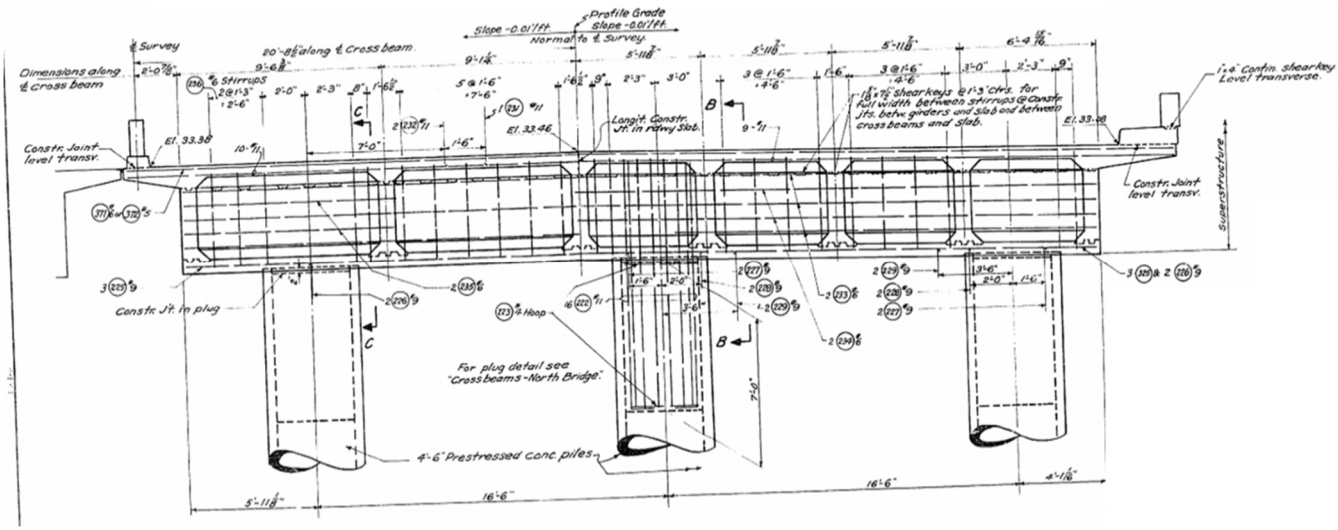

Figure A-15. Elevation of Typical Box Girder Cross Beam (Green River)

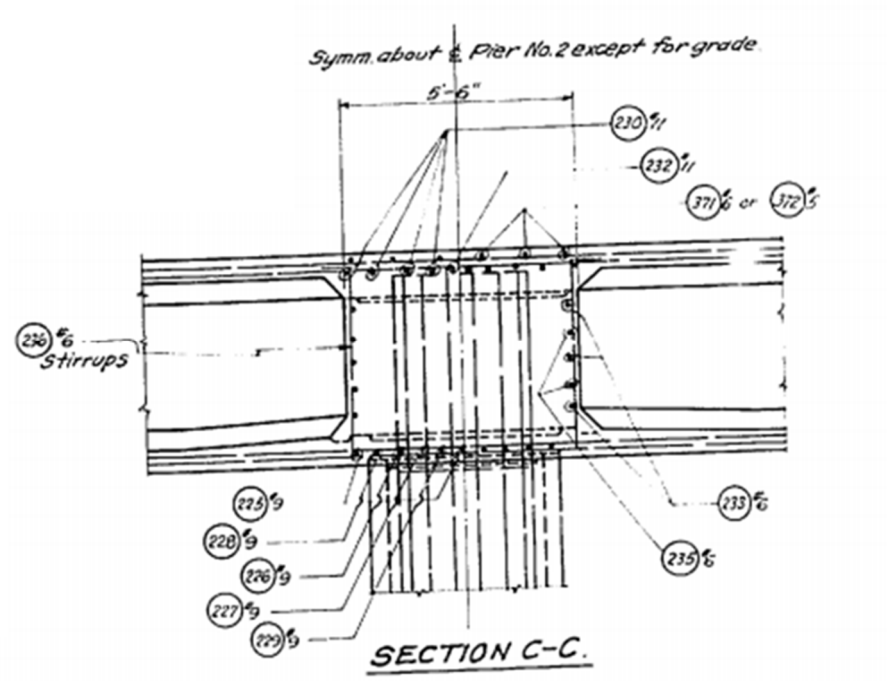

Figure A-16. Cross Beam cross-section for Typical Bent (Green River)

APPENDIX B: ANALYTICAL INVESTIGATION CALCULATION DETAILS

The numerical model in Chapter 3 used the formulation for a finite beam on an elastic foundation to represent the below-grade pile element embedded in soil of constant stiffness given by the modulus of subgrade reaction β_{soil}. The formulation is based on Hetenyi (1946).
The beam formulation has the following sign convention (Figure B-1).

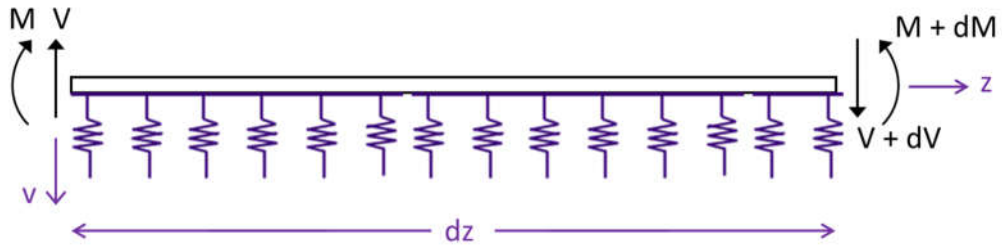

Figure B-17. Beam Formulation

The element formulation has the following sign convention (Figure B-2).

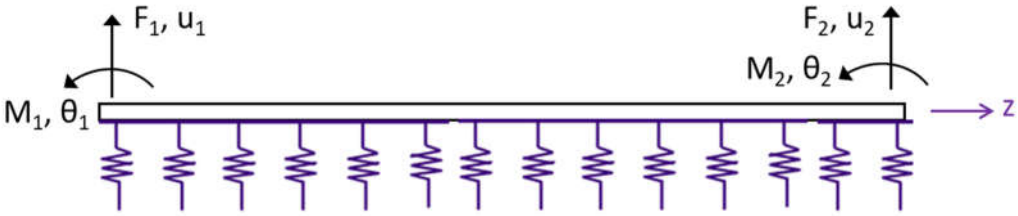

Figure B-18. Element Formulation

The pile was modelled as a beam on elastic foundations, following the Winkler approach. It was modelled using a single element, but it was necessary to allow for the calculation of values, such as displacement and moment, at internal locations.

The equation of equilibrium is

$$EIv'''' + kv = 0 \qquad (1)$$

for which the solution is

$$v = e^{-\lambda z}[A\cos\lambda z + B\sin\lambda z] + e^{\lambda z}[C\cos\lambda z + D\sin\lambda z] \quad (2)$$

given $\lambda = \sqrt[4]{\frac{\beta_{soil}}{4EI}}$

The constants *A, B, C, D* can be related to the end forces and moments by

$$\underline{R}\{A\} = \{f\} \quad (3)$$

where

$$\underline{R} = \begin{bmatrix} -2 & -2 & +2 & -2 \\ 0 & -2 & 0 & +2 \\ 2e^{-\lambda L}(\cos\lambda L - \sin\lambda L) & 2e^{-\lambda L}(\cos\lambda L + \sin\lambda L) & 2e^{\lambda L}(-\cos\lambda L - \sin\lambda L) & 2e^{\lambda L}(\cos\lambda L - \sin\lambda L) \\ 2e^{-\lambda L}\sin\lambda L & 2e^{-\lambda L}(-\cos\lambda L) & 2e^{\lambda L}(-\sin\lambda L) & 2e^{\lambda L}(2\cos\lambda L) \end{bmatrix}$$

$$\{A\} = \begin{Bmatrix} A \\ B \\ C \\ D \end{Bmatrix} \quad \text{and} \quad \{f\} = \begin{Bmatrix} F_1/EI\lambda^3 \\ M_1/EI\lambda^2 \\ F_2/EI\lambda^3 \\ M_2/EI\lambda^2 \end{Bmatrix}$$

It should be noted that the signs in the matrix must take account of the change from the beam sign convention in the equilibrium equation and the nodal sign convention used in the matrices.
The vector of {A} values can also be related to the end displacement and slopes by

$$\underline{Q}\{A\} = \{u\} \quad (4)$$

where

$$\underline{Q} =$$

$$\begin{bmatrix} -1 & 0 & -1 & 0 \\ +1 & -1 & -1 & -1 \\ -e^{-\lambda L}(\cos \lambda L) & -e^{-\lambda L}(\sin \lambda L) & -e^{\lambda L}(\cos \lambda L) & -e^{\lambda L}(\sin \lambda L) \\ e^{-\lambda L}(\cos \lambda L + \sin \lambda L) & e^{-\lambda L}(-\cos \lambda L + \sin \lambda L) & e^{\lambda L}(-\cos \lambda L + \sin \lambda L) & e^{\lambda L}(-\cos \lambda L - \sin \lambda L) \end{bmatrix}$$

and $$\{u\} = \begin{Bmatrix} u_1 \\ \theta_1/\lambda \\ u_2 \\ \theta_2/\lambda \end{Bmatrix}$$

The 4x4 stiffness matrix, $\underline{K}$ for the pile element can be obtained as

$$\underline{K} = \underline{R} * \underline{Q}^{-1} \qquad (5)$$

The 4x4 pile matrix can then be added to the 4x4 column matrix to form a 6x6 global stiffness matrix.

The global displacements are obtained from the global stiffness matrix and the applied loads, which in this structure occur at the two degrees of freedom at the top of the column.

Under elastic conditions, the loads are all zero except for the lateral load *Q* at the cap beam. Once the displacements are known, the constants *A, B, C, D* can be obtained from Eqn. 3. The displacements and forces at any depth *z* can then be obtained using Eqns. 3 and 4 with *z* substituted for *L*.

If the pile is infinitely long, the two degrees of freedom at the bottom of the pile can be discarded, and the pile behavior is then represented by the 2x2 matrix

$$\begin{Bmatrix} V \\ M \end{Bmatrix} = EI \begin{bmatrix} 4\lambda^3 & 2\lambda^2 \\ 2\lambda^2 & 2\lambda \end{bmatrix} \begin{Bmatrix} v \\ \Theta \end{Bmatrix} \qquad (6)$$

Use of this matrix, for values of *L* greater than about $10/\lambda$, helps to avoid overflow problems with the terms in $e^{\lambda L}$ in matrices *R* and *Q*.

APPENDIX C: ANALYSIS OF PLUG SHEAR FRICTION TEST RESULTS

This appendix details the analysis of the plug shear friction test results to find a coefficient of friction, μ and a cohesion value, c to find the interface transfer strength between the column-pile wall and the plug, using the AASHTO model of shear friction (Eq. 5.8.4.1-3).

$$V_{ni} = cA_{cv} + \mu(A_{vf}f_y + P_c) \quad (1)$$

There is no steel crossing the interface of shear friction transfer in the case of the column-pile wall and plug so that Eqn. 1 becomes

$$V_{ni} = cA_{cv} + \mu P_c \quad (2)$$

where

$$V_{ni} = shear\ friction\ strength\ at\ interface = peak\ applied\ force\ for\ tests$$
$$c = cohesion\ stress$$
$$A_{cv} = area\ of\ shear\ interface = \pi L_{plug} D_{plug}$$
$$\mu = coefficient\ of\ friction\ at\ shear\ interface$$
$$P_c = clamping\ force = hoop\ forces$$

C.1 MODEL CR: NON-JACKETED SPECIMENS

Assumption: All cohesion is lost after first slip of the inner plug (post-peak behavior).

1. *Did the spiral yield?*

Consider the total circumferential displacement as the sum of the width of all longitudinal cracks formed around the circumference of the pipe wall. The average crack width, w_{cr_ave} can be given in terms of the average measured hoop strain ε_{hoop_ave} and the number of cracks formed at the peak load, n_{cr}.

$$w_{cr\,ave} = \frac{\pi D_o \varepsilon_{hoop_{ave}}}{n_{cr}} \quad (3)$$

Two cases are possible. First, if the wire is anchored by bond stresses on either side of the crack, and the bond stress is assumed to be constant, the wire stress varies linearly with distance from the crack face. When the steel is at incipient yielding, integration of the strains in the bond region shows that the crack width will be $L_d\,\varepsilon_y$, where L_d is the development length. If the wire is anchored by the cross-wires, rather than by bond, the crack width at incipient yielding will be $s_{wire}\,\varepsilon_y$, where s_{wire} is the spacing of the cross-wires. These two conditions can be expressed in a single equation

$$w_{cr\,ave} = \varepsilon_y L_{eff} \tag{4}$$

where

$$L_{eff} = min\{L_d, s_{wire}\} \tag{5}$$

$$s_{wire} = longitudinal\ wire\ spacing = 8\ inches$$

Combining Equations (3) and (4) gives

$$\varepsilon_y L_{eff} = w_{cr\,ave} = \frac{\pi D_o \varepsilon_{hoop\,ave}}{n_{cr}} \tag{6}$$

or

$$\varepsilon_{hoop\,ave} = \frac{\varepsilon_y L_{eff} n_{cr}}{\pi D_o} \tag{7}$$

This is the value of the average hoop strain at which the spiral could be expected to yield.

Current codes do not give values for the development length of smooth bars. For want of a better alternative, the values for deformed bars were used. ACI and AASHTO give

ACI 318-14 Eqn. 25.4.2.3a: $$L_d = \left(\frac{3}{40}\frac{f_y}{\sqrt{f'_c}}\frac{\psi_t\psi_e\psi_s}{\left(\frac{c_b+K_{tr}}{d_b}\right)}\right)d_b$$

where $K_{tr} = \frac{40A_{tr}}{sn}$ and $\frac{c_b+K_{tr}}{d_b} \leq 2.5$

AASHTO (2012) Article 5.11.2.1: $$L_d = \frac{0.95 d_b f_y}{\sqrt{f'_c}}$$

The ACI and AASHTO values for L_d are similar, and the average (of 4") was used here. That is smaller than the cross-wire spacing, so L_{eff} was 4" in all cases. Taking the yield strain of the spiral to be

$$\varepsilon_{y_{sp}} = {f_{y_{sp}}}/{E_{sp}} = {60\ ksi}/{30000\ ksi} = 2167\ \mu\varepsilon \qquad (8)$$

It can be determined whether the spiral steel in the pipe wall yielded when the average hoop strain reaches approximately 92×10^{-6} n_{cr} in/in.

2. *Determine the coefficient of friction, μ*

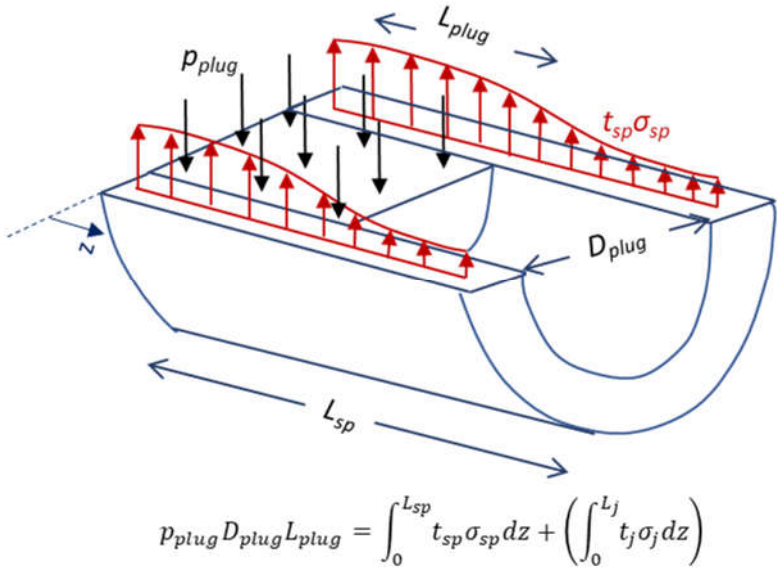

Figure C-19. Horizontal forces in equilibrium at plug-wall interface

Horizontal force equilibrium requires

$$pD_{plug}L_{plug} = P_{c\,spiral} \qquad (9)$$

$$pD_{plug}L_{plug} = 2\sigma_{sp}t_{sp}L_{sp} \qquad (10)$$

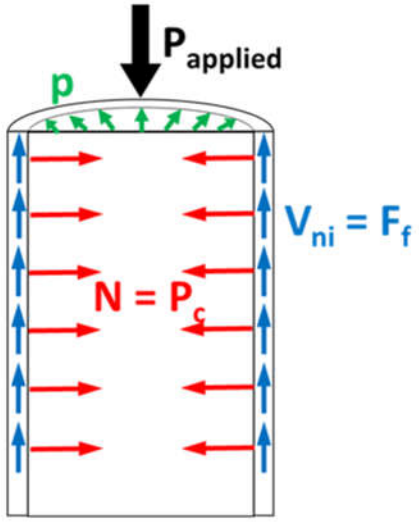

Figure C-20. Vertical force equilibrium at plug-wall interface

After peak load and assuming no cohesion, vertical force equilibrium requires

$$P_{applied} = P_{residual} = F_f \quad (11)$$

$$F_f = \mu \pi P_c \quad (12)$$

From Eqns. 9 and 12,

$$F_f = \mu \pi p D_{plug} L_{plug} \quad (13)$$

From Eqns. 10 and 13,

$$F_f = 2\mu \pi \sigma_{sp} t_{sp} L_{sp} \quad (14)$$

From Eqns. 11 and 14

$$\mu = \frac{P_{residual}}{2\pi \sigma_{sp} t_{sp} L_{sp}} \quad (15)$$

where

$$\sigma_{sp} = E \varepsilon_{sp} \quad (16)$$

$$L_{sp} = length\ of\ wall = 36\ inches$$

If the spiral yielded throughout the length of the specimen (according to measured data and Eqns. 7 and 8)

$$\sigma_{sp} = f_{y_{sp}} = 65\ ksi \qquad (17)$$

If the spiral did not yield through the length of the specimen,

$$\sigma_{sp} L_{sp} = \int_0^{L_{sp}} E\varepsilon_{sp,z}\, dz \qquad (18)$$

C.2 MODEL CR: JACKETED SPECIMENS

1. *Find the radial pressure acting at the plug-wall interface*

For the jacketed specimens, the measured hoop strains represent the hoop strains in the jacket only. However, both the spiral steel and the jacket will be providing hoop tension. An analysis is needed to relate the jacket strains to the normal pressure acting across the plug-wall interface.

Consider a cylinder in which the wall is made up from a series of concentric concrete shells, between each of which is a reinforcing layer. The radii to the reinforcing layers are R_i, and the layers are each of thickness t_i, modulus E_i, yield strength f_{yi}. The concrete is assumed to be cracked so that it carries no hoop stress, but it can carry radial stress. The following procedure is described for one reinforcing layer; the others all use the same procedure. The outer layer (in this case the jacket) is treated like an interior layer with no outer pressure. The procedure starts with an assumed hoop strain in the outer layer, and proceeds inwards, resulting in a radial pressure at the innermost layer.

Stiffness Method for Cracked, Jacketed Specimen Analysis

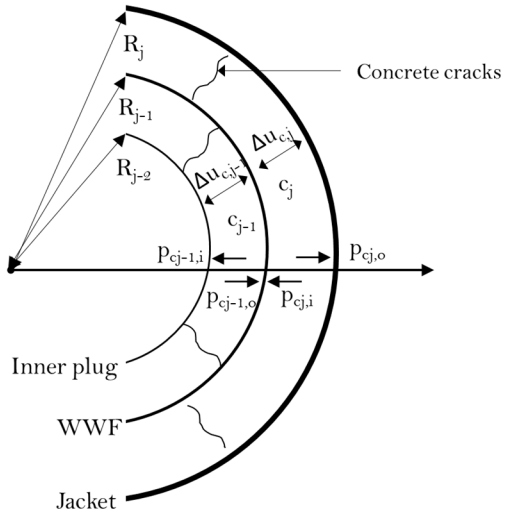

Figure C-21. Details of Stiffness Method for Cracked, Jacketed Specimens

From measured data, the hoop strain ε_j in reinforcing layer j is known.

$$\varepsilon_j = \varepsilon_{hoop_{ave}}$$

- Calculate the hoop stress, σ_j

$$\sigma_j = \min\{E_j\varepsilon_j, f_{yj}\} \quad (19)$$

- Calculate the change in radial pressure Δp_j due to the reinforcing layer

$$\Delta p_j = \frac{\sigma_j t_j}{R_j} \quad (20)$$

- Calculate the radial pressure at the outer edge of concrete layer j, $p_{cj,o}$

$$p_{cj,o} = p_{cj+1,i} + \Delta p_j \quad (21)$$

- Calculate the radial displacement at reinforcing layer j, u_j

$$u_j = \varepsilon_j R_j \quad (22)$$

- Calculate the pressure at the inner radius of concrete layer j, $p_{cj,i}$

$$p_{cj,i} = p_{cj,o}\frac{R_j}{R_{j-1}} \quad (23)$$

- Calculate the radial compressive displacement within concrete layer j, $\Delta u_{c,j}$

$$\Delta u_{c,j} = \frac{0.5t_{cj}(p_{cj,i}+p_{cj,o})}{E_{cj}} \quad (24)$$

- Calculate the radial displacement at reinforcing layer j-1, u_{j-1}

$$u_{j-1} = u_j + \Delta u_{c,j} \quad (25)$$

- Calculate the hoop strain at reinforcing layer j-1, ε_{j-1}

$$\varepsilon_{j-1} = \frac{u_{j-1}}{R_{j-1}} \quad (26)$$

- Proceed for layer j-1 as before until the radial pressure at the innermost layer is found.

The hoop strain ε_j is known at a particular height z along the length of the specimen from the measured data therefore the above procedure can be done at each discretely measured height.

2. *Find the coefficient of friction, μ*

Eqns. 9 and 10 can be modified to account for the presence of an external jacket as follows.

$$pD_{plug}L_{plug} = P_{c_{spiral}} + P_{c_{jacket}} \quad (27)$$

$$pD_{plug}L_{plug} = 2(\sigma_{sp}t_{sp}L_{sp} + \sigma_j t_j L_j) \quad (28)$$

From Eqn. 28, it can be seen that p now accounts for the contributions of the spiral steel and external jacket to the hoop force. This is the normal pressure acting across the plug-wall interface and is the result of the previous procedure to find the radial pressure at the innermost layer of concentric circles.

Therefore, using Eqns. 11 and 13 and the normal pressure found from the stiffness method, the coefficient of friction can be calculated.

$$\mu = \frac{P_{residual}}{\pi p D_{plug} L_{plug}} \tag{29}$$

To account for measurements at discrete heights, the pressures can be integrated over the height of the specimen.

$$\mu = \frac{P_{residual}}{\pi D_{plug} \int_0^L p dz} \tag{30}$$

C.3 MODEL UN: PRE-PEAK BEHAVIOR

Assumption: The coefficient of friction does not change after slip occurs so that the value remains the same throughout testing.

The cohesion stress acting at the plug-wall interface when the peak load is reached can be found by using the coefficient of friction μ found from Model CR and substituting it into Eqn. 2. The peak load P_{peak} can be taken as the shear friction strength V_{ni} at the plug-wall interface of interest.

$$V_{ni} = P_{peak} \tag{31}$$

$$c = \frac{P_{peak} - \mu \pi P_c}{A_{cv}} \tag{32}$$

Before the peak load is reached the spiral steel, concrete and external jacket, if present, are all contributing to the clamping force, P_c. Therefore

$$P_c = P_{c\,spiral} + P_{c\,jacket} + P_{c\,concrete} \tag{33}$$

The normal radial pressure p would also be in equilibrium with the three contributions, modifying Eqn. 27 to give

$$p D_{plug} L_{plug} = P_{c\,spiral} + P_{c\,jacket} + P_{c\,concrete} \tag{34}$$

Before cracking which occurs at the peak load, the three materials can be assumed to be elastic. In order to find p, the measured hoop strain can be related to it by using an equivalent elastic stiffness for the wall system, K_{el} such that

$$p = K_{el}\varepsilon_{hoop_{ave}} \quad (35)$$

1. *Determine equivalent elastic stiffness, Kel*

The equivalent elastic stiffness of the uncracked system before peak load is reached can be calculated by considering the wall of the system as a series of thick-walled concentric cylinder layers.

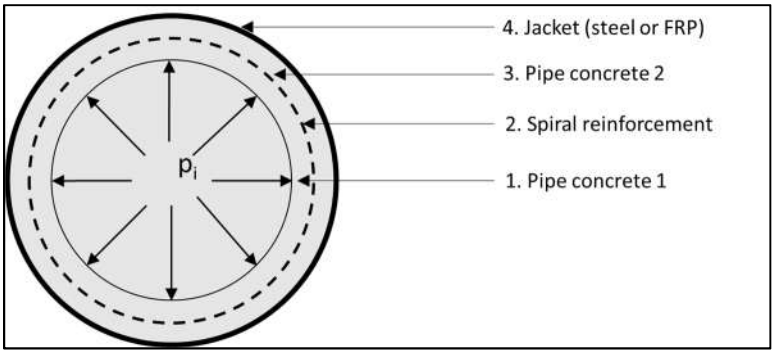

Figure C-22. Model of pipe wall as a series of concentric thick-walled cylinders

Thick-walled Cylinder Analysis for Uncracked Specimen Stiffness

Consider two thick-walled cylinders concentrically fitted within one another as shown in the figure below. Note that the displacements and pressures are taken as positive outwards.

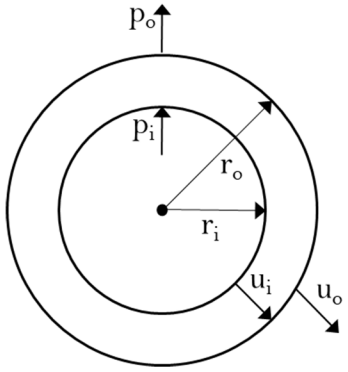

Figure C-23. Details of Thick-walled Cylinder Analysis for Uncracked Specimen Stiffness

For a thick walled cylinder, the radial displacements and pressures on the outer (u_o, p_o) and inner (u_i, p_i) walls are linked by Eqns. 36 and 37 (Timoshenko, 1941).

$$u_i = \left(\frac{1-\nu}{E}\right)\left(\frac{r_i{}^2 p_i - r_o{}^2 p_o}{r_o{}^2 - r_i{}^2}\right) r_i + \left(\frac{1+\nu}{E}\right)\left(\frac{r_i{}^2 r_o{}^2 (p_i - p_o)}{(r_o{}^2 - r_i{}^2) r_i}\right) \qquad (36)$$

$$u_o = \left(\frac{1-\nu}{E}\right)\left(\frac{r_i{}^2 p_i - r_o{}^2 p_o}{r_o{}^2 - r_i{}^2}\right) r_o + \left(\frac{1+\nu}{E}\right)\left(\frac{r_i{}^2 r_o{}^2 (p_i - p_o)}{(r_o{}^2 - r_i{}^2) r_o}\right) \qquad (37)$$

These can be expressed as a flexibility matrix $\bar{F}$ of the form:

$$\begin{Bmatrix} u_i \\ u_o \end{Bmatrix} = \frac{1}{E(r_o^2 - r_i^2)} \begin{bmatrix} r_i[r_i^2(1-\nu) + r_o^2(1+\nu)] & 2r_i r_o^2 \\ 2r_i^2 r_o & r_o[r_o^2(1-\nu) + r_i^2(1+\nu)] \end{bmatrix} \begin{Bmatrix} p_i \\ p_o \end{Bmatrix} \qquad (38)$$

or simply,

$$\{u\} = \overline{F}\{p\} \qquad (39)$$

It should be noted that the flexibility matrix is not symmetric since pressures, not forces, are related to the displacements.

The flexibility matrix in Eqn. 38 can be inverted to provide an "element" stiffness matrix for each thick-walled cylinder.

$$\{p\} = \overline{K_{el}}\{u\} \qquad (40)$$

Different elements represent the inner concrete, the spiral steel, the outer concrete and the jacket (if present).

For the test specimens, the hoop strain at the outside was the known quantity. The hoop strain is related to the radial displacement by

$$u = r\varepsilon_{hoop_{ave}} \tag{41}$$

The system of equations can be solved by applying a trial internal pressure and scaling it so that the outer radial displacement has the known value. The hoop stress in the internal elements, for example the spiral steel, can be obtained from equilibrium with radial stresses.
When the stiffness matrix is found for all elements in the system, they can be combined and condensed to relate the outermost hoop strain that is the known quantity to the inner pressure of the innermost layer by a single value K_{el} as in Eqn. 35.

2. *Find the cohesion stress, c*

Since the wall is uncracked, it can be assumed that the equivalent elastic stiffness is uniform along the height. Substituting Eqn. 33, 34 and 35 into Eqn. 32, the cohesion stress, c can be calculated for the specimen.

$$c = \frac{P_{peak} - \mu\pi D_{plug} L_{plug} K_{el} \varepsilon_{hoop_{ave}}}{\pi D_{plug} L_{plug}} \tag{42}$$

The average hoop strain ε_{hoop_ave} can be taken as the arithmetic mean of the average hoop strains measured at discrete heights along the height of the specimen since before cracking the strains are all very small and similar to each other.